Thin-walled beams and joints

Hansen, Anders Bau

Publication date:
2019

Document Version
Publisher's PDF, also known as Version of record

DTU

PhD Thesis R-410
Department of Civil Engineering

Thin-walled beams and joints

Anders Bau Hansen

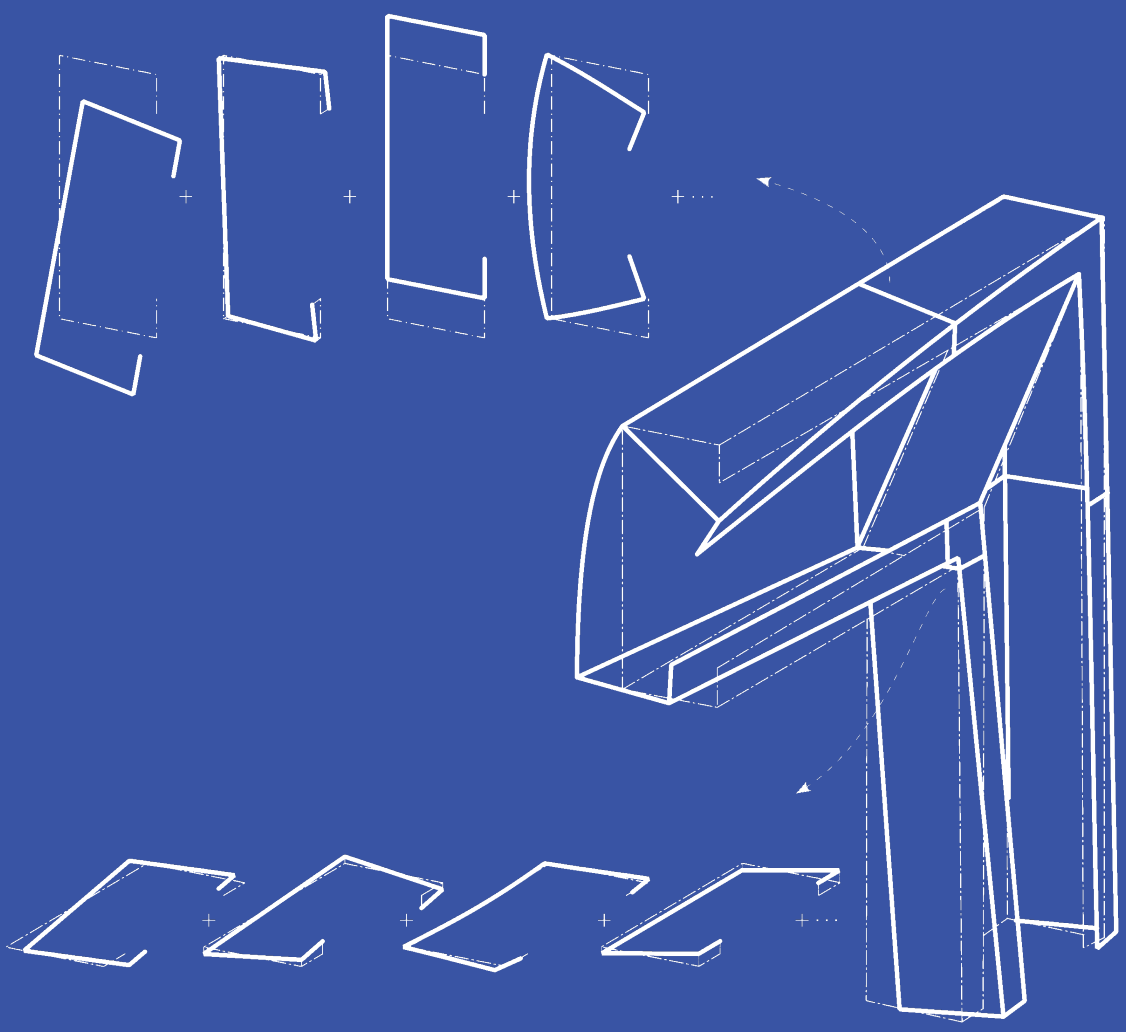

Innovation Fund Denmark

NIRAS

Thin-walled beams and joints
– *Advanced modelling of beams and connection components*

PhD dissertation

Department of Civil Engineering
Technical University of Denmark

Report R-410
ISBN 8778775086

Printed by STEP
Typeset in LaTeX

Principal supervisor

Professor Jeppe Jönsson
Department of Civil Engineering
Technical University of Denmark

Co-supervisors

Senior Specialist, Civil Engineer, PhD Thomas Hansen
Department of Structural Design
NIRAS A/S, Denmark

Associate Professor Michael Joachim Andreassen
Department of Civil Engineering
Technical University of Denmark

Assessment Committee

Associate Professor Jens Henrik Nielsen (Head of committee)
Department of Civil Engineering
Technical University of Denmark

Professor Eduardo Bayo
Department of Structural Analysis and Design
University of Navarra, Spain

Associate Professor Ádány Sándor
Department of Structural Mechanics
Budapest University of Technology and Economics, Hungary

Chairman at defence

Assistant Professor Evangelos Katsanos
Department of Civil Engineering
Technical University of Denmark

Preface

The present thesis is a result of a three year Industrial PhD project submitted in candidacy for a Danish PhD degree from the Civil Engineering PhD School at the Technical University of Denmark. The work was conducted from June 2016 till May 2019 with the Technical University of Denmark as the primary workplace and NIRAS A/S as the primary, supplementary working place. Besides this, two scientific visits took place during the study. The first research stay was a two weeks research stay with Professor Kim Rasmussen at the Faculty of Engineering and Information Technologies at the University of Sydney in Australia in late 2017. The second stay was a two months visit at the Department of Civil Engineering at the Technical University of Lisbon in Portugal under the supervision of Assistant Professor Ricardo Vieira. The stay took place from February till April 2018.

The thesis at hand begins with an introduction to thin-walled steel structures, followed by the research objectives and theoretical approach to the work carried out. A general discussion of the results and the conclusions is performed with focus on an assessment of the mechanical behaviour of steel frames, which is the core of this thesis. The content is written as a synopsis based on four papers appended to this thesis. These are referred to by a roman numeral. Paper I reviews the development of theories assessing thin-walled beams and joints and states how a displacement-based mode assessment may contribute to a detailed understanding of a global frame behaviour. A new thin-walled beam theory is presented and discussed in Paper II and III, while Paper IV presents and assesses a novel mode-based joint formulation.

The thesis was submitted 31 May 2019 and was defended at a public defence at the Technical University of Denmark 16 September 2019. Minor corrections have been made to this version of the PhD thesis based on comments given by the assessment committee at the defence.

Anders Bau Hansen
Kgs. Lyngby, September 2019

Acknowledgements

At first, I would like to thank the NIRAS ALECTIA Fund and the Innovation Fund Denmark (grant no. 5189-00005B) who jointly funded this Industrial PhD project.

I want to thank my excellent team of supervisors. Especially, I want to thank my highly qualified scientific advisor Jeppe Jönsson for his outstanding scientific overview. Additionally, I appreciated his guidance through all aspects of the PhD work, and for always finding ways through the most dreadful problems. His dedication to this project has been outstanding – always ready for a discussion and always able to keep up the spirit. Nonetheless, not only Jeppe but the whole team of supervisors have had an encouraging approach throughout the past three years. Thomas Hansen and Michael Andreassen have been part of good discussions. In addition to his scientific overview, Michael always had the result oriented view on any part of the project, which had resulted in well structured plans. Thomas has an excellent talent in keeping the link between a high level of academic research and engineering practice. A great acknowledgement should also be given to Jesper Gath who was the primary person formulating the project in its very beginning.

I thank Kim Rasmussen at the University of Sydney who gave me the possibility to join his group. I appreciated the excellent discussions we had. Moreover, my stay in Sydney would not have been as fruitful if it was not for Shen Yan, who taught me what academia is and inspired me in so many ways! I would also like to thank Ricardo Vieira for his guidance during my stay at the Technical University of Lisbon and Loís Vieira, who I had the joy to share an office with during my stay.

At the Department of Civil Engineering at DTU, I became a part of an academic society driven by a curiosity to research that has been a great inspiration to me. Besides the staff at the department, I would like to thank my colleagues and my fellow PhD students for always being motivated and always have an encouraging approach to the life as a PhD student. Especially, I want to thank Jesper Sørensen for all his guidance as well as all the wonderful early-morning coffee breaks we have shared. To my colleagues at NIRAS, I want to thank you for showing interest and curiosity to the work I was doing.

Lastly, I want to thank my family and friends for always being there and supporting me whenever I needed it. I want to mention Aslak and Lasse, who have encouraged me and reminded me that doing a PhD is more than programming and writing papers. A special thanks go to Mom & Lars, Dad & Monika, my brother Mads, and my partner Sarah for outstanding care and support – Thank you!

Summary

Structural systems of thin-walled steel members have gained increasing attention during the last decades. This increased attention is mainly due to an efficient material utilisation. However, the methods for structural analysis existing today concern primarily single member analysis that does not include the actual interaction between members. Despite that, the modelling of the beams, columns, and especially the connections between them is essential for the assessment of the overall structural performance and for the ability to provide more economical design.

This thesis presents a generic methodology to perform a first-order linear elastic analysis of thin-walled frame structures based on a modal decomposition of beam displacement modes. For this purpose, an advanced beam element and a detailed three-dimensional joint element model is developed. The main novelty is the ability to transform the degrees of freedom at the interface between a beam and a joint into a reduced number of beam displacement mode-related degrees of freedom. Accordingly, the efficiency of this procedure is achieved by having a limited number of degrees of freedom. However, detailed information is available due to decomposition into displacement modes.

The beam element that is developed throughout the study enables an analysis of thin-walled prismatic members with either open or closed cross-sections and covers cross-sectional displacements related to distortion, Poisson effects, and shear. The formulation of the beam element is based on semi-analytic displacement solution modes, which are deduced by a new procedure that results in fundamental and distortional beam modes, with polynomial and exponential variations along the beam axis. Due to the kinematic assumptions, local shear transmission between non-aligned wall elements is accounted for, which is not typically seen in thin-walled beam formulations or shell models. Nonetheless, this is confirmed by a finite element analysis with solid elements. An overall good agreement is seen when comparing the obtained results with a commercial finite element software (Abaqus, 2016).

In conclusion, the obtained results show that the methodology is attractive and well-suited for further development and practical use as it enables an enhanced structural analysis with advanced beam elements and joint models that allows the transfer of torsional and distortional displacement modes. Furthermore, a detailed analysis of various steel frames with a reasonable number of degrees of freedom can be carried out. The formulation is general and thereby suited for implementation in other approaches, which use displacement modes for analysing structural systems.

Resumé

I løbet af de sidste årtier har der været et øget fokus på bærende konstruktioner bestående af tyndvæggede stålelementer. Denne øgede opmærksomhed skyldes hovedsageligt en effektiv udnyttelse af materialet. De nuværende metoder til analyse af konstruktioner vedrører dog primært de enkelte elementer, hvorfor interaktionen imellem disse ikke medtages. Trods dette er modelleringen af bjælker, søjler og især samlingerne imellem disse af afgørende betydning for den overordnede bestemmelse af en konstruktions bæreevne, samt mulighed for et bedre økonomisk design.

Denne afhandling præsenterer en generisk metodik til at udføre en første ordens lineær elastisk analyse af tyndvæggede rammekonstruktioner, der er baseret på en modal opdeling i bjælke-deformationsformer. Til dette formål er der blevet udviklet et avanceret bjælkeelement og en detaljeret model for et tredimensionelt samlingselement. Den primære nyhed er muligheden for at frihedsgraderne på grænsefladen mellem en bjælke og en samling transformeres om til et reduceret antal frihedsgrader, der relaterer sig til bjælkedeformationsformer. Herved opnås en øget effektivitet ved at have et begrænset antal frihedsgrader. Dog er detaljerede oplysninger fortsat tilgængelige på grund af opdelingen i flytningsformer.

Bjælkeelementet, som er udviklet, muliggør en analyse af tyndvæggede prismatiske elementer med enten åbne eller lukkede tværsnit og dækker tværsnitsdeformationer, der relaterer sig til tværsnitsændringer, Poisson-effekter og forskydning. Formuleringen af bjælkeelementet er baseret på semi-analytiske løsninger beskrevet ved flytningsformer, som udledes af en ny procedure, der resulterer i fundamentale bjælkeformer og bjælkeformer med tværsnitsændringer, hvis aksiale variation kan beskrives ved enten et polynomium eller en eksponentiel funktion. På grund af de kinematiske antagelser medtages lokal forskydning mellem ikke-parallelle vægelementer, hvilket typisk ikke ses i tyndvæggede bjælketeorier eller skalmodeller. Ikke desto mindre bekræftes dette ved en finit element analyse med solide elementer. Samlet set er der opnået en overordnet god overensstemmelse ved at sammenligne resultater med et kommercielt finit element software (Abaqus, 2016).

Ud fra de opnåede resultater konkluderes det, at metoden er attraktiv og velegnet til videreudvikling og praktisk anvendelse, da den muliggør en forbedret analyse af konstruktioner ved brug af avancerede bjælke- og samlingselementer, der muliggør en overførsel af torsions- og tværsnitsmæssige deformationsformer. Desuden kan en detaljeret analyse af forskellige stålrammer med et rimeligt antal frihedsgrader udføres. Formuleringen er generel og derfor egnet til implementering i andre metoder, som anvender deformationsformer til analyse af bærende konstruktioner.

Contents

List of publications

This thesis is written as a synopsis based on the following papers written during this PhD study.

Paper I:
Anders Bau Hansen and Jeppe Jönsson, Modelling of steel frames using advanced beam and joint elements with interfaces governed by beam modes, published in *Thin-Walled Structures*, 145:106430, 2019.

Paper II:
Anders Bau Hansen and Jeppe Jönsson, Displacement modes of a thin-walled beam model with deformable cross sections, published in *Thin-Walled Structures*, 141:576–592, 2019.

Paper III:
Anders Bau Hansen and Jeppe Jönsson, A Thin-Walled Beam Element Based on Semi-Analytical Solution Modes, published in *Thin-Walled Structures*, 144:106344, 2019.

Paper IV:
Anders B. Hansen, Jeppe Jönsson and Ricardo F. Vieira, Mode-based assessment of joints and structural elements in thin-walled steel frames, submitted to *Thin-Walled Structures* 2019.

The following papers were carried out during the PhD, but have not been included as a part of this thesis:

Proceedings paper at the EUROSTEEL 2017 conference held in Copenhagen, Denmark, 13-15 September 2017.
Anders Bau Hansen and Jeppe Jönsson, A GBT-framework towards modal modelling of steel structures. *Published by Ernst & Sohn, Ce/Papers* 1 no. 2–3, 1822–1830, 2017.

Proceedings paper at the 14$^{\text{th}}$ Nordic Steel Construction Conference held in Copenhagen, Denmark, 18-20 September 2019.
Anders Bau Hansen and Jeppe Jönsson, Mode-based Beam and Connection Analysis of Frames. *Published by Ernst & Sohn, Ce/Papers* 3 no. 3–4, 355–360, 2019.

1 Introduction

Steel frames commonly consists of beams and columns joined together by bolts and welds. To optimise the efficiency of these structures, the beams and the columns are often designed with a thin-walled cross-section to reduce the self-weight. In building structures, this could, for example, be a beam with either an I-shaped cross-section or a hollow square cross-section instead of a solid square cross-section, see Figure 1.1. However, many different designs for different purposes are commonly seen and it is possible to tailor any cross-sectional shape based on relevant requirements and demands.

A frame made of thin-walled elements is normally used where there is a need for a light but stiff structures. Examples of such structures are factories, sport facilities, power plants, and offshore structures. Here, the high stiffness-to-weight and strength-to-width ratios, which is associated with the thin-walled structures, are beneficial.

The deformation of a frame includes, but is not limited to, bending and torsion of beams and columns, as well as internal rotations at the connections. Nonetheless, the current best practise for assessment of frames is in most cases based on simplified assumptions. An example of this is the rigidity of connections, which often is associated with rough assumptions of the rotational stiffness. This is at the expense of missing essential knowledge of true behaviour of the connections in the frame analysis. Therefore, to improve a frame analysis, it is necessary to understand beam, column, as well as connection mechanics and their interactions. In the following, both beams and columns will be referred to as beam elements or simply beams.

The overarching aim of this thesis is to contribute to the mechanical understand-

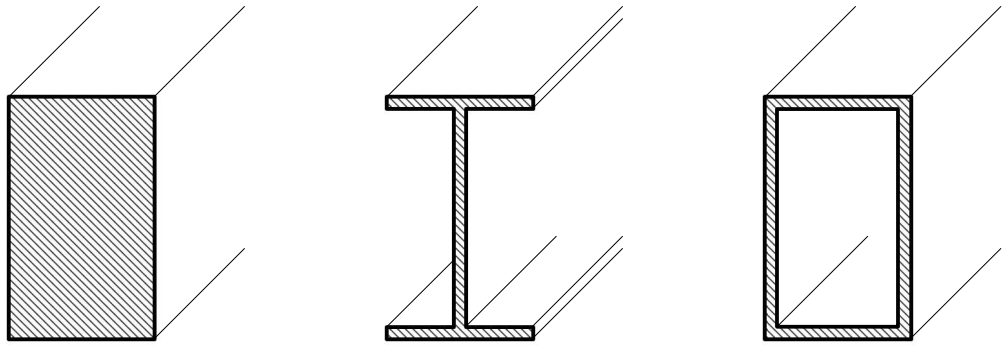

Figure 1.1: A solid and two thin-walled cross-sections sharing the same height and width but with different cross-sectional areas and properties

ing of thin-walled steel frames. First, a general introduction to the development of thin-walled beam theories will be given. Next, an overview of the development of methods to assess connections in frames is presented. In both parts, a displacement-based mode formulation is developed to form the basis for analysis of both beam elements as well as joint elements, which is the main focus of this thesis.

1.1 Thin-walled beam theories

The use of thin-walled steel members in building structures became increasingly common throughout the twentieth century. A reason for this was a general strive for lighter and more optimised structural systems. This development was not limited to the construction industry, as the fields of mechanical, maritime and aerospace engineering also shared the interest. A common feature of all thin-walled components is that they are made of thin plates joined along their edges and that the plate thickness is small compared to the other dimensions (Murray, 1986). As a rule of thumb, a structural element may be categorised as thin-walled if the wall thickness is less or equal to one-tenth of the characteristic cross-sectional dimension (width or height), and again, this characteristic dimension is less or equal to one-tenth of the beam length (Vlasov, 1961). Hence, cold-formed elements with a thickness from 0.378 mm to 6.35 mm can often be considered thin-walled (Yu and LaBoube, 2010), as well as the standardised hot rolled profiles with wall thicknesses in the range of 5 mm up to 40 mm (Plum et al., 2009). Even in offshore structures, where the wall thickness of the superstructures can be 10 mm to 40 mm thick, or even up to 150 mm, the elements may be categorised as thin-walled. However, special attention should be given considering elements of these extreme dimension. The wide use of thin-walled components is due to these elements utilising the material in a very efficient way, as the location of the material is optimised based on strength and stiffness requirements. In the construction industry thin-walled members are for example used as folded steel decks, in bridge girders, and frame structures. Examples of structural thin plate components are illustrated in Figure 1.2.

1.1.1 Background for the classic beam theories

Beam theories are continuously being developed and refined to optimise and utilise the material in the best possible way. Galilei conducted the very first investigations on beam mechanics in the sixteenth century, and Hooke made the essential formulation of the theory of elasticity in 1660 (Timoshenko, 1953). Since then, the classic beam theories have been developed continuously. The first consistent theory presented was the Euler-Bernoulli beam theory (in 1744) valid for members

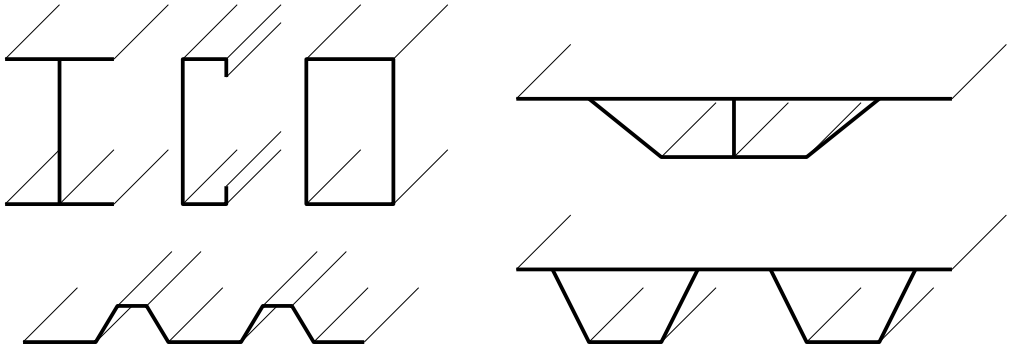

(a) Beam and deck members (b) Box-girders

Figure 1.2: Examples of thin-walled structural components represented by its middle surface lines, letting the actual thickness vanish

in pure bending with the absence of shear (Love, 1944). This theory was deduced by Euler on the hypothesis expressed by Bernoulli that *plane sections remain plane and perpendicular to the deflection curve* (Timoshenko and Goodier, 1970). Additionally, in 1826 Navier reformulated the Euler-Bernoulli theory into the one we know today by introducing the term: moment of inertia. Extensions were given by Saint-Venant (1855) adding homogeneous (free) torsion and by Timoshenko (1921) who derived a beam theory that includes shear flexibility.

In these theories, it is common practice to separate a deformation into a sum of well-known displacement modes such as axial extension, flexure, and torsion. Each mode may then be factorised into an in-plane and out-of-plane cross-sectional displacement field that is multiplied by an axial amplitude function. This amplitude function describes the axial variation of the cross-sectional displacement fields along the beam member. Based on the kinematic assumptions in the classic beam theories, it is possible to formulate a set of twelve fundamental beam displacement modes. These consist of six rigid beam displacement modes, and six beam displacement modes with a polynomial amplitude function. At first, the six rigid modes are three translational movements and three rotational movements. Common to these six rigid modes is that they do not produce any strain energy, i.e. no deformation of the body being displaced. The remaining six fundamental beam modes are as follows: a linear axial extension mode, a free torsion mode with linear variation, two bending modes with the absence of shear described by a quadratic polynomial amplitude, and two bending modes with constant shear having cubic polynomial amplitude functions. Examples are given in Figure 1.3 illustrating the twelve fundamental beam modes presented by the use of a hollow box section.

1.1.2 Elastic plate theories

Thin-walled beam theories are closely related to plate theories as thin-walled sections are made of thin plates. This section briefly introduces some of the key

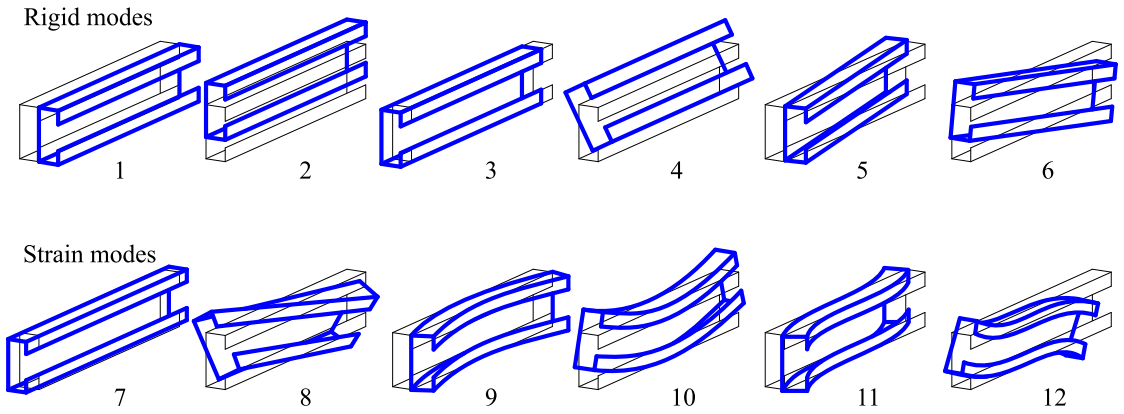

Figure 1.3: Illustration of the twelve fundamental beam displacement modes

investigations made on elastic plate theory. The development of plate theories has followed the theoretical development of beam theories. The first to publish investigations on the theory of plates was Euler in 1766. He studied vibration of perfectly flexible membranes. The flexure theory was investigated further by Bernoulli in 1789 and by Navier in 1823 (Timoshenko, 1953). Kirchhoff (1850) included proper boundary conditions and gave the first convincing plate theory. Then, in 1877 Kirchhoff developed a theory of plates combining membrane action and flexural effects. St. Venant introduced similar developments in 1883. To this end, the theory of plates was governed by the Kirchhoff hypothesis being: *normals to the middle surface remain normals during deformation* (Jönsson, 1995). Later, Reissner (1945) and Mindlin (1951) relaxed this hypothesis to include influences from shear, which is relevant as the plate thickness increases. Hence, the Kirchhoff plate theory is typically referred to as the "thin plate theory", whereas the Mindlin-Reissner plate theory is the "thick plate theory".

1.1.3 The classic thin-walled formulations

Until now, only the homogeneous torsion, which was deduced by St. Venant (Saint-Venant, 1855), has been a part of the classic beam theories. This introduces a constant rate of twist along the beam, and all cross-sections experience the same amount of warping (see Figure 1.3 mode 8). To clarify, here and throughout this thesis warping is defined as an out-of-plane distortional deformation of the cross-section in the beam axis direction as illustrated in Figure 1.4a.

With the increased use of thin-walled members, it was realised that St. Venant's theory became inadequate when examining members exposed to torsion. This was because the torsional deformations of the thin walls resulted in axial stresses and additional shear stresses within the cross-section. This additional contribution was neglected in St. Venant's formulation, which only takes the shear stresses occuring from warping deformations induced by homogeneous torsion into account. Non-

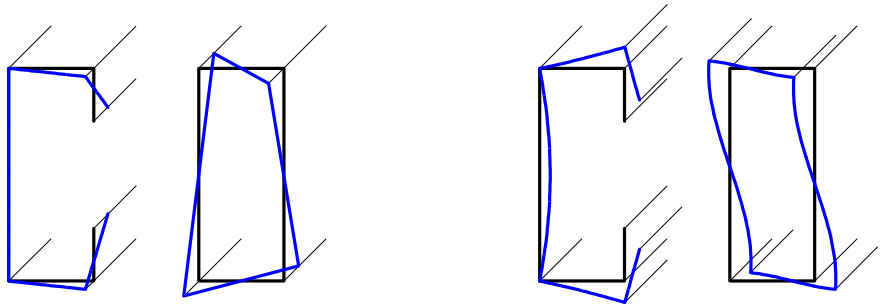

(a) out-of-plane distortional warping (b) in-plane distortion

Figure 1.4: Examples of deformations occurring in thin-walled beams with open and closed cross-sections

etheless, more suitable methods were not deduced until Timoshenko (1910) solved a general problem of mixed torsion for beams with an I-shaped cross-section. This was performed by introducing the phenomenon of non-homogeneous (warping) torsion in combination with homogeneous torsion (the St. Venant torsion). The warping torsion is characterised by a non-linear variation of the rate of twist moving along the beam axis. Indeed, thin-walled members do not comply with the assumption that plane sections remain plane since they are prone to warp (Figure 1.4a)(Kollbrunner and Basler, 1969).

One of the main founders of thin-walled beam theories was Vlasov. He succeeded in formulating a consistent beam theory for thin-walled open sections, where he incorporated the free torsion, deduced by St. Venant, and the warping torsion for arbitrary shaped thin-walled members (Vlasov, 1961). This was done by formulating the Vlasov hypothesis requiring *null shear strain at the middle surface of open sections*. With this hypothesis, it was possible for Vlasov to formulate an expression describing the cross-sectional warping, i.e. out-of-plane deformations. This expression is a function of the changes in the transverse cross-sectional rotation combined with an introduced parameter – the novel sectorial coordinate. From the warping deformation and axial stresses, Vlasov introduced a new fourth generalised force denoted the bimoment. This being a generalised balanced force system that is statically equivalent to zero. In fact, with this new generalised force, it became possible to handle torque as the bimoment is related to additional torsional moment contributions. Consequently, it was possible to describe the behaviour of the cross-section in terms of seven generalised displacements. This was adopted in finite element analysis, and a beam element was developed, which takes the cross-sectional warping deformations into account. This element may be referred to as the "Vlasov element" and fulfils Vlasov's thin-walled beam theory. Such a beam element differed in the sense of having seven degrees of freedom at its nodes instead of only six, which is used in traditional beam elements. Thus, the six standard degrees of freedom are incorporated as well as the extra seventh

degree of freedom representing the torsional deformation coupled to the bimoment and warping deformations. Examples of the use of this Vlasov element were given by Krajcinovic (1969) who investigated the stability and dynamics of thin-walled beams or by Barsoum and Gallagher (1970) who investigated torsion and lateral stability for thin-walled beams.

Besides the well-formulated thin-walled beam theory of members having open cross-sections, Vlasov formulated a theory for closed thin-walled sections as well. This theory is based on a frame analogy with movements at the cross-section corners multiplied by simple linear interpolation functions. Hence, with this analogy Vlasov was able to present a thin-walled theory for closed sections (single and multi cells) that includes cross-sectional warping deformations as well as in-plane *"torsion and deformation of the contour"* (Vlasov, 1961, p. 235), i.e. distortion. To explain, distortion is a non-rigid deformation of the cross-section occurring in the cross-sectional plane only. See e.g. Figure 1.4b.

A general feature of the Vlasov formulation is the potential of uncoupling the beam deformation into the usual axial extension mode as well as major/minor bending modes but also a torsion mode. Torsion is here uncoupled from bending by use of the shear centre, which can be defined as a point where shear forces result in bending without torsion. The shear centre was at first introduced by Maillart and Eggenschwyler in 1921, however, not knowing each others work (Kollbrunner and Basler, 1969).

Another pioneer within the field of thin-walled members was Timoshenko. Among others, he presented a detailed summary of the theory of open thin-walled beams (Timoshenko, 1945a,b,c). Also worth mentioning are Flügge and Marguerre (1950) who developed their thin-walled beam theory, where the use of exponential solution functions solved the equilibrium equation in the axial direction. With this approach, it was possible for Flügge and Marguerre to obtain an exponential decay effect of the cross-sectional deformation along the beam axis similar to the effect from non-homogeneous torsion. Another comprehensive work was conducted by Kollbrunner and Hajdin (1972), who assessed thin-walled beams with the assumption of undeformable cross-sections. Later, they extended their theory to assess thin-walled beams having deformable cross-sections as well (Kollbrunner and Hajdin, 1975). This theory was valid for members with both open and closed cross-sections. Their approach was based on a summation of independent cross-sectional displacement fields with associated geometrical functions describing the axial variation of each displacement field.

1.1.4 Advanced semi-analytic theories

Despite the well established thin-walled beam theories, it seems challenging to derive a proper expression for the in-plane distortional phenomena. As a consequence, more advanced thin-walled beam theories have been developed. A typical line adopted in many advanced thin-walled beam theories is the use of displacement modes. In this context, a mode is perceived as:

> *A cross-sectional displacement field that is subdivided into a part regarding displacements occurring in the cross-sectional plane and a part being displacements perpendicular to the cross-sectional plane. This displacement field is then associated with an axial amplitude function that describes the variation of the cross-sectional displacement field along the beam axis.*

An example of a thin-walled beam theory that adopted this idea was one given by Jönsson (1998, 1999a,b). He gave a proposal based on a generalisation of the classical Vlasov beam theory, where he extended the formulation to include a single general distortional displacement mode for both open and closed cross-sections. This was conducted through an analytical solution of a differential equation system. However, the coupled torsional and distortional displacements were not easily uncoupled in the solutions, which were found through an eigenvalue problem. From this theory, Jönsson deduced a distortional displacement field and a warping displacement field in addition to the classical cross-sectional displacement fields, which are associated with the regular axial extension and flexural beam modes. Nevertheless, additional general beam theories have been developed including a larger number of distortional modes. In the following, some of these theories are presented.

Generalised Beam Theory (GBT)

The Generalised Beam Theory is a one-dimensional beam theory first presented by Schardt (1966). His inspiration to this theory was found in the theory of prismatic folded structures as well as some general principles found in the work of Vlasov (Wlassow, 1958)[1]. Schardt saw his own approach as a direct and natural continuation of Vlasov's *Thin-Walled Elastic Beams* (Vlasov, 1961; Schardt, 1989).

The Generalised Beam Theory is established based on a set of orthogonal cross-sectional displacement fields with associated axial amplitude functions. Depending on load and boundary conditions, the displacement modes are added together resulting in the final deformation pattern. A cross-section is discretised into straight wall segments, see Figure 1.5a. Then, the set of orthogonal cross-sectional displace-

[1]Please notice that Wlassow is the German spelling of Vlasov

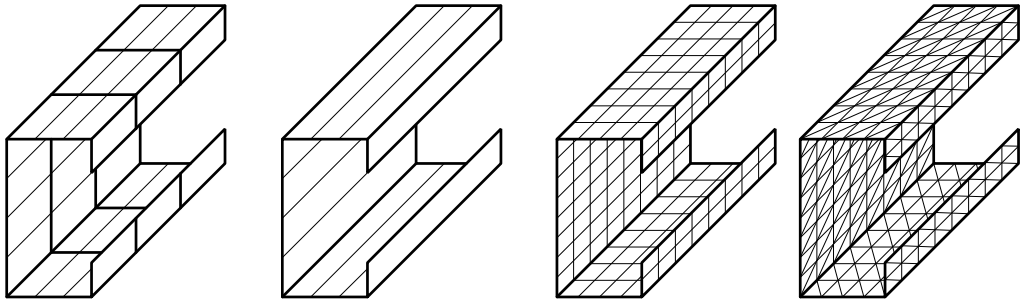

(a) GBT (b) FSM (c) FEM

Figure 1.5: Examples of different kinds of discretisation; (a) GBT discretises the cross-section and assembles the beam elements in the axial direction; (b) FSM separates the beam into narrow strips running the entire length; (c) FEM discretises the entire beam element into finite shell elements, either squared or triangular, respectively

ment fields are written as individual out-of-plane nodal unit displacements, where the nodes are examined one at the time. Based on kinematic assumptions and the out-of-plane displacement fields, transverse displacement fields are deduced as well. Next, solving specific eigenvalue problems related to the beam equilibrium equation system, regular cross-sectional displacement fields are computed. Here, the in-plane transverse displacements are interpolated using cubic polynomial interpolation functions whereas the cross-sectional warping displacements are linearly interpolated. In modern presentations of the theory, the axial variation of the beam member is interpolated using standard finite element Hermite interpolation functions that requires an axial assembling of several beam elements to analyse a single beam member.

In many years, the theory was known inside German-speaking academic societies only. Here, it was known as the: *Verallgemeinerte Technische Biegetheorie* (VTB) and was described in a book by Schardt (1989). It was not until a group of British researchers presented their research on cold-formed members that the theory became internationally known (Davies and Leach, 1994; Davies et al., 1994). The same year, Schardt presented his first papers in English (Schardt, 1994a,b). With the internationalisation of the theory it became known under the acronym: GBT, being an abbreviation for *Generalised Beam Theory*. Since then, the theory has been spread worldwide, e.g. in Slovakia by Baláž (Baláž, 1999; Rendek and Baláž, 2004), in Portugal by da Silva (Silva et al., 2000; Simão and da Silva, 2004), in Australia by Ranzi (Ranzi and Luongo, 2011; Piccardo et al., 2014), and in Italy by Miranda (Miranda et al., 2013, 2014), just to mention some of the places where GBT has been evolved. Nevertheless, the most intensive investigations regarding GBT has been conducted at the Technical University of Lisbon by the group of researchers around Professor Camotim. Their first contribution was the formu-

lation of first- and second-order analysis of members having orthotropic material properties (Silvestre and Camotim, 2002a,b). Then, research on various topics followed such as metallic non-linearities (Silvestre and Camotim, 2003; Abambres et al., 2014), aluminium and stainless steel (Gonçalves and Camotim, 2004), frames and connections (Basaglia et al., 2008, 2009), dynamics (Bebiano et al., 2013), and shear (Silvestre et al., 2011; Silvestre and Camotim, 2013). The effect of shear was incorporated by a set of extra displacement modes established from kinematic constraints. Among others, the two state-of-the-art papers (Camotim et al., 2010; Camotim and Basaglia, 2013) presents a fine summary on some of their main developments.

An essential feature of the GBT is the ability to separate a deformation into a sum of predefined displacement modes, i.e. a so-called mode decomposition. To rephrase it, a deformation is described as a sum of well-known displacement modes. This includes the classic beam modes as well as local and global distortional beam modes. The advantage of this feature is that through a post-analysis procedure it is possible to identify specific deformation patterns that the beam is susceptible to attend. This enriches the engineer with a high possibility to optimise and reinforce the structural design. Nonetheless, the efficiency of a mode-based formulation comes into its own when pronounced modes are used to reduce the number of numerical calculations. This can be done by carefully choosing modes that have an estimated high impact on the deformation. To explain, a set of judiciously chosen modes are used to perform a base change of the beam element's degrees of freedom. An example of this has been given by Abambres et al. (2014), where a reduced number of GBT-beam element modes were selected and consequently, a need of only 25% of the degrees of freedom compared to standard commercial finite element software was needed to analyse a beam.

Finite Strip Method (FSM)

An alternative to the GBT is the method named: *Finite Strip Method* (FSM). Wittrick (1968) derived the first attempt of this theory, and later it was reformulated by Przemieniecki (1973). However, the FSM in the form known today was presented by Cheung (1976).

The FSM is a semi-analytical beam theory to be used for analysis of thin-walled beams. A thin-walled beam member is subdivided into longitudinal strips running the full length of the beam, see Figure 1.5b. These strips, or elements, are rigidly joined to one another along the junction lines, and the ends are assumed simply supported. Furthermore, the kinematic assumptions originate in the Kirchhoff hypothesis. Then, stiffness matrices of each strip are set up. These are based on an assumed displacement field in the transverse direction by polynomial functions, whereas a series of geometrical functions are used in the axial direction.

Researchers who investigated buckling problems of folded plates saw this as a powerful tool and adopted this theory. As an example, Hancock (1985) used the FSM to deduce buckling curves for thin sections, i.e. so-called signature curves. This theory, however, is limited to regular geometries with simple loading and ordinary boundary conditions. Consequently, improvements were implemented by Ádány and Schafer (2006b,a) who introduced the ability to do a displacement-based mode decomposition. Their work led to the modified version of the FSM, the so-called: *constrained Finite Strip Method* (cFSM). With specific constraints introduced at the strain formulations, it is possible to subdivide an arbitrary buckling mode into a set of conventional displacement modes. These modes are categorised as global, distortional, and local modes, respectively (Ádány and Schafer, 2008). Hence, the mode decomposition, as well as the mode identification, results in a better understanding of the beam behaviour compared to the conventional FSM. Li et al. (2014) gave a favourable review of the cFSM. Other improvements to the Finite Strip Method have followed as well, e.g. the *semi-analytical Finite Strip Method* limited to simply supported boundary conditions and longitudinal loads (Cheung and Tham, 1976), or the *spline Finite Strip Method*, which replaces the axial series function with splines (van Erp and Menken, 1990).

Advanced theories with a more strict mathematical approach

Common for the theories included in this paragraph is an overall procedure of deducing the cross-sectional displacement fields directly from solving the correct eigenvalue problem related to the equilibrium equations. To explain the methodology, an arbitrary shaped thin-walled cross-section is discretised into generic wall elements, as illustrated in Figure 1.6. Each wall element is assumed straight, and its deformation is governed by nodal degrees of freedom and standard beam interpolation functions. The degrees of freedom included are two in-plane translational displacements, a single out-of-plane translation, and an in-plane rotational degree of freedom at each node. Consequently, even with a low number of wall elements global and local buckling displacement fields are obtained. Then, cross-sectional

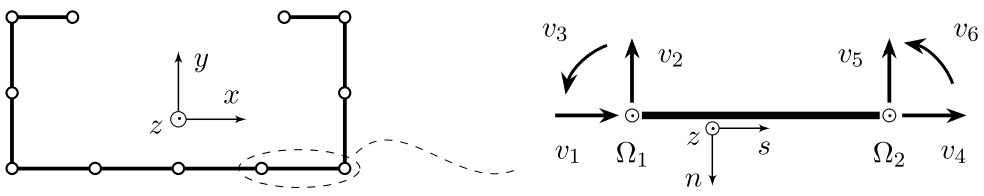

Figure 1.6: The cross-section of a thin-walled beam is discretised by wall elements. Furthermore, a wall element is shown with its nodal degrees of freedom, where v_1, v_2, v_3, v_4, v_5 and v_6 relates to in-plane deformations and Ω_1 and Ω_2 relates to out-of-plane deformations. This configuration have been used, e.g. by Jönsson and Andreassen (2011) and Vieira et al. (2014)

stiffness matrices can be formulated using an elastic strain energy formulation with kinematic assumptions originating in the Kirchhoff plate theory. The strain energy is used to determine a system of coupled homogeneous beam differential equations, which are solved with a strong approach resulting in homogeneous beam equilibrium equations that are rewritten into a polynomial eigenvalue problem. The result is a set of eigenvectors and their corresponding eigenvalues. Each eigenvector represents a cross-sectional displacement field where the eigenvalue directly relates to the axial amplitude function. If the eigenvalue is zero, the axial amplitude function will be represented as a polynomial function. On the other hand, if the eigenvalue is non-zero, the axial amplitude function will take an exponential variation, which is a direct consequence stemming from the solution of the differential equation system. As a result, displacement modes are already divided into fundamental modes and distortional modes. Here, the distortional modes are those having an exponential attenuation of the axial amplitude and relates to global and local wall bending modes. Hence, a series of higher order deformation modes is obtained.

As an example of this approach the work conducted by Jönsson and Andreassen (2011) could be mentioned. They presented a linear elastic, homogeneous beam theory to assess thin-walled components. Improvements were introduced by formulating a non-homogeneous beam element that takes body forces into account and a column buckling analysis was included as well (Andreassen and Jönsson, 2012a,b). An adequate elaboration is given in (Andreassen, 2012). To highlight some of their considerations, the simplification of letting the constitutive relations uncouple the strains by neglecting the Poisson effect should be mentioned. Moreover, through a constraint equation, the shear is uncoupled from the normal stresses. In the end, a fourth-ordered beam differential equation system is deduced and based on a procedure to reduce the differential order, the equilibrium equation system is solved as a generalised eigenvalue problem (Hanf, 1989; Tisseur and Meerbergen, 2001).

Another example is the approach presented by Vieira et al. (2013, 2014). At first glans, this formulation seems more general as it includes the Poisson effect in the constitutive relations and it contains different amplitude functions in the three principal directions regarding the deformation formulations. However, the Poisson effect is neglected in the examples from the papers, and identical expressions are used for the three amplitude functions. This makes it questionable whether these effects are fully incorporated or not. Nevertheless, Vieira and co-workers presented a procedure to deduce and identify the twelve fundamental beam modes from the classic beam theory. These were limited to an axial polynomial variation of maximum third-order, see e.g. Figure 1.3, where similar variation functions are illustrated. Vieira (2010) used a refined procedure inspired by the Jordan Chain algorithm to identify the twelve modes depending on their polynomial order. This approach was also used by e.g. Morandini et al. (2010). Now, continuing to the

higher order thin-walled beam modes, a number of distortional beam modes were included as well. Exponential amplitude functions described these to simulate the attenuation of the cross-sectional displacement field.

Method comparison

A comprehensive comparison between the GBT and the cFSM have been conducted by Ádány et al. (2009). The conclusion was that the results correlate very well, but minor deviations were observed stemming from differences in the formulation of the constitutive relations. Another point distinguishing the two approaches is the fact that the cFSM only allows for simply supported boundary conditions, whereas the GBT is more general in this regard. A comparison at a kinematic level between the two theories was carried out by Silvestre et al. (2011). Among others, they concluded that the formulation of stiffness matrices is different in the two approaches. The GBT is based on cross-sectional stiffness matrices whereas the cFSM formulates stiffness matrices of the entire beam element.

An advantage of the mathematical approaches compared to the GBT is the determination of the cross-sectional displacement fields. Here, the approach used in the GBT is not as familiar or intuitive as the rigorous formulation developed in the mathematical approaches, where the modes are deduced automatically when solving the equilibrium equations. The similarities may be associated with a finite element frame analogy. Furthermore, with the mathematical approaches, not only the cross-sectional displacement fields are automatically determined but also their exact axial amplitudes and thus, no approximations are needed concerning the axial variation of the beam element.

Having reviewed only a few of the thin-walled beam theories, which have been presented through time, the following section introduces a numerical approach to analyse and assess structural components based on polynomial interpolations.

1.2 Finite Element Method

The *Finite Element Method*, shortly FEM, is a very versatile method being used in many different contexts. Around 1942, Courant proposed the version used today. Courant used the principle of stationary energy and piecewise polynomial interpolation. However, the method was not applied in practice until the growth of the aerospace industry in the 1950s developed a need, which was supported by the increased computer power, which gradually became available through the 1960s (Cook et al., 1989; Zienkiewics et al., 1977). Since then, the method has been used in a broad range of fields as it, in its simplest form, is suitable to solve any differential equation system. In general, the idea of FEM is that a domain is partitioned into a finite number of minor parts, namely the so-called finite elements. Then,

the accuracy of the solution depends on how well the variation of the unknown variables is approximated within each element. The purest form used in structural analysis is obtained by having a linear elastic material behaviour in combination with the hypothesis of small displacements. With this set-up, a system of linear equations is obtained.

In line with the increased use of the method, the number of different elements has been expanding. With regards to structural analysis, not only one-dimensional beam elements exist but also shell elements, which are commonly used in a refined analysis of thin-walled beams, see Figure 1.5c. Here, both triangular and squared shell elements have been developed that comply with the Kirchhoff hypothesis as well as shell elements that fulfil the Mindlin plate theory. With these shell elements, it is possible to discretise even complex geometries by use of the finite element method.

Recently, an improved shell element has been developed. The element was presented by Ádány (2016) in a so-called: *constrained Finite Element Method* (cFEM). This method was derived from the semi-analytical FSM. The transverse interpolation of the element's displacements was maintained, but the longitudinal interpolation was changed to classical polynomials as used in the classic FEM formulation. Furthermore, constraints were added to the kinematic formulations as done in the cFSM. Hence, the constraints were added to the strain formulations by requiring the transverse displacement derivatives to be equal to zero. Further improvements have been given, e.g. in (Ádány, 2017, 2018; Ádány et al., 2018).

The FEM is probably the most popular method compared to the different approaches listed in Section 1.1.4. In structural analysis, it is a powerful tool due to its versatile use. One of the main achievements is the flexibility related to beam geometry. It becomes more accessible to, e.g. model internal holes or other non-continuous features. However, the main drawback is the high amount of degrees of freedom needed. This may limit the use of the method due to a low calculation speed in more extensive assessments. Furthermore, in the case of structural elements with simple geometry and boundary conditions, the group of advanced one-dimensional beam theories, e.g. GBT, seems entirely sufficient. Besides, these theories yield a high level of accuracy with a reduced number of degrees of freedom. Moreover, the advanced one-dimensional methods enable the powerful mode decomposition, which is not supported by the FEM. Indeed, this mode decomposition results in a high level of information regarding the beam deformations.

The FEM has not only been used for beam analysis. Throughout the following section, it turns out that FEM has been used for assessing the joint behaviour in steel frameworks as well. Hence, the next section focuses on the assembling of non-aligned beam elements and the joint mechanical behaviours in steel frameworks,

where FEM among others have been used.

1.3 Frame analysis and joint mechanics

In line with the increased use of thin-walled structural components, the transmission of warping and distortional effects, which occur in these thin-walled members, becomes a topic of interest when analysing frames and especially its connections. However, to be able to include these effects, a detailed analysis of the joint is needed. Simplifications may be introduced by focusing on the global frame behaviour and neglecting these higher order effects. A primary focus is the rigidity of the connection. The joint rigidity describes the joints susceptibility to deform due to internal rotations. In fact, a connection is commonly categorised in one of the three following categories: (a) ideally pinned, (b) fully rigid or (c) semi-rigid (see Figure 1.7). The ideally pinned connection permits free rotation between the connected members and therefore only normal, and shear forces can be transferred. On the other hand, a fully rigid connection prevents all internal rotations and thus, bending moments will be fully transmitted. Between these two types of connections, the semi-rigid connections are found. A semi-rigid connection is characterised by allowing relative rotations to occur when bending moments are transferred between adjacent components. Therefore, since connections seldom fulfil the criteria of being neither ideally pinned nor fully rigid, the semi-rigid behaviour should be considered in most cases of frame analysis (Cunningham, 1990).

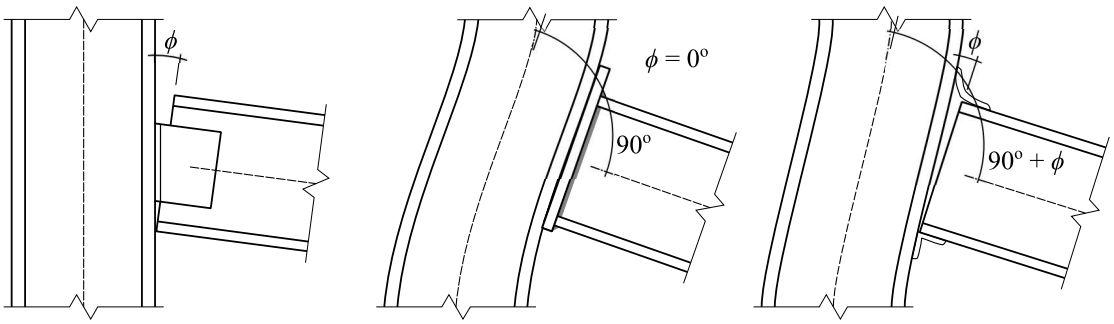

(a) Pinned connection (b) Rigid connection (c) Semi-rigid connection

Figure 1.7: Different joint behaviours that depends on the configuration. In the figure, ϕ indicates the angular rotation between the beam and the column

1.3.1 Semi-rigid connections and the Component Method

Certainly, the analysis of steel connections in frame and truss structures is a topic that has received considerable attention in the previous decades. Wilson and Moore (1917) conducted some of the earliest investigations on the rigidity of connections. They presented some experimental results carried out on riveted connections. Since

then, the amount of research on connections has increased continuously. Around the mid-1930s the Steel Structures Research Committee (1937) published several reports on the topic of steel frame analysis. Their focus was on the global behaviour of a frame structure depending on the rigidity of connections. The rigidity of the joint itself was also assessed. This was performed by measuring the relationship between the moment and rotation occurring at specific joints. Chen and Kishi (1989) developed a database collecting experimental test data from semi-rigid steel beam-to-column connections. The data were used to give the moment-rotation characteristics of different joint configurations. A procedure that is still used to describe the joint rigidity today, e.g. see Figure 1.8. Furthermore, investigations have reported that savings in the range of $7\% - 26\%$ could be achieved by analysing frames with semi-rigid connections instead of assuming pinned or rigid behaviours only (Jones et al., 1983; Sarma and Adeli, 2000; Díaz et al., 2012).

In a review given by Díaz et al. (2011), the topic of semi-rigid connections was discussed. Different approaches and methods to determine the joint behaviour were considered. In general, Díaz et al. commented on five models to assess the mechanical behaviour of a joint. These models are: empirical, analytical, mechanical, numerical and informational. Especially the mechanical model, known as the *Component Method*, has gained ground in recent years and was adopted in the European standard for connection design, i.e. Eurocode 3 part 1–8 (EN1993-1-8, 2007). Furthermore, an essential part of such a model is the formulation of the moment-rotation curve. Díaz et al. concluded that an experimental approach yields the most correct results; however, a procedure which is not suitable for daily engineering practise. Therefore, in for example the mechanical models a multi-linear approximation is often used, which is either based on tests and empirical curve fitting or more basic assumptions of the material behaviour.

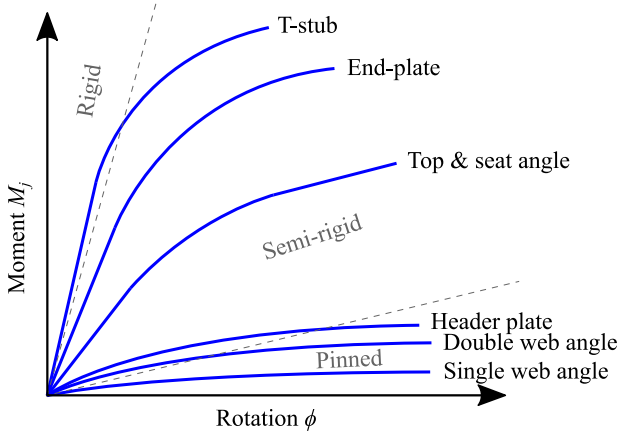

Figure 1.8: Schematic presentation of moment-rotation relationships for different joint configurations (illustration from Paper I)

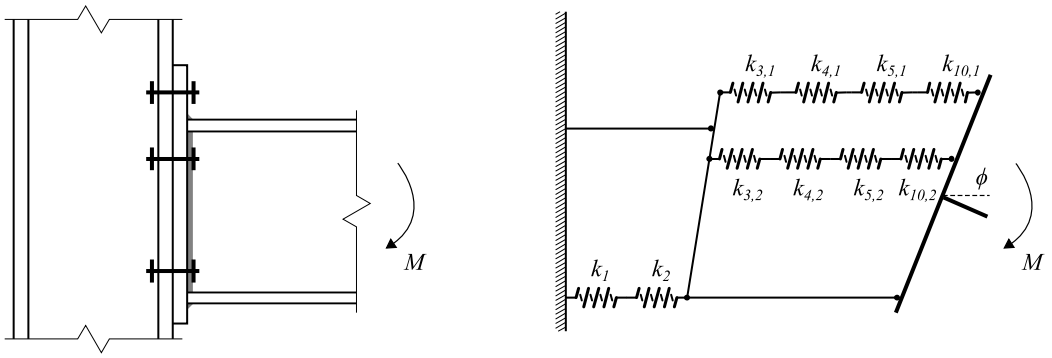

(a) Joint configuration of a beam-to-column end-plate connection between I-sections

(b) Idealised spring model of the end-plate connection, with the two upper bolt-rows in tension

Figure 1.9: Example of a beam-to-column end-plate connection, which is idealised for analysis by use of the Component Method

The Component Method is, in general, a tool to determine a rotational spring stiffness of arbitrary steel joints. This spring stiffness is then to be used in a global frame analysis as an artificial stiffness added to the ordinary beam stiffness matrices. The spring stiffness may influence the beam/column bending deformations as well as the global frame sway deflections. The procedure to compute this rotational spring stiffness is as follows: The joint is subdivided into so-called basis components. Each component is represented by a strength and a stiffness. This could, for example, be a bolt in tension or a column web panel in shear (Jaspart, 2000). Then, the joint is represented in an idealised form by use of rigid links and linear springs, each representing a component. An example of this subdivision of a connection using the Component Method is shown in Figure 1.9. Based on experiments and empirical expressions the stiffness of each component can be computed (Zoetemeijer, 1990) and in the end, the total stiffness of the spring model can be determined (Weynand et al., 1996; Jaspart and Weynand, 2016). This method, however, is limited to transmission of bending moments only, since the normal force of a connected member must not exceed 5 % of the axial design resistance (EN1993-1-8, 2007, §6.2.3(3)).

In recent years, improvements to the Component Method have been presented. Instead of using a linear spring to represent a component, Silva et al. (2000) proposed a bi-linear spring model. Here, a component was represented by a bi-linear spring models where the first part represented the linear elastic behaviour and the second part represented the plastic strain hardening effect. This idea was extended by Zhu et al. (2019) including a multi-linear spring model to represent a post-yielding effect as well.

To overcome some of the iteration steps needed in the Component Method, Bayo et al. (2006, 2017) came up with an idea of letting a joint element represent

the connection. The advantage of such a joint element is that eccentricities, which may be related to the connection, are directly incorporated in this approach. Then, the stiffness of this joint element is to be determined based on springs as in the Component Method. However, this approach is limited to joints in two-dimensional frames and at the beam interfaces, only translation and rotation can be transferred. In a recent article, Bayo and Gracia (2019) introduced a procedure to estimate the stiffness of the joint element by use of mode shapes. This was introduced through a "metamodel based on mode shapes". Hence, from a number of detailed finite element analyses of joints, the idea was to predict the stiffness of joints with similar properties but varying dimensions. This was conducted through a surrogate modelling procedure. To explain, a number of connections were modelled in a detailed finite element environment to generate a basis for the metamodelling. From the finite element analysis, the stiffness matrix of a joint was condensed to a system with only three degrees of freedom at each beam-to-joint interface for the two-dimensional case. These were two translation degrees of freedom and one rotational degree of freedom. Then, through solving an eigenvalue problem, a set of deformation modes (eigenvectors) with associated stiffness intensities (eigenvalues) were computed. The deformation modes became the governing part of the subsequent prediction of the joint stiffness matrix. The modes were assumed to be the same for similar joints, and thus, only the stiffness intensities for scaling the modes had to be predicted in a surrogate modelling procedure. Therefore, computing the newly predicted stiffness intensities and knowing the deformation modes, it was possible to compute a stiffness matrix of the joint without doing a detailed finite element analysis.

To this end, the accuracy of a global frame analysis may be highly improved by taking advantage of the semi-rigid joint design. However, only the global bending effects will be covered by these approaches. In case of frames with thin sections, it is essential to take warping into account as well (Bernuzzi et al., 2014). For this reason, the following section elaborates on the inclusion of warping and distortion in the analysis of joints.

1.3.2 The transmission of warping and distortion

In line with the increased use of constructional elements having a thin-walled cross-section, it became clear that torsion and indeed warping deformations were essential (Vlasov, 1961). In the following, an introduction to some of the key aspects concerning an investigation of the effect of warping of non-aligned thin-walled connections is presented.

One of the very first assessments of warping transmission were conducted by Vacharajittiphan and Trahair (1974). They investigated connections of non-aligned double symmetric I-sections with web continuity and different inclinations between

the beam and the column. They examined four different stiffness configurations. These are illustrated in Figure 1.10, being: (a) unstiffened, (b) partly stiffened with a diagonal stiffening plate, (c) box stiffened, and (d) fully stiffened by a combination of the diagonal and box stiffeners. Vacharajittiphan and Trahair concluded that warping and distortion were interdependent. In addition to this, it was concluded that the stiffening effect highly depends on the exact joint configuration. This was based on the argument that the stiffening plates prevent distortion of the flanges and thus, increase the resistance towards warping.

With the introduction of Vlasov's thin-walled beam theory and the following use of the Vlasov beam element with the extra warping degree of freedom, it became possible to include warping in a global frame analysis. However, it was realised that special attention should be given when handling the problem of restrained warping (Ettouney and Kirby, 1981; Yang and McGuire, 1984). Therefore, they introduced a *warping restraint factor*, and a *warping indicator*, which depended on the joint configuration and by such, the amount of warping being transmitted can be regulated. Nonetheless, these approaches are limited to either approximated calculations of specific cross-sectional shapes or simply an engineering judgement of the restrained effect.

An alternative joint configuration compared to those presented in Figure 1.10 was presented by Baigent and Hancock (1982). It was a method to connect open thin-walled channel sections so that the warping transmission was avoided. This was performed by connecting the elements with a flat plate so that the beam ends were free to warp. However, more conventional joint configurations were investigated by Sharman (1985). Based on an assumption of the rate of twist being equal at the two connected beam ends, Sharman incorporated the warping effect into the standard stiffness matrix for a uniform beam. Examples of both I and open channel sections were reported and compared to test results.

Krenk (1990) and especially Krenk and Damkilde (1991) presented a procedure to determine warping parameters suitable for buckling analysis using classical thin-

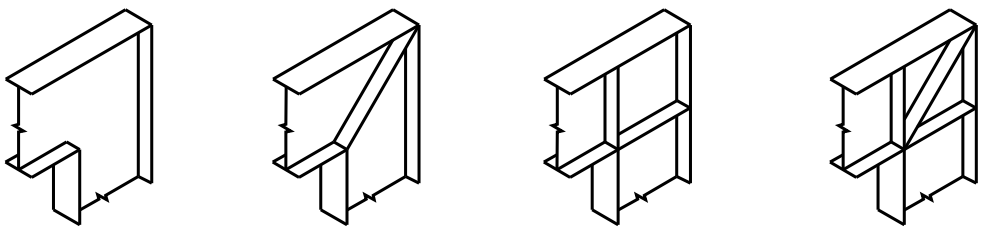

(a) Unstiffened (b) Diagonal stiffened (c) Box stiffened (d) Fully stiffened

Figure 1.10: I-sections assembled at orthogonal frame corners with web continuity and different stiffness configurations

walled beam theory. They conducted both analytical computations and thin-walled beam finite element calculations and their derivations were based on kinematic relations at the beam interfaces. The procedure was deduced for arbitrary oriented thin-walled I-beams (with web continuity) similar to the configurations examined by Vacharajittiphan and Trahair (presented in Figure 1.10). A special feature was that in-plane cross-sectional distortion was incorporated as an in-plane spring stiffness. Similar investigations were carried out by Tong et al. (2005) regarding the diagonal stiffened case only.

Morrel et al. (1996) studied the influence of providing stiffeners to a connection between thin-walled elements when transmitting torsion from one member to another through an orthogonal joint between open plane channel members. More arbitrary stiffening arrangements were examined for thin-walled portal frames by use of finite shell elements, Masarira (2002). The influence of stiffeners on the stability was investigated and in conclusion, it was pointed out that the joint configuration influences the frame stability.

Shayan and Rasmussen (2014) used the idea of letting a joint element represent a connection in a structural framework. They formulated a joint element that takes partial warping continuity through the joint into account. The joint element is to be used in combination with finite beam elements (Vlasov elements) in a linear elastic buckling analysis. They succeeded in formulating an approach that does not require changes in the beam element stiffness matrices but instead uses linear springs and linear constraint equations to represent the joint stiffness. Consequently, this approach can be implemented directly in a finite element environment. However, before the analysis, a shell finite element analysis of the joint is required to determine the correct warping stiffness parameters. This results in the ability to include joints, which are not limited to a specific number of adjoining elements or geometry and thus, complex two- and three-dimensional thin-walled steel frames can be assessed.

The significance of the reviewed methods presented in this section is the ability to include warping effects. However, distortional effects have only been considered peripherally and as a consequence of warping. Furthermore, the contributions mentioned earlier aim for adoption in either an analytical analysis of thin-walled components or as a restrained warping stiffness to be included in a thin-walled beam finite element assessment. Due to the development of more refined beam theories, such as the GBT, it is meaningful to include higher order beam modes as well. For this purpose, a method has been developed within the framework of the GBT. The work was initiated by investigations on different support conditions for the GBT-beam element (Basaglia et al., 2006; Camotim et al., 2008). Then, the first fully implemented attempt of analysing frames using the GBT was presented

by Basaglia et al. (2008). With this paper, Basaglia and co-workers introduced the idea of a joint element connecting non-aligned GBT-beam elements. One of the significant difficulties of this approach, was the handling of GBT-beam modes since these are not directly compatible with standard degrees of freedom. To overcome this hurdle, it was considered to constrain the end cross-section and by such transform the beam end displacements into the classic seven degrees of freedom. With this transformation, it was possible for Basaglia et al. (2008) to analyse the global buckling behaviour of plane and space frames constructed by open thin-walled members. By use of kinematic relations, it was possible to transmit section forces from one beam end to another. However, only the global beam behaviours were considered, i.e. no distortional effects. Later, local buckling and distortional effects were implemented by adding constraint equations to ensure compatibility between the beam elements (Basaglia et al., 2009). By adding extra elastic stiffness to the beam element stiffness matrices, bracing systems and in-span supports were implemented as well (Basaglia et al., 2010). In recent years, the approach has been extended to include beam members with circular hollow cross-sections as well as dynamic analysis for open sections (Basaglia et al., 2015, 2018). The essence of this approach is that instead of describing a deformation in terms of generalised displacements or standard nodal degrees of freedom, it uses a set of structurally meaningful displacement modes. The formulation requires a transformation from beam modes at the beam end into a set of seven generalised displacements representing the motions of the joint element. In addition, some constraint equations can be added to take distortional effects into account as well. However, a mode decomposition and thus a detailed mode assessment of the joint element itself is not supported within this formulation. Consequently, the designer cannot subtract the essential knowledge of the joint deformations from the analysis.

Several approaches have been referenced to analyse and assess thin-walled beams and frames. A methodology that has indicated great potential is the mode-based approach. Despite a great effort given by Abambres et al. (2014); Bayo and Gracia (2019); Camotim and Basaglia (2013), a full displacement-based mode analysis of an entire frame or truss structure has not yet been successfully developed.

2 Objectives

Since no sufficient assessment of steel frame structures fully exploit the potential of the efficient mode-based analysis method, this present work aims to improve the formulation that is based on displacement modes, and thereby contribute to the general knowledge of steel frames. This will be done by adopting a linear elastic analysis of beams and connections, which is described throughout the following papers, which are appended.

Paper I

Aims:

1. To give an overview of thin-walled beam theories as well as methods to implement a semi-rigid connection behaviour and warping effects in frame analysis.
2. To present a brief overall presentation of the idea of establishing a mode-based frame analysis.

Paper II

Aims:

1. To determine a linear elastic thin-walled beam theory that includes cross-sectional, detailed shear, and Poisson effect deformations.
2. To deduce cross-sectional displacement fields and their axial amplitude functions.
3. To identify fundamental and distortional beam displacement modes.

Paper III

Aim:

1. To formulate an advanced thin-walled beam element with a deformable cross-section and extended shear kinematics.

Paper IV

Aims:

1. To present a joint element transformation from standard degrees of freedom into beam cross-sectional displacement-based mode degrees of freedom.
2. To give explicit illustrations of the displacement-based mode decomposition of a frame structure.

3 Theoretical approach

The Papers II and III include the full description of the advanced thin-walled beam element, which is used in the mode-based frame analysis. Paper IV describes the joint element and the assembling of the beam elements and joint elements in a mode-based formulation. In the following, the theoretical approaches used in this PhD work will be discussed, and comments on considerations relevant to these choices will be given.

In general, the entire work is based on a linear elastic material assumption with isotropic properties. Furthermore, the kinematics are described by adapting the small displacement hypothesis. This, in addition to the linear elastic material behaviour, is chosen to keep the formulation in its purest form.

The developed theory has been implemented in the numerical software MATLAB (2016). This software includes a wide range of built-in routines using the function library: `LAPACK` (Linear Algebra PACKage). Besides, the analytical software Maple (2016) has been used as well.

3.1 Novel semi-analytic beam element

The kinematic formulation extends the number of nodal degrees of freedom compared to the methods presented by Jönsson and Andreassen (2011) and Vieira et al. (2014). Hence, a Mindlin formulation has been used through the wall thickness in the axial direction and thereby the Kirchhoff hypothesis is relaxed. Besides, additional axial deformations are taken into account by adding rotational degrees of freedom. This has been chosen to get a versatile formulation of the nodal degrees of freedom at the cross-section, which returns nodes with six standard degrees of freedom. This, however, increases the total number of nodal degrees of freedom and thereby the number of equilibrium equations. Nonetheless, with this general formulation of nodal degrees of freedom, it is an easy task to assemble the end cross-section to finite elements.

The developed theory adopts a semi-analytical procedure to solve beam equilibrium equations. These beam equilibrium equations are deduced using the variational principle on the strain energy functional, which is an efficient tool to set up finite element equations for arbitrary systems. This equation system is solved numerically. The solution is a set of cross-sectional displacement fields with associated axial amplitude functions. Thus, the beam element is formulated using an analytical approach with a direct formulation based on known axial variations

as the solution functions of the beam differential equilibrium equations. This is performed by adopting the axial amplitude functions as interpolation functions between beam end cross-sections.

The semi-analytic beam model is chosen because it results in a detailed mode decomposition with a limited amount of degrees of freedom. However, a straight extrusion of the cross-sectional shape is required, and thus, discontinuities such as holes are not easily included as it might be using the FEM.

3.2 Joint element

A joint element is based on a finite element discretisation of an arbitrary three-dimensional connection geometry by using standard finite elements, e.g. triangular plane shell elements as used in this study. This element is based on the Kirchhoff hypothesis and includes six degrees of freedom at each node, which is located at each of the three corners. However, the drilling degree of freedom, which induces in-plane deformations, requires special attention (Cook et al., 1989). Hence, artificial stiffnesses have been added to these particular degrees of freedom. Consequently, this may result in displacement discontinuities when assembling a beam element and a joint element, but this inconsistency is assumed to have a little influence on the global response.

3.3 Mode-based formulation

The essence of the mode-based formulation is a base change from a set of standard finite element degrees of freedom into a set of modal degrees of freedom. Hence, the cross-sectional displacement solution modes from the beam element have been chosen as the new set of degrees of freedom at the beam-to-joint interfaces. The hypothesis is that the beam modes govern the displacement of an interface. This has been chosen since these modes relate to structural meaningful deformations. With this formulation it is possible to judiciously select modes that shall be represented at an interface. However, this also introduces the risk of not including enough modes and thus, erroneous results may be obtained.

It is important to consider the normalisation of the cross-sectional displacement fields, which are used as the new modal degrees of freedom. This is especially important with regards to the post-analysing mode decomposition when assessing the deformed structure. Therefore, the magnitude of the largest absolute translational degree of freedom in each mode is normalised to unity. This gives a comparable basis to differentiate and identify modes of either high or vanishing influence. The reason why rotational degrees of freedom are not considered is that these might lead to a misleading visualisation of the mode intensities.

4 Results and general discussion

The results of the study is presented in detail in the four appended papers. Accordingly, a summary and a discussion of the main findings will be given throughout this chapter.

4.1 The idea of a mode-based frame analysis

The first part of Paper I concentrates on different approaches used to analyse thin-walled frame structures. This being individual members, connections, as well as global behaviours. Hence, through a background overview, some of the essential improvements in methods used to model connections and advanced beam elements in thin-walled structures are discussed. In conclusion, the properties of an entire methodology that uses displacement modes as degrees of freedom is identified as an approach with an unexploited potential. Accordingly, an idea is presented in the second part of Paper I that enriches the assessment of thin-walled frames by a detailed insight into the mechanical behaviours of beams and connections. The principal that provides the designer with a superior level of information is the newly developed approach based on beam displacement modes. The essence of this methodology is a base change with respect to the degrees of freedom. Hence, the nodal degrees of freedom at an interface between a beam and a joint element are transformed into a mode-based expression governed by few carefully chosen beam displacement modes. Thereby, a set of beam cross-sectional displacement fields can be used as novel degrees of freedom. Furthermore, this formulation allows the deformation of each member to be decomposed into structural meaningful displacement modes, which reveal the amount of extension, rotation, twist, etc.

The use of beam displacement modes as degrees of freedom has been used among others by Abambres et al. (2014) on GBT-beam elements. However, an extension to include connections in the mode-based formulation within the theoretical framework of GBT has not been fully developed yet. This despite the work conducted by Basaglia et al. (2008, 2009, 2015), who presented an approach comparable to the idea presented in Paper I. Nonetheless, several divergent points can be identified when comparing the two approaches. A fundamental difference is found in the way the joints are included in the analysis. The idea outlined in Paper I achieves a fully mode-based formulation by the inclusion of three-dimensional joint elements, whereas the GBT handles the joints by a single node with seven standard degrees of freedom and a set of constraint equations, which is not directly compatible with

the mode formulation used in GBT. Consequently, the GBT mode formulation fails to be extended directly to joint elements. Besides, prior knowledge of the mechanical behaviours of a joint element is required to set up the constraint equations, which are needed to ensure compatibility including higher order cross-sectional displacements. In contrast, the novel idea from Paper I uses a three-dimensional joint element that can be expressed in terms of displacement modes governed by the beam-to-joint interfaces and thereby allows the joint element to be expressed in terms of displacement modes as well. Furthermore, the general formulation of the joint element makes it valid for any geometry, i.e. not limited to open or circular cross-sections, which is the case in GBT.

Indeed, with the present methodology, it seems possible to analyse entire frame structures with a low level of degrees of freedom due to the use of displacement modes as degrees of freedom.

4.2 The advanced thin-walled beam element

In combination, Paper II and III presents the essential theory needed to formulate an advanced thin-walled beam element. This element shall be used in a mode-based analysis of frames. In general, Paper II concentrates on the derivation of beam displacement modes, including identification of fundamental and distortional beam modes, whereas Paper III focus on the formulation of the beam element.

4.2.1 Paper II

Thin-walled beams with both open and closed cross-sections – even multi-cell sections with branched parts, can be assessed with the approach presented in Paper II. Here, beam displacement modes are obtained for linear beam analysis. Hence, the beam displacement modes were deduced as solutions to a polynomial eigenvalue problem, which relates to the second-order beam differential equation system. The beam modes consist of a cross-sectional displacement field and an associated axial variation of the cross-sectional displacement field. The cross-sectional displacement fields are computed as the eigenvectors, and the associated axial variation of each displacement field is found based on the eigenvalues. Consequently, the beam displacement modes are determined directly from the methodology itself. Furthermore, the procedure is organised such that the displacement modes are grouped depending on their eigenvalues and accordingly the displacement modes are subdivided into two categories – the fundamental beam modes having a polynomial axial variation, and distortional beam modes having an exponential axial variation, as discussed in Section 1.1.4 as part of the subsection *Advanced theories with a more strict mathematical approach.*

To this end, effects such as warping from torsion, cross-sectional distortion with

related warping, and Poisson effects with transverse displacements due to normal stresses have been identified as part of the fundamental beam modes. Thereby, it can be concluded that the fundamental modes are not simple solutions based on constrained assumptions, which is typically seen in other similar approaches (Silvestre and Camotim, 2002a; Jönsson and Andreassen, 2011). At the same time, the distortional beam modes relate to global and local distortional deformations of the cross-section. Thus, local plate distortional behaviours and effects that relate to shear lag, as an example, are included in the solutions. Through a comparison of the distortional modes, which are deduced using the procedure described in Paper II, with other mode-based thin-walled beam theories, such as GBT and cFSM, resonable compliance is seen. To exemplify, Figure 4.1 shows the first number of global and local in-plane distortional cross-sectional displacement fields deduced from the approach given in Paper II as well as modes presented by Ádány et al. (2009). To highlight some of the similarities, the first two shapes in all three approaches are similar. Moreover, the modes 33–34, 8 and *vii* indicates also the same displacement pattern. Remembering that the ordering of the modes are method depended and the number of degrees of freedom deviate. The web height

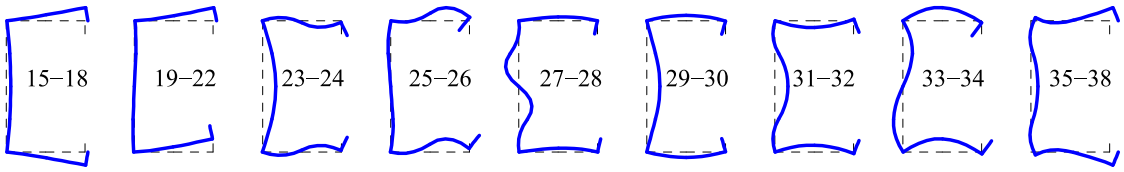

(a) Modes deduced according to the present theory in Paper II (regarding modes 15–18, 19–22, and 35–38, only the real part of the displacement fields are illustrated)

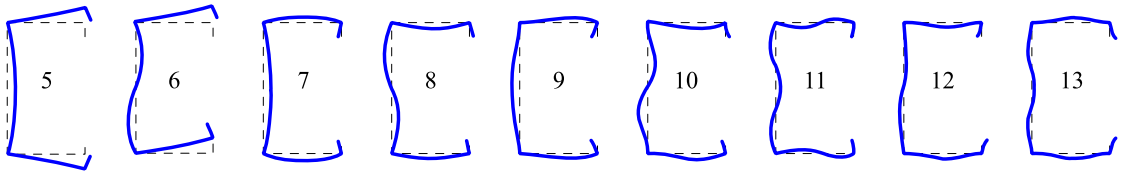

(b) Global and local distortional in-plane modes deduced using the GBT. The modes are interpreted from Ádány et al. (2009), Figure 6 and 7

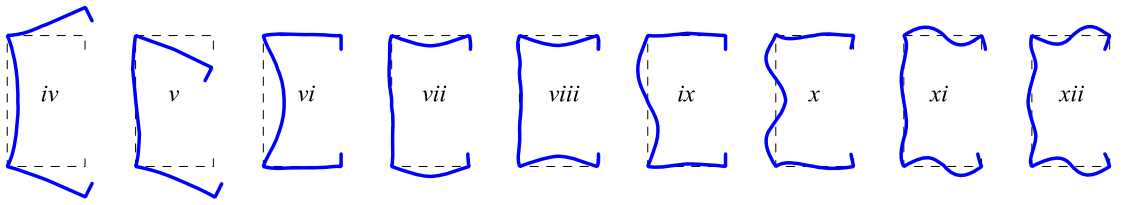

(c) Global and local cross-sectional modes deduced by the cFSM. Modes *iv* and *v* are two distortional length-independent orthogonal modes, and *vi* to *xii* are the first seven local length-independent orthogonal modes. The modes are interpreted from Ádány et al. (2009), Figure 11 and 12

Figure 4.1: In-plane cross-sectional displacement fields

of the cross-section being examined is 100 mm, the flange width is 60 mm, the lip height is 10 mm, and the plate thickness is 2 mm. The elastic constants are: $E = 210$ GPa, and $\nu = 0.3$, respectively. Moreover, the discretisation of the cross-section is as follows: a single element at each lip, two elements at each flange, and four elements at the web panel.

4.2.2 Paper III

Paper III presents the formulation of an advanced beam element, which can account for cross-sectional distortion and warping. The result is a beam element that can be used to analyse prismatic thin-walled beams where the beam deformation is found as a linear combination of pre-established beam displacement modes, i.e. those deduced in Paper II. In particular, it is found that the post-analysing assessment of a beam element provides the user with an in-depth understanding of its behaviour due to the ability to decompose a deformation into structural meaningful beam displacement modes. Not only the identification of activated modes is given, but also the intensities of each mode. In addition to this, the axial decay related to a distortional mode can be calculated from its eigenvalue, which represents the mode length scale parameter as discussed by Jönsson (1999a).

Validation of the theory is obtained by comparing obtained results with those computed using a commercial finite element software (`Abaqus`, 2016). Various examples are used to highlight special features that are covered by the advanced beam element and the results found are in general consistent with those obtained from `Abaqus`. However, due to the kinematic formulation, a refined distribution of shear stresses is obtained. This distribution deviated from a finite element analysis using shell elements, which complies the Kirchhoff hypothesis. Especially when re-distributing the shear stresses between non-aligned wall elements, deviations are seen. Consequently, the deviation in shear stresses leads to an in-depth analysis of the shear transmission between non-aligned wall elements. Thus, a finite element model with solid elements is used to assess the shear stress transmission. In conclusion, the finite element model verifies that the re-distribution of shear stresses is an actual effect localised close to corners and it is an effect that is neglected in other beam theories as well as finite element analysis with shell elements, which complies with the Kirchhoff hypothesis.

4.3 A joint element in mode-space

The primary objective of the work conducted in Paper IV is to present the theoretical interpretation of the methodology based on displacement modes to analyse thin-walled frames in accordance with the idea outlined in Paper I. This formulation contributes to an in-depth understanding of frame behaviours through an

assessment of each element within the frame, i.e. beam and joint elements. The mode-based formulation allows for a decomposition of the deformations calculated for each element into structural displacement modes, which leads to a better understanding of the structural behaviour of both the entire frame structure as well as every single element. It is found that with the mode-based approach and proper joint design, it is possible to reduce the number of degrees of freedom substantially, without a notable change in the global deformations.

This study finds that a reduced number of modes may provide satisfactory results, and in-depth knowledge can be extracted from the mode decomposition. Thereby, it supports the use of a mode-based approach for assessing larger thin-walled frame structures due to the efficient use of degrees of freedom as displacement modes reducing the amount of equations needed in an analysis, and thus saving computational time. The combination of these techniques contribute to the interpretation of the work conducted during the PhD study. Especially, the findings of unique transformation modes strengthen the procedure to be general for other mode-based beam theories as well.

Finally, a comparison of the present method with a finite element analysis, which discretises the entire frame with finite shell elements, is conducted. The conclusion of this comparison gives two primary points.

- The number of degrees of freedom deviates markedly. Two reasons have been identified in explaining this difference. Firstly, the present method uses advanced beam elements with exact axial interpolation functions and thus, degrees of freedom between beam end cross-sections becomes superfluous. The FEM, on the other hand, needs more finite elements in the beam axial direction due to the approximated polynomial interpolation functions. Secondly, the use of interface modes as degrees of freedom reduces the number of degrees of freedom further.

- The information that can be gained from a post-analysing assessment of the structure is different between the two methods. The procedure in Paper IV supports a displacement mode decomposition, and therefore knowledge can be extracted that can increase the mechanical understanding of a structural system or a single component. This can lead to a better understanding of how to design and optimise connections and frames efficiently. A similar assessment is not easily performed by the FEM, as it does not directly support decomposition of deformation into structural meaningful displacement modes (Ádány et al., 2010; Li et al., 2013).

5 Conclusions and perspectives

A novel methodology for first-order linear elastic analysis of three-dimensional thin-walled steel frame structures has been presented. The methodology uses an advanced beam element theory, which has been developed as a part of the study, and a joint element is introduced to describe the complexity that occurs when assembling beams and columns in global frame analysis. The result is a method to perform frame analysis based on displacement modes which includes a detailed displacement pattern of each frame member, i.e. beam elements and joint elements, as well as three-dimensional stress distributions in each member. Hence, the analysis enables an informative evaluation of the overall behaviour of the frame structure and information regarding the local member as well.

The advanced beam element is based on beam displacement modes that include cross-sectional displacements from distortion, Poisson effects, and shear. This method results in a more realistic transmission of shear stresses between non-aligned wall panels within a thin-walled cross-section, which is not typically seen in thin-walled beam formulations or shell models. The beam displacement modes are deduced from a systematic procedure by first solving a homogeneous beam differential equation system as a generalised eigenvalue problem. The modes are then categorised as fundamental or distortional beam modes depending on the axial amplitude function being polynomial or exponential, respectively. These beam displacement modes are then used to formulate the beam element stiffness matrix that is the core of the advanced thin-walled beam element, which includes cross-sectional deformations and extended shear kinematics. The joint element is modelled by the use of standard shell finite elements. These finite elements are used to discretise the geometry of the connection and thereby to assemble an entire joint element stiffness matrix. In combination, the beam elements and the joint elements can be used in a global frame analysis governed by cross-sectional displacement modes at the interfaces between the elements instead of the standard degrees of freedom. The findings suggest that a reduced number of cross-sectional displacement modes can be used to increase efficiency through a reduction of the number of mode-related degrees of freedom. Follow-up studies could be designed to extend the theory to include elasto-plastic analysis by including yielding of the material, which possibly could be performed by adding a bi-linear behaviour of the displacement modes.

Aside from using the present method for first-order frame analysis, the methodology could also be used for buckling analysis by adding geometrical stiffness terms. This could strengthen the methodology since the risk of failure due to instability

is essential for thin-walled members.

Finally, the shell finite element discretisation of a joint element used in this study, could be combined with other kinds of finite elements. For example, to include effects from bolts within the joint mechanics.

In conclusion, the work on thin-walled beams and joints has indicated and proved the potential of an efficient approach to analyse thin-walled steel frame structures, e.g. power plants or other industrial buildings. The analysis results in a detailed assessment of critical displacement modes and presents the intensities of all the interface modes that occur at a connected face. Furthermore, such analysis can be conducted by use of a reasonable number of degrees of freedom due to the use of displacement mode-related degrees of freedom and advanced beam elements. In comparison, a finite element analysis that discretises the entire structure by finite shell elements would usually result in a larger number of degrees of freedom being several orders of magnitude higher than the proposed methodology. The methodology has the potential to contribute to future analyses of thin-walled frames by enabling an enhanced structural analysis with advanced beam elements and joint elements that, among several effects, include distortion. This general formulation using displacement modes at interfaces as degrees of freedom can be suitable for implementation in other approaches, which use displacement modes for analysis of structural systems.

Bibliography

Abambres, M., Camotim, D., Silvestre, N., and Rasmussen, K. J. R. (2014). GBT-based structural analysis of elastic-plastic thin-walled members. *Computers & Structures*, 136:1–23.

`Abaqus` (2016). *Abaqus/CAE 2016; Abaqus® and SIMULIA® used for finite element analysis*. Abaqus Inc., SIMULIA © Dassault Systèmes, 2015, Version 2016.

Ádány, S. (2016). Shell element for constrained finite element analysis of thin-walled structural members. *Thin-Walled Structures*, 105:135–146.

Ádány, S. (2017). Constrained shell finite element method for thin-walled members with holes. *Thin-Walled Structures*, 121:41–56.

Ádány, S. (2018). Constrained shell finite element method for thin-walled members, part 1: constraints for single band or finite elements. *Thin-Walled Structures*, 128:43–55.

Ádány, S., Joó, A. L., and Schafer, B. W. (2010). Buckling mode identification of thin-walled members by using cFSM base functions. *Thin-Walled Structures*, 48:806–817.

Ádány, S. and Schafer, B. W. (2006a). Buckling mode decomposition of single-branched open-section members via finite strip method: Application and examples. *Thin-Walled Structures*, 44:585–600.

Ádány, S. and Schafer, B. W. (2006b). Buckling mode decomposition of single-branched open-section members via finite strip method: Derivation. *Thin-Walled Structures*, 44:563–584.

Ádány, S. and Schafer, B. W. (2008). A full modal decomposition of thin-walled, single-branched open cross-section members via the constrained finite strip method. *Journal of Constructional Steel Research*, 64(1):12–29.

Ádány, S., Silvestre, N., Schafer, B. W., and Camotim, D. (2009). GBT and cFSM: Two modal approaches to the buckling analysis of unbranched thin-walled members. *Advanced Steel Construction*, 5(2):195–223.

Ádány, S., Visy, D., and Nagy, R. (2018). Constrained shell finite element method, part 2: application to linear buckling analysis of thin-walled members. *Thin-Walled Structures*, 128:56–70.

Andreassen, M. J. (2012). *Distortional Mechanics of Thin-Walled Structural Elements*. PhD thesis, Technical University of Denmark - Civil Engineering. Report R-273 (UK).

Andreassen, M. J. and Jönsson, J. (2012a). Distortional buckling modes of semi-discretized thin-walled columns. *Thin-Walled Structures*, 51:53–63.

Andreassen, M. J. and Jönsson, J. (2012b). Distortional solutions for loaded semi-discretized thin-walled beams. *Thin-Walled Structures*, 50:116–127.

Baigent, A. H. and Hancock, G. J. (1982). Structural analysis of assemblages of thin-walled members. *Engineering Structures*, 4:207–216.

Baláž, I. (1999). Dünnwandige stäbe mit offenem oder geschlossenem deformierbarem querschnitt. *Stahlbau*, 68:70–77. (in German).

Barsoum, R. S. and Gallagher, R. H. (1970). Finite element analysis of torsional and torsional-flexural stability problems. *International Journal for Numerical Methods in Engineering*, 2:335–352.

Basaglia, C., Camotim, D., and Coda, H. B. (2018). Generalized beam theory (GBT) formulation to analyse the vibration behaviour of thin-walled steel frames. *Thin-Walled Structures*, 127:259–274.

Basaglia, C., Camotim, D., and Silvestre, N. (2006). GBT-based global buckling analysis of plane and space thin-walled steel frames. *in: Proceedings of the International Collquium on Stability and Ductility of Steel Structures, SDSS 2006*, pages 381–388.

Basaglia, C., Camotim, D., and Silvestre, N. (2008). Global Buckling Analysis of Plane and Space Thin-Walled Frames in the Context of GBT. *Thin-Walled Structures*, 46:79–101.

Basaglia, C., Camotim, D., and Silvestre, N. (2009). GBT-based local, distortional and global buckling analysis of thin-walled steel frames. *Thin-Walled Structures*, 47:1246–1264.

Basaglia, C., Camotim, D., and Silvestre, N. (2010). GBT-based buckling analysis of thin-walled steel frames with arbitrary loading and support conditions. *International Journal of Structural Stability and Dynamics*, 10:363–385.

Basaglia, C., Camotim, D., and Silvestre, N. (2015). Buckling and Vibration Analysis of Cold-Formed Steel CHS Members and Frames Using Generalized Beam Theory. *International Journal of Structural Stability and Dynamics*, 15:1540021.

Bayo, E., Cabrero, J. M., and Gil, B. (2006). An effective component-based method to model semi-rigid connections for the global analysis of steel and composite structures. *Engineering Structures*, 28:97–108.

Bayo, E. and Gracia, J. (2019). Stiffness modelling of 2d welded joints using metamodels based on mode shapes. *Journal of Constructional Steel Research*, 156:242–251.

Bayo, E., Loureiro, A., Lopez, M., and da Silva, L. S. (2017). General component based cruciform finite elements to model 2d steel joints with beams of equal and different depths. *Engineering Structures*, 152:698–708.

Bebiano, R., Camotim, D., and Silvestre, N. (2013). Dynamic analysis of thin-walled members using Generalised Beam Theory (GBT). *Thin-Walled Structures*, 72:188–205.

Bernuzzi, C., Pieri, A., and Squadrito, V. (2014). Warping influence on the static design of unbraced steel storage pallet racks. *Thin-Walled Structures*, 79:71–82.

Camotim, D. and Basaglia, C. (2013). Buckling Analysis of Thin-Walled Structures Using Generalized Beam Theory (GBT): A State-of-the-art Report. *Steel Construction*, 6:117–131.

Camotim, D., Basaglia, C., and Silvestre, N. (2010). GBT Buckling Analysis of Thin-Walled Steel Frames: A State-of-the-art Report. *Thin-Walled Structures*, 48:726–743.

Camotim, D., Silvestre, N., Basaglia, C., and Bebiano, R. (2008). GBT-based buckling analysis of thin-walled members with non-standard support conditions. *Thin-Walled Structures*, 46:800–815.

Chen, W.-F. and Kishi, N. (1989). Semirigid steel beam-to-column connections: Data base and modeling. *Journal of Structural Engineering*, pages 105–119.

Cheung, Y. K. (1976). *Finite Strip Method in Structural Analysis*. Pergamon Press, Oxford, New York, Toronto, Sydney, Paris, Frankfurt.

Cheung, Y. K. and Tham, L. G. (1976). *Finite Strip Method*. Boca Raton FL: CRC Press.

Cook, R. D., Malkus, D. S., and Plesha, M. E. (1989). *Concepts and applications of finite element analysis*. John Wiley & Son, NewYork Chichester Brisbane Toronto Singapore, 3. edition.

Cunningham, R. (1990). Some aspects of semi-rigid connections in structural steelwork. *Structural Engineer London*, pages 85–92.

Davies, J. M. and Leach, P. (1994). First-order generalised beam theory. *Journal of Constructional Steel Research*, 31:187–220.

Davies, J. M., Leach, P., and Heinz, D. (1994). Second-order generalised beam theory. *Journal of Constructional Steel Research*, 31:221–241.

Díaz, C., Martí, P., Victoria, M., and Querin, O. M. (2011). Review on the modelling of joint behaviour in steel frames. *Journal of Constructional Steel Research*, 67:741–758.

Díaz, C., Victoria, M., Querin, O. M., and Martí, P. (2012). Optimum design of semi-rigid connections using metamodels. *Journal of Constructional Steel Research*, 78:97–106.

EN1993-1-8 (2007). *Eurocode 3 - Design of steel structures. Part 1-8: Design of joints.* CEN Brussels, 2. edition.

Ettouney, M. M. and Kirby, J. B. (1981). Warping restraint in three-dimensional frames. *Journal of Structural Division - ASCE*, 107:1643–1656.

Flügge, W. and Marguerre, K. (1950). Wölbkräfte in dünnwandingen profilstäben. *Ingenieur-archiv*, 18(1):23–38. Published by Springer-Verlag, (in German).

Gonçalves, R. and Camotim, D. (2004). GBT local and global buckling analysis of aluminium and stainless steel columns. *Computers & Structures*, pages 1473–1484.

Hancock, G. J. (1985). Distortional buckling of steel storage rack columns. *Journal of Structural Engineering*, 111:2770–2783.

Hanf, M. (1989). *Die geschlossene Lösung der linearen Differentialgleichungssysteme der Verallgemeinerten Technishen Beigetheorie mit einer Anwendung auf die Ermittlung plasticher Grenzlasten.* PhD thesis, Technische Hochschule Darmstadt - Institut für Statik. Report 9 (in German).

Jaspart, J.-P. (2000). General report: session on connections. *Journal of Constructional Steel Research*, 55:68–89.

Jaspart, J.-P. and Weynand, K. (2016). *Design of Joints in Steel and Composite Structures.* ECCS – European Convention for Constructional Steelwork.

Jones, S. W., Kirby, P. A., and Nethercot, D. A. (1983). The analysis of frames with semi-rigid connections – a state-of-the-art report. *Journal of Constructional Steel Research*, 3:2–13.

Jönsson, J. (1995). *Continuum Mechanics of Beam and Plate Flexure.* Aalborg University.

Jönsson, J. (1998). Determination of shear stresses, warping functions and section properties of thin-walled beams using finite elements. *Computers & Structures*, 68:393–410.

Jönsson, J. (1999a). Distortional theory of thin-walled beams. *Thin-Walled Structures*, 33:269–303.

Jönsson, J. (1999b). Distortional warping functions and shear distribution in thin-walled beams. *Thin-Walled Structures*, 33:245–268.

Jönsson, J. and Andreassen, M. J. (2011). Distortional eigenmodes and homogeneous solutions for semi-discretized thin-walled beams. *Thin-Walled Structures*, 49:691–707.

Kirchhoff, G. (1850). Über das gleichgewicht und die bewegung einer elastischen scheibe. *Journal für die reine und angewandte Mathematik*, 1850(40):51–88. (in German).

Kollbrunner, C. F. and Basler, K. (1969). *Torsion in Structures*. Springer-Verlag, Berlin Heidelberg New York. Translation of original edition: Torsion, from 1966 in German.

Kollbrunner, C. F. and Hajdin, N. (1972). *Dünnwandige Stäbe · Band 1, Stäbe mit undeformierbaren Querschnitten*. Springer-Verlag. (in German).

Kollbrunner, C. F. and Hajdin, N. (1975). *Dünnwandige Stäbe · Band 2, Stäbe mit deformierbaren Querschnitten, Nicht-elastisches Verhalten dünnwandiger Stäbe*. Springer-Verlag. (in German).

Krajcinovic, D. (1969). A consistent discrete elements technique for thinwalled assemblages. *International Journal of Solids and Structures*, 5:639–662.

Krenk, S. (1990). Constrained lateral buckling of i-beam gable frames. *Journal of Structural Engineering (ASCE)*, 116:3268–3284.

Krenk, S. and Damkilde, L. (1991). Warping of joints in i-beam assemblages. *Journal of Engineering Mechanics (ASCE)*, 117:2457–2474.

Li, Z., Abreu, J. C. B., Leng, J., Ádány, S., and Schafer, B. W. (2014). Review: Constrained finite strip method developments and applications in cold-formed steel design. *Thin-Walled Structures*, 81:2–18.

Li, Z., Ádány, S., and Schafer, B. W. (2013). Modal identification for shell finite element models of thin-walled members in nonlinear collapse analysis. *Thin-Walled Structures*, 67:15–24.

Love, A. E. H. (1944). *A Treatise of the Mathematical Theory of Elasticity*. Dover Publication, New York, 4. edition.

Maple (2016). *Maple® used for analytical computations*. Maple - © Waterloo Maple Inc. 1981-2017, Version 2016.2.

Masarira, A. (2002). The effect of joints on the stability behaviour of steel frame beams. *Journal of Constructonal Steel Research*, 58:1375–1390.

MATLAB (2016). MATLAB® *and Simulink® used for technical computing*. MATLAB - © 1984-2016 The MathWorks, Inc., Version 2016a.

Mindlin, R. D. (1951). Influence of rotatory inertia and shear on flexural motions of isotropic, elastic plates. *Journal of Applied Mechanics*, 18:31–38.

Miranda, S., Gutiérrez, A., Miletta, R., and Ubertini, F. (2013). A generalized beam theory with shear deformation. *Thin-Walled Structures*, 67:88–100.

Miranda, S., Madeo, A., Miletta, R., and Ubertini, F. (2014). On the relationship of the shear deformable generalized beam theory with classical and non-classical theories. *International Journal of Solids and Structures*, 51:3698–3709.

Morandini, M., Chierichetti, M., and Mantegazza, P. (2010). Characteristic behavior of prismatic anisotropic beam via generalized eigenvectors. *International Journal of Solids and Structures*, 47:1327–1337.

Morrel, P. J. B., Riddington, J. R., Ali, F. A., and Hamid, H. A. (1996). Influence of joint detail on the flexural torsional interaction of thin-walled structures. *Thin-Walled Structures*, 24:97–111.

Murray, N. W. (1986). *Introduction to the Theory of Thin-Walled Structures*. Oxford University Press.

Piccardo, G., Ranzi, G., and Luongo, A. (2014). A direct approach for the evaluation of the conventional modes within the GBT formulation. *Thin-Walled Structures*, 74:133–145.

Plum, C. M., Svensson, E., and Søndergaard, E. (2009). *Teknisk Ståbi*. Nyt Teknisk Forlag, 20. edition. Chapter 6 (in Danish).

Przemieniecki, J. S. (1973). Finite element structural analysis of local instability. *AIAA Journal (American Institute of Aeronautics and Astronautics Journal)*, 11(1):33–39.

Ranzi, G. and Luongo, A. (2011). A new approach for thin-walled member analysis in the framework of GBT. *Thin-Walled Structures*, 49:1404–1414.

Reissner, E. (1945). The effect of transverse shear deformation on the bending of elastic plates. *Journal of Applied Mechanics*, 12(2):69–77.

Rendek, S. and Baláž, I. (2004). Distortion of thin-walled beams. *Thin-Walled Structures*, 42:255–277.

Saint-Venant, B. (1855). Mémoire sur la torsion des prismes. *Mem. Acad. Sci. Savants Etrangers*, 14:233–560.

Sarma, K. C. and Adeli, H. (2000). Cost optimization of steel structures. *Engineering Optimization*, 32:777–802.

Schardt, R. (1966). Eine erweiterung der technishen biegelehre für die berechnung biegestreifer prismatischer falfwerke. *Der Stahlbau*, 35:161–171. (in German).

Schardt, R. (1989). *Verallgemeinerte Technische Biegetheorie - Band 1, Lineare Theorie*. Metrum-Verlag,Darmstadt, 2. edition. (in German).

Schardt, R. (1994a). Generalized beam theory - an adequate method for coupled stability problems. *Thin-Walled Structures*, 19:161–180.

Schardt, R. (1994b). Lateral torsional and distortional buckling of channel- and hat sections. *Journal of Constructional Steel Research*, 31:243–265.

Sharman, P. W. (1985). Analysis of structures with thin-walled open sections. *International Journal of Mechanical Sciences*, 27:665–677.

Shayan, S. and Rasmussen, K. J. R. (2014). A model for warping transmission through joints of steel frames. *Thin-Walled Structures*, 82:1–12.

Silva, L. S., Coelho, A. G., and Neto, E. L. (2000). Equivalent post-buckling models for the flexural behaviour of steel connections. *Computers & Structures*, 77:615–624.

Silvestre, N. and Camotim, D. (2002a). First-order generalised beam theory for arbitrary orthotropic materials. *Thin-Walled Structures*, 40:755–789.

Silvestre, N. and Camotim, D. (2002b). Second-order generalised beam theory for arbitrary orthotropic materials. *Thin-Walled Structures*, 40:791–820.

Silvestre, N. and Camotim, D. (2003). Nonlinear generalized beam theory for cold-formed steel members. *International Journal of Structural Stability and Dynamics*, 3(4):461–490.

Silvestre, N. and Camotim, D. (2013). Shear deformable generalized beam theory for the analysis of thin-walled composite members. *Journal of Engineering Mechanics (ASCE)*, 139:1010–1024.

Silvestre, N., Camotim, D., and Silva, N. F. (2011). Generalized beam theory revisited: from kinematical assumptions to the deformation mode determination. *International Journal of Structural Stability and Dynamics*, 11:969–997.

Simão, P. and da Silva, L. S. (2004). A unified energy formulation for the stability analysis of open and closed thin-walled members in the framework of the generalized beam theory. *Thin-Walled Structures*, 42:1495–1517.

Steel Structures Research Committee (1937). Final report of the steel structures research committee. *Nature*, 139:5–6.

Timoshenko, S. P. (1910). Einige Stabilitätsprobleme der Elastizitätstheorie. *Zeitschrift für Mathematik und Physik*, 58:337–385. (in German) first published in 1905 in Russian.

Timoshenko, S. P. (1921). LXVI. On the Correction for Shear of the Differential Equation for Transverse Vibrations of Prismatic Bars. *Philosophical magazine series 6*, 41(245):744–746.

Timoshenko, S. P. (1945a). Theory of bending, torsion and buckling of thin-walled members of open cross section. *Journal of the Franklin Institute*, 239:201–219. part I.

Timoshenko, S. P. (1945b). Theory of bending, torsion and buckling of thin-walled members of open cross section. *Journal of the Franklin Institute*, 239:249–268. part II.

Timoshenko, S. P. (1945c). Theory of bending, torsion and buckling of thin-walled members of open cross section. *Journal of the Franklin Institute*, 239:343–361. part III.

Timoshenko, S. P. (1953). *History of Strength of Materials.* McGraw-Hill Book Company, inc.

Timoshenko, S. P. and Goodier, J. N. (1970). *Theory of Elasticity.* McGraw-Hill Book Company, inc., 3. edition.

Tisseur, F. and Meerbergen, K. (2001). The quadratic eigenvalue problem. *Society for Industrial and Applied Mathematics*, 43(2):235–286.

Tong, G. S., Yan, X. X., and Zhang, L. (2005). Warping and bimoment transmission through diagonally stiffened beam-to-column joints. *Journal of Constructional Steel Research*, 61:749–763.

Vacharajittiphan, P. and Trahair, N. S. (1974). Warping and distortion at I-section joints. *Journal of the Structural Division (ASCE)*, pages 547–564.

van Erp, G. M. and Menken, C. M. (1990). The spline fininte-strip method in the buckling analysis of thin-walled structures. *Communications in Applied Numerical Methods*, 6:477–484.

Vieira, R. F., Virtuoso, F. B., and Pereira, E. B. R. (2014). A higher order model for thin-walled structures with deformable cross-sections. *International Journal of Solids and Structures*, pages 575–598.

Vieira, R. F., Virtuoso, F. B. E., and Pereira, E. B. R. (2013). A higher order thin-walled model including warping and shear modes. *International Journal of Mechanical Sciences*, pages 67–82.

Vieira, R. J. (2010). *A Higher Order Thin-Walled Beam Model.* PhD thesis, Universidade Técnica de Lisboa - Instituto Superior Técnico.

Vlasov, V. Z. (1961). *Thin-Walled Elastic Beams.* Jerusalem, 2. edition. Israel program for scientific translations.

Weynand, K., Jaspart, J. P., and Steenhuis, M. (1996). The stiffness model of revised Annex J of Eurocode 3. *in: R Bjorhovde and A Colson and R Zandonini (Eds.), Connections in Steel Structures III. Procedings of the 3rd Int. Workshop on Connections, Elsevier, Trento*, pages 441–452.

Wilson, W. M. and Moore, H. F. (1917). Tests to determine the rigidity of riveted joints of steel structures. *Bulletin of the University of Illinois Engineering Experiment Station*, 104:55pp.

Wittrick, W. H. (1968). General sinusoidal stiffness matrices for buckling and vibration analyses of thin flat-walled structures. *International Journal of Mechanical Sciences*, 10:949–966.

Wlassow, W. S. (1958). *Allgemeine Schalentheorie und ihre Anwendung in der Technik.* Akademie Verlag Berlin. (Wlassow is the German spelling of Vlasov).

Yang, Y.-B. and McGuire, W. (1984). A procedure for analysing space frames with partial warping restraint. *International Journal for Numerical Methods in Engineering*, 20:1377–1398.

Yu, W.-W. and LaBoube, R. A. (2010). *Cold-Formed Steel Design*. John Wiley & Sons, 4. edition.

Zhu, C., Rasmussen, K. J. R., and Yan, S. (2019). Generalised component model for structural steel joints. *Journal of Constructional Steel Research*, 153:330–342.

Zienkiewics, O. C., Taylor, R. L., and Zhu, J. Z. (1977). *The Finite Element Method Set – Its Basis and Fundamentals*. McGraw-Hill, 6. edition.

Zoetemeijer, P. (1990). Summary of the research on bolted beam-to-column connections. Technical report, TU-Delft. Report 25-6-90-2.

Appendices

I. Anders Bau Hansen and Jeppe Jönsson, Modelling of steel frames using advanced beam and joint elements with interfaces governed by beam modes. *Thin-Walled Structures*, 145:106430, 2019.

II. Anders Bau Hansen and Jeppe Jönsson, Displacement Modes of a Thin-Walled Beam Model with Deformable Cross Sections, *Thin-Walled Structures*, 141:576–592, 2019.

III. Anders Bau Hansen and Jeppe Jönsson, A Thin-Walled Beam Element Based on Semi-Analytical Solution Modes. *Thin-Walled Structures*, 144:106344, 2019.

IV. Anders B. Hansen, Jeppe Jönsson and Ricardo F. Vieira, Mode-based assessment of joints and structural elements in thin-walled steel frames. Paper submitted to Thin-Walled Structures.

Paper I

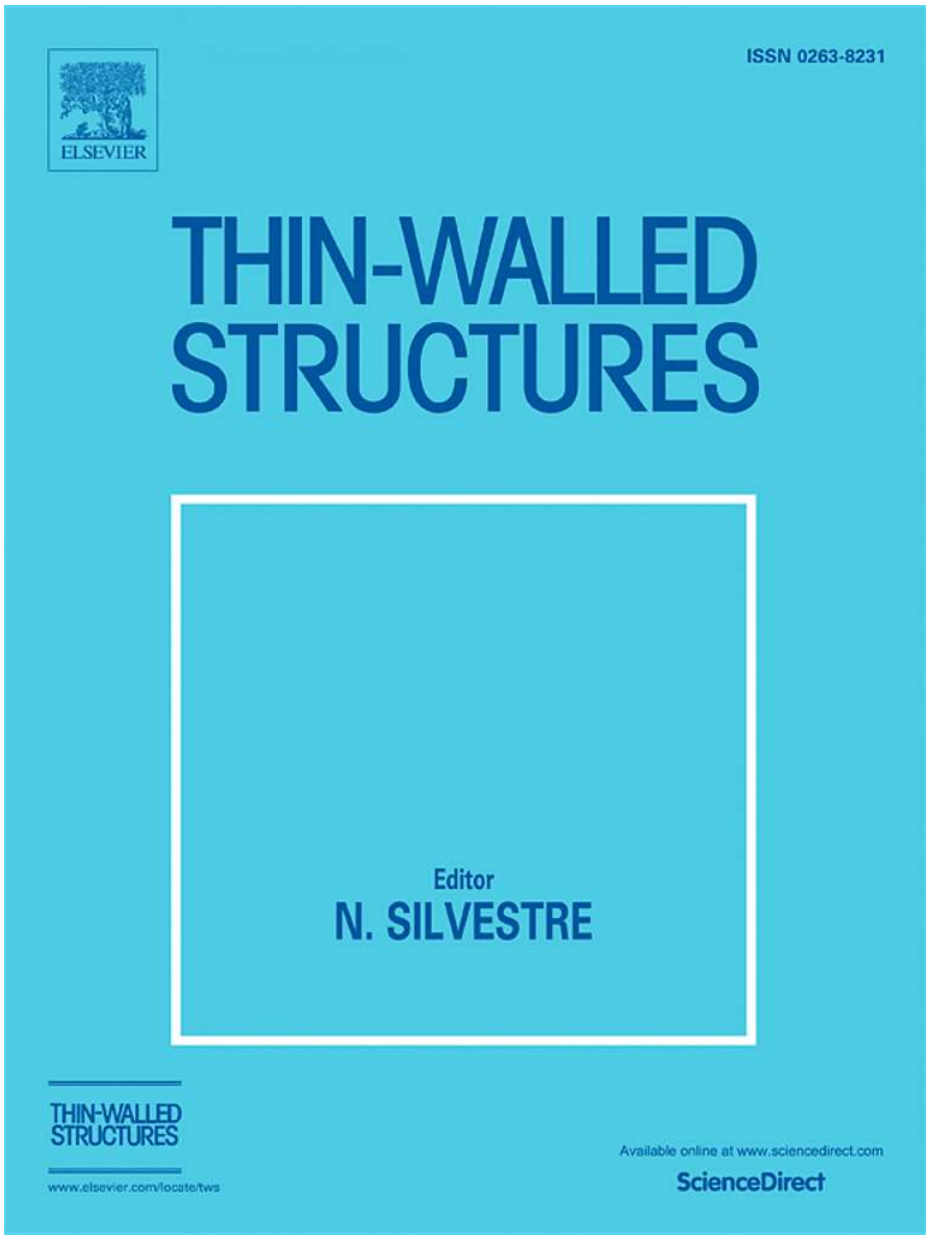

Modelling of steel frames using advanced beam and joint elements with interfaces governed by beam modes

Anders Bau Hansen[a,b], Jeppe Jönsson[a,*]

[a] *Technical University of Denmark, Department of Civil Engineering, Brovej Building 118, DK-2800 Kgs. Lyngby, Denmark*
[b] *NIRAS A/S, Sortemosevej 19, DK-3450 Allerød, Denmark*

Abstract

For decades, engineers have assessed and analysed steel frames using simple joints between beams and columns. These joints are often based on oversimplified assumptions using hinges or a direct transfer of beam displacements without any relative displacements. More seldom is the use of spring models that allow relative beam and column displacements at the joints. This despite the standardised component method approach, which can be used to determine the rotational spring stiffness of the relative rotation in a joint. This paper gives a background overview of essential developments in joint modelling and generalised thin-walled beam modelling, including torsional, distortional and related warping effects. For particular situations, some recent proposals for joint models can be applied to joints between thin-walled beams. On this basis, this paper presents a novel idea and a generic methodology that allows the interface between an extended number of generalised beam displacement modes and joints that are modelled using shell elements. The main novelty is the idea to transform from standard degrees of freedom of the interface into a reduced number of beam displacement mode related degrees of freedom. Thus, the number of degrees of freedom of the joint can be reduced to the corresponding total sum of beam modes that have been chosen for the modelling of each of the connected beam elements. The total number of degrees of freedom used for modelling the complete framework will depend on the selected number of modes in each beam element and on the number of extra internal modes chosen in the joint models. For enhanced structural analysis with advanced beam elements and joints that allow relevant distortions and built-in refined connection components, it is believed that this methodology will enable the full detailed analysis of large steel frameworks with a reasonable number of degrees of freedom.

Keywords: Steel frames, beam theories, joint analysis, mode-based formulation

1. Introduction

Steel frameworks have been used for decades in a broad range of engineering fields; maritime, aerospace, offshore, civil and mechanical engineering. In the construction industry, steel is commonly used in larger frame and truss structures such as sports arenas, power plants, cranes, high rise buildings and bridges. This paper focus on the analysis of steel frameworks using advanced generalised thin-walled beams with an expanded number of displacement modes and the interface to shell joint models. Thus, achieving a more detailed assessment of the steel framework with a much-improved beam and joint modelling. In fact, this paper presents the general idea of a novel generic methodology to model joints interfacing between beams and columns. The proposed methodology extends the usability of mode-based beam elements to model frames.

The daily practice in the design of structural steel frameworks is to use the simplified approach of assuming the joints to be either ideally pinned or fully rigid. This practice happens despite that design codes, such as Eurocode 3 [1], allows engineers to consider a semi-rigid behaviour of steel joints through the 'Component Method' and also despite that studies have indicated savings in the range of $7\,\% - 26\,\%$ considering semi-rigid behaviours [2, 3, 4]. The simplified approach is often chosen to keep the analysis as simple as possible even though connections seldom fulfil such behaviours [5]. Usually a joint should be categorised as semi-rigid, reflecting a behaviour where relative rotations occur when transmitting bending moments between adjacent members. Furthermore, considering such a simplified approach, valuable knowledge regarding joint behaviour is lost. Especially in thin-walled structures in which effects such as warping becomes an essential issue [6].

Consequently, the structural designer is left with the choice to perform quite costly experimental investigations or numerical investigations by consulting sophisticated finite element computer software, which requires a time-consuming process of data input and result interpretation. Furthermore, such finite element assessment is prohibited for routine applications in frame analysis. Thus,

*Corresponding author
Email address: jej@byg.dtu.dk (Jeppe Jönsson)

dedicated methods for frame analysis with enhanced thin-walled beam modelling and enhanced joint modelling are in demand. It has been shown in [7] that advanced analysis of thin-walled beam members can be achieved with a reduced number of degrees of freedom by considering a displacement-based mode formulation where judiciously chosen deformation modes are selected and thereby only 25 % of the degrees of freedom are needed compared to commercial finite element software using shell elements. However, by using only one advanced thin-walled beam element between joints in linear analysis, this reduction is believed to be even higher depending on the number of beam modes taken into account.

The following subsections give a background overview of some of the crucial developments in joint modelling and generalised thin-walled beam modelling.

1.1. Semi-rigid connections

The very first reported investigations on the rigidity of joints in steel structures was assessed by Wilson & Moore in 1917 [8] regarding experiments on riveted connections. Later, around the mid-1930s, a more general elaboration on the rigidity of joints was given considering the relationship between the moment and rotation occurring at the joint as well as the overall influence on the global structure, see e.g. [9]. Modifications have been implemented in theories, such as rotational springs between beam-ends to reflect the joint stiffness [10]. In such cases, the joint is represented by a finite stiffness, and improved structural response is achieved. However, the task of establishing an adequate spring stiffness is difficult. In a review given by Diaz et al. [11] referring 180 papers a broad range of models and procedures are given on how to implement and take advantage of the semi-rigid joint design. It is concluded that the most accurate prediction is through experiments yielding a true non-linear behaviour between moment and rotation as shown in Figure 1, which illustrates the idealised moment-rotation curves of different joint configurations. Furthermore, Diaz et al. states that one of the most used methods is the mechanical model also adopted in the Eurocode 3 [1, 12] namely the 'Component Method'.

The Component Method is an idealisation of a joint into a mechanical model including linear springs and rigid links. As an example of mechanical modelling see the simple beam-to-column connection in Figure 2. This connection is exposed to a bending moment M that will cause a relative rotation ϕ that will induce tension, compression and shear within the connection. Hence, the Component Method represents these effects through mechanical components. For this purpose, the joint is divided into components each represented by a spring stiffness. In the simplified case illustrated in Figure 2 these are: k_1 column web panel in shear, k_2 column web in transverse compression, and k_3 column web in transverse tension. The linear spring stiffness/behaviour of each component is derived depending on the geometrical joint configurations. This derivation is to a great extent based on empirical equations, e.g. [13]. The method is, however, limited to asses joints exposed to bending moments and not able to take shear and normal forces into account [1]. Recently, modifications have been presented by Bayo et al. [14, 15]. They use a 'joint element' to which beams and columns are attached. The stiffness of this joint element is then found using the same component stiffness's as in the Component Method, but with this method, eccentricities are incorporated right away while several iterations are avoided compared to the classic Component Method. Another variation in the Component Method is given by Silva et al. [16] presenting a bi-linear spring model to achieve more accurate results covering the plastification of the joint. A special spring model is developed and gives an idealised bi-linear behaviour of each component. Hence, each component may be represented by a linear elastic part followed by a linear plastic strain hardening zone (see Figure $2c_2$). A 'Generalized Component Method' was presented by Zhu et al. [17] adopting Silva's approach. Zhu and co-workers consider a tri-linear model to include both elastic, plastic and post yielding behaviours. See Figure $2c_3$.

1.2. Torsional effects in thin-walled beams

In the second half of the twentieth century, the interest in using thin-walled steel components increased heavily. This increase was highly due to its excellent stiffness-to-weight ratio and its strength-to-width ratio with the main purpose of lightening engineering structures by saving materials. Some of the pronounced pioneers with respect to thin-walled structures were Timoshenko [18, 19, 20], Flügge & Marguerre [21], Vlasov [22], and Kollbrunner & Hajdin [23]. They realised that non-negligible normal stresses were developed leading to warping deformations not included in the beam theories at that time. Therefore a demand for new theories was born. Accordingly, theories, such as Vlasov's 'Thin-Walled Elastic Beams', were implemented considering an extra seventh degree of freedom representing the warping effect based on torsion and the *sectorial coordinate* also introduced by Vlasov.

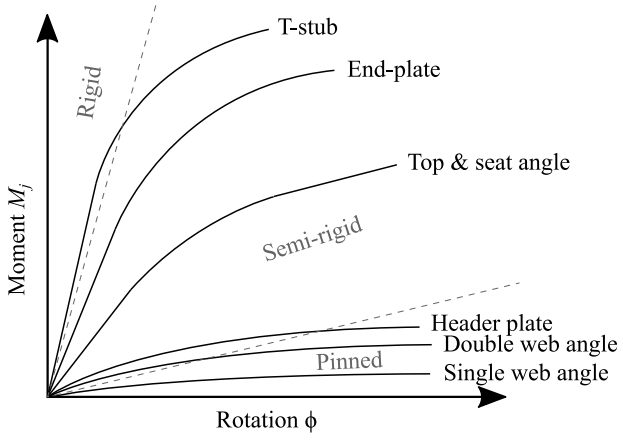

Figure 1: Idealised moment-rotation curves

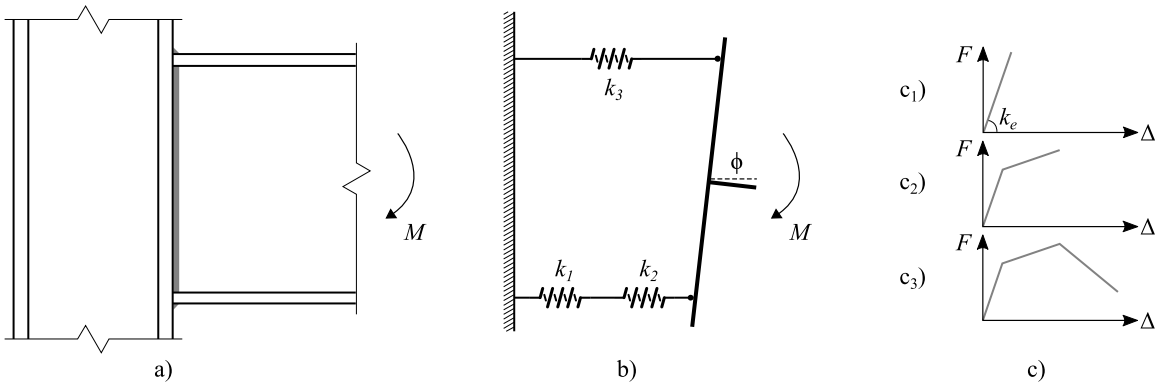

Figure 2: The Component Method: a) A welded beam-to-column connection consisting of two I-beams exposed to a bending moment M, b) idealisation of the connection (k_1, k_2, k_3 being spring stiffness's and ϕ the relative rotation), and c) spring behaviours of different approaches; c_1) the classic Component Method [1], c_2) proposed by Silva et al. [16] having a bi-linear behaviour, and c_3) used by Zhu et al. [17] with a tri-linear behaviour

Examples on approaches adopting the seventh degree of freedom are Krajcinovic [24] and Barsoum & Gallagher [25] who investigated stability and dynamics, and torsion and lateral stability of thin-walled beams, respectively. They introduced finite beam elements with the seventh degree of freedom reflecting Vlasov's theory. With the proposed finite beam elements it is possible to analyse frames more accurately by taking warping into account. However, depending on the joint configuration, the amount of warping being transmitted is restrained and a Vlasov beam element yield erroneous results due to inadequate warping restraint and transmission. Thus, with the recognition of warping's presence, the transmission of local warping, as well as rotation and warping from torsion occurring at beam-ends, became the main task to include when connecting non-aligned beams, for example at frame corners. However, a proposal to avoid this was given by Baigent & Hancock [26] connecting non-aligned open channel profiles with flat plates. More regular joint configurations were assessed by Vacharajittiphan & Trahair [27] investigating the warping restraint stiffness in non-aligned doubly symmetric I-sections in four different joint configurations being: unstiffened, partially stiffened with a single diagonal stiffener, box stiffened, and fully stiffened with three stiffening plates, see Figure $3a_1$ to $3d_1$. Similar investigations on warping transmission through joints were carried out by Morrell et al. [28] considering the relationship between end section torsional rotations in orthogonal plain open channel section members, or Sharman [29] and Krenk & Damkilde [30] who dealt with warping transmission of arbitrarily oriented members both assessing I-sections and open channel sections. Different joint configurations were assessed where the member webs were laying in the same plane. Lastly, Masarira [31] deduced coefficients approximating the joint effect on lateral torsional buckling load of steel frames based on a shell finite element analysis concluding that the warping effect profoundly influences the stability.

To this end, it seems that warping torsion is a significant effect and should be incorporated in the analysis of the structural response assessing open thin-walled members. However, methods taking this into account in frame analysis often fail. Yang & McGuire proposed a 'warping indicator' adjusting the restriction of warping at each beam-end [32] (a warping spring to characterise warping). Another approach was given by Tong et al. [33] presenting a warping transmission model for beam-to-column rigid joints with diagonal stiffeners. A third approach to be mentioned modelling joints in thin-walled frames have been given by Shayan & Rasmussen [34] introducing a 'joint element' in a beam finite element environment. Here, beam-ends are connected by the use of springs and linear constraint equations, which are derived beforehand based on a shell finite element discretisation and assessment of the joint element. Nevertheless, the mentioned approaches are all limited to seven degrees of freedom not considering detailed cross-section investigations able to include distortional effects.

1.3. Distortional effects in thin-walled beams

The cross-sections of thin-walled beams do not keep their shape during deformation – they distort. A small infinitesimal cut-out of a wall element has to be in equilibrium and to establish this equilibrium the cross-section deforms. Furthermore, instability effects will also induce local and distortional buckling. Thus, beams and columns with thin-walled cross-sections are prone to non-rigid in-plane deformations.

A well-known beam theory that handles this effect is the one Schardt introduced in 1966. Namely, the 'Generalised Beam Theory', (GBT). He introduced it in Germany as 'Verallgemeinerte Technische Biegetheorie' (VTB) assessing open thin-walled cross-sections, [35, 36]. Later, he modified it to include closed cross-sections as well. The theory is essentially based on a folded plate theory and the idea of expanding the displacements as a sum of displacement modes. To explain, this theory is a mode-based beam theory relying on orthogonal cross-section displacement fields with associated axial variations. All modes

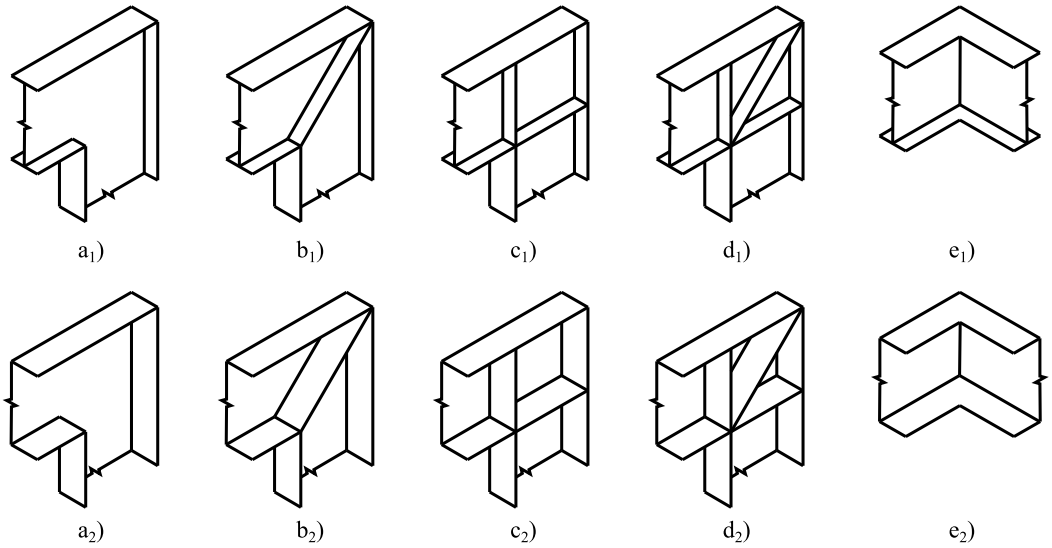

Figure 3: Frame corners with different stiffness configurations connecting two in-plane I-beams or two open channel sections, respectively. a) to d) having web continuity and a) unstiffened, b) diagonal stiffened, c) box stiffened, d) box and diagonal stiffened, whereas e) unstiffened with flange continuity

are linearly combined with varying intensities yielding the final deformation response. That is, a deformation is decomposed into a number of known displacement modes. Another proposal to a thin-walled beam theory taking distortion into account was given by Kollbrunner & Hajdin. They extended their thin-walled theory to include distortional in-plane deformations as well, even considering both open and closed cross-sections [37]. British investigators on cold-formed steel members adopted the Generalised Beam Theory and published several papers, [38, 39], leading to an internationalisation of the theory and whereby it became known by the acronym 'GBT'. Subsequently, GBT was extended to handle orthotropic materials such as fibre reinforced polymers (FRP) by Silvestre and Camotim [40, 41]. In the latest decades inclusion of non-linearities [42], plasticity [7], and a more general shear strain formulation [43, 44] have been incorporated, besides the already implemented first-order, buckling and post-buckling analysis as well as dynamic assessments. See also [45, 46].

Simultaneously with the development of GBT, the 'Finite Strip Method' (FSM) has been further developed. Based on the work of Wittrick [47] and Przemieniecki [48], Cheung [49] formulated the FSM as we know it today. The essentials of this theory are: the discretisation of the beam element into narrow strips running the entire beam length being rigidly joint together, the cross-sectional deformations being interpolated by polynomial functions assuming a Kirchhoff plate bending behaviour, and the axial variation found as sinusoidal functions. Among others, Hancock used this theory to deduce buckling curves or so-called signature curves for thin-walled members, [50]. However, the main lack in this theory is the missing decomposition of deformations into known displacement modes. Accordingly, Ádány & Schafer introduced this to the FSM, [51, 52] leading to the theory named 'constrained FSM' (cFSM) enabling mode decomposition and identification, [53, 54]. Silvestre et al. [55] compare the derivations of the cross-sectional displacement fields in the GBT and FSM being on same mechanical properties. Furthermore, Ádány et al. [56] compares the results obtained using the two approaches concluding nearly similar results. However, GBT and cFSM differ in the determination of the axial variation functions. Where, GBT formulates finite beam elements with a variation between end cross-sections as interpolations by use of Hermite cubic standard finite beam element functions, the cFSM uses a geometrical approach having sinusoidal amplitude functions.

As a matter of fact, the displacement mode decomposition has been seen as an efficient tool by many. Hence, others who adopted the idea of separating the beam deformation responses into orthogonal displacement modes were, for example Jönsson [57] who deduces the extra warping and distortional mode for thin-walled beams, or Jönsson & Andreassen [58, 59, 60], and Vieira et al. [61, 62] who determined cross-sectional displacement fields based on a generalised eigenvalue problem. This also reveals the axial amplitude functions as polynomial and exponential functions without limiting the beam element to have a finite length, which for example is the case in GBT. Garcea et al. [63] deduce cross-sectional displacement fields as generalised eigenvectors (GE) as well. The obtained results are compared with the GBT nearly being coincidental.

A new development is also the 'constrained finite element method' (cFEM) by Ádány [64, 65, 66, 67], in which a special purpose finite element is formulated and constrained to adhere to certain displacement mode constraints. A common point of the theories mentioned above is the inclusion of cross-sectional distortion effects. Often the displacement modes are also ordered in local, distortional and global modes.

Although very detailed beam theories have been developed, it is difficult to use these for analysis of frame structures. The main reason is the lack of methods that satisfyingly allow an interface between connected members at a joint. The most successful proposals have been implemented in the framework of GBT by Basaglia et al. [68, 69, 70, 71, 72, 73, 74, 75]. The primary focus has been on joint configurations as illustrated in Figure 3. With their approach, they introduced a 'joint element' between non-aligned finite GBT beam elements. However, difficulties have been met due to the modal nature of GBT (being a GBT-method with non-standard nodal degrees of freedom for cross-sectional displacements), which was not able to be transferred to the joint element formulation. In their formulation, the joint element is represented by the seven generalised displacements known from the Vlasov theory allowing a warping transmission from non-uniform torsion. Additionally, a number of constraint equations have been added to fulfil displacement continuity between adjacent members (i.e. to include local and distortional effects). The constraint equations highly depend on the joint geometry. This method requires prior knowledge of the joint to establish the correct constraint prerequisites before performing a proper frame analysis.

2. Proposal of a new methodology

Although Basaglia and co-workers have presented procedures for assessing frames of thin-walled members including torsional and distortional effects, the methods are limited to specific types of cross-sections and joints. It is believed that a more generic and general methodology needs to be developed so that joints between advanced thin-walled beams can be established and modelled by use of more conventional finite element modelling, which can be performed by engineering offices.

2.1. The idea

In general, the idea is to model beam and column members using an advanced beam element formulation that is based on displacement modes, which includes warping and distortional deformations. On the other hand, the connections between advanced beam elements shall be modelled by use of more traditional finite elements, e.g. finite shell elements. Both the advanced beam elements and the joint elements are modelled such that all nodes within a discretised interface have six degrees of freedom each.

The mode-based formulation is performed by letting an advanced beam element be expressed by beam displacement modes instead of traditional nodal degrees of freedom. Each beam displacement mode is formulated as a combination of cross-sectional displacement fields, which contains transverse as well as warping displacements, and an amplitude function that describes the variation of the cross-sectional displacement field along the beam member. Hence, instead of standard finite element degrees of freedom at the interfaces between beam elements and joint elements the connected faces will be governed by the cross-sectional beam displacement fields that will be used as novel modal degrees of freedom. Accordingly, the connected faces at a joint element must likewise be transformed into this modal-based formulation, which is governed by the beam displacement modes. Furthermore and of utmost importance, with a modal formulation of the thin-walled beam elements, it is possible to reduce the number of modes to the most relevant, judiciously selected modes, and thereby reduce the number of modal degrees of freedom at the interfaces both regards to the beam member and the joint element. This reduction is done by transforming the conventional displacement degrees of freedom of the cross-section interface between a beam element and a joint element into the chosen modal displacements of the beam, and then use these modal displacements as the degrees of freedom at the interfaces. Hence, the nodal degrees of freedom at the connected faces are transformed into the chosen beam modal degrees of freedom. The unselected (irrelevant) modal degrees of freedom are assumed to be non-existing (zero). As a result, the frame behaviour is expressed in a displacement-based modal language yielding the opportunity of regulating the number of included modal degrees of freedom.

It is reasonable to assume that the same beam and joint configurations are represented several times within a frame structure. This may be utilised during the programming of the stiffness formulations and during back substitution of displacements, stresses and strains in members and joints.

To give the best possible grasp of the idea presented, a two-dimensional example will be referred to throughout the following subsections. For simplicity this illustrative example only includes in-plane degrees of freedom even though the presented idea is valid for a full three-dimensional analysis. The example includes three advanced beam elements and a single joint element, which for example could represent a beam-to-column connection in a larger frame structure as illustrated in Figure 4.

2.2. Beam elements

In-between connections, beam members and column members will be modelled using a beam element based on an advanced beam theory with torsional and distortional effects including the related cross-sectional warping deformations. To be able to describe the cross-sectional displacements, the cross-section is discretised into wall segments between nodes that have six displacement degrees of freedom each. Thus, the ends of a beam have several wall elements and several nodes, see also Figure 5. This results in an interface to which joints modelled using finite (shell) elements with conventional translational and rotational degrees of freedom at the nodes can be connected to. To derive the conventional linear elastic stiffness equation that governs the advanced beam element problem, a set of orthogonal cross-sectional displacement modes is used and

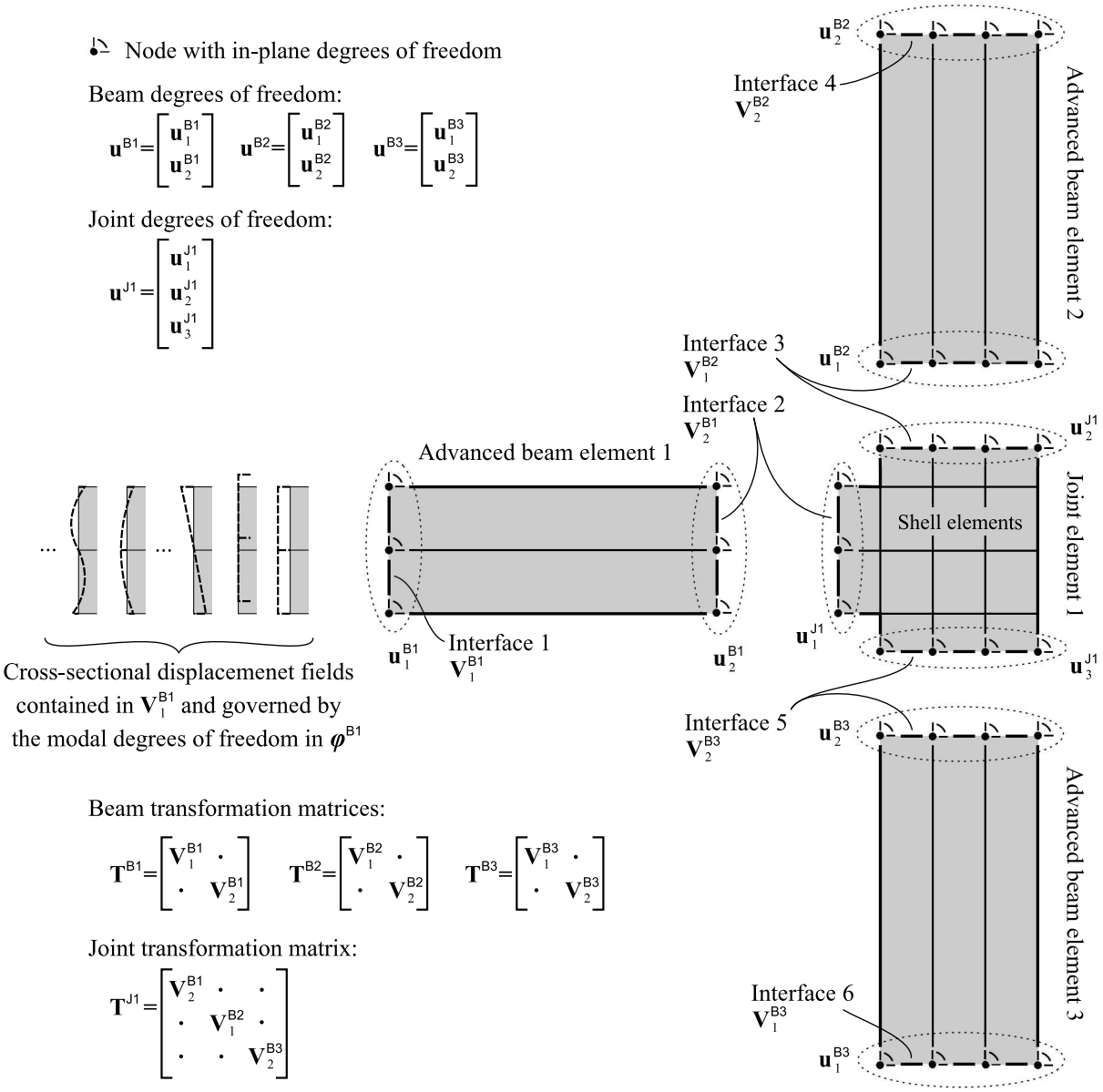

Figure 4: A two-dimensional example for illustration purpose

hence:

$$\mathbf{K}^{\mathsf{B}}\,\mathbf{u}^{\mathsf{B}} = \mathbf{f}^{\mathsf{B}} \quad \text{where } \mathbf{u}^{\mathsf{B}} = \begin{bmatrix} \mathbf{u}_1^{\mathsf{B}} \\ \mathbf{u}_2^{\mathsf{B}} \end{bmatrix} \tag{1}$$

in which $\mathbf{K}^{\mathsf{B}}$ is the beam element stiffness matrix, $\mathbf{f}^{\mathsf{B}}$ is a load vector, and $\mathbf{u}^{\mathsf{B}}$ is the displacement vector that contains $\mathbf{u}_1^{\mathsf{B}}$ and $\mathbf{u}_2^{\mathsf{B}}$ holding the standard nodal finite element degrees of freedom with regards to the two beam ends, respectively.

Thus, we achieve an accurate beam element governed by its degrees of freedom in all the nodes at the two end cross-sections. Furthermore, these degrees of freedom correspond to those in the joint element formulation sharing the same interface. Therefore, it is possible to assemble a beam element with a joint element having the same discretisation at the interfaces.

The beam cross-section analysis results in a set of beam solution modes containing orthogonal cross-sectional displacement fields, which we assemble as columns in the matrix $\mathbf{V}^{\mathsf{B}}$. In Figure 4 the cross-sectional displacement fields concerning the 'Advanced beam element 1' are shown on the left hand side of the beam end.

Using conventional finite element methods, it is possible to find a transformation between the three-dimensional beam modes and all the nodal degrees of freedom at the end cross-sections.

The degrees of freedom at each beam end cross-section ($\mathbf{u}_1^{\mathsf{B}}$ and $\mathbf{u}_2^{\mathsf{B}}$ according to Equation (1)) are transformed into orthogonal modal degrees of freedom with the following transformation:

$$\mathbf{u}_i^{\mathsf{B}} = \mathbf{V}_i^{\mathsf{B}}\,\boldsymbol{\varphi}_i^{\mathsf{B}} \quad \text{for } i = 1, 2 \tag{2}$$

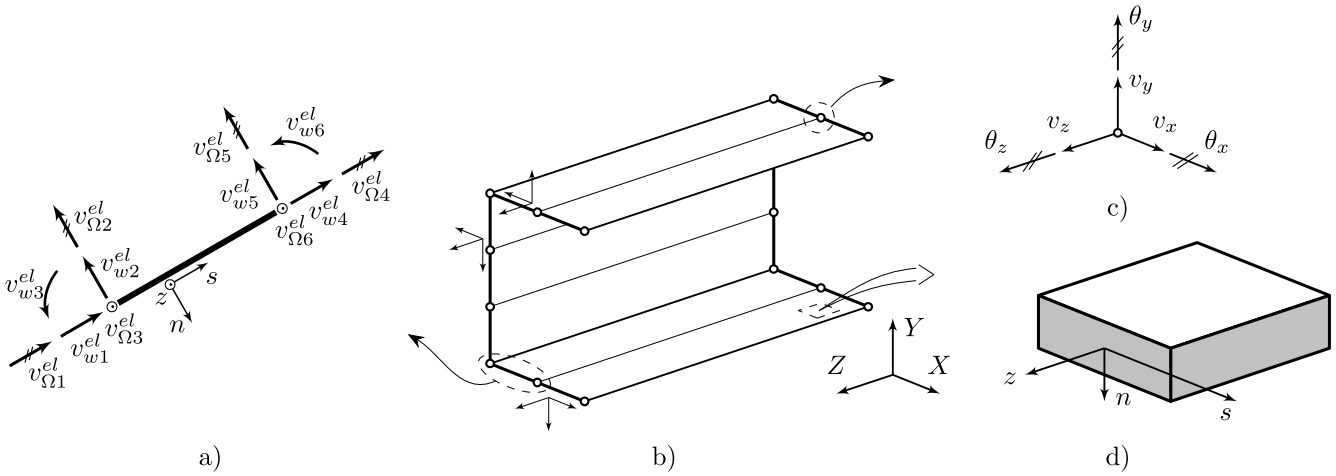

Figure 5: Beam element: a) Wall element and its local degrees of freedom, b) Beam element with discretised end cross-sections, c) Nodal degrees of freedom, and d) Wall cut-out with the local coordinate system

where the column vector $\boldsymbol{\varphi}_i^{\mathsf{B}}$ contains the modal degrees of freedom at the one end of the beam. In fact, these modal degrees of freedom correspond to intensities of the cross-sectional displacement fields given as the columns in $\mathbf{V}^{\mathsf{B}}$. Then, the entire transformation of a beam element can be performed using the transformation matrix $\mathbf{T}^{\mathsf{B}}$:

$$\mathbf{u}^{\mathsf{B}} = \mathbf{T}^{\mathsf{B}}\,\boldsymbol{\varphi}^{\mathsf{B}} \quad \text{with } \mathbf{T}^{\mathsf{B}} = \begin{bmatrix} \mathbf{V}_1^{\mathsf{B}} & \cdot \\ \cdot & \mathbf{V}_2^{\mathsf{B}} \end{bmatrix}, \quad \boldsymbol{\varphi}^{\mathsf{B}} = \begin{bmatrix} \boldsymbol{\varphi}_1^{\mathsf{B}} \\ \boldsymbol{\varphi}_2^{\mathsf{B}} \end{bmatrix} \tag{3}$$

where a single dot $[\,\cdot\,]$ represents a suitable zero-matrix. The matrices $\mathbf{V}_1^{\mathsf{B}}$ and $\mathbf{V}_2^{\mathsf{B}}$ contain the exact same modes and number of modes as we operate on a single beam element. The column vector $\boldsymbol{\varphi}^{\mathsf{B}}$ contains the beam modal degrees of freedom, which is separated into $\boldsymbol{\varphi}_1^{\mathsf{B}}$ and $\boldsymbol{\varphi}_2^{\mathsf{B}}$ representing each of the beam end cross-sections, respectively.

Now, using the transformations in Equation (3) and applying the laws of transformation on the equation system in Equation (1) we have:

$$\tilde{\mathbf{K}}^{\mathsf{B}}\,\boldsymbol{\varphi}^{\mathsf{B}} = \tilde{\mathbf{f}}^{\mathsf{B}} \tag{4}$$

where $\tilde{\mathbf{K}}^{\mathsf{B}}$ is the beam element modal stiffness matrix defines as:

$$\tilde{\mathbf{K}}^{\mathsf{B}} = {\mathbf{T}^{\mathsf{B}}}^{\mathsf{T}}\mathbf{K}^{\mathsf{B}}\,\mathbf{T}^{\mathsf{B}} \tag{5}$$

However, please note that, since solution modes formulate the beam element we may judiciously choose a relevant number of these modes in $\mathbf{V}^{\mathsf{B}}$ and perform a transformation of the end nodal degrees of freedom into a reduced number of modal degrees of freedom and hence, the equation system does not necessarily contain all modal degrees of freedom, but instead represents a reduced equation system.

2.3. Joint elements

The complexity met in connecting beam members and column members are accommodated by introducing a 'joint element'. This joint element is in itself an assembly of standard (shell) finite elements used to discretise the often complex plated joint geometry. The joint element is modelled so that the interfaces to the connected beams have the same nodes and nodal degrees of freedom. Hence, many 'joint element' geometries even including other types of special purpose finite elements can be incorporated in the joint model. Consequently, a single joint element allows a detailed assessment of displacements and stresses due to the finite element formulation, but the main drawback is the inclusion of a high number of degrees of freedom. The assembly of finite elements results in the following equation system:

$$\mathbf{K}^{\mathsf{J}}\,\mathbf{u}^{\mathsf{J}} = \mathbf{f}^{\mathsf{J}} \quad \text{where } \mathbf{u}^{\mathsf{J}} = \begin{bmatrix} \mathbf{u}_1^{\mathsf{J}} \\ \mathbf{u}_2^{\mathsf{J}} \\ \vdots \end{bmatrix} \tag{6}$$

Here, $\mathbf{K}^{\mathsf{J}}$ is the stiffness matrix, $\mathbf{f}^{\mathsf{J}}$ is the load vector, and $\mathbf{u}^{\mathsf{J}}$ is the displacement vector, which is grouped into displacement vectors that contain the displacement degrees of freedom at each of the connected faces indicated by the index. If any secondary degrees of freedom exist within the joint element these may be condensed.

Since it is the idea to let the joint element interfaces be governed by the displacement fields of the connected beam elements then the nodal degrees of freedom at these connected faces are transformed into modal degrees of freedom governed by the related beam transformations from Equation (2). Hence, the nodal degrees of freedom at an interface are transformed into modal degrees of freedom using:

$$\mathbf{u}_i^{\mathsf{J}} = \mathbf{V}_j^{\mathsf{B}}\,\boldsymbol{\varphi}_i^{\mathsf{J}} \quad \text{for } i = 1, 2, .., n_{\mathrm{I}} \tag{7}$$

where index i indicates an interface and n_{I} is the total number of connected faces for a single joint element. With respect to the example in Figure 4 this corresponds to $n_{\mathrm{I}} = 3$. In Equation (7), $\mathbf{V}_j^{\mathsf{B}}$ is the exact same matrix

used for the beam transformation in Equation (3) at the exact same interface and therefore index j is a reference to which of the beam ends that is located at the interface, being either $j = 1$ or $j = 2$. Since the interfaces at a joint element not necessary contain the same number of nodes, the matrices $\mathbf{V}_j^{\mathsf{B}}$ may not be of the same size. Accordingly for the entire joint element in Figure 4 the transformation matrix will be:

$$\mathbf{u}^{\mathsf{J}} = \mathbf{T}^{\mathsf{J}}\,\boldsymbol{\varphi}^{\mathsf{J}} \quad \text{with } \mathbf{T}^{\mathsf{J}} = \begin{bmatrix} \mathbf{V}_2^{\mathsf{B1}} & \cdot & \cdot \\ \cdot & \mathbf{V}_1^{\mathsf{B2}} & \cdot \\ \cdot & \cdot & \mathbf{V}_2^{\mathsf{B3}} \end{bmatrix} \tag{8}$$

Then, applying the transformations from Equation (8) to the equation system in Equation (6) the mode-based equation system for the joint element will be:

$$\tilde{\mathbf{K}}^{\mathsf{J}}\,\boldsymbol{\varphi}^{\mathsf{J}} = \tilde{\mathbf{f}}^{\mathsf{J}} \quad \text{where } \boldsymbol{\varphi}^{\mathsf{J}} = \begin{bmatrix} \boldsymbol{\varphi}_1^{\mathsf{J}} \\ \boldsymbol{\varphi}_2^{\mathsf{J}} \\ \boldsymbol{\varphi}_3^{\mathsf{J}} \end{bmatrix} \tag{9}$$

where $\tilde{\mathbf{K}}^{\mathsf{J}}$ is the joint element stiffness matrix transformed into modal space, $\boldsymbol{\varphi}^{\mathsf{J}}$ is the modal displacement degrees of freedom, and $\tilde{\mathbf{f}}^{\mathsf{J}}$ is the load vector in modal space. Explicitly we define the joint element stiffness matrix and the modal displacement degree of freedom vector as:

$$\tilde{\mathbf{K}}^{\mathsf{J}} = \mathbf{T}^{\mathsf{J}^{\mathsf{T}}}\mathbf{K}^{\mathsf{J}}\,\mathbf{T}^{\mathsf{J}} \quad \text{and} \quad \tilde{\mathbf{f}}^{\mathsf{J}} = \mathbf{T}^{\mathsf{J}^{\mathsf{T}}}\mathbf{f}^{\mathsf{J}} \tag{10}$$

Note that the degrees of freedom at the interfaces are transformed into modal beam type displacements of the individually connected beam and thus, a judiciously chosen reduction in the number of degrees of freedom in the joint interfaces can be performed.

2.4. Mode-based formulation

Thus as mentioned, to increase efficiency, this methodology allows us to utilise the modal formulation of the beam elements to decreases the number of degrees of freedom. This is achieved by transforming the beam degrees of freedom in the interface section into a mode-based degree of freedom space, i.e. a mode space containing a few numbers of relevant and unique cross-section displacement fields. The joint elements are likewise transformed into a displacement-based mode formulation. Here, the nodal degrees of freedom at the interfaces are transformed into few beam modal degrees of freedom and the remaining internal degrees of freedom can be eliminated for example by condensation. This allows a mode-based assembly of the structural framework by assembly of the different element contributions from Equation (4) and (9). Hence, we end up with an equation system for the entire frame structure being in a modal format:

$$\tilde{\mathbf{K}}^{\mathsf{sys}}\,\boldsymbol{\varphi}^{\mathsf{sys}} = \tilde{\mathbf{f}}^{\mathsf{sys}} \tag{11}$$

This is achieved by using conventional assembly and transformation procedures as in the finite element method (see for example Cook et al. [76]).

3. Illustration of key aspects

The purpose of this section is to illustrate and highlight some of the key aspects of the idea. To do so, we examine a rectangular portal frame corner connecting two thin-walled lipped channel sections by a diagonally stiffened joint element. Furthermore, to ease the implementation, there are two minor joint elements incorporated at the beam and column ends, respectively. These are implemented as a continuation of the beam/column element to simplify the application of load and boundary conditions. The general configurations and dimensions concerning this example are illustrated in Figure 6. The modulus of elasticity used is given as: $E = 210$ GPa and the Poisson ratio is: $\nu = 0.3$. The boundary conditions are as follows: at point A and C the mid point of the web is restrained against any translation, and at point B the translation out of the frame-plane is restrained. Moreover, the cross-section in A is loaded by a vertical unit displacement δ applied at the upper flange on top of the lip. The portal frame corner is assessed by a first-order linear elastic analysis.

3.1. The beam element

The advanced beam theory used to model the beam and column members is an advanced theory, which includes cross-sectional deformations and allows for a mode-based formulation, resently developed by the authors [77, 78]. This theory is based on the small displacement hypothesis as well as a linear elastic analysis of the beam cross-section. Using this theory, the cross-section is discretised by wall elements as illustrated in Figure 5 having six degrees of freedom at cross-section nodes. This new thin-walled beam theory embraces a shear variation through a

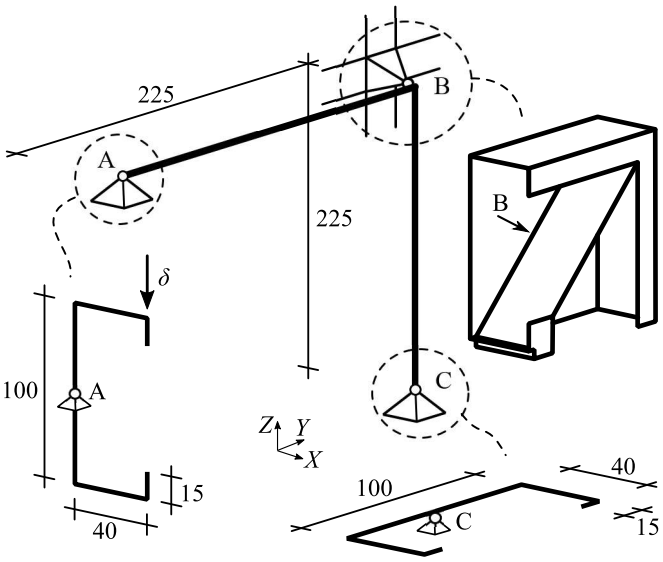

Figure 6: Frame set-up with load and support conditions. Dimensions in millimetre [mm] and the plate thickness is equal to 3 mm

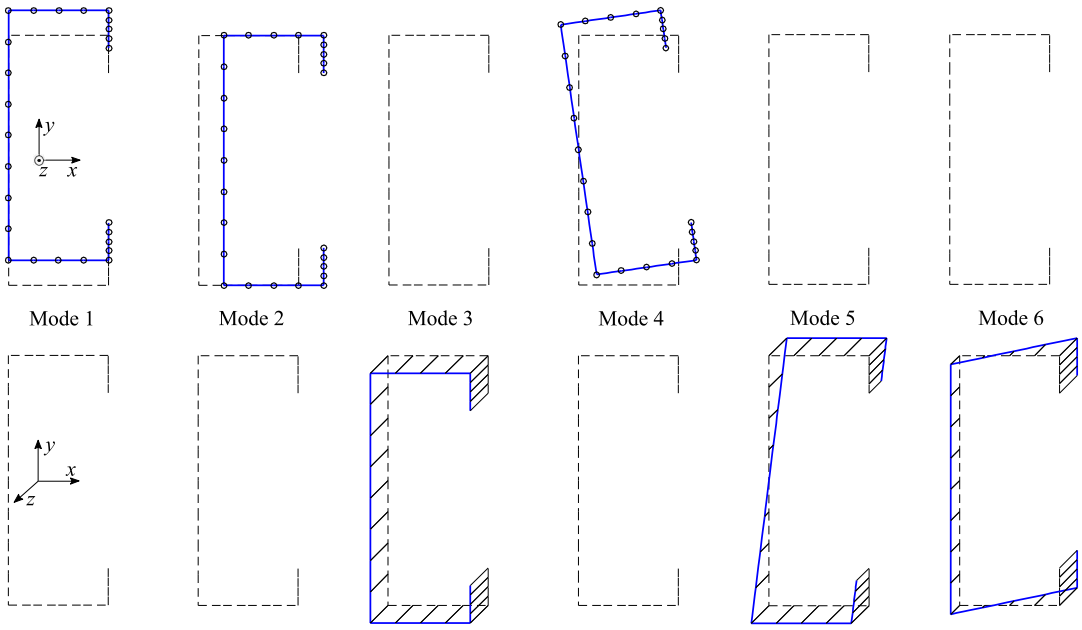

Figure 7: Interface modes 1–6 (the six rigid displacement fields). The upper row illustrates the translational part of the modes whereas the lower row represents the corresponding out-of-plane displacements (plotted in a local beam coordinate system)

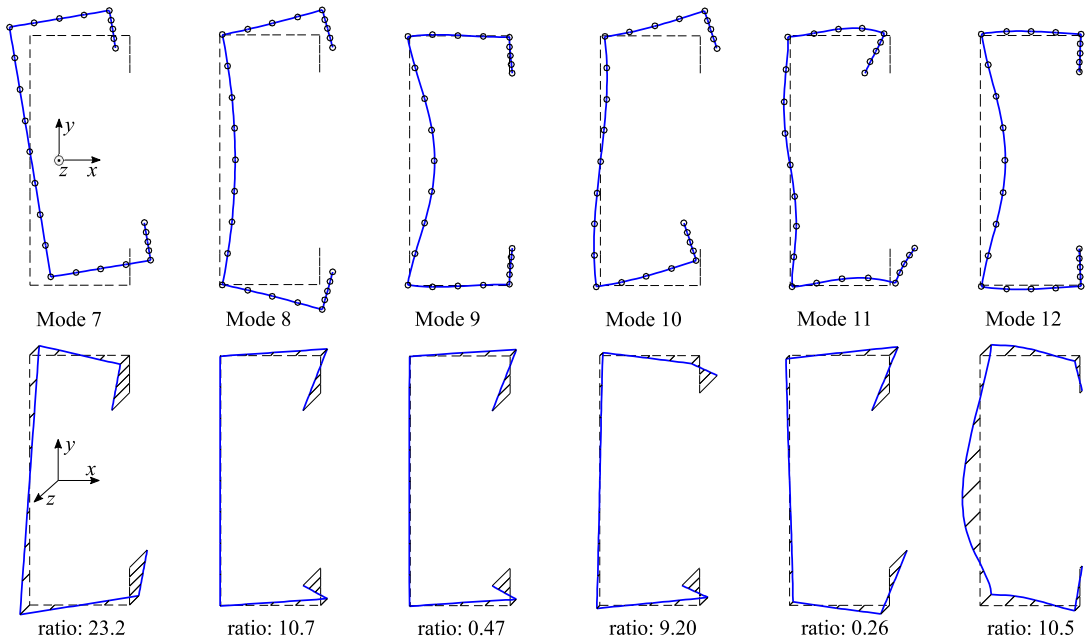

Figure 8: Interface modes 7–12 (first six distortional modes). The upper row illustrates the translational part of the modes whereas the lower row represents the corresponding out-of-plane displacements (plotted in a local beam coordinate system). The 'ratio' indicates the scaling between the largest in-plane displacement and the largest out-of-plane displacement

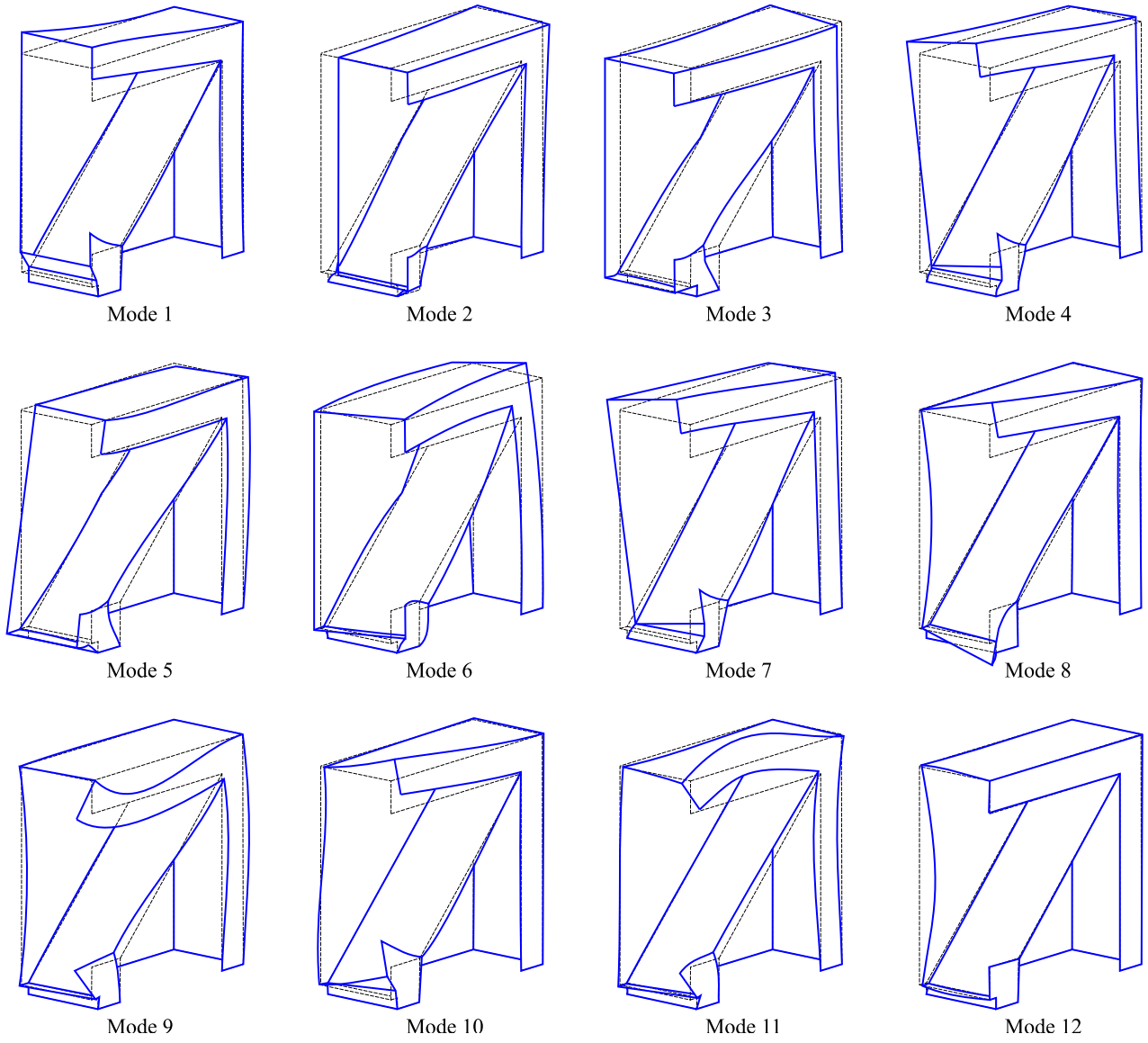

Figure 9: Joint deformation modes related to the first twelve modal degrees of freedom at the beam-to-joint interface

Timoshenko like beam behaviour and a Mindlin-Reissner like wall plate behaviour. Such a formulation is hardly found in other advanced beam theories despite the approach given by Miranda et al. [44, 79] who formulated a beam element in the framework of GBT, which probably also could have been used here.

The cross-section analysis results in a set of beam displacement modes that can be subdivided into cross-sectional displacement fields and their associated axial amplitude functions, which describes the axial variation of the cross-sectional displacement field along the beam axis. These amplitude functions are either polynomials of maximum third-order (reflecting the twelve fundamental beam modes) or having exponential functions with varying decay (reflecting beam displacement modes of higher order). Each higher order mode has an exponential amplitude that decays away from one of the beam ends. This decay is controlled by a length scale parameter. The lower the length scale parameter, the longer the decay is. It is common practise to sort the modes based on their length scale since this often also reflect their influence.

In this example the cross-section is discretised into twenty-four wall elements; eight in the web panel and four in each of the other panels. This corresponds to 150 degrees of freedom, and in our case, this results in 150 unique interface modes (cross-sectional displacement fields) to be used for transforming both the beam and the column elements as well as the joint elements into the mode-based formulation. In fact, the transformation matrices $\mathbf{V}^{\mathsf{B}}$ in Equation (2) and (7) contains 150 columns representing the interface modes. These interface modes are deduced in the beam element cross-section analysis and are sorted with regards to decay length (this being related to the axial variation of the beam modes). To exemplify, the first

twelve interface modes are illustrated in Figure 7 and 8. In fact, Figure 7 shows the six rigid cross-sectional interface modes and Figure 8 shows the next six modes, which are the first six distortional cross-sectional interface modes.

3.2. The joint element

The joint elements are discretised by use of triangular shell finite elements having six degrees of freedom at each node, see for example Cook et al. [76]. To be able to assemble beam and column members to a joint element, the joint element mesh is chosen in such a way that the nodes at the interfaces are in the exact same locations as the nodes of the adjacent beam and column cross-sections.

Based on the interface modes that are deduced during the beam element analysis and contained in $\mathbf{V}^{\mathsf{B}}$, each joint element is transformed into the mode-based formulation using the transformation in Equation (7). Hence, the displacement of a joint element may now be expressed in terms of modal degrees of freedom instead of conventional nodal degrees of freedom. To give a visual understanding of this modal degree of freedom formulation Figure 9 illustrates the effect of activating a single modal degree of freedom at a time. This has been done for the first twelve modal degrees of freedom at the beam-to-joint interface. Explicitly we have for Mode 1: $\boldsymbol{\varphi}^{\mathsf{J}} = [1, 0, 0, \cdots]^{\mathsf{T}}$, for Mode 2: $\boldsymbol{\varphi}^{\mathsf{J}} = [0, 1, 0, 0, \cdots]^{\mathsf{T}}$ and so on for the remaining ten modes illustrated. In fact, the twelve modal degrees of freedom that are activated in Figure 9 corresponds to the twelve interface modes shown in Figure 7 and 8.

3.3. Assessment

After the portal frame corner has been analysed by solving Equation (11) and according to the conditions given in Figure 6, we draw the deformed shape in Figure 10. To be observed is the ability to include the distortional deformations of the beam element due to the advanced beam element formulation. Furthermore, it is seen how the joint configuration is able to transmit both torsional and distortional deformation from the beam through the joint and into the column.

The frame corner has also been analysed using the commercial finite element program `Abaqus` [80]. Here, triangular finite shell elements (S3 in `Abaqus` nomenclature) with a maximum side length of 10 mm has been used to discretise the entire model. A brief comparison is given next.

The horizontal displacement at the upper left corner in cross-section A has been compared to the finite element model and a relative deviation of $-2.89\,\%$ is found. At the same corner, Von Mises stresses are compared and shows a relative deviation of $-0.22\,\%$. Furthermore, the entire Von Mises stress distribution of both models are shown in Figure 11. A close-up of the corner is shown in Figure 12. The colours represent the surface stress at the mid-point of each element(Note that the two colour scales are not identical within the scale from 0 to 80MPa).

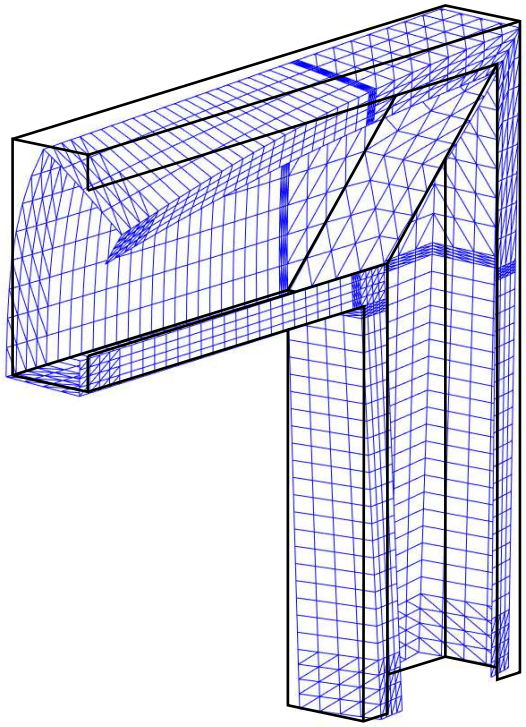

Figure 10: Full deformation pattern of the frame structure (the deformation is scaled 30 times)

3.4. Displacement mode identification

The main idea of this methodology is to identify those displacement modes that have an important influence on the structure and to reduce the number of included modes within the analysis. The joint element that connects the beam and the column is assessed in order to identify which modes that are activated at its interfaces. This assessment is shown in Figure 13. In Figure 13a the deformation of the joint element is drawn based on the present methodology. Furthermore, the deformations of the interfaces are shown as well. For comparison Figure 13b shows the deformation of the corner from the `Abaqus` analysis. The intensities of the modal degrees of freedom at the two interfaces are determined directly as $\boldsymbol{\varphi}^{\mathsf{sys}}$ when solving the frame equation in Equation (11). These intensities are also illustrated in Figure 13c and 13d. Besides the deformation patterns, it should be observed that the activated interface modes are limited to the first number of modes. The primary modes are 1, 2, 4, 7, and 8; and 1, 2, 4, 7 and 8 for the beam-to-joint interface and the column-to-joint interface, respectively. Common to these modes is that they are either part of the polynomial modes or belong to the distortional modes that have a long decay length. This illustrates that a reduced set of modes related to the longer length scales of the modes of the connected beam elements may be chosen and that the influence of the modes having a short length scale may be neglected. This is one of the essential reasons for formulating this theory with a mode-based interface approach. This has been tested at the frame corner by performing an analysis including the

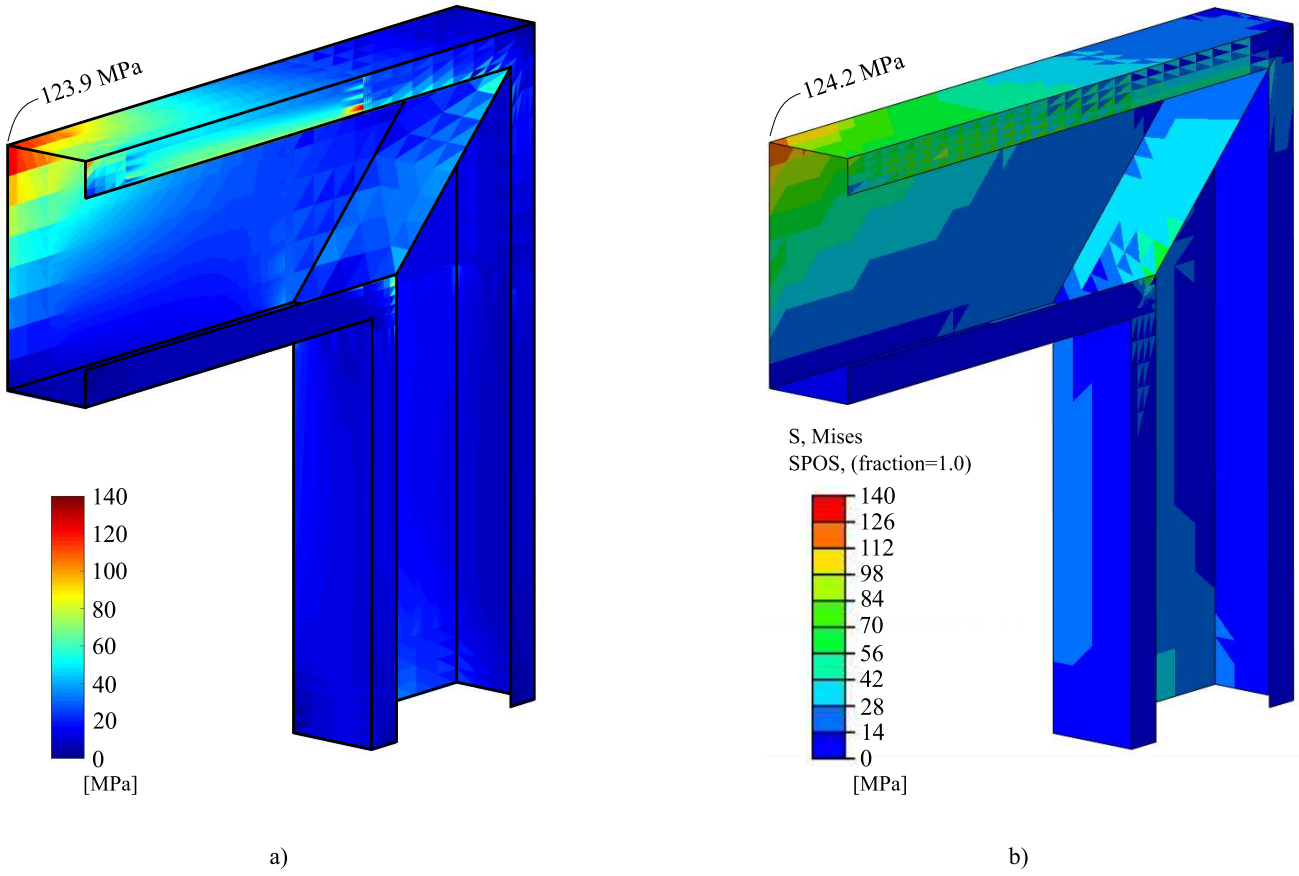

Figure 11: Three-dimensional illustration of the Von Mises surface stress in the frame. a) Present method; b) `Abaqus` model

first twenty modes at each interface only. If we then compare the displacements and Von Mises stresses at the upper left corner in cross-section A to the results obtained with the same methodology but with all 150 interface modes we get a relative deviation of $-2.1\,\%$ for the displacements and $0.65\,\%$ for the stresses.

4. Discussion

The motivation for this paper originates in several studies reporting that savings can be obtained by applying proper semi-rigid joint modelling. One of the popular methods is the mechanical one, namely the Component Method, which is adopted in the Eurocode 3 as well [1]. However, only global deformations are considered, and the method is limited to the transmission of bending moments. Other approaches exist, however, these are limited to the transmission of the seven generalised displacements of Vlasov beams. As a consequence, no cross-sectional distortion effects are taken into account at joints between non-aligned members despite the increasing amount of advanced beam theories, such as GBT and cFSM. These beam theories include this cross-sectional distortion effects, but the proper methodology to assemble these for global frame analysis with a reduced distortional and local mode space is lacking.

It is believed that the idea being presented in this paper enriches the analysis of connected non-aligned thin-walled beam members with a totally new mode-based interface approach that gives an in-depth insight into the mechanics of beam and joint behaviour. This new methodology may be used for optimising the joint design or may lead to better utilisation of materials within the entire frame structure. The methodology is mainly based on the use of beam-end displacement modes, formulated by standard nodal displacement parameters. The beam element used in this paper is based on an advanced beam theory developed by the authors [77, 78]. The formulation allows a displacement-based mode decomposition. Concerning the joint element, it is discretised by (shell) finite elements and therefore able to adopt complex geometries, for example including plate stiffeners. The technique presented has some similarity with that reported by Wu & Mohareb [81] and Sahraei & Mohareb [82], which models frame joints using shell elements and the structural members by conventional finite element beam elements. However, unlike the work in [81, 82], the present study captures distortional modes.

The beam and joint elements are transformed from a

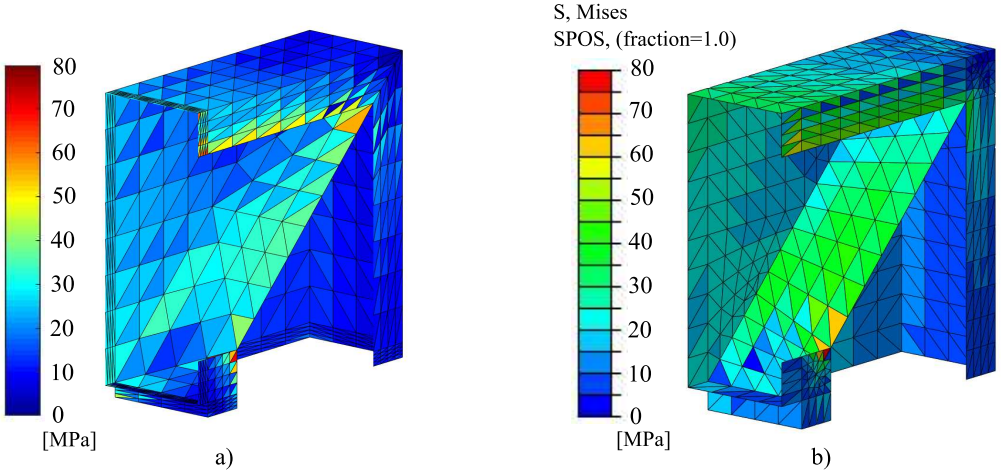

Figure 12: Three-dimensional illustration of the Von Mises surface stress in the frame corner. a) present method; b) `Abaqus` model

standard degree of freedom space into a formulation governed by a few selected interface modes, which relates to the cross-section interface between beam elements and a joint. Hence, instead of having standard nodal degrees of freedom, a set of beam-end cross-sectional displacement fields are used as modal degrees of freedom. Such a mode could, for example, be a rigid translation of the cross-section or a distortional deformation (see Figure 7 and 8).

Due to the use of an advanced beam theory as well as a detailed (shell) finite element discretisation of the joints, frame analysis can include very sophisticated deformation patterns. Comparing to the proposals based on Vlasov elements together with more overall joint formulations, such as the procedure presented by Shayan & Rasmussen [34], shows that these approaches only include the warping effects and not the in-plane distortional effects.

Comparing this novel approach to full finite element analysis using shell elements, the amount of degrees of freedom required is orders of magnitude less, which results in much faster execution times for linear analysis with only a minor risk of decreasing accuracy. Moreover, the illustrative example indicates a reasonable agreement of the obtained displacements as well as Von Mises stresses when comparing the present approach to a commercial finite element model.

The presented methodology is more general than the approach given by Basaglia et al. within the framework of GBT [69, 70]. Both methods are based on a mode-based displacement formulation using advanced beam elements that includes higher order effects. However, the GBT approach includes advanced beam elements, but the joint element formulation supports only the seven generalised displacements. Furthermore, in-depth prior knowledge of the joint mechanics is needed to establish constraint equations to ensure compatibility if including higher order displacement modes. In contrast, the joint element presented here includes the mechanical properties as well as being compatible at connected faces without prior assessment or constraint equations. In fact, due to the general formulation of the joint, it is believed that most displacement-based beam theories can adopt the presented methodology. The only requirement present is the need of a set of cross-sectional displacement fields to be used for transforming the standard degrees of freedom at the cross-section interfaces into the chosen mode-based interface governed degree of freedom space. In this paper, the new methodology is illustrated by a single example that highlights some of the key aspects of this novel idea. The example clearly illustrates that only a limited number of interface modes are activated. Therefore, a reduction of degrees of freedom modes is a possibility (this, however, will vary depending on the corner and frame geometry).

Despite that this simple example does not include any connection components, such as bolts, it is known that such components can be implemented as springs or other elements as a part of the joint formulation. The stiffness of such components could perhaps also be adopted from the Component Method. Other possibilities and improvements that can be considered is the introduction of a bi- or multi-linear behaviour. In other words, the approach could be extended to have a set of rigid plastic displacement modes. This feature is essential because the regions near a connection are highly exposed to plastic behaviour. This type of response is often simplified in frame analysis using spring stiffness's [83, 84]. Furthermore, research is needed to include both buckling and multi-linear elastic-plastic analysis in this mode-based formulation.

5. Acknowledgement

The first author gratefully acknowledges the financial support given to a scholarship by the Danish consultancy company NIRAS A/S and the Innovation Fund Denmark (grant 5189-00005B).

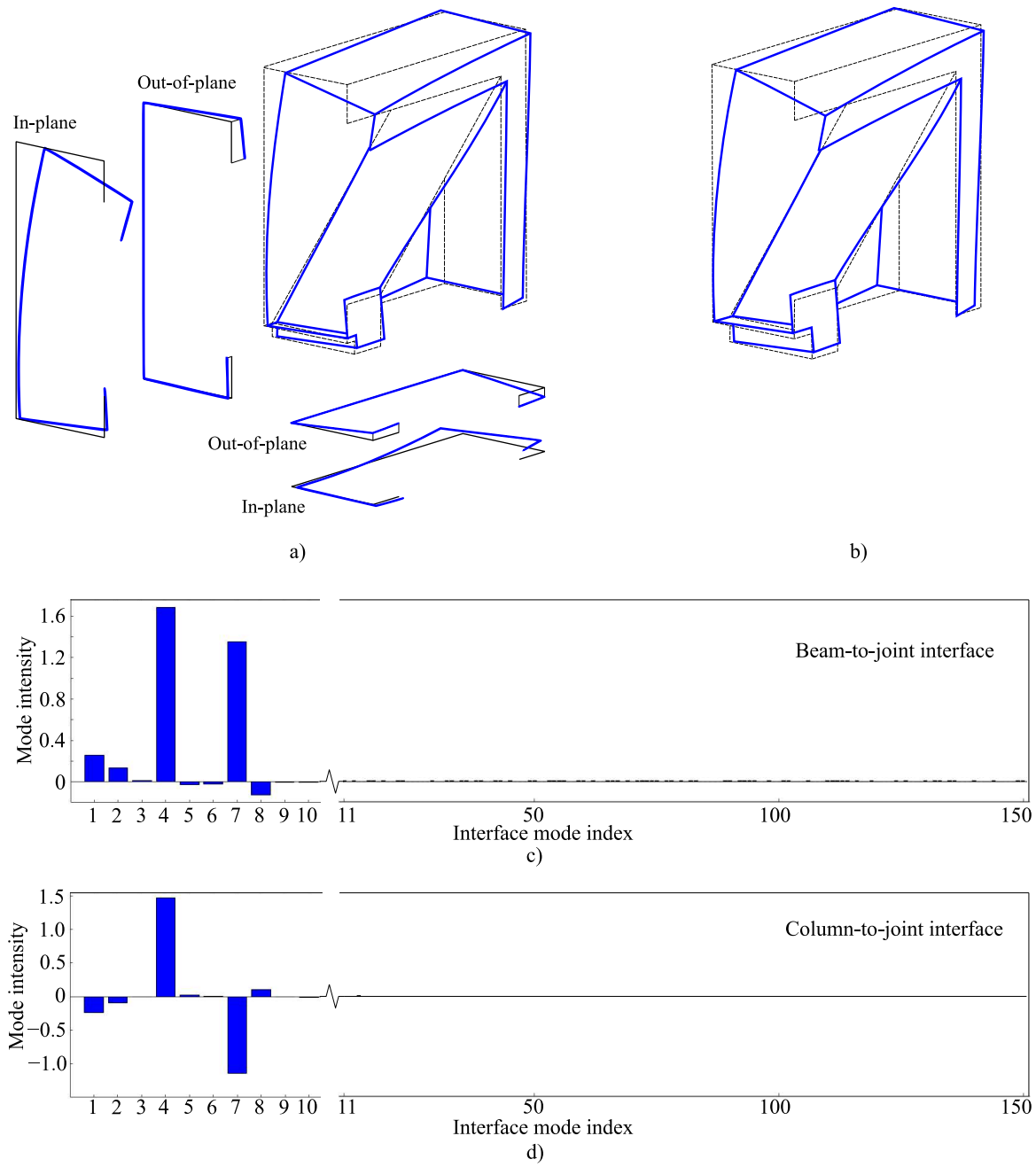

Figure 13: Deformation of the joint element: a) based on the present method, b) from `Abaqus` shell model, c) intensities of the beam-to-joint interface modes, d) intensities of the column-to-joint interface modes

References

[1] EN1993-1-8, Eurocode 3 - Design of steel structures. Part 1-8: Design of joints, 2nd Edition, CEN Brussels, 2007.

[2] S. W. Jones, P. A. Kirby, D. A. Nethercot, The analysis of frames with semi-rigid connections – a state-of-the-art report, Journal of Constructional Steel Research 3 (1983) 2–13. doi:10.1016/0143-974X(83)90017-2.

[3] K. C. Sarma, H. Adeli, Cost optimization of steel structures, Engineering Optimization 32 (2000) 777–802. doi:10.1080/03052150008941321.

[4] C. Díaz, M. Victoria, O. M. Querin, P. Martí, Optimum design of semi-rigid connections using metamodels, Journal of Constructional Steel Research 78 (2012) 97–106. doi:10.1016/j.jcsr.2012.06.013.

[5] R. Cunningham, Some aspects of semi-rigid connections in structural steelwork, Structural Engineer London (1990) 85–92.

[6] C. Bernuzzi, A. Pieri, V. Squadrito, Warping influence on the static design of unbraced steel storage pallet racks, Thin-Walled Structures 79 (2014) 71–82. doi:10.1016/j.tws.2014.01.024.

[7] M. Abambres, D. Camotim, N. Silvestre, K. J. R. Rasmussen, GBT-based structural analysis of elastic-plastic thin-walled members, Computers and Structures 136 (2014) 1–23. doi:10.1016/j.compstruc.2014.01.001.

[8] W. M. Wilson, H. F. Moore, Tests to determine the rigidity of riveted joints of steel structures, Bulletin of the University of Illinois Engineering Experiment Station 104 (1917) 55pp.

[9] Steel Structures Research Committee, Final report of the steel structures research committee, Nature 139 (1937) 5–6. doi:10.1038/139005a0.

[10] P. Zoetemeijer, Summary of the research on bolted beam-to-column connections, Tech. rep., TU-Delft, report 25-6-90-2 (1990).

[11] C. Díaz, P. Martí, M. Victoria, O. M. Querin, Review on the modelling of joint behaviour in steel frames, Journal of Constructional Steel Research 67 (2011) 741–758. doi:10.1016/j.jcsr.2010.12.014.

[12] K. Weynand, J. P. Jaspart, M. Steenhuis, The stiffness model of revised Annex J of Eurocode 3, in: R Bjorhovde and A Colson and R Zandonini (Eds.), Connections in Steel Structures III. Procedings of the 3rd Int. Workshop on Connections, Elsevier, Trento (1996) 441–452.

[13] J.-P. Jaspart, K. Weynand, Design of Joints in Steel and Composite Structures, ECCS – European Convention for Constructional Steelwork, 2016.

[14] E. Bayo, J. M. Cabrero, B. Gil, An effective component-based method to model semi-rigid connections for the global analysis of steel and composite structures, Engineering Structures 28 (2006) 97–108. doi:10.1016/j.engstruct.2005.08.001.

[15] E. Bayo, A. Loureiro, M. Lopez, L. S. da Silva, General component based cruciform finite elements to model 2d steel joints with beams of equal and different depths, Engineering Structures 152 (2017) 698–708. doi:10.1016/j.engstruct.2017.09.042.

[16] L. S. da Silva, A. G. Coelho, E. L. Neto, Equivalent post-buckling models for the flexural behaviour of steel connections, Computers and Structures 77 (2000) 615–624. doi:10.1016/S0045-7949(00)00015-8.

[17] C. Zhu, K. J. R. Rasmussen, S. Yan, Generalised component model for structural steel joints, Journal of Constructional Steel Research 153 (2019) 330–342. doi:10.1016/j.jcsr.2018.10.026.

[18] S. P. Timoshenko, Theory of bending, torsion and buckling of thin-walled members of open cross section, Journal of the Franklin Institute 239 (1945) 201–219, part I. doi:10.1016/0016-0032(45)90093-7.

[19] S. P. Timoshenko, Theory of bending, torsion and buckling of thin-walled members of open cross section, Journal of the Franklin Institute 239 (1945) 249–268, part II. doi:10.1016/0016-0032(45)90161-X.

[20] S. P. Timoshenko, Theory of bending, torsion and buckling of thin-walled members of open cross section, Journal of the Franklin Institute 239 (1945) 343–361, part III. doi:10.1016/0016-0032(45)90013-5.

[21] W. Flügge, K. Marguerre, Wölbkräfte in dünnwandingen profilstäben, Ingenieur-archiv 18 (1) (1950) 23–38, published by Springer-Verlag, (in German). doi:10.1007/BF00537588.

[22] V. Z. Vlasov, Thin-Walled Elastic Beams, 2nd Edition, Jerusalem, 1961, Israel program for scientific translations.

[23] C. F. Kollbrunner, N. Hajdin, Dünnwandige Stäbe · Band 1, Stäbe mit undeformierbaren Querschnitten, Springer-Verlag, 1972.

[24] D. Krajcinovic, A consistent discrete elements technique for thinwalled assemblages, International Journal of Solids and Structures 5 (1969) 639–662. doi:10.1016/0020-7683(69)90085-7.

[25] R. S. Barsoum, R. H. Gallagher, Finite element analysis of torsional and torsional-flexural stability problems, International Journal for Numerical Methods in Engineering 2 (1970) 335–352. doi:10.1002/nme.1620020304.

[26] A. H. Baigent, G. J. Hancock, Structural analysis of assemblages of thin-walled members, Engineering Structures 4 (1982) 207–216. doi:10.1016/0141-0296(82)90010-4.

[27] P. Vacharajittiphan, N. S. Trahair, Warping and distortion at I-section joints, Journal of the Structural Division (ASCE) (1974) 547–564.

[28] P. J. B. Morrel, J. R. Riddington, F. A. Ali, H. A. Hamid, Influence of joint detail on the flexural torsional interaction of thin-walled structures, Thin-Walled Structures 24 (1996) 97–111. doi:10.1016/0263-8231(95)00048-8.

[29] P. W. Sharman, Analysis of structures with thin-walled open sections, International Journal of Mechanical Sciences 27 (1985) 665–677. doi:10.1016/0020-7403(85)90048-7.

[30] S. Krenk, L. Damkilde, Warping of joints in i-beam assemblages, Journal of Engineering Mechanics (ASCE) 117 (1991) 2457–2474.

[31] A. Masarira, The effect of joints on the stability behaviour of steel frame beams, Journal of Constructonal Steel Research 58 (2002) 1375–1390. doi:10.1016/S0143-974X(02)00017-2.

[32] Y.-B. Yang, W. McGuire, A procedure for analysing space frames with partial warping restraint, International Journal for Numerical Methods in Engineering 20 (1984) 1377–1398. doi:10.1002/nme.1620200803.

[33] G. S. Tong, X. X. Yan, L. Zhang, Warping and bimoment transmission through diagonally stiffened beam-to-column joints, Journal of Constructional Steel Research 61 (2005) 749–763. doi:10.1016/j.jcsr.2004.12.002.

[34] S. Shayan, K. J. R. Rasmussen, A model for warping transmission through joints of steel frames, Thin-Walled Structures 82 (2014) 1–12. doi:10.1016/j.jtws.2014.03.017.

[35] R. Schardt, Eine erweiterung der technishen biegelehre für die berechnung biegestreifer prismatischer falfwerke, Der Stahlbau 35 (1966) 161–171.

[36] R. Schardt, Verallgemeinerte Technische Biegetheorie - Band 1, Lineare Theorie, 2nd Edition, Metrum-Verlag,Darmstadt, 1989.

[37] C. F. Kollbrunner, N. Hajdin, Dünnwandige Stäbe · Band 2, Stäbe mit deformierbaren Querschnitten, Nicht-elastisches Verhalten dünnwandiger Stäbe, Springer-Verlag, 1975.

[38] J. M. Davies, P. Leach, First-order generalised beam theory, Journal of Constructional Steel Research 31 (1994) 187–220. doi:10.1016/0143-974X(94)90010-8.

[39] J. M. Davies, P. Leach, D. Heinz, Second-order generalised beam theory, Journal of Constructional Steel Research 31 (1994) 221–241. doi:10.1016/0143-974X(94)90011-6.

[40] N. Silvestre, D. Camotim, First-order generalised beam theory for arbitrary orthotropic materials, Thin-Walled Structures 40 (2002) 755–789. doi:10.1016/S0263-8231(02)00025-3.

[41] N. Silvestre, D. Camotim, Second-order generalised beam theory for arbitrary orthotropic materials, Thin-Walled Structures 40 (2002) 791–820. doi:10.1016/S0263-8231(02)00026-5.

[42] N. Silvestre, D. Camotim, Nonlinear generalized beam theory for cold-formed steel members, International Journal of Structural Stability and Dynamics 3 (4) (2003) 461–490. doi:

10.1142/S0219455403001002.
[43] R. Gonçalves, M. Ritto-Corrêa, D. Camotim, A new approach to the calculation of cross-section deformation modes in the framework of generalized beam theory, Computational Mechanics 46 (2010) 759–781. doi:10.1007/s00466-010-0512-2.
[44] S. de Miranda, A. Gutiérrez, R. Miletta, F. Ubertini, A generalized beam theory with shear deformation, Thin-Walled Structures 67 (2013) 88–100. doi:10.1016/j.tws.2013.02.012.
[45] D. Camotim, C. Basaglia, N. Silvestre, GBT Buckling Analysis of Thin-Walled Steel Frames: A State-of-the-art Report, Thin-Walled Structures 48 (2010) 726–743. doi:10.1016/j.tws.2009.12.003.
[46] D. Camotim, C. Basaglia, Buckling Analysis of Thin-Walled Structures Using Generalized Beam Theory (GBT): A State-of-the-art Report, Steel Construction 6 (2013) 117–131. doi:10.1002/stco.201310021.
[47] W. H. Wittrick, General sinusoidal stiffness matrices for buckling and vibration analyses of thin flat-walled structures, International Journal of Mechanical Sciences 10 (1968) 949–966. doi:10.1016/0020-7403(68)90049-0.
[48] J. S. Przemieniecki, Finite element structural analysis of local instability, AIAA Journal (American Institute of Aeronautics and Astronautics Journal) 11 (1) (1973) 33–39. doi:10.2514/3.50433.
[49] Y. K. Cheung, Finite Strip Method in Structural Analysis, Pergamon Press, Oxford, New York, Toronto, Sydney, Paris, Frankfurt, 1976.
[50] G. J. Hancock, Distortional buckling of steel storage rack columns, Journal of Structural Engineering 111 (1985) 2770–2783. doi:10.1061/(ASCE)0733-9445(1985)111:12(2770).
[51] S. Ádány, B. W. Schafer, Buckling mode decomposition of single-branched open-section members via finite strip method: Derivation, Thin-Walled Structures 44 (2006) 563–584. doi:10.1016/j.tws.2006.03.013.
[52] S. Ádány, B. W. Schafer, Buckling mode decomposition of single-branched open-section members via finite strip method: Application and examples, Thin-Walled Structures 44 (2006) 585–600. doi:10.1016/j.tws.2006.03.014.
[53] S. Ádány, B. W. Schafer, A full modal decomposition of thin-walled, single-branched open cross-section members via the constrained finite strip method, Journal of Constructional Steel Research 64 (1) (2008) 12–29. doi:10.1016/j.jcsr.2007.04.004.
[54] Z. Li, J. C. B. Abreu, J. Leng, S. Ádány, B. W. Schafer, Review: Constrained finite strip method developments and applications in cold-formed steel design, Thin-Walled Structures 81 (2014) 2–18. doi:10.1016/j.tws.2013.09.004.
[55] N. Silvestre, D. Camotim, N. F. Silva, Generalized beam theory revisited: from kinematical assumptions to the deformation mode determination, International Journal of Structural Stability and Dynamics 11 (2011) 969–997. doi:10.1142/S0219455411004427.
[56] S. Ádány, N. Silvestre, B. W. Schafer, D. Camotim, GBT and cFSM: Two modal approaches to the buckling analysis of unbranched thin-walled members, Advanced Steel Construction 5 (2) (2009) 195–223.
[57] J. Jönsson, Distortional theory of thin-walled beams, Thin-Walled Structures 33 (1999) 269–303. doi:10.1016/S0263-8231(98)00050-0.
[58] J. Jönsson, M. J. Andreassen, Distortional eigenmodes and homogeneous solutions for semi-discretized thin-walled beams, Thin-Walled Structures 49 (2011) 691–707. doi:10.1016/j.tws.2010.12.009.
[59] M. J. Andreassen, J. Jönsson, Distortional solutions for loaded semi-discretized thin-walled beams, Thin-Walled Structures 50 (2012) 116–127. doi:10.1016/j.tws.2011.08.013.
[60] M. J. Andreassen, J. Jönsson, Distortional buckling modes of semi-discretized thin-walled columns, Thin-Walled Structures 51 (2012) 53–63. doi:10.1016/j.tws.2011.11.002.
[61] R. F. Vieira, F. B. E. Virtuoso, E. B. R. Pereira, A higher order thin-walled model including warping and shear modes, International Journal of Mechanical Sciences (2013) 67–82doi:10.1016/j.ijmecsci.2012.10.009.
[62] R. F. Vieira, F. B. Virtuoso, E. B. R. Pereira, A higher order model for thin-walled structures with deformable cross-sections, International Journal of Solids and Structures (2014) 575–598doi:10.1016/j.ijsolstr.2013.10.023.
[63] G. Garcea, R. Gonçalves, A. Billota, D. Manta, R. Bebiano, N. Leonetti, D. Magisano, D. Camotim, Deformation modes of thin-walled members: a comparison between the method of generalized eigenvectors and generalized beam theory, Thin-Walled Structures 100 (2016) 192–212. doi:10.1016/j.tws.2015.11.013.
[64] S. Ádány, Shell element for constrained finite element analysis of thin-walled structural members, Thin-Walled Structures 105 (2016) 135–146. doi:10.1016/j.tws.2016.04.012.
[65] S. Ádány, Constrained shell finite element method for thin-walled members with holes, Thin-Walled Structures 121 (2017) 41–56. doi:10.1016/j.tws.2017.09.021.
[66] S. Ádány, Constrained shell finite element method for thin-walled members, part 1: constraints for single band or finite elements, Thin-Walled Structures 128 (2018) 43–55. doi:10.1016/j.tws.2017.01.015.
[67] S. Ádány, D. Visy, R. Nagy, Constrained shell finite element method, part 2: application to linear buckling analysis of thin-walled members, Thin-Walled Structures 128 (2018) 56–70. doi:10.1016/j.tws.2017.01.022.
[68] D. Camotim, N. Silvestre, C. Basaglia, R. Bebiano, GBT-based buckling analysis of thin-walled members with non-standard support conditions, Thin-Walled Structures 46 (2008) 800–815. doi:10.1016/j.tws.2008.01.019.
[69] C. Basaglia, D. Camotim, N. Silvestre, Global Buckling Analysis of Plane and Space Thin-Walled Frames in the Context of GBT, Thin-Walled Structures 46 (2008) 79–101. doi:10.1016/j.tws.2007.07.007.
[70] C. Basaglia, D. Camotim, N. Silvestre, GBT-based local, distortional and global buckling analysis of thin-walled steel frames, Thin-Walled Structures 47 (2009) 1246–1264. doi:10.1016/j.tws.2009.04.003.
[71] C. Basaglia, D. Camotim, N. Silvestre, GBT-based buckling analysis of thin-walled steel frames with arbitrary loading and support conditions, International Journal of Structural Stability and Dynamics 10 (2010) 363–385. doi:10.1142/S0219455410003531.
[72] C. Basaglia, D. Camotim, N. Silvestra, Torsion warping transmission at thin-walled frame joints: Kinematics, modelling and structural response, Journal of Constructional Steel Research 69 (2012) 39–53. doi:10.1016/j.jcsr.2011.07.016.
[73] C. Basaglia, D. Camotim, N. Silvestre, Post-buckling analysis of thin-walled steel frames using generalised beam theory (gbt), Thin-Walled Structures 62 (2013) 229–242. doi:10.1016/j.tws.2012.07.003.
[74] C. Basaglia, D. Camotim, N. Silvestre, Buckling and vibration analysis of cold-formed steel chs members and frames using generalized beam theory, International Journal of Structural Stability and Dynamics 15 (2015) 1540021. doi:10.1142/S0219455415400210.
[75] C. Basaglia, D. Camotim, H. B. Coda, Generalized beam theory (GBT) formulation to analyse the vibration behaviour of thin-walled steel frames, Thin-Walled Structures 127 (2018) 259–274. doi:10.1016/j.tws.2018.01.038.
[76] R. D. Cook, D. S. Malkus, M. E. Plesha, Concepts and applications of finite element analysis, 3rd Edition, John Wiley & Son, NewYork Chichester Brisbane Toronto Singapore, 1989.
[77] A. B. Hansen, J. Jönsson, Displacement modes of a thin-walled beam model with deformable cross sections, Thin-Walled Structures 141 (2019) 576–592. doi:10.1016/j.tws.2019.01.052.
[78] A. B. Hansen, J. Jönsson, A thin-walled beam element formulated on exact displacement modes, approved for publishing in: Thin-Walled Structures (2019).
[79] S. de Miranda, A. Madeo, R. Miletta, F. Ubertini, On the relationship of the shear deformable generalized beam theory with classical and non-classical theories, International Journal

of Solids and Structures 51 (2014) 3698–3709. doi:10.1016/j.ijsolstr.2014.07.001.

[80] Abaqus, Abaqus/CAE 2016; Abaqus© and SIMULIA® used for finite element analysis, 2016, abaqus Inc., SIMULIA © Dassault Systèmes, 2015, Version 2016.

[81] L. Wu, M. Mohareb, Finite-element formulation for the lateral torsional buckling of plane frames, Journal of Engineering Mechanics 139 (2013) 512–524. doi:10.1061/(ASCE)EM.1943-7889.0000492.

[82] A. Sahraei, M. Mohareb, Lateral torsional buckling analysis of moment resisting plane frames, Thin-Walled Strucures 134 (2019) 233–254. doi:10.1016/j.tws.2018.10.006.

[83] S.-E. Kim, S.-H. Choi, Practical advanced analysis for semi-rigid space frames, International Journal of Solids and Structures 38 (2001) 9111–9131. doi:10.1016/S0020-7683(01)00141-X.

[84] R. G. L. da Silva, A. C. C. Lavall, R. S. Costa, H. F. Viana, Formulation for second-order inelastic analysis of steel frames including shear deformation effect, Journal of Constructional Steel Research 151 (2018) 216–227. doi:10.1016/j.jcsr.2018.09.011.

Paper II

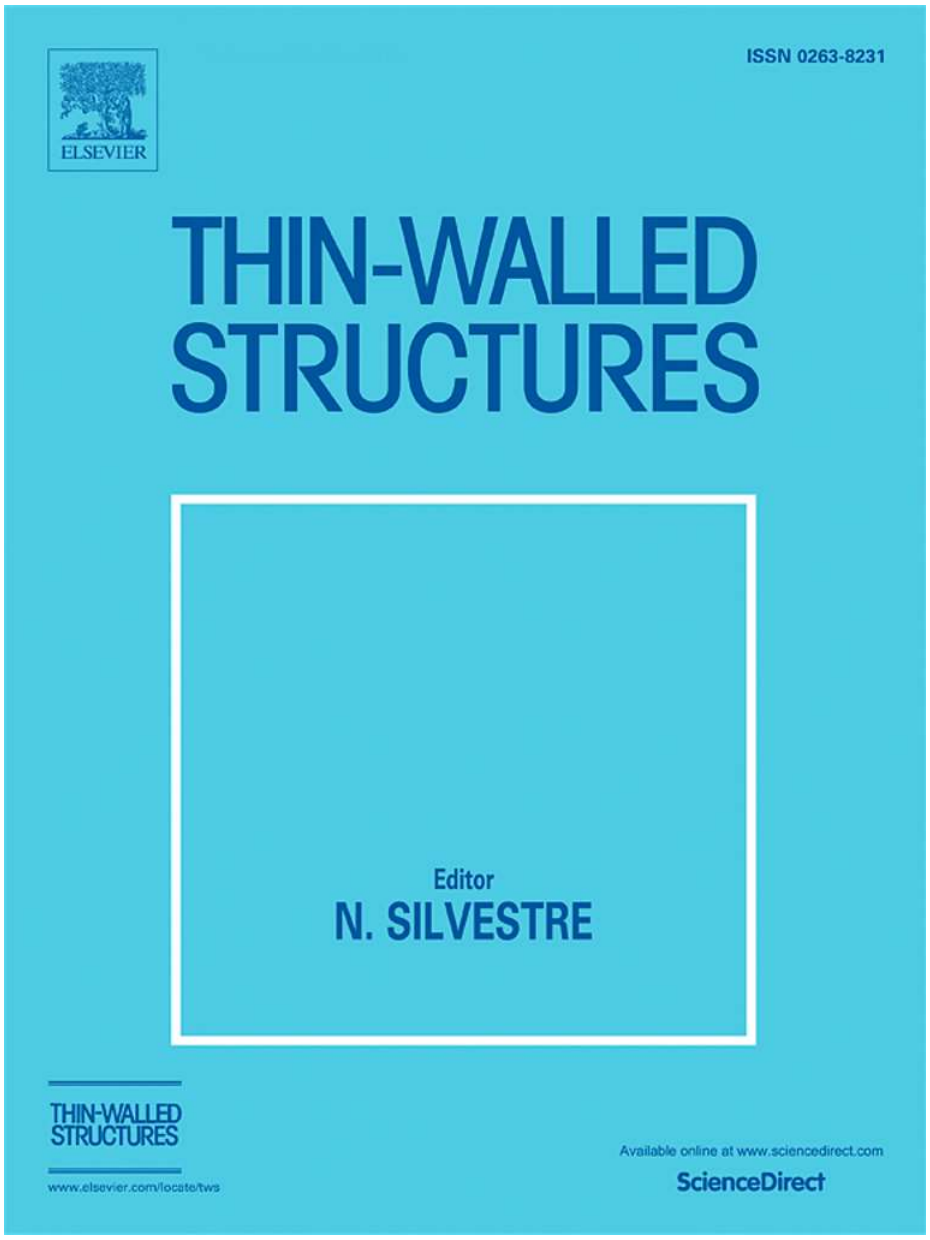

Displacement Modes of a Thin-Walled Beam Model with Deformable Cross Sections

Anders Bau Hansen[a,b], Jeppe Jönsson[a,*]

[a] *Technical University of Denmark, Department of Civil Engineering, Brovej Building 118, DK-2800 Kgs. Lyngby, Denmark*
[b] *NIRAS A/S, Sortemosevej 19, DK-3450 Allerød, Denmark*

Abstract

A novel one dimensional beam model for analysis of prismatic thin-walled beams with deformable cross sections is introduced and a novel cross section mode determination procedure, which leads to the three dimensional beam displacement modes, is derived. The first order beam model for linear analysis includes: shear deformations related to both Timoshenko and Mindlin-Reissner type shear deformations, the warping effects of torsion, cross section distortion with related warping effects, as well as the Poisson effect with transverse displacements due to normal stress. The generality of the model allows it to handle open, closed and multi-cell cross sections with branched walls. The cross section analysis procedure leads to two types of beam displacement modes referred to as distortional beam modes and fundamental beam modes, with exponential and polynomial variations along the beam axis, respectively. It turns out that each of the beam deformation modes consists of a sum of one to four cross section displacement fields each with an individual axial variation. The displacement modes can facilitate the formulation of an advanced thin-walled beam element. The beam displacement modes will be illustrated for an open and a closed cross section.

Keywords: Thin-walled beams, Beam eigenvalue problem, Warping, Distortion, Shear deformations, Fundamental beam modes, Beam theory

1. Introduction

Through centuries, beam models have been developed and especially in the twentieth century the development of thin-walled models increased due to the emerging ship and aircraft industries. It was realized that theories, such as the Euler-Bernoulli and the Timoshenko theories were not sufficient for assessing thin-walled structures even when unconstrained uniform St. Venant torsion was included. A reason was the missing cross sectional warping effect, thus, new theories had to be derived. The best known consistent theory is the torsional thin-walled beam theory presented by Vlasov [1]. This theory includes the warping phenomenon by introducing the sectorial coordinate. With this new "coordinate", the axial displacement field of the cross section is defined as a warping function. With this warping function, a decoupling of the displacement field into the classic extension and flexural modes is still possible, similar to earlier classic beam theories. However, Vlasov's theory of torsion does not include distortion of the cross section, since the cross section is assumed to maintain its shape. A generalization of Vlasov's thin-walled beam theory for open cross sections including distortion was given by Schardt [2]. Later, Schardt extended the theory to include closed cross sections as well, [3]. To do this he relaxed the Vlasov hypothesis of negligible shear strain adopting "Bredt's shear flow" in closed cells. At first, Schardt's theory was named: "Verallgemeinerte Technishe Biegetheorie" (VTB), but with its international spread, due to the work done by Davies and co-workers [4, 5], it is now known as GBT, i.e. Generalized Beam Theory, in the international academic society.

An expansion of Vlasovs thin-walled beam theory to include a single distortional deformation mode, which is directly applicable to both open and closed cross sections, was given by Jönsson in [6]. This reference illustrates the coupling of the differential equations, which are not easily uncoupled even in this relatively simple theory.

In recent years Silvestre and Camotim contributed heavily to the development and refinement of GBT and they also include orthotropic material behaviour [7, 8].

The general idea of modern GBT is to use a cross section discretization to determine orthogonal cross section displacement modes, i.e. displacement fields of a cross section. These modes are then interpolated using cubic Hermite functions in the axial direction. The cross section displacement modes are found from solving special eigenvalue problems related to equilibrium equations of the cross section using frame analogy. This approach, deriving displacement modes based on a discretized cross section, has become popular among researchers, since only a relatively small number of unknowns are needed. Modern GBT establishes a thin-walled beam model through rationalized and automated cross section analysis procedures and numerical analysis, see for example Bebiano et al. [9]

*Corresponding author
Email address: jej@byg.dtu.dk (Jeppe Jönsson)

and recently GBT has been extended to curved members by Peres et al. [10].

The "Finite Strip Method" (FSM) is another very popular method used to model the behaviour of thin-walled beams with deformable cross sections. With the refined "constrained Finite Strip Method" (cFSM) developed by Ádány and Schafer [11], it is possible to group the modes into categories; local modes, distortional mode, and beam modes as already done using GBT. A comparison of these two methods can be found in Ádány et al. [12].

The "constrained Finite Element Method" (CFEM) in which shell finite elements are used to model thin-walled beams by constraining displacements may also be used to create approximate beam models. The accuracy of these models depend on the underlying discretization in both transverse and longitudinal directions as well as on the constraints adapted. The constraints reduce the number of degrees of freedom and lead to advanced thin-walled beam elements, see for example Ádány [13].

Other generalized beam models based on discretization of the cross section adapt a more strict mathematical approach by formulating and solving the coupled equilibrium equations, i.e. they adapt the strong solution form. See for example the appoaches by Jönsson and Andreassen [14], Morandini et al. [15] and Vieira et al. [16]. All of these authors solve eigenvalue problems as part of a standard procedure for finding the solution to the coupled homogeneous beam differential equations for arbitrary cross sections. As opposed to GBT, these approaches lead to eigenvectors being the cross section displacement fields multiplied by the exponential eigenfunction determined by the eigenvalues. The polynomial modes (related to the classic beam modes) are derived from a detailed evaluation of the null-eigenvalue modes, hence, two sets of solutions are obtained. Morandini et al. find twelve fundamental beam solutions for solid cross sections using a special procedure based on the Jordan chain method. Furthermore, they find the eigenvalues of the exponential solutions and relate these to length scales as well as the St. Venant principle. Vieira et al. also uses a Jordan chain method to establish the polynomial solution modes, which are identified as fundamental beam modes, e.g. extension, flexure, etc. Furthermore, they use isospectral transformations of exponential modes to define generalized solution modes.

The prismatic thin-walled beam model presented in the following also adheres to the more strict mathematical approach of solving the coupled equilibrium equations. Some of the kinematic assumptions are made in order to facilitate the secondary goal of being able to connect to joints, which are modeled using conventional finite shell elements with three translational and three rotational degrees of freedom at each node. Furthermore it has also been the goal to achieve a formulation including shear deformations and the Poisson effect as opposed to the theoretical model presented in Jönsson and Andreassen [14], which does not include these effects. As opposed to Morandini et al. and Vieira et al. the present work retains the complex eigenvalues and exponential solution modes of the quadratic eigenvalue problem and therefore the solutions do not diagonalize all matrices of the original coupled differential equilibrium equations of the beam, since this is unnecessary as the modes span the solution space.

In this paper, the exact solution modes of the coupled differential beam equations are found through cross section discretization and separation of variables into cross section displacement fields and attenuation functions. The solutions to the differential equations leads to solutions consisting of fundamental polynomial beam solutions modes and exponential distortional solution modes (decaying from each beam end). The solution modes involve from one to four cross section displacement fields combined into a single three-dimensional solution mode being either polynomial or exponential. The advantage of this beam model is that the full solution is obtained between beam-ends and not as in GBT in which a beam must be discretized into several GBT finite elements with Hermitian interpolation along the axis of the beam.

2. The thin-walled beam model

The prismatic one dimensional thin-walled beam model is introduced in the following subsections. It is assumed that the beam displacements can be subdivided into a sum of separate beam displacement modes, which all obey the equilibrium equations. In the first subsection the kinematics and strains of one displacement mode is introduced and illustrated. Then, in the second subsection we introduce the strain energy function using the introduced displacement assumptions. Hereafter in the third subsection the cross section is discretized into straight wall elements and interpolation functions and related degrees of freedom are introduced and chosen. The fourth subsection introduces the discretization into the strain energy, which leads to the definition of wall element stiffness matrices, which in turn assemble into the stiffness matrices of the cross section. In the last and fifth subsection the variation of the discretized strain energy leads to the strong formulation of displacement mode equilibrium as a set of coupled second order differential equations expressed by the cross sectional stiffness matrices.

2.1. Kinematics

The prismatic thin-walled beam member is located in a global rectangular, right-handed Cartesian coordinate system (X, Y, Z). The Z-axis is pointing in the longitudinal direction of the member and the cross section is located in the X, Y-plane. To navigate through the cross section a local coordinate system is introduced in the walls as (n, s, z) following the right-hand convention and where z is parallel to the global Z-axis. The s-coordinate is a curve parameter running along the center line of the cross section and n indicates the normal to the s, z-plane. In figure 1 both local (n, s, z) and global (X, Y, Z) coordinate systems are

illustrated. The notation used in the following for derivatives with respect to the cross section wall coordinates will be a subscript comma followed by the local coordinate, e.g. as: $(\cdot)_{,n} \equiv d(\cdot)/dn$ or $(\cdot)_{,ss} \equiv d^2(\cdot)/ds^2$; however, derivatives with respect to the axial coordinate will be denoted by a prime, i.e. $(\cdot)' \equiv d(\cdot)/dz$.

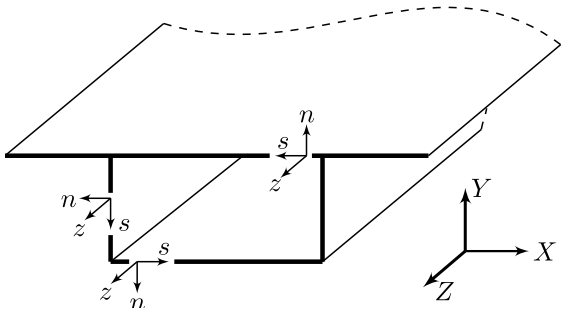

Figure 1: Illustration of local and global coordinate systems

Beam displacement modes are introduced by separation of variables through the sum of products between displacement variables dependent on the cross section coordinates (n, s) and amplitude functions dependent on the axial coordinate z. The cross section displacements are given in the local coordinate directions as functions of the local coordinates (n, s) and the axial coordinate z. The displacements of one displacement mode thus consists of transverse displacements (u_n, u_s) and (axial) warping displacements u_z. The kinematic displacement parameters are illustrated in figure 2.

Let us start by introducing the transverse displacements (u_n, u_s) of one displacement mode as:

$$u_n(s, z) = w_n(s)\psi(z) \tag{1}$$

$$u_s(n, s, z) = \Big[\; w_s(s) - nw_{n,s}(s) \;\Big]\psi(z) \tag{2}$$

in which $w_n(s)$ and $w_s(s)$ are the center line displacements in local directions factorized by a function of the axial coordinate, $\psi(z)$, referred to as an axial amplitude function. This displacement formulation corresponds to that of thin-plate theory or Kirchhoff theory in the transverse s-direction. This assumption will in a later subsection allow us to use beam like wall elements with a traditional beam type interpolation.

Then, let us introduce the axial warping displacements u_z of the displacement mode as:

$$u_z(n, s, z) = \Big[\; \Omega(s) + n\alpha(s) \;\Big]\eta(z) \tag{3}$$

where $\Omega(s)$ is the axial displacement of the wall center line, $\alpha(s)$ is the additional inclination through the thickness, and $\eta(z)$ is the related amplitude function, see figure 2. This formulation corresponds to a Timoshenko like shear formulation in the planes of each wall element $(s, z$-plane) and a Mindlin-Reisner like shear formulation through the wall element thickness in the axial z-direction $(n, z$-plane). This warping displacement formulation has been chosen to allow a strict local warping compatibility at the corners under the hypothesis that this would allow an enhanced modeling of shear, see for example the related GBT type assumptions and illustrations in Miranda et al. [17] and [18]. In a later subsection these assumptions also allow the introduction of six degrees of freedom per node in the cross section interpolation. Furthermore, the kinematic displacement assumptions also allow torsional shear flow around closed cells as considered by Jönsson and Andreassen [14].

In the elastic first order model, the linear strain definitions are applicable and they can be expressed by the introduced displacement description as follows:

$$\begin{aligned}
\varepsilon_{ss} = u_{s,s} \quad &= (w_{s,s} - nw_{n,ss})\,\psi \\
\varepsilon_{zz} = u_z' \quad &= (\Omega + n\alpha)\,\eta' \\
\gamma_{zs} = u_s' + u_{z,s} \quad &= (w_s - nw_{n,s})\,\psi' \\
&\quad + (\Omega_{,s} + n\alpha_{,s})\,\eta \\
\gamma_{zn} = u_n' + u_{z,n} \quad &= w_n\psi' + \alpha\eta
\end{aligned} \tag{4}$$

where ε_{ss} are the transverse distortional strains, ε_{zz} are axial normal strains, γ_{zs} are the membrane shear strains of the wall, and γ_{zn} are the through-wall axial shear strains. It follows that $\varepsilon_{nn} = 0$ and $\gamma_{sn} = 0$. It is seen that, due to the displacement formulations, we achieve non-null γ_{zn}-strains. It is also seen that the kinematics presented here includes transverse extension along the cross section mid-line as well as membrane shear strain, which both are neglected in the Vlasov theory (the Vlasov hypothesis).

In the following, vectors and matrices will be denoted by non-slanted, boldfaced, roman letters.

2.2. Discretization and interpolation of strain energy

The constitutive relations between stresses and strains are not as simple as in conventional beam theories, since the theory not only includes axial stresses σ_{zz} but also transverse stresses σ_{ss}, membrane wall shear stresses τ_{sz}, as well as transverse wall shear stresses τ_{nz}. As in plate theory we base the constitutive relation of the wall on the assumption of zero out of plane normal stress, i.e. $\sigma_{nn} = 0$. The axial and transverse in-plane normal stresses are coupled through the Poisson ratio, ν, and enables the Poisson effect, which induces changes in the geometry of the cross section. Using Young's modulus of elasticity E, we introduce the shear modulus $G = E/(2(1+\nu))$ and the plate elasticity modulus $E_s = E/(1-\nu^2)$. Hence, the linear constitutive relations are:

$$\begin{bmatrix} \sigma_{ss} \\ \sigma_{zz} \\ \tau_{sz} \\ \tau_{nz} \end{bmatrix} = \begin{bmatrix} E_s & \nu E_s & 0 & 0 \\ \nu E_s & E_s & 0 & 0 \\ 0 & 0 & G & 0 \\ 0 & 0 & 0 & G \end{bmatrix} \begin{bmatrix} \varepsilon_{ss} \\ \varepsilon_{zz} \\ \gamma_{sz} \\ \gamma_{nz} \end{bmatrix} \tag{5}$$

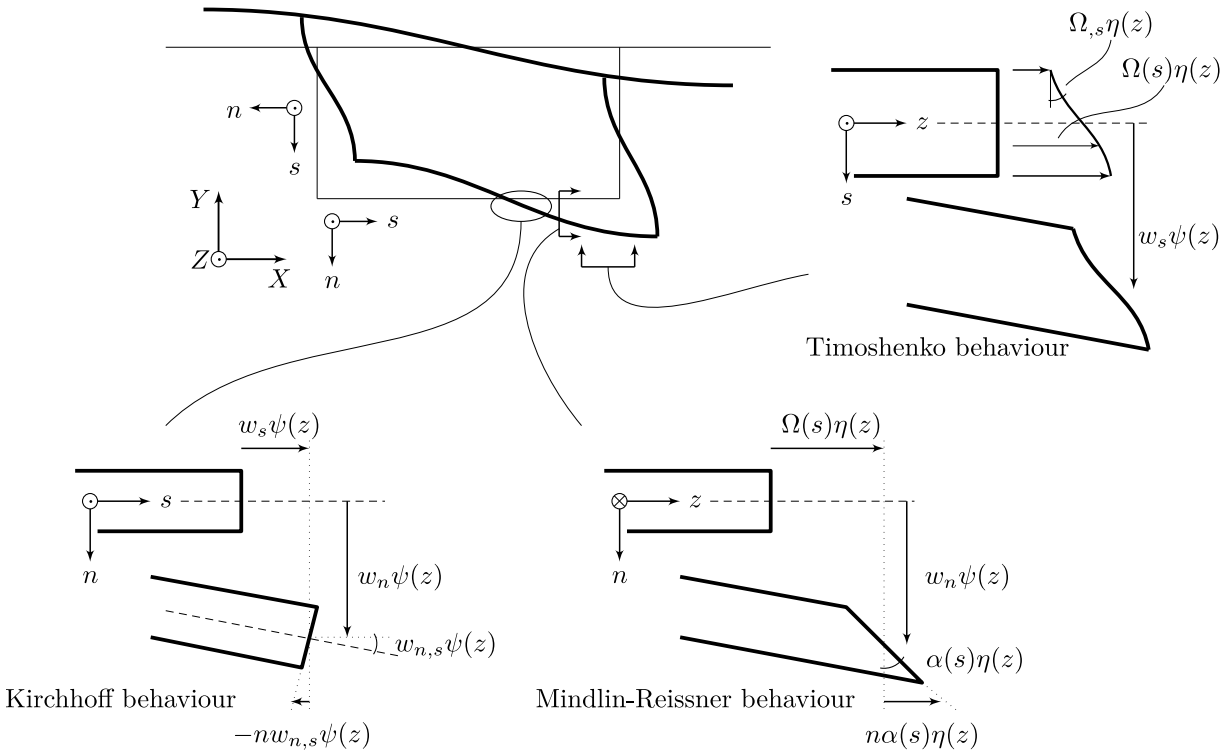

Figure 2: Deformations with respect to the cross section in different orientations

With the introduced constitutive relations, the linear elastic strain energy can be written as follows:

$$U = \frac{1}{2}\int_V \{E_s\varepsilon_{ss}^2 + E_s\varepsilon_{zz}^2 + 2\nu E_s\varepsilon_{ss}\varepsilon_{zz} + G\gamma_{nz}^2 + G\gamma_{sz}^2\}dV \tag{6}$$

Let us introduce the strains, equation (4), expressed by the displacement parameters into the strain energy. Then, let us perform the volume integration by subdividing the cross section into a sum of integrals over each straight wall element and let us perform the integration through the thickness. Thus, the middle-surface of a thin-walled cross section is assembled by straight wall elements as illustrated in figure 3. In the current formulation a wall element is characterized by a constant plate thickness t_{el} and an element length of b_{el}. The strain energy equation (6) for one displacement mode of a beam of length ℓ becomes:

$$\begin{aligned} U = &\tfrac{1}{2}\int_0^\ell \sum_{\text{el}} \int_0^{b_{el}} \Big\{ E_s\left(t_{el}\left(w_{s,s}\psi\right)^2 + \frac{1}{12}t_{el}^3\left(w_{n,ss}\psi\right)^2\right) \\ &+ E_s\left(t_{el}\left(\Omega\eta'\right)^2 + \frac{1}{12}t_{el}^3\left(\alpha\eta'\right)^2\right) \\ &+ 2\nu E_s\left(t_{el}\left(w_{s,s}\psi\Omega\eta'\right) - \frac{1}{12}t_{el}^3 w_{n,ss}\psi\alpha\eta'\right) \\ &+ G\left(t_{el}\left(w_s\psi'\right)^2 + 2t_{el}w_s\psi'\Omega_{,s}\eta + \frac{1}{12}t_{el}^3\left(w_{n,s}\psi'\right)^2\right. \\ &\quad \left. -2\frac{1}{12}t_{el}^3 w_{n,s}\psi'\alpha_{,s}\eta + t_{el}\left(\Omega_{,s}\eta\right)^2 + \frac{1}{12}t_{el}^3\left(\alpha_{,s}\eta\right)^2\right) \\ &+ G\left(t_{el}\left(w_n\psi'\right)^2 + t_{el}\left(\alpha\eta\right)^2 + 2t_{el}w_n\psi'\alpha\eta\right)\Big\} ds\, dz \end{aligned} \tag{7}$$

An example of the overall discretization of a cross section is illustrated in figure 3a and the configuration of a discrete wall element is shown in figure 3b illustrating its degrees of freedom. The wall element displacements are derived from approximated linear Lagrange and cubic Hermite functions. The degrees of freedom are split into two – those regarding displacements in the cross sectional plane given a w-subscript are transverse displacements, and those regarding displacements out of the cross sectional plane denoted by an Ω are in general being referred to as warping displacements. Thus, the wall element de-

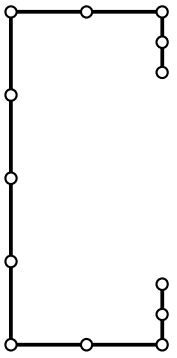

(a) Cross section discretized into minor wall elements

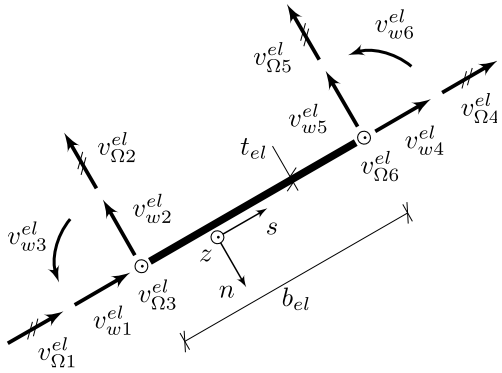

(b) A wall element with its twelve degrees of freedom and local coordinate system

Figure 3: A discretized thin-walled cross section and a wall element

grees of freedom are collected in two vectors being:

$$\begin{aligned}\mathbf{v}^{el}_{w} &= \begin{bmatrix} v^{el}_{w1} & v^{el}_{w2} & v^{el}_{w3} & v^{el}_{w4} & v^{el}_{w5} & v^{el}_{w6}\end{bmatrix}^{\mathsf{T}} \\ \mathbf{v}^{el}_{\Omega} &= \begin{bmatrix} v^{el}_{\Omega1} & v^{el}_{\Omega2} & v^{el}_{\Omega3} & v^{el}_{\Omega4} & v^{el}_{\Omega5} & v^{el}_{\Omega6}\end{bmatrix}^{\mathsf{T}}\end{aligned} \tag{8}$$

The introduced cross section displacement parameters are interpolated within the cross section using standard interpolation functions as follows (for clarity we have kept the related amplitude functions):

$$\begin{aligned} w_s\ \psi &= \mathbf{N}_s\ \mathbf{v}^{el}_{w}\ \psi\ \ , \quad \alpha\ \eta = \mathbf{N}_\alpha\ \mathbf{v}^{el}_{\Omega}\ \eta \\ w_n\ \psi &= \mathbf{N}_n\ \mathbf{v}^{el}_{w}\ \psi\ \ , \quad \Omega\ \eta = \mathbf{N}_\Omega\ \mathbf{v}^{el}_{\Omega}\ \eta \end{aligned} \tag{9}$$

in which the interpolation vectors are given in table 1. Furthermore, $\mathbf{N}_s$ and $\mathbf{N}_\alpha$ are linear whereas $\mathbf{N}_n$ and $\mathbf{N}_\Omega$ are cubic, see [19].

Table 1: Interpolation vectors

$\mathbf{N}_s = [N_1 \quad 0 \quad 0 \quad N_4 \quad 0 \quad 0]$
$\mathbf{N}_n = [0 \quad -N_2 \quad -N_3 \quad 0 \quad -N_5 \quad -N_6]$
$\mathbf{N}_\alpha = [-N_1 \quad 0 \quad 0 \quad -N_4 \quad 0 \quad 0]$
$\mathbf{N}_\Omega = [0 \quad -N_3 \quad N_2 \quad 0 \quad -N_6 \quad N_5]$

2.3. Cross section stiffness matrices

If the displacement interpolation functions, from equation (9), are substituted into equation (7), local wall element stiffness matrices given in table 2 may be found by integration over the element wall length. Regarding the superscripts, these indicate whether a stiffness matrix relates to transverse, normal or shearing stiffness, denoted: s, σ or γ, respectively. The coupling terms between axial and transverse normal strain are given by $\mathbf{k}^{s\sigma}_{w\Omega}$ and its transpose, which becomes $\mathbf{k}^{\sigma s}_{\Omega w}$.

Table 2: Local stiffness matrices

$\mathbf{k}^{s}_{ww} = \int_0^{b_{el}} \left(t_{el} E_s \mathbf{N}^{\mathsf{T}}_{s,s} \mathbf{N}_{s,s} + \frac{t^3_{el}}{12} E_s \mathbf{N}^{\mathsf{T}}_{n,ss} \mathbf{N}_{n,ss} \right) ds$
$\mathbf{k}^{\sigma}_{\Omega\Omega} = \int_0^{b_{el}} \left(t_{el} E_s \mathbf{N}^{\mathsf{T}}_{\Omega} \mathbf{N}_{\Omega} + \frac{t^3_{el}}{12} E_s \mathbf{N}^{\mathsf{T}}_{\alpha} \mathbf{N}_{\alpha} \right) ds$
$\mathbf{k}^{s\sigma}_{w\Omega} = \int_0^{b_{el}} \left(t_{el} \nu E_s \mathbf{N}^{\mathsf{T}}_{s,s} \mathbf{N}_{\Omega} - \frac{t^3_{el}}{12} \nu E_s \mathbf{N}^{\mathsf{T}}_{n,ss} \mathbf{N}_{\alpha} \right) ds$
$\mathbf{k}^{\sigma s}_{\Omega w} = \int_0^{b_{el}} \left(t_{el} \nu E_s \mathbf{N}^{\mathsf{T}}_{\Omega} \mathbf{N}_{s,s} - \frac{t^3_{el}}{12} \nu E_s \mathbf{N}^{\mathsf{T}}_{\alpha} \mathbf{N}_{n,ss} \right) ds$
$\mathbf{k}^{\gamma}_{\Omega\Omega} = \int_0^{b_{el}} \left(t_{el} G \mathbf{N}^{\mathsf{T}}_{\alpha} \mathbf{N}_{\alpha} + t_{el} G \mathbf{N}^{\mathsf{T}}_{\Omega,s} \mathbf{N}_{\Omega,s} + \frac{t^3_{el}}{12} G \mathbf{N}^{\mathsf{T}}_{\alpha,s} \mathbf{N}_{\alpha,s} \right) ds$
$\mathbf{k}^{\gamma}_{ww} = \int_0^{b_{el}} \left(t_{el} G \mathbf{N}^{\mathsf{T}}_{n} \mathbf{N}_{n} + t_{el} G \mathbf{N}^{\mathsf{T}}_{s} \mathbf{N}_{s} + \frac{t^3_{el}}{12} G \mathbf{N}^{\mathsf{T}}_{n,s} \mathbf{N}_{n,s} \right) ds$
$\mathbf{k}^{\gamma}_{\Omega w} = \int_0^{b_{el}} \left(t_{el} G \mathbf{N}^{\mathsf{T}}_{\alpha} \mathbf{N}_{n} + t_{el} G \mathbf{N}^{\mathsf{T}}_{\Omega,s} \mathbf{N}_{s} - \frac{t^3_{el}}{12} G \mathbf{N}^{\mathsf{T}}_{\alpha,s} \mathbf{N}_{n,s} \right) ds$
$\mathbf{k}^{\gamma}_{w\Omega} = \int_0^{b_{el}} \left(t_{el} G \mathbf{N}^{\mathsf{T}}_{n} \mathbf{N}_{\alpha} + t_{el} G \mathbf{N}^{\mathsf{T}}_{s} \mathbf{N}_{\Omega,s} - \frac{t^3_{el}}{12} G \mathbf{N}^{\mathsf{T}}_{n,s} \mathbf{N}_{\alpha,s} \right) ds$

Formulating the assembled cross section stiffness matrices and vectors containing all degrees of freedom it is convenient to express the local degrees in terms of a global reference frame. Thus, using a formal standard transformation matrix, the local degrees are written in global coordinates ($\mathbf{v}^{el} = \mathbf{T}^{el}\mathbf{v}$). Therefore, the local stiffness matrices can be assembled using a common assembling procedure yielding global cross sectional stiffness matrices (see e.g. [20]). Following this procedure, the strain energy from equation (7) takes the form:

$$U = \frac{1}{2}\int_0^{\ell} \begin{bmatrix} \mathbf{v}_w\psi \\ \mathbf{v}_\Omega\eta \\ \mathbf{v}_w\psi' \\ \mathbf{v}_\Omega\eta' \end{bmatrix}^{\mathsf{T}} \begin{bmatrix} \mathbf{K}^{s}_{ww} & \cdot & \cdot & \mathbf{K}^{s\sigma}_{w\Omega} \\ \cdot & \mathbf{K}^{\gamma}_{\Omega\Omega} & \mathbf{K}^{\gamma}_{\Omega w} & \cdot \\ \cdot & \mathbf{K}^{\gamma}_{w\Omega} & \mathbf{K}^{\gamma}_{ww} & \cdot \\ \mathbf{K}^{\sigma s}_{\Omega w} & \cdot & \cdot & \mathbf{K}^{\sigma}_{\Omega\Omega} \end{bmatrix} \begin{bmatrix} \mathbf{v}_w\psi \\ \mathbf{v}_\Omega\eta \\ \mathbf{v}_w\psi' \\ \mathbf{v}_\Omega\eta' \end{bmatrix} dz \tag{10}$$

using global stiffness matrices. Here and in the following a dot '$\cdot$' represents a suitable size null-matrix.

2.4. Displacement mode equilibrium

The differential equations for the displacement modes are derived using variational principles on the strain en-

ergy functional. The delta symbols, δ, in front of the displacement vectors are introduced to represent the variational terms. Integration by parts is performed on the variational terms, which are differentiated with respect to the axial coordinate. Thereby we eliminate axial derivatives (the primes) of the variational terms $\delta(\mathbf{v}_w\psi')$ and $\delta(\mathbf{v}_\Omega\eta')$ and the first variation of the strain energy takes the form:

$$\begin{aligned}\delta U = \int_0^\ell \delta \begin{bmatrix} \mathbf{v}_w\psi \\ \mathbf{v}_\Omega\eta \end{bmatrix}^{\mathsf{T}} \Bigg(& \begin{bmatrix} -\mathbf{K}^{\gamma}_{ww} & \cdot \\ \cdot & -\mathbf{K}^{\sigma}_{\Omega\Omega} \end{bmatrix} \begin{bmatrix} \mathbf{v}_w\psi \\ \mathbf{v}_\Omega\eta \end{bmatrix}'' \\ & + \begin{bmatrix} \cdot & \mathbf{K}^{s\sigma}_{w\Omega} - \mathbf{K}^{\gamma}_{w\Omega} \\ \mathbf{K}^{\gamma}_{\Omega w} - \mathbf{K}^{\sigma s}_{\Omega w} & \cdot \end{bmatrix} \begin{bmatrix} \mathbf{v}_w\psi \\ \mathbf{v}_\Omega\eta \end{bmatrix}' \\ & + \begin{bmatrix} \mathbf{K}^{s}_{ww} & \cdot \\ \cdot & \mathbf{K}^{\gamma}_{\Omega\Omega} \end{bmatrix} \begin{bmatrix} \mathbf{v}_w\psi \\ \mathbf{v}_\Omega\eta \end{bmatrix} \Bigg) \, dz \\ + \Bigg[\delta \begin{bmatrix} \mathbf{v}_w\psi \\ \mathbf{v}_\Omega\eta \end{bmatrix}^{\mathsf{T}} \Bigg(& \begin{bmatrix} \mathbf{K}^{\gamma}_{ww} & \cdot \\ \cdot & \mathbf{K}^{\sigma}_{\Omega\Omega} \end{bmatrix} \begin{bmatrix} \mathbf{v}_w\psi \\ \mathbf{v}_\Omega\eta \end{bmatrix}' \\ & + \begin{bmatrix} \cdot & \mathbf{K}^{\gamma}_{w\Omega} \\ \mathbf{K}^{\sigma s}_{\Omega w} & \cdot \end{bmatrix} \begin{bmatrix} \mathbf{v}_w\psi \\ \mathbf{v}_\Omega\eta \end{bmatrix} \Bigg) \Bigg]_0^\ell \end{aligned} \tag{11}$$

In this equation the last bracketed terms, i.e. $[\cdots]_0^\ell$, represent boundary terms, that ensure equilibrium with the boundary loads, which we have not introduced at this stage.

It follows from calculus of variations that, the first variation of the energy must vanish in order to have minimum energy. Therefore, the δU should vanish, i.e. $\delta U = 0$, for arbitrary variations in $\delta(\mathbf{v}_w\psi)$ and $\delta(\mathbf{v}_\Omega\eta)$, satisfying kinematic boundary conditions. This requirement is the condition of stationarity, which leads to the following set of equilibrium equations.

$$\begin{aligned} & \underbrace{\begin{bmatrix} -\mathbf{K}^{\gamma}_{ww} & \cdot \\ \cdot & \mathbf{K}^{\sigma}_{\Omega\Omega} \end{bmatrix}}_{\mathbf{K}_2} \underbrace{\begin{bmatrix} \mathbf{v}_w\psi \\ \mathbf{v}_\Omega\eta \end{bmatrix}''}_{\mathbf{u}''} \\ & + \underbrace{\begin{bmatrix} \cdot & \mathbf{K}^{s\sigma}_{w\Omega} - \mathbf{K}^{\gamma}_{w\Omega} \\ \mathbf{K}^{\sigma s}_{\Omega w} - \mathbf{K}^{\gamma}_{\Omega w} & \cdot \end{bmatrix}}_{\mathbf{K}_1} \underbrace{\begin{bmatrix} \mathbf{v}_w\psi \\ \mathbf{v}_\Omega\eta \end{bmatrix}'}_{\mathbf{u}'} \\ & + \underbrace{\begin{bmatrix} \mathbf{K}^{s}_{ww} & \cdot \\ \cdot & -\mathbf{K}^{\gamma}_{\Omega\Omega} \end{bmatrix}}_{\mathbf{K}_0} \underbrace{\begin{bmatrix} \mathbf{v}_w\psi \\ \mathbf{v}_\Omega\eta \end{bmatrix}}_{\mathbf{u}} = \begin{bmatrix} \mathbf{0} \\ \mathbf{0} \end{bmatrix} \end{aligned} \tag{12}$$

Please note that to achieve symmetry in the matrix formulation the lower block-row-equation is multiplied by -1. Furthermore, we have, in the above equation, introduced the matrices $\mathbf{K}_2$, $\mathbf{K}_1$ and $\mathbf{K}_0$ as well as the vector of displacements $\mathbf{u}$. This has been done in order to obtain the following more compact formulation of these differential equilibrium equations:

$$\mathbf{K}_2\mathbf{u}'' \; + \; \mathbf{K}_1\mathbf{u}' \; + \; \mathbf{K}_0\mathbf{u} \; = \; \mathbf{0} \tag{13}$$

Consequently, we have achieved a set of second order displacement mode differential equations and not as in other higher order beam theories, such as GBT, a fourth order differential equation system. The reason why a second-order beam differential equation system is derived here, is the use of warping fields $\Omega\eta$ and $\alpha\eta$, which until otherwise stated are independent of ψ.

3. Cross section mode determination procedure

The cross section mode determination procedure reflects the solution of the displacement mode differential equations using the approach of assuming exponential solutions and finding these through the solution of the characteristic equations being a quadratic eigenvalue problem. However, hereby we have not found the complete homogeneous solution, since there will be $n_z = 12$ null eigenvalues corresponding to the classic polynomial solutions including constant strain modes and rigid body motions also referred to as *fundamental modes*. The polynomial solutions are found by seeking a set of n_z third order polynomial solutions. Since there are a multitude of possible combinations of these modes an engineering based procedure, which enables the direct relation to classic beam theory, is described. This task, however, is not as straight forward as expected.

3.1. Exponential modes

Let us start out seeking exponential solutions. In the previous section separation of variables was used to formulate displacements as product terms of cross sectional displacements and the amplitude functions. Thus, we need to find solutions to the differential equations (13) with the displacement vector:

$$\mathbf{u}(z) \; = \; \begin{bmatrix} \mathbf{v}_w\psi(z) \\ \mathbf{v}_\Omega\eta(z) \end{bmatrix} \tag{14}$$

in which the vectors $\mathbf{v}_w$ and $\mathbf{v}_\Omega$ contains cross sectional degrees of freedom with respect to transverse and warping displacements, respectively. It is clear that two related amplitude functions $\psi(z)$ and $\eta(z)$ have been introduced. This, however, has been done in order to keep the relation to conventional formulations of beam theories. Nonetheless, to solve the coupled differential equations we now assume that $\eta = \psi$. This enables us to write the displacement using a single amplitude function as:

$$\mathbf{u}(z) = \mathbf{v} \; \psi(z) \; c \tag{15}$$

in which the cross section displacement mode vector is given by:

$$\mathbf{v} = \begin{bmatrix} \mathbf{v}_w \\ \mathbf{v}_\Omega \end{bmatrix} \tag{16}$$

The complex constant to be determined by boundary conditions, $c_p \in \mathbb{C}$ has been introduced in equation (15) to scale the whole solution mode.

A general solution of the beam differential equations (13) is sought by assuming an exponential amplitude function: $\psi = e^{\lambda z}$, whereby the assumed solution vector from equation (15) becomes:

$$\mathbf{u}_e \;=\; \mathbf{v}_e \; e^{\lambda z} \; c_e \tag{17}$$

Here, we have introduced the subscript e to distinguish an exponential solution mode from a polynomial one. Inserting this assumed solution into the differential equations (13) and simplifying by dividing by $e^{\lambda z} c_e$ the following algebraic system of equations is found.

$$\left(\lambda^2 \mathbf{K}_2 \;+\; \lambda \mathbf{K}_1 \;+\; \mathbf{K}_0\right) \mathbf{v}_e = \mathbf{0} \quad \text{with } \lambda \in \mathbb{C} \tag{18}$$

This algebraic system of equations is a quadratic matrix eigenvalue problem with λ as the eigenvalue variable and $\mathbf{v}_e$ being the eigenvector representing an associated deformation mode. Solution modes can be derived by reducing the differential order of equation (13) to an equivalent system of first order differential equations introducing a state vector as proposed by Tisseur and Meerbergen [21] leading to a generalized eigenvalue problem but also doubling the number of solution modes, or directly by solving the quadratic eigenvalue problem by use of the built-in function `polyeig` in MATLAB [22]. It is worth noting that it is the state vectors that become orthogonal (with respect to the total strain energy).

The eigenvectors associated with non-null eigenvalues are the cross section displacement vectors related to the exponential modes. The eigenvalues can be viewed as inverse length scale parameters and the importance of each mode depends on the length scale. The larger the scale, the more important is the related displacement mode in relation to the beam model. Thus, we will sort the modes hierarchically such that modes with low eigenvalues are those of higher importance and comes first. The more localized and detailed behaviour that has to be assessed by the beam model, the more short scale modes will have to be included. The sum of all exponential modes may be written as:

$$\mathbf{u}_e = \mathbf{V}_e \; \mathbf{\Psi}_e \; \mathbf{c}_e \tag{19}$$

where $\mathbf{V}_e$ contains all the sorted eigenvectors of the associated non-null eigenvalues λ_i as its columns, $\mathbf{\Psi}_e$ is a diagonal amplitude matrix and $\mathbf{c}_e$ is a column vector containing a constant to each mode. In other words, the components in equation (19) are given as follows:

$$\mathbf{V}_e = \begin{bmatrix} \mathbf{v}_{e_1} & \mathbf{v}_{e_2} & \dots & \mathbf{v}_{e_{n_e}} \end{bmatrix} ,$$

$$\mathbf{\Psi}_e = \begin{bmatrix} \psi_{e_1} & & & \\ & \psi_{e_2} & & \\ & & \ddots & \\ & & & \psi_{e_{n_e}} \end{bmatrix} , \quad \mathbf{c}_e = \begin{bmatrix} c_{e_1} \\ c_{e_2} \\ \vdots \\ c_{e_{n_e}} \end{bmatrix} \tag{20}$$

in which the ith exponential diagonal amplitude function is given as $\psi_{e_i} = e^{\lambda_i z}$ and where n_e is the number of exponential modes being $n_e = 2n - n_z$, where n is six times the number of nodes in the discretized cross section.

Not considering the null-eigenvalues the solution of the quadratic eigenvalue problem contains pairs of real eigenvalues $\{\lambda, -\lambda\}$ as well as complex quadruples $\{\lambda, -\lambda, \overline{\lambda}, -\overline{\lambda}\}$. The quadruples have a real part representing the axial decay effect accompanied by an oscillatory amplitude related to the imaginary part. In case of complex eigenvalues the eigenvectors also become complex.

To be able to present and discuss unique eigenmodes, all the distortional vectors in $\mathbf{V}_e$ have been normalized by multiplication by a complex constant. This constant is determined in such a way that the largest absolute value of all components in each transverse displacement vector $\mathbf{v}_w$ is one and that this component is real. This has to be done in order to make them unique since complex eigenvectors are determined by the eigenvalue problem except for an arbitrary complex constant given in $\mathbf{c}_e$.

The eigenvectors related to the $n_z = 12$ null-eigenvalues are coupled, since many of them are related to rigid body displacements and constant strain displacement fields, which have polynomial amplitude functions. The following subsection derives these fundamental modes.

3.2. Fundamental modes

Eigenvectors associated with null-eigenvalues of the quadratic eigenvalue problem in equation (18) are assumed to be fundamental beam modes having a polynomial amplitude function along the beam axis without any exponential components. These represent the classical beam mode solutions as those illustrated in figure 4. From classic beam theory, we know that the rigid body displacements corresponds to constant and linear amplitude functions, that pure extension and unrestrained torsion corresponds to constant strain and linear displacements, where as constant bending strain corresponds to quadratic displacements. Moreover, constant shear strain does not exist alone but corresponds to a mode that also has linear varying bending strains and therefore has a cubic variation of the transverse displacements. It is important to note that the deformation shapes are not known beforehand as in ordinary beam theory, since shear deformation and the Poisson expansion of the cross section are now included in the theory. With this in mind, we assume a third order polynomial function to embrace the fundamental modes. Thus, let us seek n_z solutions of the form:

$$\mathbf{u}_p = \left(\frac{z^3}{3!}\mathbf{v}_3 + \frac{z^2}{2!}\mathbf{v}_2 + z\mathbf{v}_1 + \mathbf{v}_0 \right) c_p \tag{21}$$

where $\{\mathbf{v}_3,\ \mathbf{v}_2,\ \mathbf{v}_1,\ \mathbf{v}_0\}$ is a set of cross section deformation vectors altogether representing one polynomial displacement mode factored by the constant c_p. Each vector contains both the in-plane and out-of-plan components as

in equation (16). Now, substituting this assumed polynomial solution function and its derivatives into the beam differential equations from equation (13) results in the following set of equations that must be fulfilled in order to maintain equilibrium:

$$\Big(\tfrac{1}{6}z^3(\mathbf{K}_0\mathbf{v}_3) + \tfrac{1}{2}z^2(\mathbf{K}_1\mathbf{v}_3 + \mathbf{K}_0\mathbf{v}_2) + z(\mathbf{K}_2\mathbf{v}_3 + \mathbf{K}_1\mathbf{v}_2 + \mathbf{K}_0\mathbf{v}_1) + (\mathbf{K}_2\mathbf{v}_2 + \mathbf{K}_1\mathbf{v}_1 + \mathbf{K}_0\mathbf{v}_0)\Big)c_p = 0 \tag{22}$$

By assembling the polynomial terms in a vector and assembling the deformation mode vectors in a vector as well, the equilibrium equations may be expressed by an assembled matrix notation as follows:

$$\begin{bmatrix} \frac{1}{6}z^3\mathbf{I}_n \\ \frac{1}{2}z^2\mathbf{I}_n \\ z\mathbf{I}_n \\ \mathbf{I}_n \end{bmatrix}^{\mathsf{T}} \begin{bmatrix} \mathbf{K}_0 & \cdot & \cdot & \cdot \\ \mathbf{K}_1 & \mathbf{K}_0 & \cdot & \cdot \\ \mathbf{K}_2 & \mathbf{K}_1 & \mathbf{K}_0 & \cdot \\ \cdot & \mathbf{K}_2 & \mathbf{K}_1 & \mathbf{K}_0 \end{bmatrix} \begin{bmatrix} \mathbf{v}_3 \\ \mathbf{v}_2 \\ \mathbf{v}_1 \\ \mathbf{v}_0 \end{bmatrix} c_p = \mathbf{0} \tag{23}$$

In which we have introduced the unit matrix $\mathbf{I}_n$, where n is a reference to the number of degrees of freedom in each block.

Mode space of the fundamental modes

The non-trivial solutions to these equilibrium equations (22), i.e. with $c_p \neq 0$ for all values of z, can be found as the null space of $\mathbb{K}$ being:

$$\mathbb{V} = \mathcal{N}(\mathbb{K}) \tag{24}$$

where $\mathcal{N}$ is the null space algebraic operation and the solution satisfies $\mathbb{K}\mathbb{V} = \mathbf{0}$ where $\mathbb{K}$ is given in equation (25) by the block matrices defined in equation (12) and $\mathbb{V}$ may be separated into equivalent blocks also illustrated in equation (25). The subscripts on the block matrices $\mathbf{V}_k$ in $\mathbb{V}$ refers to their position in the polynomial solution from equation (21) – the coefficient numbers k reflects the associated polynomial order of z, i.e. a column in $\mathbf{V}_k$ will be linked to $\frac{1}{k!}z^k$.

$$\mathbb{K} = \begin{bmatrix} \mathbf{K}_0 & \cdot & \cdot & \cdot \\ \mathbf{K}_1 & \mathbf{K}_0 & \cdot & \cdot \\ \mathbf{K}_2 & \mathbf{K}_1 & \mathbf{K}_0 & \cdot \\ \cdot & \mathbf{K}_2 & \mathbf{K}_1 & \mathbf{K}_0 \end{bmatrix} \quad \text{and} \quad \mathbb{V} = \begin{bmatrix} \mathbf{V}_3 \\ \mathbf{V}_2 \\ \mathbf{V}_1 \\ \mathbf{V}_0 \end{bmatrix} \tag{25}$$

Computing the null space, in equation (24), yields twelve solutions given as the columns in $\mathbb{V}$. This corresponds exactly to the number of null-eigenvalues associated with the quadratic eigenvalue problem in equation (18). Moreover, this also corresponds to the number of classic solutions, e.g. the *elementary solutions* considered by Morandini et al. [15] determined using a slightly different procedure considering a Jordan chain formulation. However, the modes found as solutions to the null space of $\mathbb{K}$ are coupled in the sense that they represent a mix of the classic beam modes. These modes may be used in the continued beam analysis, however, they would not give a clear engineering connection to classic beam theory. Hence, a mode identification procedure is required in order to decouple classic solution modes, which are representative.

From an engineering perspective, we know that the twelve fundamental solution modes can be subdivided into six rigid body deformation modes; and six strain modes corresponding to pure extension, (unconstrained) free torsion, pure bending and constant shear strain with linear varying normal strains; as illustrated in figure 4. From the displacement fields, illustrated in the figure, it can be deduced that the individual solution modes may have contributions from up to four cross section displacement vectors $\mathbf{v}_3$, $\mathbf{v}_2$, $\mathbf{v}_1$ and $\mathbf{v}_0$ with the corresponding polynomial amplitude functions $\{\frac{1}{6}z^3, \frac{1}{2}z^2, z, 1\}$ according to equation (21). Note that each of these four cross section displacement vectors $\mathbf{v}_k$ have a transverse part $\mathbf{v}_{kw}$ and a warping part $\mathbf{v}_{k\Omega}$ as indicated in equation (16). Table 3 gives an overview of the twelve fundamental modes in relation to cross section displacement vectors and their related polynomial terms as seen from an engineering point of view. The intent of the fourth line in the table is to give a reference to the principal axis of displacement, rotation or bending as 1 or 2 diThe fundamental modes shown in figure 13 and 14 of the results section 4 may clarify the principle. However, the displacement vectors need to be found and identified. Furthermore, from table 3 it can be seen that this subdivision of fundamental modes leads to a logical separation based on polynomial order related to these modes. Thus, the polynomial order may be used in a mode identification procedure, which follows in next section.

Identification of modes dependent on polynomial order

The procedure adopted to identify the cubic, quadratic, linear and constant amplitude function modes is similar to the procedure described by Vieira [23]. The ordering and the orthogonalization procedure, which we apply is new. The orthogonalization procedure is based on strain energy for strain modes and on inertial energy for rigid modes.

In the following, four superscripts are introduced – one for each polynomial "family". The four superscripts used for sub-columns of $\mathbb{V}$ are: C, L, B and S assigned to constant modes of zero order, linear modes of first order, bending modes of second order, and shear modes of third order, respectively. Having found the null space in equation (24), the columns in the block vector $\mathbf{V}_3$ contains the displacement content of third order. From our engineering viewpoint only two modes with constant shear and linear bending should be identified with this particular order. Therefore the columns in $\mathbb{V}$ must be decoupled using $\mathbf{V}_3$. To do this and in order to identify displacement modes with a cubic content, a singular value decomposition (SVD) is applied to $\mathbf{V}_3$. The SVD results in a decomposition of $\mathbf{V}_3$ in a null part "$\cdot$" and a non-null part $\mathbf{V}_3^{\mathrm{S}}$. However, the

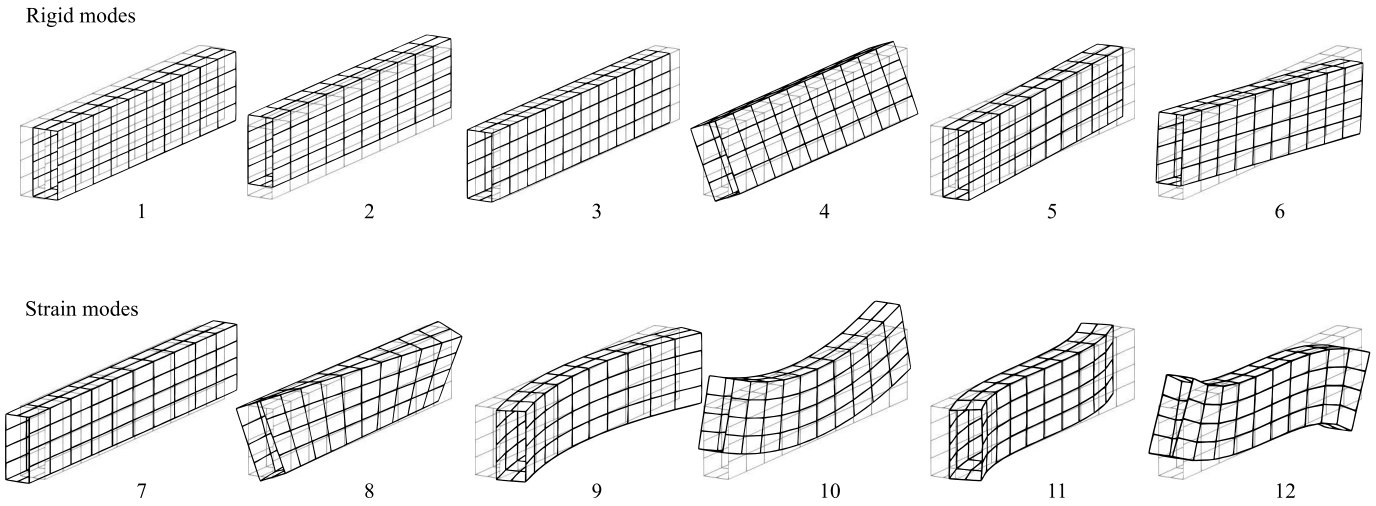

Figure 4: Illustration of fundamental displacement modes

Table 3: Amplitude functions of cross section displacement vectors related to the fundamental displacement modes.

Type		**Rigid modes**						**Strain modes**					
		Translations in			Rotations about			Extension & Torsion		Pure Bending abt		Constant Shear in	
		X	Y	Z	Z	Y	X	Ext.	Tors.	Y	X	X	Y
Mode i		1	2	3	4	5	6	7	8	9	10	11	12
$\mathbf{V}_3$	$\mathbf{v}^i_{3w}$ $\mathbf{v}^i_{3\Omega}$											$\frac{1}{6}z^3$	$\frac{1}{6}z^3$
$\mathbf{V}_2$	$\mathbf{v}^i_{2w}$ $\mathbf{v}^i_{2\Omega}$									$\frac{1}{2}z^2$	$\frac{1}{2}z^2$	$\frac{1}{2}z^2$	$\frac{1}{2}z^2$
$\mathbf{V}_1$	$\mathbf{v}^i_{1w}$ $\mathbf{v}^i_{1\Omega}$					z	z	z	z	z	z	$z^\dagger$	$z^\dagger$
$\mathbf{V}_0$	$\mathbf{v}^i_{0w}$ $\mathbf{v}^i_{0\Omega}$	1	1	1	1	1	1	$1^\dagger$	1	$1^\dagger$	$1^\dagger$	1	1
Max. order		**0**				**1**				**2**		**3**	

†Poisson effect

decomposition is applied not only to $\mathbf{V}_3$ but to the whole mode space matrix $\mathbb{V}$, such that it is subdivided into a remaining mode space $\mathbf{V}^r$ of lower order and a third order mode space $\mathbf{V}^{\mathrm{S}}$, which we relate to shear. Hence, the null space of $\mathbb{K}$ takes the form $\mathbb{V} = [\mathbf{V}^r, \mathbf{V}^{\mathrm{S}}]$, which may also be written as:

$$\mathbb{V} = \begin{bmatrix} \cdot & \mathbf{V}_3^{\mathrm{S}} \\ \mathbf{V}_2^r & \mathbf{V}_2^{\mathrm{S}} \\ \mathbf{V}_1^r & \mathbf{V}_1^{\mathrm{S}} \\ \mathbf{V}_0^r & \mathbf{V}_0^{\mathrm{S}} \end{bmatrix} \tag{26}$$

Next, the modes of second order, i.e. bending modes, are identified by performing a SVD on the remaining block matrix $\mathbf{V}_2^r$. This similarly leads to a decoupling into new remaining modes $\mathbf{V}^{nr}$ and second order bending modes $\mathbf{V}^{\mathrm{B}}$. The null space of $\mathbb{K}$ now has the form $\mathbb{V} = [\mathbf{V}^{nr}, \mathbf{V}^{\mathrm{B}}, \mathbf{V}^{\mathrm{S}}]$. Finally, the last step is to decouple linear and constant terms through a SVD on the remaining sub-matrix $\mathbf{V}_1^{nr}$, whereafter those modes related to the non-null singular values receive a superscript L where as the remaining part a superscript C. The number of modes having a given order complies with the numbers expected from table 3. Furthermore, the result of this successive procedure is that we have decomposed the polynomial displacement modes according to polynomial order and the matrix $\mathbb{V}$ now takes the form:

$$\mathbb{V} = \begin{bmatrix} \cdot & \cdot & \cdot & \mathbf{V}_3^{\mathrm{S}} \\ \cdot & \cdot & \mathbf{V}_2^{\mathrm{B}} & \mathbf{V}_2^{\mathrm{S}} \\ \cdot & \mathbf{V}_1^{\mathrm{L}} & \mathbf{V}_1^{\mathrm{B}} & \mathbf{V}_1^{\mathrm{S}} \\ \mathbf{V}_0^{\mathrm{C}} & \mathbf{V}_0^{\mathrm{L}} & \mathbf{V}_0^{\mathrm{B}} & \mathbf{V}_0^{\mathrm{S}} \end{bmatrix} \tag{27}$$

Even though the modes have been identified and sorted according to their polynomial order, the linear modes are not separated into a rigid part and a strain part. Furthermore, the modes are not pure and for example the third order modes $\mathbf{V}^{\mathrm{S}}$ may be contaminated by parts of the lower order modes $\mathbf{V}^{\mathrm{B}}$, $\mathbf{V}^{\mathrm{L}}$ and $\mathbf{V}^{\mathrm{C}}$ and so forth. It would also be convenient that the strain modes are orthogonal with respect to strain energy, for example that they represents the principal axis bending modes.

To achieve all this, a procedure following the steps listed here, will be executed on the modes in equation (27).

a) Split linear modes into rigid modes and orthogonal strain modes.

b) Remove lower order strain modes from higher order strain modes.

c) Find principal bending modes from the second order modes.

d) Find shear modes following the principal axis of bending.

e) Transform rigid modes according to principal directions.

f) Remove lower order rigid modes from higher order modes.

The following subsections will describe the individual procedural steps.

a) Split linear modes into rigid modes and strain modes

To identify the classic beam modes we need to introduce and relate to the strain energy formulated with respect to the polynomial cross section displacement modes. In this regard, consider the strain energy from equation (10), where the integration over the beam length is not of interest since we investigate cross section behaviours at an arbitrary point along the beam, however, the energy depends on the product of the amplitude functions. Thus, we consider the strain energy in a cross section or rather the strain energy density per beam length, which takes the form:

$$U' = \frac{1}{2} \begin{bmatrix} \mathbf{v}_w\psi \\ \mathbf{v}_\Omega\eta \\ \mathbf{v}_w\psi' \\ \mathbf{v}_\Omega\eta' \end{bmatrix}^{\mathsf{T}} \begin{bmatrix} \mathbf{K}_{ww}^{s} & \cdot & \cdot & \mathbf{K}_{w\Omega}^{s\sigma} \\ \cdot & \mathbf{K}_{\Omega\Omega}^{\gamma} & \mathbf{K}_{\Omega w}^{\gamma} & \cdot \\ \cdot & \mathbf{K}_{w\Omega}^{\gamma} & \mathbf{K}_{ww}^{\gamma} & \cdot \\ \mathbf{K}_{\Omega w}^{\sigma s} & \cdot & \cdot & \mathbf{K}_{\Omega\Omega}^{\sigma} \end{bmatrix} \begin{bmatrix} \mathbf{v}_w\psi \\ \mathbf{v}_\Omega\eta \\ \mathbf{v}_w\psi' \\ \mathbf{v}_\Omega\eta' \end{bmatrix} \tag{28}$$

As stated previously, we assume the functions ψ and η to be polynomials of third order multiplied by a set of coefficient vectors introduced as displacement vectors. As a result, the mode vectors in equation (28) may be formulated, for a single mode, as:

$$\begin{aligned} \mathbf{v}_w\psi &= \tfrac{1}{6}\mathbf{v}_{3w}z^3 + \tfrac{1}{2}\mathbf{v}_{2w}z^2 + \mathbf{v}_{1w}z + \mathbf{v}_{0w} \\ \mathbf{v}_\Omega\eta &= \tfrac{1}{6}\mathbf{v}_{3\Omega}z^3 + \tfrac{1}{2}\mathbf{v}_{2\Omega}z^2 + \mathbf{v}_{1\Omega}z + \mathbf{v}_{0\Omega} \end{aligned} \tag{29}$$

and its first derivatives as:

$$\begin{aligned} \mathbf{v}_w\psi' &= \tfrac{1}{2}\mathbf{v}_{3w}z^2 + \mathbf{v}_{2w}z + \mathbf{v}_{1w} \\ \mathbf{v}_\Omega\eta' &= \tfrac{1}{2}\mathbf{v}_{3\Omega}z^2 + \mathbf{v}_{2\Omega}z + \mathbf{v}_{1\Omega} \end{aligned} \tag{30}$$

Based on our engineering intuition and mathematics we foresee the following:

- Inserting the zero order rigid modes $\mathbf{V}^{\mathrm{C}}$ will all result in zero energy density, hence, all being rigid motions.
- For the first order modes $\mathbf{V}^{\mathrm{L}}$ corresponding to rotational rigid body modes, extension and torsion will result in four modes with some constant energy density, since the modes are not pure.
- The second order modes $\mathbf{V}^{\mathrm{B}}$ corresponding to bending will result in two modes with constant energy density.
- The third order modes $\mathbf{V}^{\mathrm{S}}$ will result in a constant energy density term corresponding to pure shear and a quadratic energy term corresponding to linear varying bending moments.

Consequently, it is convenient to introduce an inner product based on the strain energy density to be able to com-

bine mode vectors. This inner product we formulate as:

$$\left\langle \begin{bmatrix} \mathbf{V}^i_k \\ \mathbf{V}^i_{(k+1)} \end{bmatrix}, \begin{bmatrix} \mathbf{V}^j_l \\ \mathbf{V}^j_{(l+1)} \end{bmatrix} \right\rangle_E = \begin{bmatrix} \mathbf{v}^i_{kw} \\ \mathbf{v}^i_{k\Omega} \\ \mathbf{v}^i_{(k+1)w} \\ \mathbf{v}^i_{(k+1)\Omega} \end{bmatrix}^{\mathsf{T}} \begin{bmatrix} \mathbf{K}^s_{ww} & \cdot & \cdot & \mathbf{K}^{s\sigma}_{w\Omega} \\ \cdot & \mathbf{K}^{\gamma}_{\Omega\Omega} & \mathbf{K}^{\gamma}_{\Omega w} & \cdot \\ \cdot & \mathbf{K}^{\gamma}_{w\Omega} & \mathbf{K}^{\gamma}_{ww} & \cdot \\ \mathbf{K}^{\sigma s}_{\Omega w} & \cdot & \cdot & \mathbf{K}^{\sigma}_{\Omega\Omega} \end{bmatrix} \begin{bmatrix} \mathbf{v}^j_{lw} \\ \mathbf{v}^j_{l\Omega} \\ \mathbf{v}^j_{(l+1)w} \\ \mathbf{v}^j_{(l+1)\Omega} \end{bmatrix} \tag{31}$$

If $\mathbf{V}^i$ and $\mathbf{V}^j$ represent columns i and j, the inner product computes a number (representing the work and related stiffness of the two modes). On the other hand if $\mathbf{V}^i$ and $\mathbf{V}^j$ each represent a number of columns (for example a mode family) the inner product computes a subspace (stiffness) matrix related to these modes. Thus, the subscripts k and l refer to the coefficient numbers related to the polynomial degree (see equation (25)) whereas i and j refers to the solution family or a column number. Note that the $+1$ in subscripts $(k+1)$ and $(l+1)$ stem from differentiated terms in equation (30); when for example gathering energy terms of constant or quadratic dependency on z.

In order to separate the rigid modes and strain modes all having a linear amplitude, we use the inner product in equation (31) and substitute $\mathbf{V}^i$ and $\mathbf{V}^j$ with $\mathbf{V}^{\mathrm{L}}$. As highlighted, modes of first order have either zero strain or constant strain. Consequently, we use the cross section displacement vectors $\mathbf{v}_{0w}$, $\mathbf{v}_{0\Omega}$, $\mathbf{v}_{1w}$ and $\mathbf{v}_{1\Omega}$ in the inner product (i.e. $k = l = 0$). Hence, let us analyze this strain energy density of the four first order modes resulting in a 4×4 matrix $\mathbf{K}^{\mathrm{L}}$ as follows:

$$\mathbf{K}^{\mathrm{L}} = \left\langle \begin{bmatrix} \mathbf{V}^{\mathrm{L}}_0 \\ \mathbf{V}^{\mathrm{L}}_1 \end{bmatrix}, \begin{bmatrix} \mathbf{V}^{\mathrm{L}}_0 \\ \mathbf{V}^{\mathrm{L}}_1 \end{bmatrix} \right\rangle_E \tag{32}$$

From the four dimensional subspace $\mathbf{K}^{\mathrm{L}}$ we can now extract eigenvalues and eigenvectors in order to identify and separate the rigid modes $\mathbf{V}^{\mathrm{L}_R}$ from the strain modes $\mathbf{V}^{\mathrm{L}_E}$. As a bonus the extensional and torsional modes are separated into individual principal eigenmodes as well. The rigid body motions have zero eigenvalues whereas extension and torsion modes have separate eigenvalues related to axial stiffness and torsional stiffness. The full polynomial vector space takes the following form:

$$\mathbb{V} = \left[\begin{array}{cc|ccc} \cdot & \cdot & \cdot & \cdot & \mathbf{V}^{\mathrm{S}}_3 \\ \cdot & \cdot & \cdot & \mathbf{V}^{\mathrm{B}}_2 & \mathbf{V}^{\mathrm{S}}_2 \\ \cdot & \mathbf{V}^{\mathrm{L}_R}_1 & \mathbf{V}^{\mathrm{L}_E}_1 & \mathbf{V}^{\mathrm{B}}_1 & \mathbf{V}^{\mathrm{S}}_1 \\ \mathbf{V}^{\mathrm{C}}_0 & \mathbf{V}^{\mathrm{L}_R}_0 & \mathbf{V}^{\mathrm{L}_E}_0 & \mathbf{V}^{\mathrm{B}}_0 & \mathbf{V}^{\mathrm{S}}_0 \end{array}\right] \begin{array}{l} \\ \\ \\ \\ \end{array} \tag{33}$$

$$\underbrace{\qquad\qquad}_{\text{Rigid modes}} \quad \underbrace{\qquad\qquad\qquad}_{\text{Strain modes}}$$

b) Remove lower order strain modes from higher order strain modes

Since the higher order strain modes are contaminated by parts of lower order strain modes the next step is to remove this contamination. For this purpose, we will use a matrix projection procedure with an adequate inner product related to the energy. Since both the linear strain modes and the second order bending strain modes correspond to constant strain and constant strain energy density we will use the inner product defined in equation (31). Furthermore, we will use dots below a matrix symbol to indicate the updated matrix, however, in the following subsections with independent operations we will discard the dots of previous subsections. Thus, subtracting the linear strain modes from the bending modes can be done as shown here:

$$\dot{\mathbf{V}}^{\mathrm{B}} = \mathbf{V}^{\mathrm{B}} - \mathbf{V}^{\mathrm{L}_E}\, \boldsymbol{\mathcal{P}}^{\mathrm{L}_E\mathrm{B}}_E \tag{34}$$

in which $\boldsymbol{\mathcal{P}}^{\mathrm{L}_E\mathrm{B}}_E$ is given by:

$$\boldsymbol{\mathcal{P}}^{\mathrm{L}_E\mathrm{B}}_E = \left\langle \begin{bmatrix} \mathbf{V}^{\mathrm{L}_E}_0 \\ \mathbf{V}^{\mathrm{L}_E}_1 \end{bmatrix}, \begin{bmatrix} \mathbf{V}^{\mathrm{L}_E}_0 \\ \mathbf{V}^{\mathrm{L}_E}_1 \end{bmatrix} \right\rangle^{-1}_E \left\langle \begin{bmatrix} \mathbf{V}^{\mathrm{L}_E}_0 \\ \mathbf{V}^{\mathrm{L}_E}_1 \end{bmatrix}, \begin{bmatrix} \mathbf{V}^{\mathrm{B}}_0 \\ \mathbf{V}^{\mathrm{B}}_1 \end{bmatrix} \right\rangle_E \tag{35}$$

The inner strain products in the angular brackets were defined in equation (31).

Similar, linear strain and second order bending are removed from the third order modes using:

$$\dot{\mathbf{V}}^{\mathrm{S}} = \mathbf{V}^{\mathrm{S}} - \left(\mathbf{V}^{\mathrm{L}_E}\, \boldsymbol{\mathcal{P}}^{\mathrm{L}_E\mathrm{S}}_E + \dot{\mathbf{V}}^{\mathrm{B}}\, \boldsymbol{\mathcal{P}}^{\mathrm{BS}}_E\right) \tag{36}$$

where

$$\boldsymbol{\mathcal{P}}^{\mathrm{L}_E\mathrm{S}}_E = \left\langle \begin{bmatrix} \mathbf{V}^{\mathrm{L}_E}_0 \\ \mathbf{V}^{\mathrm{L}_E}_1 \end{bmatrix}, \begin{bmatrix} \mathbf{V}^{\mathrm{L}_E}_0 \\ \mathbf{V}^{\mathrm{L}_E}_1 \end{bmatrix} \right\rangle^{-1}_E \left\langle \begin{bmatrix} \mathbf{V}^{\mathrm{L}_E}_0 \\ \mathbf{V}^{\mathrm{L}_E}_1 \end{bmatrix}, \begin{bmatrix} \mathbf{V}^{\mathrm{S}}_0 \\ \mathbf{V}^{\mathrm{S}}_1 \end{bmatrix} \right\rangle_E \tag{37}$$

and

$$\boldsymbol{\mathcal{P}}^{\mathrm{BS}}_E = \left\langle \begin{bmatrix} \dot{\mathbf{V}}^{\mathrm{B}}_0 \\ \dot{\mathbf{V}}^{\mathrm{B}}_1 \end{bmatrix}, \begin{bmatrix} \dot{\mathbf{V}}^{\mathrm{B}}_0 \\ \dot{\mathbf{V}}^{\mathrm{B}}_1 \end{bmatrix} \right\rangle^{-1}_E \left\langle \begin{bmatrix} \dot{\mathbf{V}}^{\mathrm{B}}_0 \\ \dot{\mathbf{V}}^{\mathrm{B}}_1 \end{bmatrix}, \begin{bmatrix} \mathbf{V}^{\mathrm{S}}_0 \\ \mathbf{V}^{\mathrm{S}}_1 \end{bmatrix} \right\rangle_E \tag{38}$$

Now we have made sure that the strain modes are pure, however, bending and shear modes are not in principal directions and the modes may also be contaminated by rigid modes.

c) Find principal bending modes from the second order modes

At the present stage we have sorted the modes into rigid modes and strain modes according to order. Pure extension and restrained torsion have been found. However, the bending modes and shear modes do not reflect bending about principal axes. Let us therefore extract a 2×2 stiffness matrix: $\mathbf{K}^{\mathrm{B}}$ from a bending subspace using the inner strain product in terms of equation (31) and the two second order modes in $\mathbf{V}^{\mathrm{B}}$, i.e.

$$\mathbf{K}^{\mathrm{B}} = \left\langle \begin{bmatrix} \mathbf{V}^{\mathrm{B}}_0 \\ \mathbf{V}^{\mathrm{B}}_1 \end{bmatrix}, \begin{bmatrix} \mathbf{V}^{\mathrm{B}}_0 \\ \mathbf{V}^{\mathrm{B}}_1 \end{bmatrix} \right\rangle_E \tag{39}$$

From this two dimensional subspace, we now extract eigenvectors identifying the principal bending modes. Thereby we can find the bending modes related to the principal axes of classic theory. Eigenvalues are related to the bending stiffness's.

Table 4: Pseudo mass matrices of cross section elements

$\mathbf{m}^{el}_{ww} = \int_0^{b_{el}} \Big(t_{el}\mathbf{N}_n^{\mathsf{T}}\mathbf{N}_n + t_{el}\mathbf{N}_s^{\mathsf{T}}\mathbf{N}_s + \frac{1}{12}t_{el}^3\mathbf{N}_{n,s}^{\mathsf{T}}\mathbf{N}_{n,s} \Big) ds$
$\mathbf{m}^{el}_{\Omega\Omega} = \int_0^{b_{el}} \Big(t_{el}\mathbf{N}_\Omega^{\mathsf{T}}\mathbf{N}_\Omega + \frac{1}{12}t_{el}^3\mathbf{N}_\alpha^{\mathsf{T}}\mathbf{N}_\alpha \Big) ds$

d) Find shear modes following the principal axis of bending

The shear modes correspond to the third order modes, which have constant shear strain and linear varying bending shear. Thus, the bending terms are related to the quadratic energy terms (z^2-terms). Let us therefore extract a 2×2 stiffness matrix: $\mathbf{K}^{\mathrm{S}}$ of the bending part of the third order (shear) subspace again using the inner strain product and the two third order modes as follows:

$$\mathbf{K}^{\mathrm{S}} = \left\langle \begin{bmatrix} \mathbf{V}_1^{\mathrm{S}} \\ \mathbf{V}_2^{\mathrm{S}} \end{bmatrix}, \begin{bmatrix} \mathbf{V}_1^{\mathrm{S}} \\ \mathbf{V}_2^{\mathrm{S}} \end{bmatrix} \right\rangle_E \tag{40}$$

Notice that the inner product uses: $k = l = 1$ in equation (31).

From the two dimensional stiffness subspace related to the linearly varying part of the shear modes we can extract eigenvectors that identify the principal bending modes and thus transform the third order shear modes in accordance with the principal directions of the bending modes of classic beam theory.

e) Transform rigid modes according to principal directions

The principal directions are now given by the translations of the quadratic variation of the bending modes $\mathbf{V}_2^{\mathrm{B}}$ or rather $\mathbf{V}_{2w}^{\mathrm{B}}$, (since $\mathbf{V}_{2\Omega}^{\mathrm{B}}$ can be disregarded due to its diminishing magnitude). Hence, through a matrix projection procedure, it is possible to rearrange the two linear rigid modes to follow the principal axes. As we are operating on a geometric basis, we formulate the projection through a geometric inner product anticipating that the displacements correspond to velocities of a pseudo inertial energy density with unit mass density being found as:

$$\begin{aligned} U_I &= \tfrac{1}{2}\int_A u_n^i u_n^j \;+\; u_s^i u_s^j \;+\; u_z^i u_z^j \; dA \\ &= \tfrac{1}{2} \begin{bmatrix} \mathbf{v}_w^i \psi \\ \mathbf{v}_\Omega^i \eta \end{bmatrix}^{\mathsf{T}} \begin{bmatrix} \mathbf{M}_{ww} & \cdot \\ \cdot & \mathbf{M}_{\Omega\Omega} \end{bmatrix} \begin{bmatrix} \mathbf{v}_w^j \psi \\ \mathbf{v}_\Omega^j \eta \end{bmatrix} \end{aligned} \tag{41}$$

where the pseudo mass matrices $\mathbf{M}_{ww}$ and $\mathbf{M}_{\Omega\Omega}$ are found by assembly of the cross section element mass matrices $\mathbf{m}^{el}_{ww}$ and $\mathbf{m}^{el}_{\Omega\Omega}$ given in table 4.

A geometric inner product, "similar" to the one related to strains in equation (31), is formulated based on the inertial energy U_I substituting the displacement modes from equation (29). Then, a geometric inner product is formulated as:

$$\left\langle \mathbf{V}_k^i, \mathbf{V}_l^j \right\rangle_I = \begin{bmatrix} \mathbf{v}_{kw}^i \\ \mathbf{v}_{k\Omega}^i \end{bmatrix}^{\mathsf{T}} \begin{bmatrix} \mathbf{M}_{ww} & \cdot \\ \cdot & \mathbf{M}_{\Omega\Omega} \end{bmatrix} \begin{bmatrix} \mathbf{v}_{lw}^j \\ \mathbf{v}_{l\Omega}^j \end{bmatrix} \tag{42}$$

where i and j indicates a polynomial family and k and l represents a coefficient number.

Using principles from matrix projection we transform the linear modes using a subspace spanned by the second order parts of the bending modes. The linear modes following principal directions are then found through:

$$\overset{\bullet}{\mathbf{V}}^{\mathrm{L}_R} = \mathbf{V}^{\mathrm{L}_R} \boldsymbol{\mathcal{P}}_I^{\mathrm{L}_R\mathrm{B}} \tag{43}$$

where

$$\boldsymbol{\mathcal{P}}_I^{\mathrm{L}_R\mathrm{B}} = \left\langle \mathbf{V}_1^{\mathrm{L}_R}, \mathbf{V}_1^{\mathrm{L}_R} \right\rangle_I^{-1} \left\langle \mathbf{V}_1^{\mathrm{L}_R}, \mathbf{V}_2^{\mathrm{B}} \right\rangle_I \tag{44}$$

In a similar manner, it is possible to transform the rigid constant modes into principal directions. As a matter of fact, the four directions are already represented in the solution space being the first order part of the linear mode family. Thus, through a matrix projection the constant modes are projected onto the directions given in $\mathbf{V}_1^{\mathrm{L}}$. So,

$$\overset{\bullet}{\mathbf{V}}^{\mathrm{C}} = \mathbf{V}^{\mathrm{C}} \boldsymbol{\mathcal{P}}_I^{\mathrm{CL}} \tag{45}$$

where

$$\boldsymbol{\mathcal{P}}_I^{\mathrm{CL}} = \left\langle \mathbf{V}_0^{\mathrm{C}}, \mathbf{V}_0^{\mathrm{C}} \right\rangle_I^{-1} \left\langle \mathbf{V}_0^{\mathrm{C}}, \mathbf{V}_1^{\mathrm{L}} \right\rangle_I \tag{46}$$

With the above transformation the rigid modes are now directed according to the principal directions.

f) Remove lower order rigid modes from higher order modes

The last modification step missing is to make sure that no higher order modes contain any constant or linear rigid motions.

While the rigid body modes have zero strains we cannot use the procedure from step *b*) and the strain energy density. As a consequence, we need to introduce a separate inner product to remove the contamination in the higher order modes. Hence we use the geometric inner product from equation (42).

First, let us clean the linear rigid modes, i.e. let us remove the contamination with constant rigid modes from the linear rigid modes by:

$$\overset{\bullet}{\mathbf{V}}^{\mathrm{L}_R} = \mathbf{V}^{\mathrm{L}_R} - \mathbf{V}^{\mathrm{C}} \; \boldsymbol{\mathcal{P}}_I^{\mathrm{CL}_R} \tag{47}$$

with

$$\boldsymbol{\mathcal{P}}_I^{\mathrm{CL}_R} = \left\langle \mathbf{V}_0^{\mathrm{C}}, \mathbf{V}_0^{\mathrm{C}} \right\rangle_I^{-1} \left\langle \mathbf{V}_0^{\mathrm{C}}, \mathbf{V}_0^{\mathrm{L}_R} \right\rangle_I \tag{48}$$

Secondly, let us clean the linear strain modes, i.e. let us remove the constant rigid modes from the linear strain modes:

$$\overset{\bullet}{\mathbf{V}}^{\mathrm{L}_E} = \mathbf{V}^{\mathrm{L}_E} - \mathbf{V}^{\mathrm{C}} \; \boldsymbol{\mathcal{P}}_I^{\mathrm{CL}_E} \tag{49}$$

with

$$\boldsymbol{\mathcal{P}}_I^{\mathrm{CL}_E} = \left\langle \mathbf{V}_0^{\mathrm{C}}, \mathbf{V}_0^{\mathrm{C}} \right\rangle_I^{-1} \left\langle \mathbf{V}_0^{\mathrm{C}}, \mathbf{V}_0^{\mathrm{L}_E} \right\rangle_I \tag{50}$$

Then, we clean the second order modes:

$$\overset{\bullet}{\mathbf{V}}^{\mathrm{B}} = \mathbf{V}^{\mathrm{B}} - \left(\mathbf{V}^{\mathrm{C}} \; \boldsymbol{\mathcal{P}}_I^{\mathrm{CB}} \;+\; \overset{\bullet}{\mathbf{V}}^{\mathrm{L}_R} \; \boldsymbol{\mathcal{P}}_I^{\mathrm{L}_R\mathrm{B}} \right) \tag{51}$$

with

$$\boldsymbol{\mathcal{P}}_I^{\mathrm{CB}} = \left\langle \mathbf{V}_0^{\mathrm{C}}, \mathbf{V}_0^{\mathrm{C}} \right\rangle_I^{-1} \left\langle \mathbf{V}_0^{\mathrm{C}}, \underset{\bullet}{\mathbf{V}}_0^{\mathrm{B}} \right\rangle_I \tag{52}$$

and

$$\boldsymbol{\mathcal{P}}_I^{\mathrm{L}_R\mathrm{B}} = \left\langle \underset{\bullet}{\mathbf{V}}_1^{\mathrm{L}_R}, \underset{\bullet}{\mathbf{V}}_1^{\mathrm{L}_R} \right\rangle_I^{-1} \left\langle \underset{\bullet}{\mathbf{V}}_1^{\mathrm{L}_R}, \underset{\bullet}{\mathbf{V}}_1^{\mathrm{B}} \right\rangle_I \tag{53}$$

Finally, we clean the third order modes through:

$$\underset{\bullet\bullet}{\mathbf{V}}^{\mathrm{S}} = \underset{\bullet}{\mathbf{V}}^{\mathrm{S}} - \left(\mathbf{V}^{\mathrm{C}}\ \boldsymbol{\mathcal{P}}_I^{\mathrm{CS}} \ +\ \underset{\bullet}{\mathbf{V}}^{\mathrm{L}_R}\ \boldsymbol{\mathcal{P}}_I^{\mathrm{L}_R\mathrm{S}} \right) \tag{54}$$

with

$$\boldsymbol{\mathcal{P}}_I^{\mathrm{CS}} = \left\langle \mathbf{V}_0^{\mathrm{C}}, \mathbf{V}_0^{\mathrm{C}} \right\rangle_I^{-1} \left\langle \mathbf{V}_0^{\mathrm{C}}, \underset{\bullet}{\mathbf{V}}_0^{\mathrm{S}} \right\rangle_I \tag{55}$$

and

$$\boldsymbol{\mathcal{P}}_I^{\mathrm{L}_R\mathrm{S}} = \left\langle \underset{\bullet}{\mathbf{V}}_1^{\mathrm{L}_R}, \underset{\bullet}{\mathbf{V}}_1^{\mathrm{L}_R} \right\rangle_I^{-1} \left\langle \underset{\bullet}{\mathbf{V}}_1^{\mathrm{L}_R}, \underset{\bullet}{\mathbf{V}}_1^{\mathrm{S}} \right\rangle_I \tag{56}$$

Displacement formulation of polynomial modes

Having completed the steps *a*) through *f*) we can assemble the fundamental polynomial solutions into a practical displacement formulation. For us a practical displacement formulation allows the use of the Hadarmard product in which the amplitude functions are in the form of a diagonal matrix. Let us therefore introduce a polynomial displacement vector $\mathbf{V}_p$ consisting of the four block matrices of $\mathbb{V}$ in a row of blocks:

$$\mathbf{V}_p = \left[\begin{array}{cccc} \mathbf{V}_3 & \mathbf{V}_2 & \mathbf{V}_1 & \mathbf{V}_0 \end{array} \right] \tag{57}$$

Furthermore, let us introduce $\mathbf{I}_p$ as a $n_z \times n_z = 12 \times 12$ diagonal unit matrix. This allows us to write the displacement formulation of the fundamental polynomial modes as follows:

$$\begin{aligned} \mathbf{u}_p &= \begin{bmatrix} \mathbf{V}_3 \\ \mathbf{V}_2 \\ \mathbf{V}_1 \\ \mathbf{V}_0 \end{bmatrix}^{\mathsf{T}} \begin{bmatrix} \frac{1}{6}z^3\mathbf{I}_p & \cdot & \cdot & \cdot \\ \cdot & \frac{1}{2}z^2\mathbf{I}_p & \cdot & \cdot \\ \cdot & \cdot & z\mathbf{I}_p & \cdot \\ \cdot & \cdot & \cdot & \mathbf{I}_p \end{bmatrix} \begin{bmatrix} \mathbf{I}_p \\ \mathbf{I}_p \\ \mathbf{I}_p \\ \mathbf{I}_p \end{bmatrix} \mathbf{c}_p \\ &= \mathbf{V}_p\ \boldsymbol{\Psi}_p\ \mathbf{T}_p\ \mathbf{c}_p \end{aligned} \tag{58}$$

where we have taken the liberty to introduce the diagonal matrix $\boldsymbol{\Psi}_p$ that contains all polynomial amplitude functions and a polynomial transformation matrix $\mathbf{T}_p$. The column vector $\mathbf{c}_p$ holds the $n_z = 12$ constants belonging to each fundamental displacement mode. These constants are the constants belonging to each of the (mode) solutions to the differential equations and are to be determined by the use of boundary conditions.

3.3. Full displacement formulation

Finally, the full displacement solution encompassing both exponential and fundamental polynomial modes can be found. The exponential modes found in equation (19) may also be written as:

$$\mathbf{u}_e = \mathbf{V}_e\ \boldsymbol{\Psi}_e\ \mathbf{I}_e\ \mathbf{c}_e \tag{59}$$

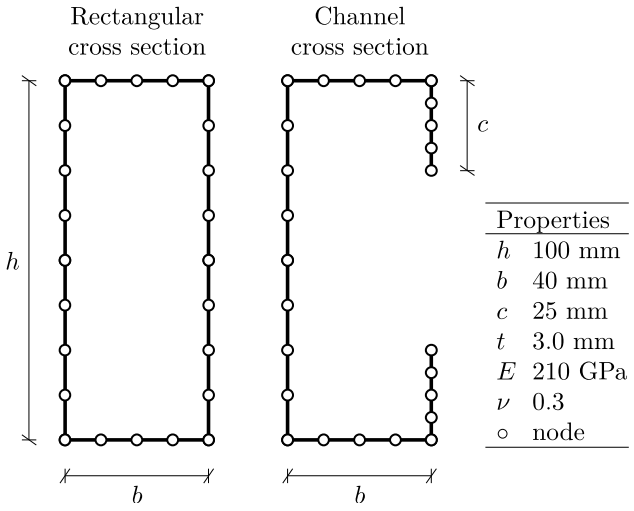

Figure 5: Geometrical and material properties of the rectangular cross section and the lipped channel cross section.

where $\mathbf{I}_e$ is just a "dummy" unit matrix of size $n_e \times n_e$that allows us to write the full displacement solution as:

$$\begin{aligned} \mathbf{u} = \mathbf{u}_p + \mathbf{u}_e &= \mathbf{V}\ \boldsymbol{\Psi}\ \mathbf{T}_c\ \mathbf{c} \\ &= \left[\begin{array}{cc} \mathbf{V}_p & \mathbf{V}_e \end{array} \right] \begin{bmatrix} \boldsymbol{\Psi}_p & \cdot \\ \cdot & \boldsymbol{\Psi}_e \end{bmatrix} \begin{bmatrix} \mathbf{T}_p & \cdot \\ \cdot & \mathbf{I}_e \end{bmatrix} \begin{bmatrix} \mathbf{c}_p \\ \mathbf{c}_e \end{bmatrix} \end{aligned} \tag{60}$$

In which we have introduced $\mathbf{V}$ as the full mode matrix, $\boldsymbol{\Psi}$ as the full diagonal amplitude matrix and $\mathbf{T}_c$ as a constant transformation matrix containing $\mathbf{T}_p$ and $\mathbf{I}_e$. This concludes the cross section mode determination procedure. Note that since each fundamental mode is a combination of four cross section displacement fields $\mathbf{v}_1^i$ to $\mathbf{v}_4^i$ the number of columns in $\mathbf{V}$ is: $4n_z+(2n-n_z) = 4n_z+n_e$, where n is the number of degrees of freedom in the cross section, n_z is the number of fundamental modes, and n_e the number of exponential modes. However, the number of constants $\mathbf{c}$ is $2n = n_z + n_e$.

4. Results of the mode determination procedure

Using the approach just presented within this paper, it is possible to identify all eigenmodes of a thin-walled beam with an arbitrary shaped cross section, based on simple elastic constitutive relations and an appropriate discritization of the cross section. In the following, results from the mode determination procedure will be presented for a rectangular cross section and a channel cross section. The cross section discretization and geometrical as well as material properties are shown in figure 5 for both cross sections. In the rectangular cross section analysed, there are 24 nodes with six degrees of freedom each giving a total of $2 \cdot 144$ modes of which 12 are the fundamental modes. In the channel cross section analysed, there are 25 nodes with six degrees of freedom resulting in a total of $2 \cdot 150$ deformation modes.

Table 5: First twenty-two non-null eigenvalues, i.e. $\lambda \neq 0$

	Rectangular cross section	Channel cross section
13	$0.0065 + 0.0060i$	0.0011
14	$0.0065 - 0.0060i$	-0.0011
15	$-0.0065 + 0.0060i$	$0.0058 + 0.0046i$
16	$-0.0065 - 0.0060i$	$0.0058 - 0.0046i$
17	$0.0363 + 0.0144i$	$-0.0058 + 0.0046i$
18	$0.0363 - 0.0144i$	$-0.0058 - 0.0046i$
19	$-0.0363 + 0.0144i$	$0.0079 + 0.0067i$
20	$-0.0363 - 0.0144i$	$0.0079 + 0.0067i$
21	$0.0366 + 0.0136i$	$-0.0079 + 0.0067i$
22	$0.0366 - 0.0136i$	$-0.0079 - 0.0067i$
23	$-0.0366 + 0.0136i$	0.0373
24	$-0.0366 - 0.0136i$	-0.0373
25	$0.0374 + 0.0186i$	0.0388
26	$0.0374 - 0.0186i$	-0.0388
27	$-0.0374 + 0.0186i$	$0.0374 + 0.0170i$
28	$-0.0374 - 0.0186i$	$0.0374 + 0.0170i$
29	$0.0401 + 0.0193i$	$-0.0374 + 0.0170i$
30	$0.0401 - 0.0193i$	$-0.0374 - 0.0170i$
31	$-0.0401 + 0.0193i$	$0.0394 + 0.0164i$
32	$-0.0401 - 0.0193i$	$0.0394 + 0.0164i$
33	0.0616	$0.0394 + 0.0164i$
34	-0.0616	$0.0394 + 0.0164i$

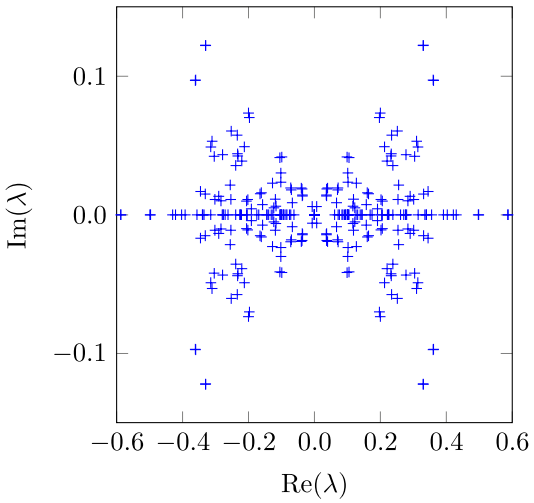

Figure 6: Plot of eigenvalues for the rectangular cross section

4.1. Exponential modes

To find the exponential modes we solve the quadratic eigenvalue problem in equation (18) using the state vector approach. This results in a pool of eigenvalues of which twelve are null, some are real pairs and others are complex quadruples. The first twenty-two non-null eigenvalues are listed in table 5 for both cross sections. These eigenvalues may be presented in the complex plane as shown in figure 6 for the rectangular cross section and in figure 7 for the channel cross section. From these figures, it is seen how the pairs of real eigenvalues $\{\lambda, -\lambda\}$ lay on the horizontal axis with Im(λ)=0, whereas the complex quadruple eigenvalues, i.e. pairs of complex conjugated eigenvalues, $\{\lambda, \overline{\lambda}, -\lambda, -\overline{\lambda}\}$, are those points which are distributed double-symmetrically in the complex plane. The eigenvalues can be seen as an inverse length scale related to the attenuation for the real part and to the period of the harmonic variations for the imaginary part. The first three sets of related amplitude functions are shown in figure 8 for the rectangular cross section and figure 9 for the channel cross section. Each row in these figures corresponds to either a couple or quadruple set of eigenvalues in which we use: $f(z) = e^{\lambda z}$ for eigenvalues with a negative real part and: $f(z) = e^{\lambda(z-\ell)}$ for eigenvalues with a positive real part, where ℓ is the beam length. These functions are also used in the amplitude matrix to limit the numerical magnitude of the exponential function. It can be seen how the imaginary parts yield positive or negative oscillation along the beam axis.

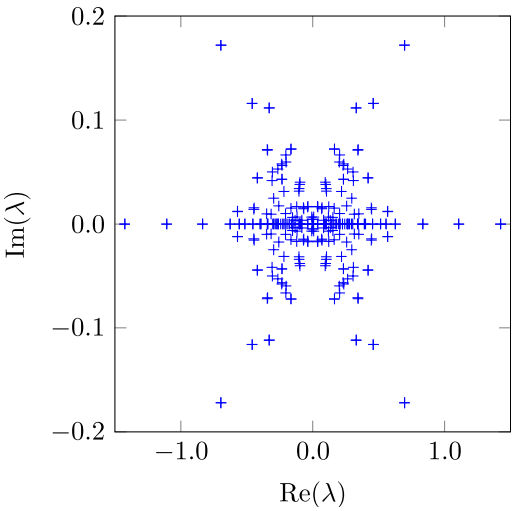

Figure 7: Plot of eigenvalues for the channel cross section

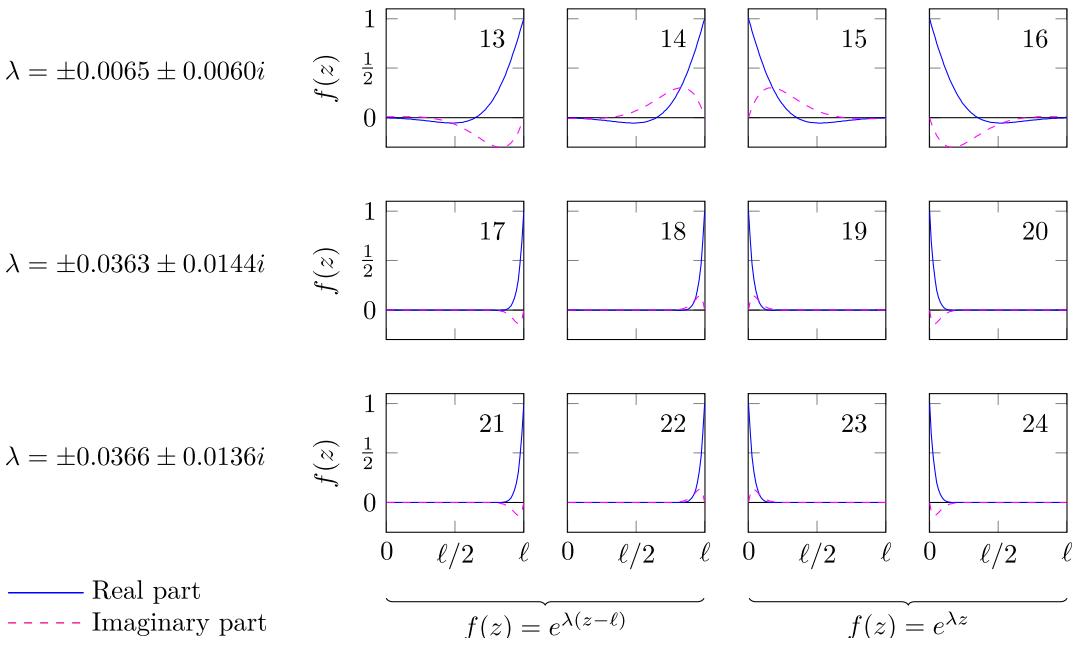

Figure 8: Amplitude functions for rectangular cross section eigenmodes (with a beam length of $\ell = 750$mm)

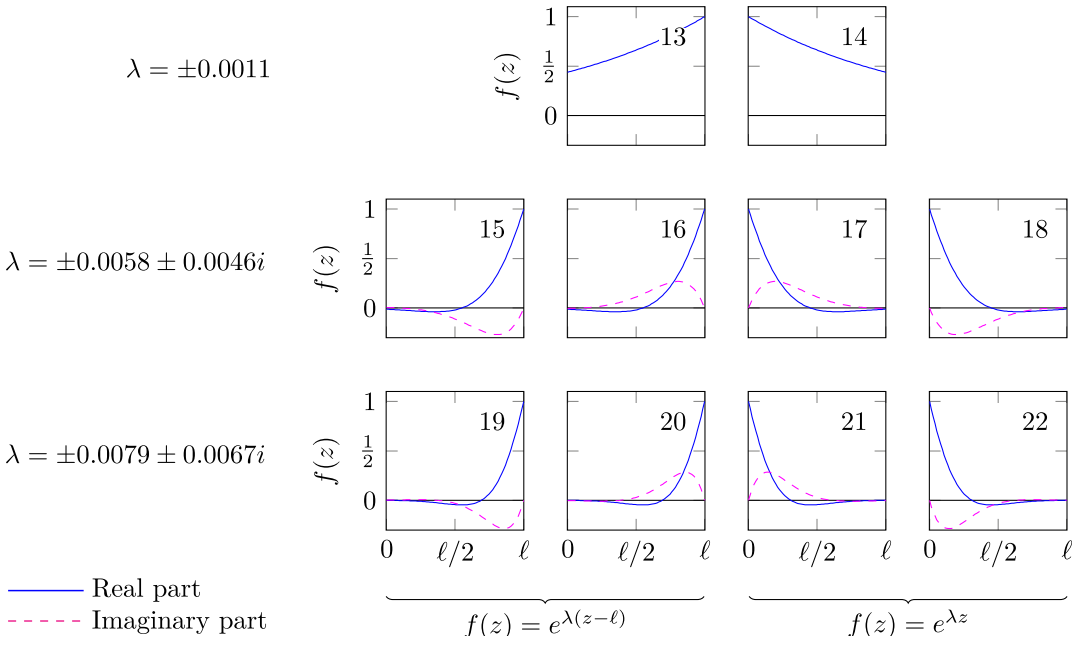

Figure 9: Amplitude functions for channel cross section eigenmodes (with a beam length of $\ell = 750$mm)

Figures 10 and 11 illustrates the first 22 exponential displacement modes of the two cross sections. The displacement modes are separated into transverse displacements and warping displacements and the modes are ordered according to their attenuation length in an increasing order. As mentioned the modes are normalized in such a way that the real, largest displacement in either the X- or Y-direction is set to unity for the transverse displacements. To be able to see the imaginary part of a mode it is scaled by a factor "scale" given below the illustration. The magnitude of the warping part of a mode depends on the normalization of the transverse displacement. We therefore need to scale the warping modes by the ratio between maximum transverse displacement and maximum warping displacement to be able to plot them corresponding to a unit out of plane deformation. Hence, the "ratio" is given in the figure below the real part of the warping mode. We also need to separately "scale" the imaginary parts of the warping displacements – also given as a "scale".

For the channel cross section it is worth noting that the first mode with the longest attenuation length is the classic exponential part of restrained torsion, i.e. with rotation and warping of the cross section (giving normal stresses). Furthermore, it is notable that the rectangular cross section does not have this kind of mode and therefore restrained torsion of the rectangular cross section will involve distortion of the cross section as well.

The quadruple complex exponential modes can be transformed into four coupled real modes with a procedure presented by Jönsson and Andreassen [14]. To illustrate this two of these four modes with attenuation towards the other end are shown in figures 12a and 12b for the rectangular cross section mode 13 through 14 and in figures 12c and 12d for the channel cross section modes 19 through 20. In both cases a beam length of $\ell = 750$ mm has been used for the illustration.

It can be seen that the eigenvalues that come in pairs are associated displacement modes, which have one cross section displacement field which attenuates in one or the other axial direction. Furthermore, the quadruple eigenvalues correspond to complex displacement modes which consist of one real cross section displacement field plus or minus one imaginary cross section displacement field, which may be combined corresponding to two different types of attenuations, one in each direction. Thus, the modes of the quadruple complex eigenvalues correspond to two cross section deformation fields, which are combined with the amplitude functions into four different spatial beam displacement modes.

4.2. Fundamental modes

The fundamental modes are found as the null space of $\mathbb{K}$ being the set of equilibrium equations to be fulfilled by the polynomial displacement modes up to third order. In the null space we then find modes of different polynomial order using SVD on the block related to a given order. Then we follow the procedure *a)* through *f)* to separate rigid body modes and strain modes and to identify the different fundamental modes illustrated in figure 4. The figures 13 and 14 illustrates these modes by only showing the relevant, either transverse displacement field or the warping displacement field depending on which is largest. In our case one of these always diminishes by a factor of about 10^{-3} or less. Furthermore we do not show displacements which are numerically so small that they are irrelevant, i.e. in our case a factor of 10^{-12} lower than the relevant part of the mode (dependent on machine precision). All displacement plots have been scaled to a maximum unit displacement. Therefore, for example in the illustration of a pure bending mode 9 in figure 13 or 14, the magnitude of the constant transverse displacements $\mathbf{v}_0^9$ related to the Poisson effect is in reality much smaller than shown compared to the quadratic transverse displacements $\mathbf{v}_2^9$.

It is very interesting, from an engineering point of view, to take a closer look at these cross section displacement fields. It can be seen that there are twelve fundamental modes combining twelve independent cross section displacement fields. The independent cross section displacement fields are identified in the bottom line of the figures corresponding to $\mathbf{V}_0$. Thus, with the theory of this paper the fundamental polynomial displacements of a thin-walled beam is described by twelve cross section displacement fields and not the conventional six or seven cross section displacement fields of three dimensional beam theory or three dimensional Vlasov beam theory, respectively. The six cross section displacement fields of classic beam theory are the 3 warping modes i.e. axial extension + two flexural and 3 transverse modes corresponding to pure axial extension and two flexural

5. Conclusion

The theory behind the novel prismatic thin-walled beam model including deformable cross sections, shear deformations and the Poisson effect has been introduced. Furthermore, a new mode determination procedure for determination of both exponential distortional displacement modes and the fundamental beam displacement modes has been presented and the modes have been illustrated in the results section. The new developments are especially related to the procedure used in determining and separating the fundamental modes mathematically and numerically. The novelty of the procedure lies in the use of both strain energy and the geometric based products relating to the order of the polynomial terms within each of the fundamental modes. Furthermore, the exponential modes presented do not decouple the original coupled quadratic differential equations, but they represent the full solution space, and decouple a related set of first order differential equations, as in Jönsson and Andreassen [14]. However, the shear and Poisson effects are now included in all modes of the present formulation and the fundamental modes are not simple solutions based on additional constraint assumptions.

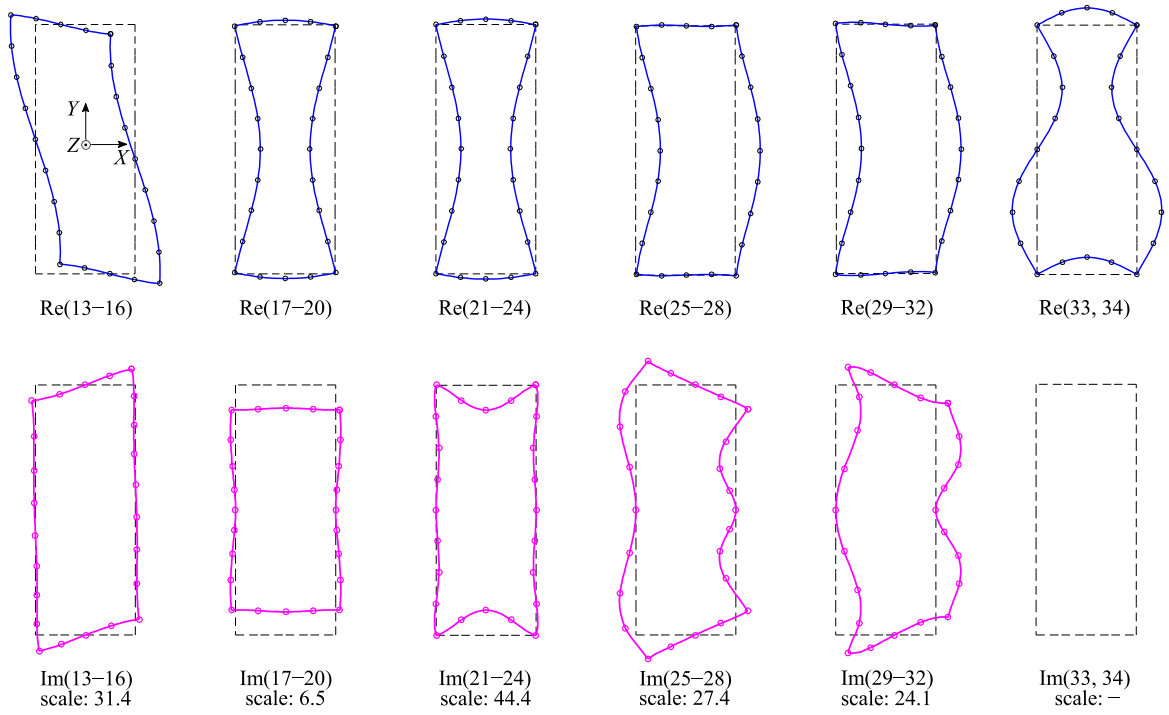

(a) Transverse displacements

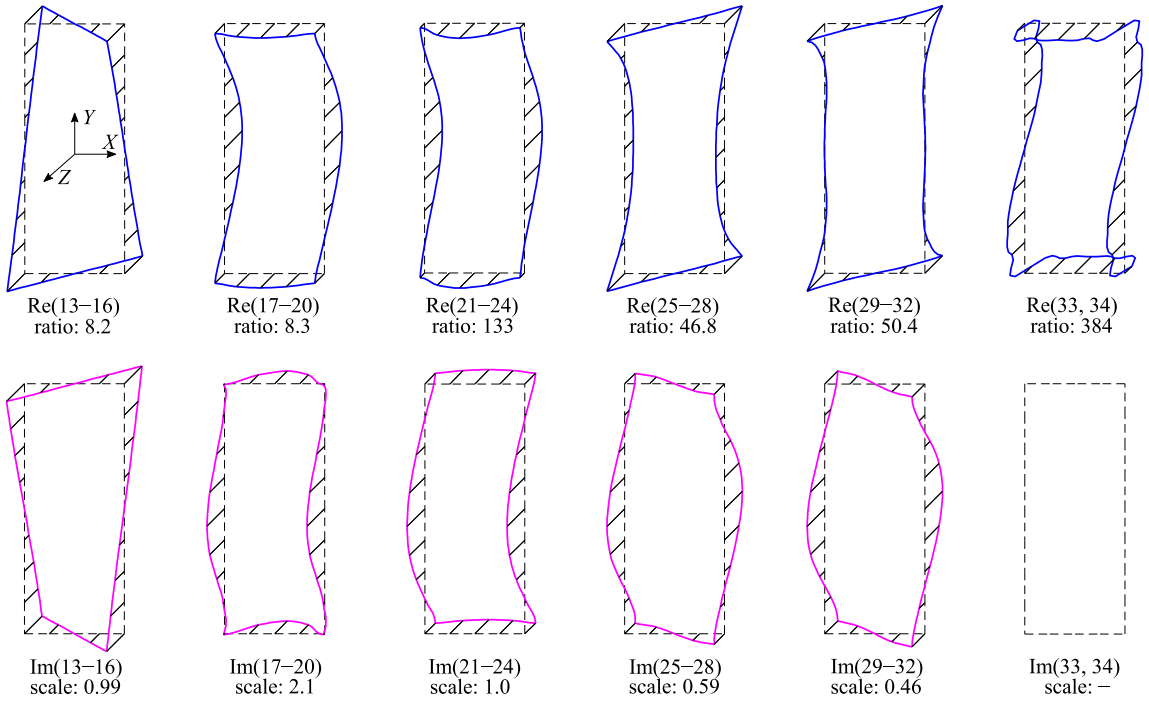

(b) Warping displacements

Figure 10: Exponential modes – Rectangular cross section

All the classic beam deformation modes have been found by the procedure and it is interesting and worth noting that restrained torsion is represented among the exponential solutions as a pure twist of open cross sections (such as the channel cross section) with the same warping function shape as the fundamental solution of unrestrained torsion. Specially noteworthy is it that for closed cross sections, this is not the case.

It is also noteworthy, by observation of figures 13 and 14, that it seems that the twelve fundamental solutions being combinations of one to four different cross section displacement fields are simple combinations of twelve cross

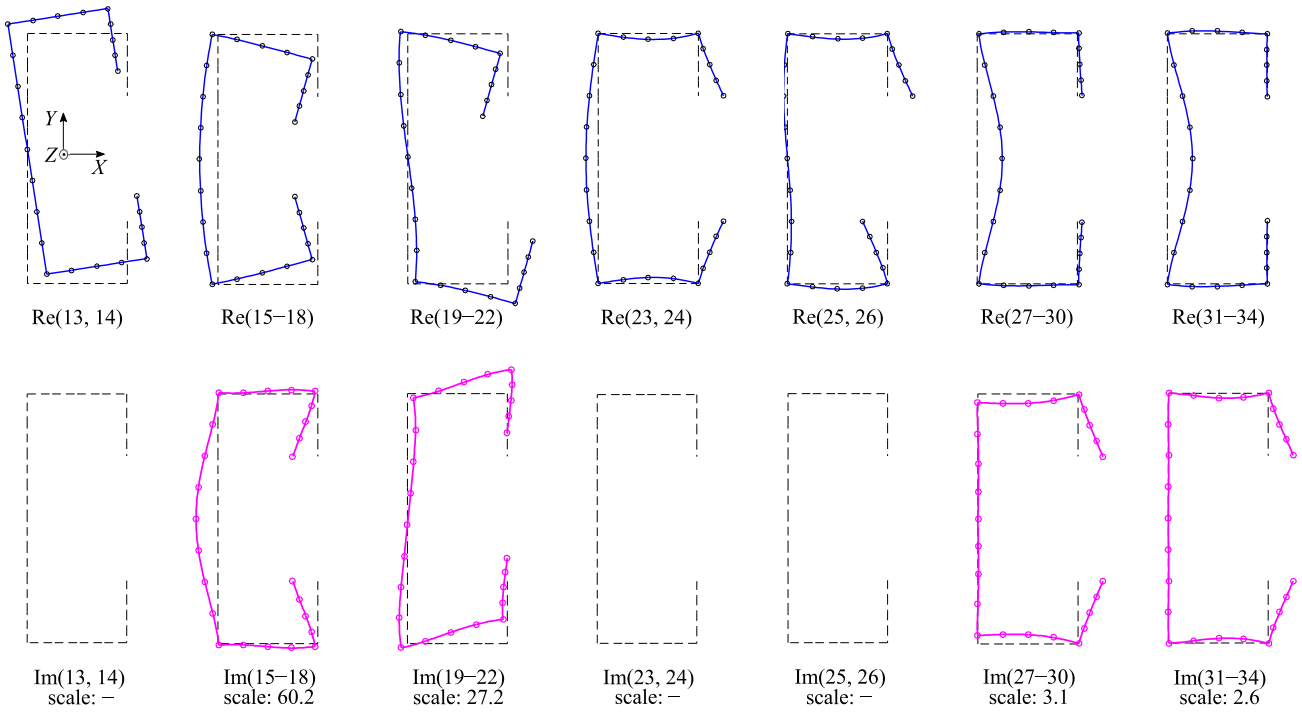

(a) Transverse displacements

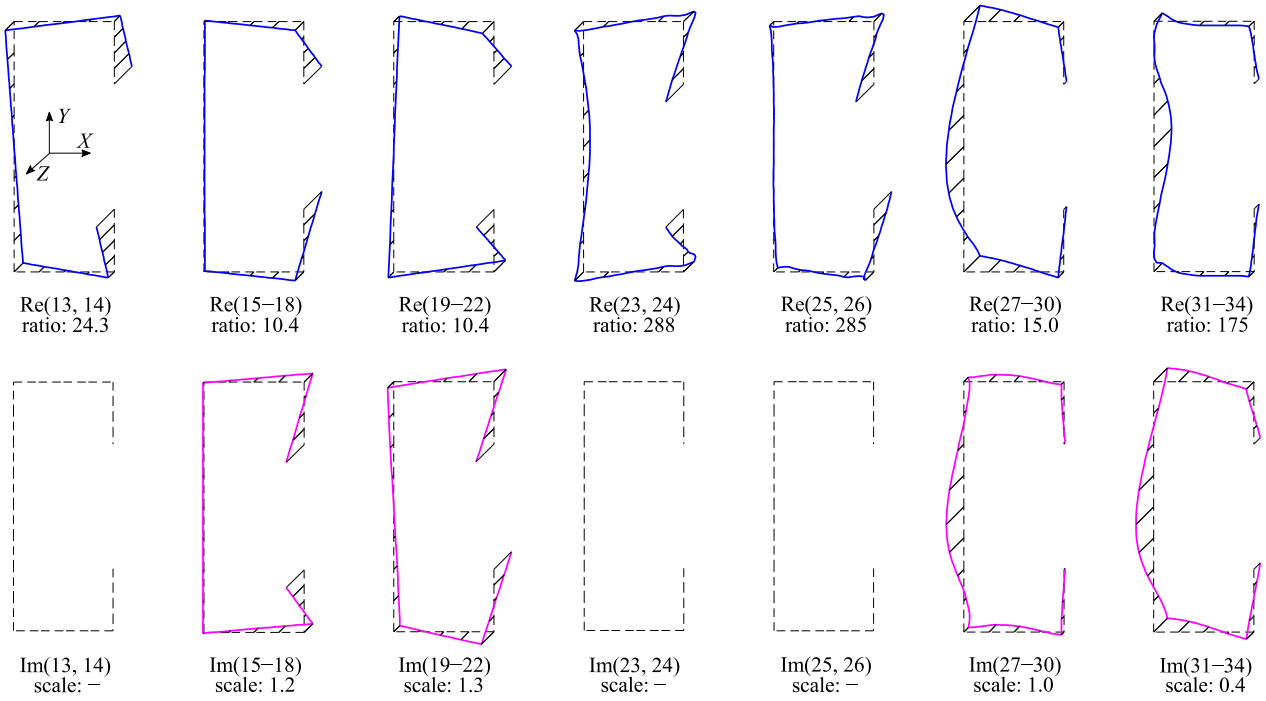

(b) Warping displacements

Figure 11: Exponential modes – Channel cross section

section displacement fields.

It is interesting that the defined internal strain energy products also can be used to find the principal direction of bending thereby giving a direct link to classic beam theory and perhaps also to the cross section properties. This link and the relation of the boundary conditions to the classic section forces of beam theory is the focus of the continued research. With the determination of all the displacement modes it is now possible to continue the research and formulate an advanced beam element based on exact axial

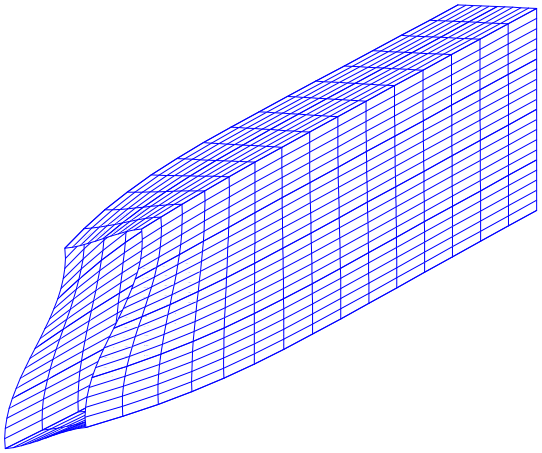

(a) The first real combination of mode 13 and 14 with respect to the rectangular cross section

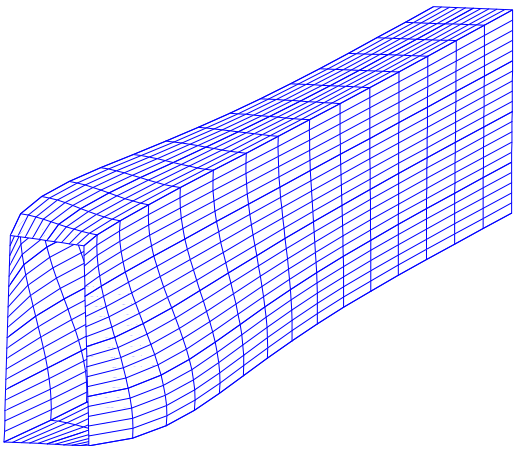

(b) The second real combination of mode 13 and 14 with respect to the rectangular cross section

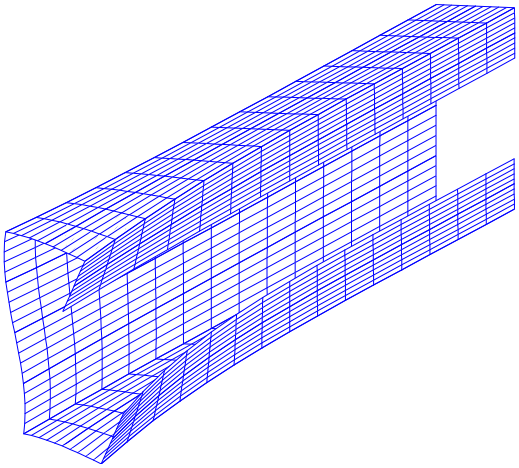

(c) The first real combination of mode 19 and 20 regarding the channel section

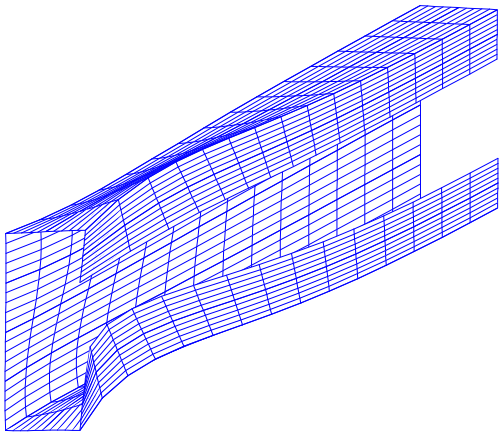

(d) The second real combination of mode 19 and 20 regarding the channel section

Figure 12: Quadruple complex distortional eigenmodes illustrated as real coupled modes

shape functions and the possibility of just choosing a reduced number of displacement modes.

6. Acknowledgement

The work presented in this paper has been supported financially by the Danish engineering consultancy NIRAS A/S and the Innovation Fund Denmark by grant: 5189-00005B.

References

[1] V. Z. Vlasov, Thin-Walled Elastic Beams, 2nd Edition, Jerusalem, 1961, israel Program for scientific translations.

[2] R. Schardt, Eine erweiterung der technishen biegelehre für die berechnung biegestreifer prismatischer falfwerke, Der Stahlbau 35 (1966) 161–171.

[3] R. Schardt, Verallgemeinerte Technische Biegetheorie - Band 1, Lineare Theorie, 2nd Edition, Metrum-Verlag,Darmstadt, 1989.

[4] J. M. Davies, P. Leach, First-order generalised beam theory, Journal of Constructional Steel Research 31 (1994) 187–220. doi:10.1016/0143-974X(94)90010-8.

[5] J. M. Davies, P. Leach, D. Heinz, Second-order generalised beam theory, Journal of Constructional Steel Research 31 (1994) 221–241. doi:10.1016/0143-974X(94)90011-6.

[6] J. Jönsson, Distortional theory of thin-walled beams, Thin-Walled Structures 33 (1999) 269–303. doi:10.1016/S0263-8231(98)00050-0.

[7] N. Silvestre, D. Camotim, First-order generalised beam theory for arbitrary orthotropic materials, Thin-Walled Structures 40 (2002) 755–789. doi:10.1016/S0263-8231(02)00025-3.

[8] N. Silvestre, D. Camotim, Nonlinear generalized beam theory for cold-formed steel members, International Journal of Structural Stability and Dynamics 3 (4) (2003) 461–490. doi:10.1142/S0219455403001002.

[9] R. Bebiano, R. Gonçalves, D. Camotim, A cross-section analysis procedure to rationalise and automate the performance of gbt-based structural analyses, Thin-Walled Structures 92 (2015) 29–47. doi:10.1016/j.tws.2015.02.017.

[10] N. Peres, R. Gonçalves, D. Camotim, A cross-section analysis procedure to rationalise and automate the performance of gbt-based structural analyses, Thin-Walled Structures 127 (2018) 769–780. doi:10.1016/j.tws.2018.03.008.

[11] S. Ádány, B. W. Schafer, A full modal decomposition of thin-walled, single-branched open cross-section members via the constrained finite strip method, Journal of Constructional Steel Research 64 (1) (2008) 12–29. doi:10.1016/j.jcsr.2007.04.004.

[12] S. Ádány, N. Silvestre, B. W. Schafer, D. Camotim, GBT and

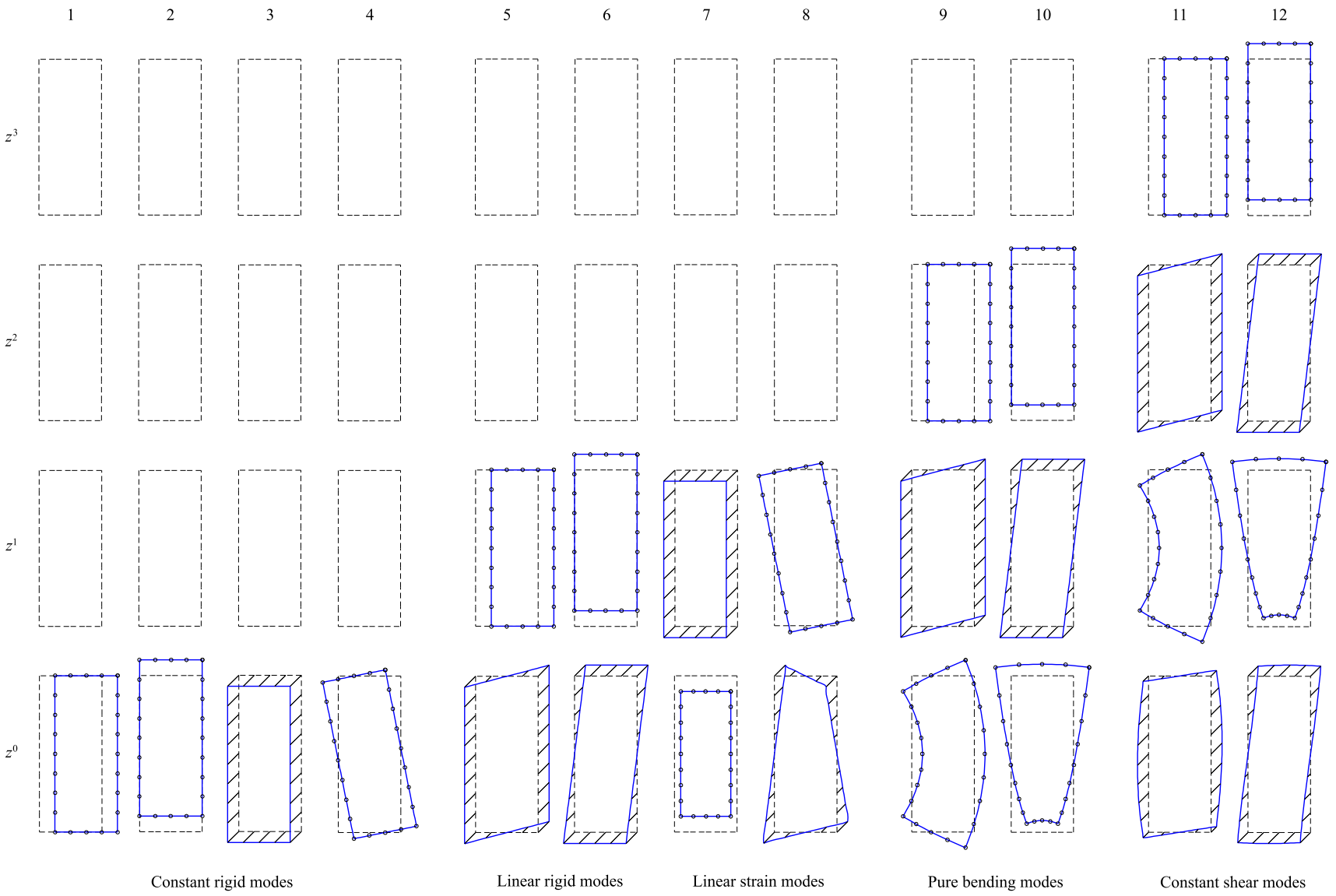

Figure 13: Fundamental modes of the box cross section

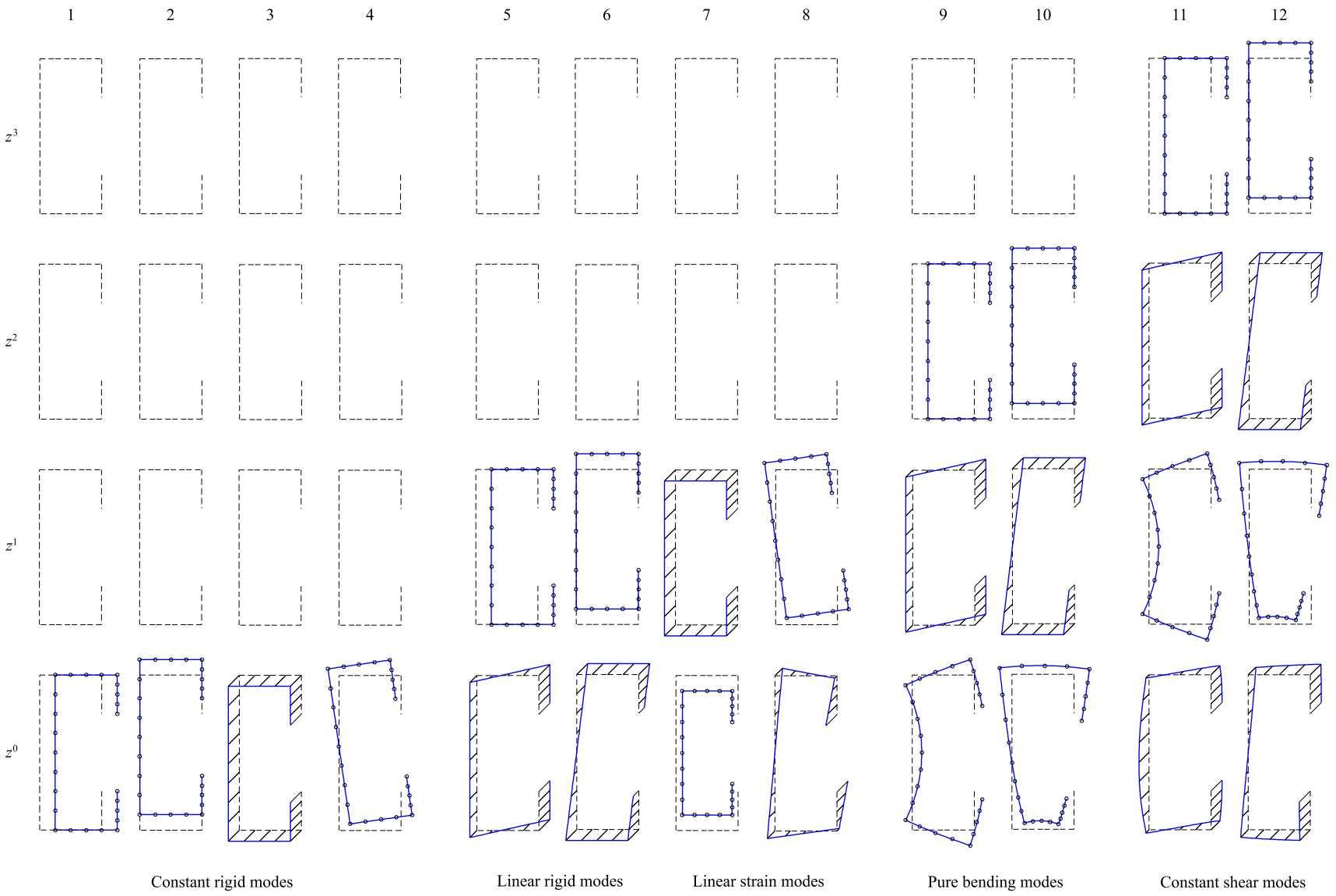

Figure 14: Fundamental modes of the channel cross section

cFSM: Two modal approaches to the buckling analysis of unbranched thin-walled members, Advanced Steel Construction 5 (2) (2009) 195–223.

[13] S. Ádány, Modal identification of thin-walled members with and without holes using CFEM, Proceedings of the Eighths International Conference on Thin-Walled Structures, ICTWS 2018.

[14] J. Jönsson, M. J. Andreassen, Distortional eigenmodes and homogeneous solutions for semi-discretized thin-walled beams, Thin-Walled Structures 49 (2011) 691–707. doi:10.1016/j.tws.2010.12.009.

[15] M. Morandini, M. Chierichetti, P. Mantegazza, Characteristic behavior of prismatic anisotropic beam via generalized eigenvectors, International Journal of Solids and Structures 47 (2010) 1327–1337. doi:10.1016/j.ijsolstr.2010.01.017.

[16] R. F. Vieira, F. B. Virtuoso, E. B. R. Pereira, A higher order model for thin-walled structures with deformable cross-sections, International Journal of Solids and Structures (2014) 575–598doi:10.1016/j.ijsolstr.2013.10.023.

[17] S. de Miranda, A. Gutiérrez, R. Miletta, F. Ubertini, A generalized beam theory with shear deformation, Thin-Walled Structures 67 (2013) 88–100. doi:10.1016/j.tws.2013.02.012.

[18] S. de Miranda, A. Madeo, R. Miletta, F. Ubertini, On the relationship of the shear deformable generalized beam theory with classical and non-classical theories, International Journal of Solids and Structures 51 (2014) 3698–3709. doi:10.1016//j.ijsolstr.2014.07.001.

[19] A. B. Hansen, J. Jönsson, A gbt-framework towards modal modelling of steel structures, John Wiley & Sons, Ltd – ce/papers (2017) 1822–1830doi:10.1002/cepa.226.

[20] R. D. Cook, D. S. Malkus, M. E. Plesha, Concepts and applications of finite element analysis, 3rd Edition, John Wiley & Son, NewYork Chichester Brisbane Toronto Singapore, 1989.

[21] F. Tisseur, K. Meerbergen, The quadratic eigenvalue problem, Society for Industrial and Applied Mathematics 43 (2) (2001) 235–286. doi:10.1.1.32.9042.

[22] MATLAB, MATLAB® and Simulink® used for technical computing, 2016, MATLAB - © 1984-2016 The MathWorks, Inc., Version 2016a.

[23] R. J. de Figueiredo Mendes Vieira, A higher order thin-walled beam model, Ph.D. thesis, Universidade Técnica de Lisboa - Instituto Superior Técnico (2010).

Paper III

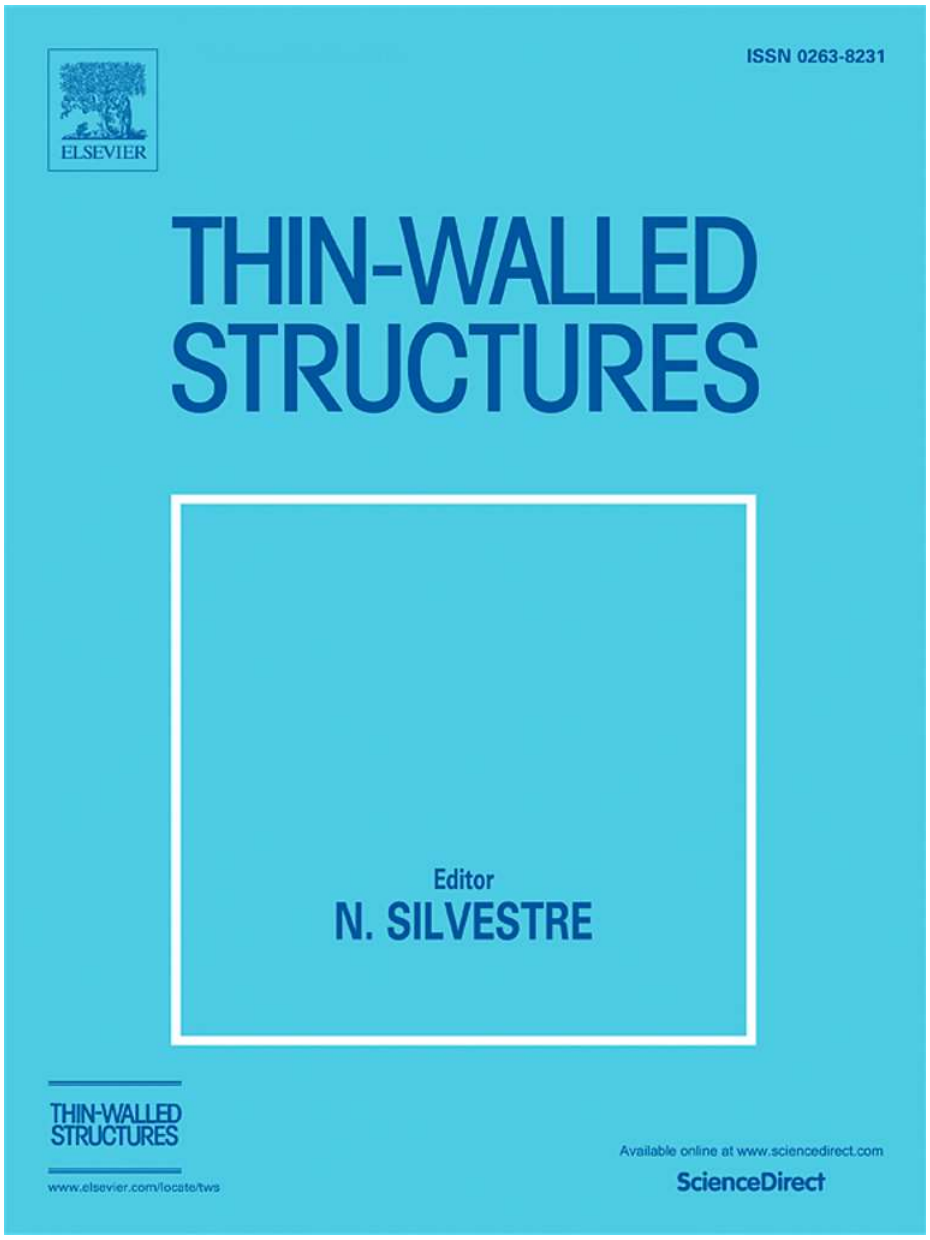

A Thin-Walled Beam Element Based on Semi-Analytical Solution Modes

Anders Bau Hansen[a,b], Jeppe Jönsson[b,*]

[a] *NIRAS A/S, Sortemosevej 19, DK-3450 Allerød, Denmark*
[b] *Technical University of Denmark, Department of Civil Engineering, Brovej Building 118, DK-2800 Kgs. Lyngby, Denmark*

Abstract

Using energy principles, a thin-walled beam element is introduced for the analysis of beams with deformable cross-sections that are prone to distortion. The beam element is based on previously attained semi-analytical displacement solution modes of an advanced thin-walled beam model. The first-order beam element for linear analysis handles shear deformations related to both Timoshenko and Mindlin-Reissner type deformations, warping effects of torsion, cross-section distortion including associated warping effects, as well as the transverse displacement effect from normal stress. The formulation can handle both open and closed cross-sections without special attention. The formulation of the displacement solution modes and the stiffness integration of the products of the advanced displacement modes using the Hadamard product are described. The paper also presents the transformations between modal degrees of freedom and element displacement degrees of freedom. Four examples show the beam element capabilities and good agreement with results obtained using the shell and solid elements of a commercial finite element program. The kinematic assumptions that the thin-walled beam model accommodates leads to local shear stress transfer at corners. This transfer of shear stresses is not normally seen in thin-walled beam formulations or shell models. However, the shear transfer is verified through examination of a finite element model using solid elements.

Keywords: Thin-walled beams, beam element, distortional beam theory, shear deformations, corner shear

1. Introduction

Since the industrialisation of steel production in the late nineteenth-century thin-walled metal members have been utilised in structures such as bridges, buildings, aeroplanes and ships, see [1]. The main reason for this is the high stiffness-to-weight ratio of the thin-walled members. This led to the development of theories enabling analysis and the assessment of such members since it was realised that during flexure and torsion, the beams generated non-negligible normal stresses due to warping displacements of the cross-section. Vlasov introduced the well-known one-dimensional thin-walled beam theory, [2]. With this theory, the torsional warping effects of open thin-walled beams were included. Kollbrunner & Hajdin [3] expanded the theory to include cross-sections with closed cells. In line with the development of the finite element method, thin-walled beam elements were introduced having a total of 14 degrees of freedom, see for example [4, 5]. The inclusion of extra degrees of freedom was to handle the torque and bimoment acting upon the member. However, such finite beam elements do not include the distortional effects of the cross-section. Consequently, a thin-walled beam formulation incorporating cross-sectional distortion is the *Generalised Beam Theory* (GBT), which was introduced by Schardt in 1966 under the name "Verallgemeinerte Technische Biegetheorie" (VTB) [6, 7]. Kollbrunner and Hajdin describe a similar approach to the introduction of a consistent distortional beam theory in [8]. Nonetheless, with the research performed by Davies and co-workers, GBT was spread outside the German-speaking academic society [9, 10]. Since then, different academic groups have contributed to its development – e.g. Simão & da Silva [11], the group around Camotim [12, 13, 14, 15, 16, 17], or by Ranzi and his colleges [18, 19] just to mention some of the many contributors. The general idea of GBT is to represent and discretise the cross-section along the wall centre line to find distortional transverse displacement modes that have orthogonal warping modes. The approximate displacement modes are achieved solving specific eigenvalue problems related to the beam equilibrium equations. Besides, each mode is affiliated to an axial amplitude function. Therefore, considering standard beam finite element formulations, the axial variations affiliated to each cross-sectional displacement field is assumed to be Hermite cubic polynomials.

Alongside the development of GBT, other thin-walled beam analysis methods were developed too. One of these methods is the *Finite Strip Method* (FSM), Cheung [20]. Several versions of the original FSM formulation have been presented, for example the *constrained Finite Strip Method* (cFSM), by Ádány & Schafer [21, 22, 23]. The constraints introduced, enables a subdivision of the displacements into

*Corresponding author
Email address: jej@byg.dtu.dk (Jeppe Jönsson)

specific displacement modes, which allows a modal decomposition as in GBT. Both Ádány et al. [24] and Silvestre et al. [15] give detailed comparisons of cFSM and GBT. The approach to *Generalised Eigenvectors* (GE), presented by Genoese and co-workers [25, 26], was recently compared to the GBT method by Garcea et al. [27]. The GE method is very versatile due to the discretisation of the cross-section using finite shell elements. On the other hand, this discretisation increases the number of elements compared to the method presented in this paper as well as the GBT method. Besides, the GE method is oriented towards anisotropic members, whereas the present theory concerns isotropic material behaviour.

In the last decade, semi-analytical methods, which are closely related to GBT, have been presented. In these methods, the cross-section is discretised into wall elements with local displacement interpolation. The beam solution modes are found through an analytic solution of the equilibrium equations related to the cross-sections. Among others, this has been done by Jönsson & Andreassen [28], and Vieira et al. [29, 30] who adapt the strong analytical approach of solving the beam differential equations. Solutions to the coupled beam equilibrium equations are deduced through the solution of a related quadratic eigenvalue problem. Both Jönsson & Andreassen [28] and Vieira et al. [29, 30] introduce a wall element with nodal degrees of freedom and displacements being interpolated by use of standard "beam" type shape functions when they discretise the cross-section. Hence, the cross-sectional displacement fields are directly found as eigenvectors. Vieira et al. [29, 30] use a spectral transformation to transform the complex eigenvectors, whereas Jönsson & Andreassen [28] as well as the method presented in this paper, directly use the complex solution vectors with the associated complex attenuation functions as beam displacement modes.

The present paper presents a novel formulation of a beam element based on the semi-analytical thin-walled beam theory introduced by the authors in [31]. The fundamental modes deduced in this paper are not identical, but similar to the semi-analytical beam modes presented by Vieira [32], they are, however, derived using a different orthogonalisation approach. Using the theory proposed by the authors, a coupled system of beam differential equilibrium equations is derived by taking variations in the strain energy. The theory approximates the cross-sectional displacement field by use of discrete wall elements and uses exact analytical solution functions to express the axial variation along the beam, which are deduced from the related differential equilibrium equations. The solution of the differential equations involves a decoupling that leads to cross-sectional displacement fields with associated solution functions that correspond to the amplitude functions. The essential idea of this beam model is that the formulation is based on approximated cross-sectional displacement fields that have associated axial amplitude functions, which are the exact analytical solutions of the homogeneous beam differential equations. While knowing the cross-sectional displacement fields and their associated amplitude functions, it is possible to formulate a beam element adopting these exact solution modes as interpolation functions. In fact, with a linear combination of these pre-established displacement modes, it is possible to develop a beam element. The main and very important feature of the presented method, when compared to GBT, is that GBT uses Hermite polynomial functions to describe the axial variation, whereas the present theory uses the exact solution functions and therefore a further discretisation with multiple elements along the beam axis is not necessary.

Another essential feature of the beam model presented here, is the use of generic wall elements having six degrees of freedom at each node. Consequently, it is possible to connect the beam end cross-section to other finite elements, e.g. finite shell elements. Accordingly, the wall elements used to discretise the cross-section are discrete straight wall elements. Both displacement degrees of freedom, as well as rotational degrees of freedom, are taken into account. Therefore, even with a coarse mesh both global and local distortional modes become a part of the solution space – a space containing cross-sectional displacement fields that are found as solutions to the equilibrium equations. These solutions are found through the solution of the related polynomial eigenvalue problem. From the eigenvalue problem, eigenvectors are extracted as cross-sectional displacement fields with associated exact axial amplitude functions depending on the eigenvalues. In combination, a displacement field and an axial amplitude function describe a beam displacement mode. The modes are grouped into two families: those having eigenvalues equal zero, and those having eigenvalues different from zero. The former include global modes with polynomial amplitudes of maximum third-order reflecting the twelve fundamental beam displacement fields. In the latter case, beam displacement modes with amplitudes having exponential decays are considered. In these cases, the eigenvalues represent an inverse length scale parameter related to the St. Venant principle through an axial decay effect.

2. The beam model

An arbitrary thin-walled beam element is located in a global Cartesian coordinate system spanned by the axes (X, Y, Z). The beam axis is assumed to be straight and parallel to the Z-axis with the cross-sectional plane being orthogonal to this, as illustrated in Figure 1. Furthermore, a local, right-handed orthogonal coordinate system is introduced in the cross-section with (n, s, z) as the normal, tangential and axial directions.

2.1. Kinematics

The displacement of a material point within a beam element is given as a sum of cross-sectional displacement fields multiplied by amplitude functions, which vary along

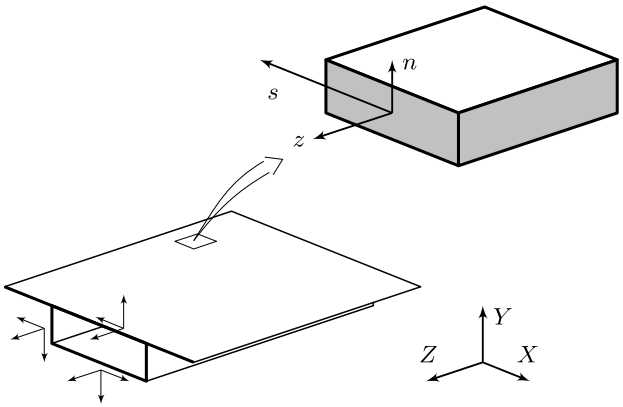

Figure 1: Global and local Cartesian coordinate systems regarding a thin-walled beam

the longitudinal beam axis. The intensities of the amplitude functions are determined by the constants of integration, which become the modal degrees of freedom of the beam model. In other words, the displacements are formulated in the three local coordinate directions u_n, u_s and u_z as a sum of m displacement fields where each displacement field is referred to by index i. Hence, the three displacements are given as:

$$\begin{aligned} u_n(s,z) &= \sum_{i=1}^{m} w_n^i(s)\,\psi_i(z)\,c_i \\ u_s(n,s,z) &= \sum_{i=1}^{m} \Big[\; w_s^i(s) - n\,w_{n,s}^i(s) \;\Big]\psi_i(z)\,c_i \\ u_z(n,s,z) &= \sum_{i=1}^{m} \Big[\; \Omega^i(s) + n\,\alpha^i(s) \;\Big]\eta_i(z)\,c_i \end{aligned} \tag{1}$$

where $w_n^i(s)$, $w_s^i(s)$, $\Omega^i(s)$ and $\alpha^i(s)$ are displacement components of the interpolated cross-section displacement mode i with reference to the mid-line of the wall elements. The displacement formulation at hand uses a Kirchhoff like displacement behaviour in the n,s-plane, a Mindlin-Reissner like shear behaviour through the wall-thickness in the n,z-plane combined with a Timoshenko like shear behaviour in the s,z-plane. For illustration purpose, Figure 2 illustrates the meaning of the different displacement components. Derivatives with respect to n- and s-coordinates are given as subscripts following a comma whereas axial derivatives are denoted by a prime. The axial amplitude functions that describe the axial variation of a given cross-section displacement field are denoted $\psi_i(z)$ and $\eta_i(z)$. The transverse displacements of a cross-section are associated with the amplitude function $\psi(z)$, whereas the amplitude function $\eta(z)$ is related to the warping displacements, which are displacements that are orthogonal to the cross-sectional plane. This distinction between amplitude functions has been chosen in order to keep a clearer relation of the kinematics in Equation (1) to the kinematics of conventional beam theories. Therefore, the two independent amplitude functions are used. Nonetheless, later, during the solution of the differential equilibrium equations, the assumption: $\psi_i(z) = \eta_i(z)$ from [31] is adopted. A comment to the deformation formulations in Equation (1) is that the intensity of each mode i is controlled by the constant c_i. These constants correspond to the modal degrees of freedom and reflect the intensities of the amplitude functions belonging to each displacement mode in the summation of modal displacements in Equation (1).

In order to determine natural cross-sectional displacement fields, this theory discretises the cross-section into straight wall elements. Each wall element has two nodes with three translational degrees of freedom and three rotational degrees of freedom. Accordingly, the twelve nodal degrees of freedom related to a wall element are collected in the column vectors $\mathbf{v}_w^{el\,i}$ and $\mathbf{v}_\Omega^{el\,i}$, respectively, with six degrees of freedom in $\mathbf{v}_w^{el\,i}$ related to translational deformations whereas the remaining six degrees of freedom are collected in $\mathbf{v}_\Omega^{el\,i}$ since they are related to warping deformations. Here and in the following, vectors and matrices will be denoted by non-slanted, boldfaced, letters. The wall element deformations are determined by use of linear interpolation functions given in the row interpolation vectors $\mathbf{N}_s(s)$ and $\mathbf{N}_\alpha(s)$, and also cubic interpolation functions given in the row vectors $\mathbf{N}_n(s)$ and $\mathbf{N}_\Omega(s)$ (see also [33]). Now, considering a cross-sectional displacement field i, the displacement vector components of a wall element may be written in terms of interpolation vectors and nodal degrees of freedom vectors as follows:

$$\begin{aligned} w_s^i(s) &= \mathbf{N}_s(s)\;\mathbf{v}_w^{el\,i}\;, \qquad \alpha^i(s) = \mathbf{N}_\alpha(s)\;\mathbf{v}_\Omega^{el\,i} \\ w_n^i(s) &= \mathbf{N}_n(s)\;\mathbf{v}_w^{el\,i}\;, \qquad \Omega^i(s) = \mathbf{N}_\Omega(s)\;\mathbf{v}_\Omega^{el\,i} \end{aligned} \tag{2}$$

Due to the mode formulation, it is convenient to introduce two wall element deformation vectors $\mathbf{u}_w^{el}(z)$ and $\mathbf{u}_\Omega^{el}(z)$ as the sum of all m displacement modes including the nodal degrees of freedom vectors, the axial amplitude functions, and the constants controlling the mode intensities. Hence, the deformation vectors of a single wall element are computed as the sum of m displacement modes as follows:

$$\begin{aligned} \mathbf{u}_w^{el}(z) &= \sum_{i=1}^{m} \mathbf{v}_w^{el\,i}\;\psi_i(z)\,c_i \\ \mathbf{u}_\Omega^{el}(z) &= \sum_{i=1}^{m} \mathbf{v}_\Omega^{el\,i}\;\psi_i(z)\,c_i \end{aligned} \tag{3}$$

The interpolation vectors in Equation (2) are independent of the specific displacement fields. Therefore, the interpolation vectors are the same for all modes with respect to the same wall element. Consequently, for a single wall element, the displacements in Equation (1) may be inter-

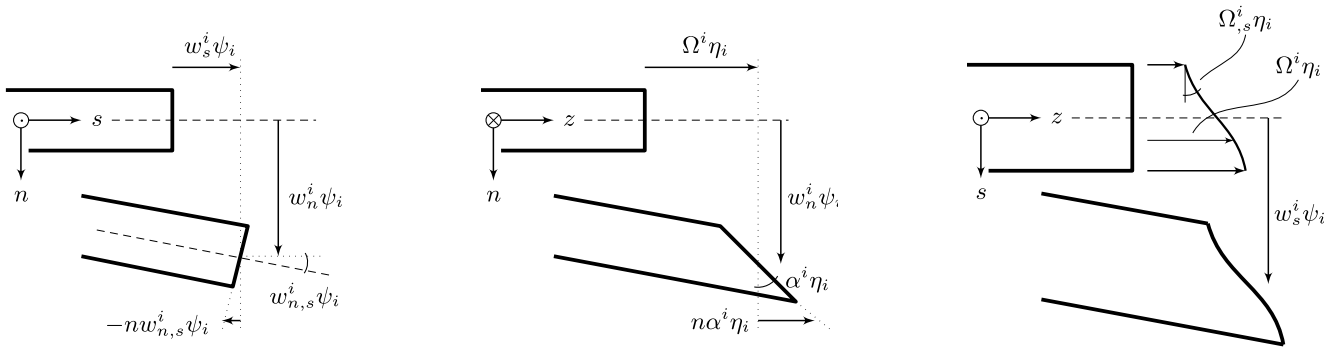

(a) n, s-plane having a Kirchhoff like behaviour

(b) n, z-plane having a Mindlin-Reissner like behaviour

(c) s, z-plane having a Timoshenko like behaviour

Figure 2: Allowable deformation patterns regarding a beam element plate for a single mode i

polated as:

$$\begin{aligned} u_n(s,z) &= \mathbf{N}_n(s)\,\mathbf{u}_w^{el}(z) \\ u_s(n,s,z) &= \Big[\ \mathbf{N}_s(s) - n\,\mathbf{N}_{n,s}(s)\ \Big]\,\mathbf{u}_w^{el}(z) \\ u_z(n,s,z) &= \Big[\ \mathbf{N}_\Omega(s) + n\,\mathbf{N}_\alpha(s)\ \Big]\,\mathbf{u}_\Omega^{el}(z) \end{aligned} \tag{4}$$

in which $\mathbf{u}_w^{el}$ and $\mathbf{u}_\Omega^{el}$ are column vectors containing the nodal deformations related to a single wall element as illustrated in Figure 3. To ease the notation, we will in the following omit the function handle (z) that shows the explicit dependency on the beam axis coordinate, except a few places where there is a specific need for it.

As in [31] the strains are based on the linear small displacement hypothesis and the deformation formulations from Equation (1). This renders the following strain formulations where the normal strain becomes zero ($\varepsilon_{nn} = 0$), but the transverse distortional normal strain and the axial normal strain are given as:

$$\varepsilon_{ss} = u_{s,s} \quad \text{and} \quad \varepsilon_{zz} = u_z' \tag{5}$$

The non-null engineering shear strains are found as:

$$\gamma_{sz} = u_s' + u_{z,s} \quad \text{and} \quad \gamma_{nz} = u_n' + u_{z,n} \tag{6}$$

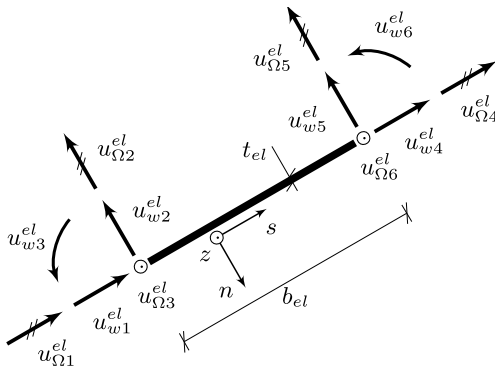

Figure 3: Wall element, which is used to discretise the cross-section also illustrating the deformation components from $\mathbf{u}_w^{el}$ and $\mathbf{u}_\Omega^{el}$, respectively

whilst $\gamma_{ns} = 0$.

2.2. Strain energy and cross-sectional stiffness matrices

Since a linear elastic first-order analysis is considered, the constitutive equations follow from the assumption of zero normal stress $\sigma_{nn} = 0$ as given in the following Equation (7). Here, the stresses are directly found from the strains. The material properties are assumed to be elastic and isotropic with a modulus of elasticity E, a shear modulus: $G = E/(2(1+\nu))$, and a plate elasticity modulus: $E_s = E/(1-\nu^2)$ in which ν is the Poisson ratio. The non-null stresses are then found using the linear constitutive relations including coupling terms between axial and transverse stresses related to deformations within the cross-sectional plane due to the Poisson effect. Hence,

$$\begin{bmatrix} \sigma_{ss} \\ \sigma_{zz} \\ \tau_{sz} \\ \tau_{nz} \end{bmatrix} = \begin{bmatrix} E_s & \nu E_s & 0 & 0 \\ \nu E_s & E_s & 0 & 0 \\ 0 & 0 & G & 0 \\ 0 & 0 & 0 & G \end{bmatrix} \begin{bmatrix} \varepsilon_{ss} \\ \varepsilon_{zz} \\ \gamma_{sz} \\ \gamma_{nz} \end{bmatrix} \tag{7}$$

The stresses σ_{ss}, σ_{zz} and τ_{sz} depend on all three local coordinates (n, s, z) whereas τ_{nz} only depends on the (s, z) coordinates, since it is constant through the plate thickness (well-knowing the true variation is parabolic). Figure 4 illustrates the included stresses and their distribution through the thickness. Due to the difference between shear formulations in the two plate directions of a wall element and due to the very limited influence of plate shear, a

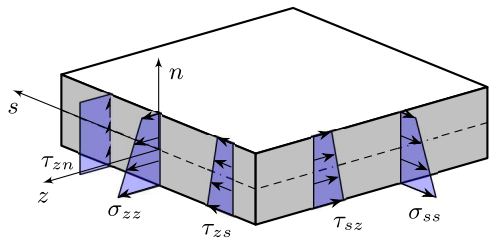

Figure 4: Allowable stress variations at the wall cut-out from Figure 1, with $\sigma_{nn} = 0$ and $\tau_{ns} = 0$

specific shear correction factor has not been implemented. This is done even though Timoshenko [34] already in 1921 introduced a correction factor to adjust the influence of shear. Through time, several considerations have been made on this correction, see for example Cowper [35] or finite element textbooks [36]. However, well-knowing the shear variation through a wall is incorrect, its influence is assumed to be small and a correction would be out of the scope of this paper.

The linear elastic strain energy is formulated by integrating the strain energy density over the full continuum and by substituting stress terms using Equation (7). Accordingly, the linear elastic strain energy becomes:

$$U = \frac{1}{2}\int_V \Big(E_s\varepsilon_{ss}^2 \;+\; E_s\varepsilon_{zz}^2 \;+\; 2E_s\varepsilon_{ss}\varepsilon_{zz}\nu \;+\; G\gamma_{nz}^2 \;+\; G\gamma_{sz}^2 \Big)\, dV \tag{8}$$

The strain energy is partly integrated by performing integration over the cross-section area. The total strain energy expression is found by adding up the cross-sectional integrations of each wall element, i.e. integrating over both wall width and wall thickness and assembling the cross-sectional wall elements into the strain energy using standard finite element methods.

The strain energy is formulated by use of cross-sectional stiffness matrices. Table 1 presents local wall element stiffness matrices deduced by substitution of the strains from Equation (5) and (6) as well as the displacements from Equation (4) into the energy in Equation (8). Accordingly, by considering standard transformations and assembling procedures, global cross-sectional stiffness matrices are derived, see also Cook et al. [36]. The assembling procedure leads to the following strain energy formulation:

$$U = \frac{1}{2}\int_0^\ell \begin{bmatrix} \mathbf{u}_w \\ \mathbf{u}_\Omega \\ \mathbf{u}_w' \\ \mathbf{u}_\Omega' \end{bmatrix}^\mathsf{T} \begin{bmatrix} \mathbf{K}_{ww}^s & \cdot & \cdot & \mathbf{K}_{w\Omega}^{s\sigma} \\ \cdot & \mathbf{K}_{\Omega\Omega}^{\gamma} & \mathbf{K}_{\Omega w}^{\gamma} & \cdot \\ \cdot & \mathbf{K}_{w\Omega}^{\gamma} & \mathbf{K}_{ww}^{\gamma} & \cdot \\ \mathbf{K}_{\Omega w}^{\sigma s} & \cdot & \cdot & \mathbf{K}_{\Omega\Omega}^{\sigma} \end{bmatrix} \begin{bmatrix} \mathbf{u}_w \\ \mathbf{u}_\Omega \\ \mathbf{u}_w' \\ \mathbf{u}_\Omega' \end{bmatrix} dz \tag{9}$$

Hence, the cross-sectional deformation vectors $\mathbf{u}_w$ and $\mathbf{u}_\Omega$ contain all wall element deformation vectors from Equation (3) as a result of the assembling procedure. Additionally, in Equation (9) and throughout the paper a dot $[\,\cdot\,]$ represents a suitable null matrix. The superscripts s, σ and γ indicate terms related to transverse, axial or shear stresses and strains, respectively.

It is convenient in the following to introduce a common deformation vector containing both translational and warping deformations:

$$\mathbf{u}(z) = \begin{bmatrix} \mathbf{u}_w(z) \\ \mathbf{u}_\Omega(z) \end{bmatrix} \tag{10}$$

At the same time, the cross-sectional stiffness matrices are

Table 1: Local wall element stiffness matrices

$$\mathbf{k}_{ww}^s = \int_0^{b_{el}} \left(t_{el}E_s\mathbf{N}_{s,s}^\mathsf{T}\mathbf{N}_{s,s} + \tfrac{t_{el}^3}{12}E_s\mathbf{N}_{n,ss}^\mathsf{T}\mathbf{N}_{n,ss} \right) ds$$
$$\mathbf{k}_{\Omega\Omega}^\sigma = \int_0^{b_{el}} \left(t_{el}E_s\mathbf{N}_{\Omega}^\mathsf{T}\mathbf{N}_{\Omega} + \tfrac{t_{el}^3}{12}E_s\mathbf{N}_{\alpha}^\mathsf{T}\mathbf{N}_{\alpha} \right) ds$$
$$\mathbf{k}_{w\Omega}^{s\sigma} = \int_0^{b_{el}} \left(t_{el}\nu E_s\mathbf{N}_{s,s}^\mathsf{T}\mathbf{N}_{\Omega} - \tfrac{t_{el}^3}{12}\nu E_s\mathbf{N}_{n,ss}^\mathsf{T}\mathbf{N}_{\alpha} \right) ds$$
$$\mathbf{k}_{\Omega w}^{\sigma s} = \int_0^{b_{el}} \left(t_{el}\nu E_s\mathbf{N}_{\Omega}^\mathsf{T}\mathbf{N}_{s,s} - \tfrac{t_{el}^3}{12}\nu E_s\mathbf{N}_{\alpha}^\mathsf{T}\mathbf{N}_{n,ss} \right) ds$$
$$\mathbf{k}_{\Omega\Omega}^\gamma = \int_0^{b_{el}} \left(t_{el}G\mathbf{N}_{\alpha}^\mathsf{T}\mathbf{N}_{\alpha} + t_{el}G\mathbf{N}_{\Omega,s}^\mathsf{T}\mathbf{N}_{\Omega,s} + \tfrac{t_{el}^3}{12}G\mathbf{N}_{\alpha,s}^\mathsf{T}\mathbf{N}_{\alpha,s} \right) ds$$
$$\mathbf{k}_{ww}^\gamma = \int_0^{b_{el}} \left(t_{el}G\mathbf{N}_{n}^\mathsf{T}\mathbf{N}_{n} + t_{el}G\mathbf{N}_{s}^\mathsf{T}\mathbf{N}_{s} + \tfrac{t_{el}^3}{12}G\mathbf{N}_{n,s}^\mathsf{T}\mathbf{N}_{n,s} \right) ds$$
$$\mathbf{k}_{\Omega w}^\gamma = \int_0^{b_{el}} \left(t_{el}G\mathbf{N}_{\alpha}^\mathsf{T}\mathbf{N}_{n} + t_{el}G\mathbf{N}_{\Omega,s}^\mathsf{T}\mathbf{N}_{s} - \tfrac{t_{el}^3}{12}G\mathbf{N}_{\alpha,s}^\mathsf{T}\mathbf{N}_{n,s} \right) ds$$
$$\mathbf{k}_{w\Omega}^\gamma = \int_0^{b_{el}} \left(t_{el}G\mathbf{N}_{n}^\mathsf{T}\mathbf{N}_{\alpha} + t_{el}G\mathbf{N}_{s}^\mathsf{T}\mathbf{N}_{\Omega,s} - \tfrac{t_{el}^3}{12}G\mathbf{N}_{n,s}^\mathsf{T}\mathbf{N}_{\alpha,s} \right) ds$$

grouped in blocks as follows:

$$\mathbf{K}_{aa} = \begin{bmatrix} \mathbf{K}_{ww}^s & \cdot \\ \cdot & \mathbf{K}_{\Omega\Omega}^\gamma \end{bmatrix},\; \mathbf{K}_{ab} = \begin{bmatrix} \cdot & \mathbf{K}_{w\Omega}^{s\sigma} \\ \mathbf{K}_{\Omega w}^\gamma & \cdot \end{bmatrix},$$
$$\mathbf{K}_{ba} = \mathbf{K}_{ab}^\mathsf{T} \;\text{ and }\; \mathbf{K}_{bb} = \begin{bmatrix} \mathbf{K}_{ww}^\gamma & \cdot \\ \cdot & \mathbf{K}_{\Omega\Omega}^\sigma \end{bmatrix} \tag{11}$$

in which each block matrix is $n \times n$, where n is six times the number of nodes used to discretise the cross-section. Thus, with this block notation, the strain energy from Equation (9) is written as:

$$U = \frac{1}{2}\int_0^\ell \begin{bmatrix} \mathbf{u} \\ \mathbf{u}' \end{bmatrix}^\mathsf{T} \begin{bmatrix} \mathbf{K}_{aa} & \mathbf{K}_{ab} \\ \mathbf{K}_{ba} & \mathbf{K}_{bb} \end{bmatrix} \begin{bmatrix} \mathbf{u} \\ \mathbf{u}' \end{bmatrix} dz \tag{12}$$

2.3. Modal displacement field and solution space

From the strain energy, in Equation (12), beam equilibrium equations are deduced using variational principles, i.e. virtual work principle and partial integration as in [31]. This leads to:

$$\mathbf{K}_2\mathbf{u}'' \;+\; \mathbf{K}_1\mathbf{u}' \;+\; \mathbf{K}_0\mathbf{u} \;=\; \mathbf{0} \tag{13}$$

where the stiffness matrices $\mathbf{K}_0$, $\mathbf{K}_1$ and $\mathbf{K}_2$ are defined as blocks of cross-sectional stiffness matrices as follows:

$$\mathbf{K}_0 = \begin{bmatrix} \mathbf{K}_{ww}^s & \cdot \\ \cdot & -\mathbf{K}_{\Omega\Omega}^\gamma \end{bmatrix},$$
$$\mathbf{K}_1 = \begin{bmatrix} \cdot & \mathbf{K}_{w\Omega}^{s\sigma} - \mathbf{K}_{w\Omega}^\gamma \\ \mathbf{K}_{\Omega w}^{\sigma s} - \mathbf{K}_{\Omega w}^\gamma & \cdot \end{bmatrix}, \tag{14}$$
$$\mathbf{K}_2 = \begin{bmatrix} -\mathbf{K}_{ww}^\gamma & \cdot \\ \cdot & \mathbf{K}_{\Omega\Omega}^\sigma \end{bmatrix}$$

The full homogeneous solution space of the second-order differential equation, i.e. Equation (13), contains two parts – one related to fundamental modes having a polynomial

amplitude function, and the second one related to modes with exponential amplitude functions. Hence, the two solution spaces are found as:

- a set of twelve fundamental displacement modes with polynomial amplitude variations collected in $\mathbf{u}_p$. Hence, $\mathbf{u}_p$ contains $n_z = 12$ modes.
- a set of displacement modes having exponential amplitude functions collected in $\mathbf{u}_e$. The number of modes in $\mathbf{u}_e$ depends on the discretisation of the cross-section such that $\mathbf{u}_e$ contains $n_e = 2n - n_z$ modes. Furthermore, these modes might include pairs of complex conjugated modes.

Let us detail the formulation of these modes in the following.

2.3.1. Fundamental modes

The twelve solutions that are categorised as fundamental modes having a polynomial amplitude function are explicitly written as:

$$\mathbf{u}_p(z) = \mathbf{V}_p \ \mathbf{\Psi}_p(z) \ \mathbf{T}_p \ \mathbf{c}_p \tag{15}$$

where the cross-sectional nodal degrees of freedom vectors are collected as columns in four block matrices in $\mathbf{V}_p = [\ \mathbf{V}_3\ \mathbf{V}_2\ \mathbf{V}_1\ \mathbf{V}_0\ ]$. The blocks act as coefficients to the polynomial functions z^3, z^2, z, and 1, respectively. However, the derivation of these cross-sectional nodal degrees of freedom vectors will not be shown here but can be found in the paper [31]. The amplitude matrix, the constant-transformation matrix, and the column vector with the intensity-constants of each mode (modal constants) have the following format:

$$\mathbf{\Psi}_p = \begin{bmatrix} \frac{z^3}{6}\mathbf{I}_p & \cdot & \cdot & \cdot \\ \cdot & \frac{z^2}{2}\mathbf{I}_p & \cdot & \cdot \\ \cdot & \cdot & z\mathbf{I}_p & \cdot \\ \cdot & \cdot & \cdot & \mathbf{I}_p \end{bmatrix}, \quad \mathbf{T}_p = \begin{bmatrix} \mathbf{I}_p \\ \mathbf{I}_p \\ \mathbf{I}_p \\ \mathbf{I}_p \end{bmatrix}, \quad \mathbf{c}_p = \begin{bmatrix} c_{p_1} \\ c_{p_2} \\ \vdots \\ c_{p_{n_z}} \end{bmatrix} \tag{16}$$

in which $\mathbf{I}_p$ is an identity matrix of size $n_z \times n_z$ that is 12×12 reflecting the number of fundamental modes.

Now, seeking the first derivative of $\mathbf{u}_p(z)$ in Equation (15) is traditionally performed by differentiating the amplitude matrix $\mathbf{\Psi}_p(z)$, which is dependent on the z-variable. However, in this (polynomial) case a state-space vector formulation will be used as in the coming exponential solution formulation. Therefore, it is realised that by keeping the amplitude matrix as it is and instead shifting the nodal degree of freedom block vectors in $\mathbf{V}_p$ one place to the right the first derivative of the displacement vector $\mathbf{u}'_p(z)$ can be written as: $\mathbf{u}'_p(z) = \dot{\mathbf{u}}_p(z)$, where the state-space formulation of the displacement-vector-derivative is given as:

$$\dot{\mathbf{u}}_p(z) = \dot{\mathbf{V}}_p \ \mathbf{\Psi}_p(z) \ \mathbf{T}_p \ \mathbf{c}_p \tag{17}$$

In which $\dot{\mathbf{V}}_p = [\ \mathbf{0}\ \mathbf{V}_3\ \mathbf{V}_2\ \mathbf{V}_1]$ is the result of the differentiation operation of $\mathbf{u}_p(z)$. Thus, we have introduced the notation $\dot{\mathbf{u}}_p$ in this special formulation of the derivative. With this refinement, the polynomial solution and its first derivative, Equation (15) and (17), is conveniently written in state-space vector format as:

$$\begin{bmatrix} \mathbf{u}_p \\ \dot{\mathbf{u}}_p \end{bmatrix} = \begin{bmatrix} \mathbf{V}_p \\ \dot{\mathbf{V}}_p \end{bmatrix} \mathbf{\Psi}_p(z) \ \mathbf{T}_p \ \mathbf{c}_p \tag{18}$$

where differentiation of the amplitude functions has been avoided by just shifting the mode vectors and keeping the amplitude matrix $\mathbf{\Psi}_p$.

2.3.2. Exponential modes

In performing the task of solving the second-order differential equation system, it is common to rewrite the equations into a first-order equation system by introducing a state-vector using a special notation for the derivative of a vector, see for example Tisseur and Meerbergen in [37]. However, this correctly and as mathematically expected expands the number of solutions and the size of the problem and ruins the conventional notion of orthogonal solution modes. Nonetheless, the variable $\dot{\mathbf{u}}$ defined as the first derivative of the displacement field is introduced. Hence,

$$\dot{\mathbf{u}}(z) \ \equiv \ \mathbf{u}'(z) \tag{19}$$

Following the procedure outlined by Tisseur and Meerbergen [37] by substituting $\dot{\mathbf{u}}(z)$ into Equation (13) for the first derivatives, the second-order differential equation system can be equivalently written as:

$$\begin{bmatrix} \mathbf{K}_0 & \cdot \\ \cdot & -\mathbf{K}_2 \end{bmatrix} \begin{bmatrix} \mathbf{u} \\ \dot{\mathbf{u}} \end{bmatrix} + \begin{bmatrix} \mathbf{K}_1 & \mathbf{K}_2 \\ \mathbf{K}_2 & \cdot \end{bmatrix} \begin{bmatrix} \mathbf{u} \\ \dot{\mathbf{u}} \end{bmatrix}' = \begin{bmatrix} \mathbf{0} \\ \mathbf{0} \end{bmatrix} \tag{20}$$

using the state-vector notation. This first-ordered differential equation system is solved as a generalised eigenvalue problem by assuming exponential solutions where each eigenvector corresponds to a vector with the nodal degrees of freedom and its derivative for a single mode, and the corresponding eigenvalue gives the exponential amplitude. Consequently, the exponential solution space $\mathbf{u}_e$ and its first derivative $\dot{\mathbf{u}}_e$ can be written as:

$$\begin{bmatrix} \mathbf{u}_e \\ \dot{\mathbf{u}}_e \end{bmatrix} = \begin{bmatrix} \mathbf{V}_e \\ \dot{\mathbf{V}}_e \end{bmatrix} \mathbf{\Psi}_e(z) \ \mathbf{c}_e \tag{21}$$

in which the nodal degrees of freedom vectors are the eigenvectors given as:

$$\begin{bmatrix} \mathbf{V}_e \\ \dot{\mathbf{V}}_e \end{bmatrix} = \begin{bmatrix} \mathbf{v}_1 & \mathbf{v}_2 & \dots & \mathbf{v}_{n_e} \\ \dot{\mathbf{v}}_1 & \dot{\mathbf{v}}_1 & \dots & \dot{\mathbf{v}}_{n_e} \end{bmatrix} \tag{22}$$

The amplitude matrix and mode intensity constant vector (modal degrees of freedom) in Equation (21) are:

$$\mathbf{\Psi}_e = \begin{bmatrix} e^{\lambda_1 z} & & & \\ & e^{\lambda_2 z} & & \\ & & \ddots & \\ & & & e^{\lambda_{n_e} z} \end{bmatrix}, \quad \mathbf{c}_e = \begin{bmatrix} c_{e_1} \\ c_{e_2} \\ \vdots \\ c_{e_{n_e}} \end{bmatrix} \tag{23}$$

Here, λ represents the non-null eigenvalue of each mode, which may be complex.

2.3.3. Homogeneous solution space

The polynomial and exponential solutions are given as Equations (18) and (21), respectively. Thus, the full homogeneous solution can be written as follows:

$$\begin{aligned}\begin{bmatrix}\mathbf{u}\\ \dot{\mathbf{u}}\end{bmatrix} &= \begin{bmatrix}\mathbf{u}_p\\ \dot{\mathbf{u}}_p\end{bmatrix} + \begin{bmatrix}\mathbf{u}_e\\ \dot{\mathbf{u}}_e\end{bmatrix}\\ &= \begin{bmatrix}\mathbf{V}_p & \mathbf{V}_e\\ \dot{\mathbf{V}}_p & \dot{\mathbf{V}}_e\end{bmatrix}\begin{bmatrix}\mathbf{\Psi}_p & \cdot\\ \cdot & \mathbf{\Psi}_e\end{bmatrix}\begin{bmatrix}\mathbf{T}_p & \cdot\\ \cdot & \mathbf{I}_e\end{bmatrix}\begin{bmatrix}\mathbf{c}_p\\ \mathbf{c}_e\end{bmatrix}\\ &= \begin{bmatrix}\mathbf{V}\\ \dot{\mathbf{V}}\end{bmatrix}\mathbf{\Psi}\ \mathbf{T}_c\ \mathbf{c} \end{aligned} \tag{24}$$

where $\mathbf{V}$ is the full mode matrix, $\mathbf{\Psi}$ is a common amplitude diagonal matrix containing $\mathbf{\Psi}_p$ and $\mathbf{\Psi}_e$ from Equation (16) and (23), respectively; and $\mathbf{T}_c$ is a constant-transformation matrix containing $\mathbf{T}_p$ from Equation (16) and an identity matrix, $\mathbf{I}_e$ of size $n_e \times n_e$. Furthermore $\mathbf{c}$ is a column vector containing all the mode intensity constants $\mathbf{c}_p$ and $\mathbf{c}_e$ (being modal degrees of freedom).

3. Beam element formulation

Having found the displacement modes of the thin-walled beam element in the previous section, based on the chosen discretisation of the cross-section, this section formulates the beam element using these exact displacement modes as axial interpolation functions between beam end cross-sections.

The theory developed here takes only nodal forces at boundaries into account, as well as nodal deformations. This has been chosen in order to keep a simple formulation. Nevertheless, distributed loads acting along the beam member axis can be implemented using a similar method as the one reported by Andreassen & Jönsson [38].

To derive the beam element formulation, the potential energy is formulated as the sum of the strain energy and the potential from applied loads:

$$V = U + \Pi \tag{25}$$

The strain energy U is given in Equation (12) and the potential Π of external nodal forces at each end of the beam element is given as:

$$\Pi = -\begin{bmatrix}\mathbf{u}(0)\\ \mathbf{u}(\ell)\end{bmatrix}^{\mathsf{T}}\begin{bmatrix}\mathbf{f}_0\\ \mathbf{f}_\ell\end{bmatrix} \tag{26}$$

where $\mathbf{f}_0$ and $\mathbf{f}_\ell$ are load vectors. Each load vector refers to one of the two beam ends as indicated by the subscripts. Furthermore, a single load vector contains a load parameter for each nodal degree of freedom in the cross-section.

3.1. Modal beam stiffness matrix

To formulate a beam element, we must derive its stiffness matrix. To do so, we consider the strain energy from Equation (12).

As interpolation functions, the natural beam displacement modes found as solutions in the previous section, i.e. Equation (24), will be used. Thus, considering the full homogeneous solution space, a formulation of a modal beam stiffness matrix is presented letting the vectors of constants be perceived as the temporary modal degree of freedom vectors. Later, these temporary modal degrees of freedom vectors are transformed into a nodal degree of freedom space containing the classic deformations and rotations at each node. Consequently, we have a beam element with a number of displacement modes that reflect the exact deformation modes derived for this specific beam element. Thus, substituting the homogeneous solution space and its first derivatives from Equation (24) into the elastic strain energy in Equation (12) we have:

$$U = \frac{1}{2}\int_0^\ell \mathbf{c}^{\mathsf{T}}\mathbf{T}_c^{\mathsf{T}}\mathbf{\Psi}^{\mathsf{T}}\begin{bmatrix}\mathbf{V}\\ \dot{\mathbf{V}}\end{bmatrix}^{\mathsf{T}}\begin{bmatrix}\mathbf{K}_{aa} & \mathbf{K}_{ab}\\ \mathbf{K}_{ba} & \mathbf{K}_{bb}\end{bmatrix}\begin{bmatrix}\mathbf{V}\\ \dot{\mathbf{V}}\end{bmatrix}\mathbf{\Psi}\ \mathbf{T}_c\ \mathbf{c}\ dz \tag{27}$$

and in integrated form it follows as:

$$U = \tfrac{1}{2}\ \mathbf{c}^{\mathsf{T}}\ \tilde{\mathbf{K}}\ \mathbf{c} \tag{28}$$

The modal stiffness matrix $\tilde{\mathbf{K}}$ is found by computing the matrix multiplications and performing the integration. However, in order to substantially ease and reduce the number of computations, a reformulation is introduced. The fact that only the (diagonal) matrix $\mathbf{\Psi}$ depends on z is utilised and therefore, only these matrices have to be integrated. We rearange the order of the terms in $\tilde{\mathbf{K}}$ to isolate the $\mathbf{\Psi}$-matrices within the integration. This is achieved by introducing the mathematical Hadamard product: $\circ$, which allows us to separate the matrices $\mathbf{\Psi}$ in the integration from the rest of the expression. Furthermore, to utilise the fact that $\mathbf{\Psi}$ contains values in its diagonal only, the Kronecker product: $\otimes$ is introduced. Hence, a combination of the Kronecker product and a re-formulation of $\mathbf{\Psi}$ into a column vector containing the diagonal components only, denoted $\hat{\mathbf{\Psi}}$, (see also [31]), the modal stiffness matrix is written as:

$$\begin{aligned}\tilde{\mathbf{K}} = \mathbf{T}_c^{\mathsf{T}}\Bigg(&\begin{bmatrix}\mathbf{V}\\ \dot{\mathbf{V}}\end{bmatrix}^{\mathsf{T}}\begin{bmatrix}\mathbf{K}_{aa} & \mathbf{K}_{ab}\\ \mathbf{K}_{ba}^{\mathsf{T}} & \mathbf{K}_{bb}\end{bmatrix}\begin{bmatrix}\mathbf{V}\\ \dot{\mathbf{V}}\end{bmatrix}\\ &\circ \int_0^\ell \hat{\mathbf{\Psi}}^{\mathsf{T}}\otimes\ \hat{\mathbf{\Psi}}\ dz\Bigg)\mathbf{T}_c\end{aligned} \tag{29}$$

With this formulation of $\tilde{\mathbf{K}}$, the integration is easily performed analytically due to the fairly simple amplitude functions by first computing the indefinite integral, and then using the fundamental theorem of calculus.

As stated previously, the energy formulation in Equation (28) considers the vector of modal constants as variables or temporary modal degree of freedom vectors. In the next subsection, a transformation is introduced where the temporary modal degrees of freedom vectors are written in terms of nodal beam element degrees of freedom vectors at the boundaries, i.e. at each end of the beam.

3.2. Beam element formulation

This subsection formulates the beam element by considering the potential energy from Equation (25), the load contributions from Equation (26), and the strain energy written in modal form in Equation (28). At first, the strain energy shall be written in terms of beam element boundary degrees of freedom instead of the temporary modal degrees of freedom. Then, substituting into the potential energy, taking variation and by requiring the first variation of the energy to be stationary, we achieve the beam element formulation.

3.2.1. Beam element degrees of freedom

The beam element degrees of freedom are directly linked to the cross-sectional degrees of freedom at the boundaries. Therefore, considering the deformation vector $\mathbf{u}(z)$ and letting the position variable z adopt the boundary values of the beam element, i.e. $z = 0$ and $z = \ell$, where ℓ is the beam length, the deformations at the boundaries in the beam element degree of freedom vector $\mathbf{u}_b$ are expressed as:

$$\mathbf{u}_b = \begin{bmatrix} \mathbf{u}(0) \\ \mathbf{u}(\ell) \end{bmatrix} \tag{30}$$

Substituting: $\mathbf{u}(z) = \mathbf{V}\boldsymbol{\Psi}(z)\mathbf{T}_c\mathbf{c}$, a part of Equation (24), we may write Equation (30) as:

$$\mathbf{u}_b = \begin{bmatrix} \mathbf{u}(0) \\ \mathbf{u}(\ell) \end{bmatrix} = \begin{bmatrix} \mathbf{V}\ \boldsymbol{\Psi}(0)\ \mathbf{T}_c \\ \mathbf{V}\ \boldsymbol{\Psi}(\ell)\ \mathbf{T}_c \end{bmatrix} \mathbf{c} \tag{31}$$

From this equation it can be seen that there is a relation between the deformations at the boundaries in $\mathbf{u}_b$ and the temporary modal degrees of freedom in $\mathbf{c}$. This relation was in fact used in Equation (28). Consequently, a transformation matrix $\mathbf{A}$ is introduced and Equation (31) is re-written into:

$$\mathbf{u}_b = \mathbf{A}\ \mathbf{c} \quad \text{where } \mathbf{A} = \begin{bmatrix} \mathbf{V}\ \boldsymbol{\Psi}(0)\ \mathbf{T}_c \\ \mathbf{V}\ \boldsymbol{\Psi}(\ell)\ \mathbf{T}_c \end{bmatrix} \tag{32}$$

With this formulation, $\mathbf{A}$ is defined as a squared, positive definite and invertible matrix that allows $\mathbf{c}$ to be written as:

$$\mathbf{c} = \mathbf{A}^{-1}\ \mathbf{u}_b \tag{33}$$

3.2.2. Beam element stiffness matrix

If Equation (33) is substituted into the modal strain energy formulation in Equation (28) we are able to express the beam element strain energy in terms of displacements at the boundaries. This is:

$$\begin{aligned} U &= \tfrac{1}{2}\ \mathbf{u}_b^{\mathsf{T}} \left[\mathbf{A}^{-1}\right]^{\mathsf{T}}\ \tilde{\mathbf{K}}\ \mathbf{A}^{-1}\mathbf{u}_b \\ &= \tfrac{1}{2}\ \mathbf{u}_b^{\mathsf{T}}\ \mathbf{K}\ \mathbf{u}_b \end{aligned} \tag{34}$$

in which the *beam element stiffness matrix* $\mathbf{K}$ is introduced as:

$$\mathbf{K} = \left[\mathbf{A}^{-1}\right]^{\mathsf{T}}\ \tilde{\mathbf{K}}\ \mathbf{A}^{-1} \tag{35}$$

3.2.3. The beam element

Substituting the strain energy from Equation (34) into the potential energy Equation (25) and the potential from the applied load in Equation (26) the full potential energy takes the form:

$$V\ =\ U + \Pi\ =\ \tfrac{1}{2}\ \mathbf{u}_b^{\mathsf{T}}\ \mathbf{K}\ \mathbf{u}_b -\ \mathbf{u}_b^{\mathsf{T}}\ \mathbf{f}$$

Then, taking the first variation in the displacement field, $\delta\mathbf{u}_b$, the potential energy becomes:

$$\delta V =\ \delta\mathbf{u}_b^{\mathsf{T}}\ \mathbf{K}\ \mathbf{u}_b - \delta\mathbf{u}_b^{\mathsf{T}}\ \mathbf{f} \tag{36}$$

and by requiring stationarity of the energy, it must equal zero for all variations ($\delta V = 0$ where $\delta\mathbf{u}_b^{\mathsf{T}} \neq \mathbf{0}$) whereby the well-known linear elastic beam formulation is derived:

$$\mathbf{K}\ \mathbf{u}_b = \mathbf{f} \tag{37}$$

With the formulation in Equation (37) a linear relation between the boundary loads $\mathbf{f}$, and the boundary deformations $\mathbf{u}_b$ is given – the *beam element formulation.*

The trivial solution procedure of the equation system in Equation (37) will not be expressed here, but reference is made to literature, such as Cook et al. [36]. In this literature, it is also described how aligned beam elements can be assembled. However, bear in mind that the presented formulation relies on exact longitudinal amplitude (shape) functions whereas traditional finite element formulations rely on approximations between end nodes through interpolation functions. Therefore, the presented beam element can adopt any length without further approximation.

3.3. Boundary conditions

The boundary conditions of a beam element are defined by the use of standard methods and operate on the deformation vector $\mathbf{u}_b$. In this deformation vector each degree of freedom within the two beam end cross-sections are represented. Therefore, it is possible to add boundary conditions related to each degree of freedom within an end cross-section. Furthermore, this allows the modelling of many kinds of supports, e.g. simple support conditions and clamped support conditions. However, support and load conditions should, if possible, be distributed to several nodes avoiding singularities and local stress concentration.

Advanced boundary conditions such as partially restrained cross-sections will not be described here, but special cross-section restraints can be added at the cross-section level, which however, is beyond the scope of this paper.

4. Element deformations, strains and stresses

Having solved Equation (37), this section describes how to find displacements, deformation derivatives, strains, and stresses in an arbitrary point within a wall element of any cross-section within the thin-walled beam element.

4.1. Deformation field

The deformations at the beam boundaries are given by the beam element deformation vector $\mathbf{u}_b$ corresponding to the cross-sectional degrees of freedom at the beam element ends. Knowing these, the modal content can be determined using Equation (33). This enables us to determine the deformation vector and the axial derivative of the deformation vector of a cross-section at a given axial position z using Equation (24). Thus, the cross-section deformation vector at the axial position z can be found as:

$$\begin{bmatrix} \mathbf{u}(z) \\ \dot{\mathbf{u}}(z) \end{bmatrix} = \begin{bmatrix} \mathbf{V} \\ \dot{\mathbf{V}} \end{bmatrix} \mathbf{\Psi}(z)\ \mathbf{T}_c\ \mathbf{A}^{-1}\mathbf{u}_b \tag{38}$$

From these cross-section deformation vectors the local wall element degrees of freedom $\mathbf{u}_w^{el}$ and $\mathbf{u}_\Omega^{el}$ as well as the corresponding axial derivatives $\dot{\mathbf{u}}_w^{el}$ and $\dot{\mathbf{u}}_\Omega^{el}$ can be extracted.

The local deformations in any point (n, s) of a wall element in the cross-section at the axial position z may now be found using Equation (4).

4.2. Strain field

Using the element wall deformations and axial deformation derivatives of a cross-section at the axial position z, the local strains at any point of a wall element is found as follows:

$$\begin{aligned}
\varepsilon_{ss}^{el}(n,s,z) &= [\mathbf{N}_{s,s} - n\mathbf{N}_{n,ss}]\,\mathbf{u}_w^{el} \\
\varepsilon_{zz}^{el}(n,s,z) &= [\mathbf{N}_\Omega + n\mathbf{N}_\alpha]\,\dot{\mathbf{u}}_\Omega^{el} \\
\gamma_{nz}^{el}(s,z) &= \mathbf{N}_n\dot{\mathbf{u}}_w^{el} + \mathbf{N}_\alpha\mathbf{u}_\Omega^{el} \\
\gamma_{sz}^{el}(n,s,z) &= [\mathbf{N}_s - n\mathbf{N}_{n,s}]\,\dot{\mathbf{u}}_w^{el} \\
&\quad + [\mathbf{N}_{\Omega,s} + n\mathbf{N}_{\alpha,s}]\,\mathbf{u}_\Omega^{el}
\end{aligned} \tag{39}$$

in which only the element wall deformation vectors $\mathbf{u}_w^{el}$ and $\mathbf{u}_\Omega^{el}$ and their axial derivative $\dot{\mathbf{u}}_w^{el}$ and $\dot{\mathbf{u}}_\Omega^{el}$ are dependent on the axial position coordinate z.

4.3. Stress field

Knowing the cross-sectional strain field for a given z-value, the corresponding stresses can be computed using the linear elastic constitutive relations for isotropic materials presented in Equation (7). Substituting the strains into the constitutive relations gives us the stresses in each wall element as a function of the local coordinates as follows:

$$\begin{aligned}
\sigma_{ss}^{el}(n,s,z) &= E_s\,\big(\ [\mathbf{N}_{s,s} - n\mathbf{N}_{n,ss}]\,\mathbf{u}_w^{el} \\
&\quad + \nu\,[\mathbf{N}_\Omega + n\mathbf{N}_\alpha]\,\dot{\mathbf{u}}_\Omega^{el}\ \big) \\
\sigma_{zz}^{el}(n,s,z) &= E_s\,\big(\ [\mathbf{N}_\Omega + n\mathbf{N}_\alpha]\,\dot{\mathbf{u}}_\Omega^{el} \\
&\quad + \nu\,[\mathbf{N}_{s,s} - n\mathbf{N}_{n,ss}]\,\mathbf{u}_w^{el}\ \big) \\
\tau_{nz}^{el}(s,z) &= G\,\big(\ \mathbf{N}_n\dot{\mathbf{u}}_w^{el} + \mathbf{N}_\alpha\mathbf{u}_\Omega^{el}\ \big) \\
\tau_{sz}^{el}(n,s,z) &= G\,\big(\ [\mathbf{N}_s - n\mathbf{N}_{n,s}]\,\dot{\mathbf{u}}_w^{el} \\
&\quad + \ [\mathbf{N}_{\Omega,s} + n\mathbf{N}_{\alpha,s}]\,\mathbf{u}_\Omega^{el}\ \big)
\end{aligned} \tag{40}$$

Distinguishing between membrane and bending stresses is common. However, this will not be incorporated directly, but could easily be achieved from Equation (40) by separating into terms that are dependent or independent of the n-coordinate.

4.4. Exponential decay

A characteristic of those modes having an exponential amplitude function is that they are either derived as real couples or complex quadruples. A real couple represents a displacement mode with an increasing amplitude along the beam axis peaking at the one end, and a mode with a decaying amplitude peaking at the other end. In case of a complex set of eigenvalues, there will be a real and an imaginary cross-section mode vector with an increasing or decreasing harmonic oscillation. This corresponds to two mode shapes with a decaying amplitude function and two modes with an increasing amplitude function, respectively.

Due to this characteristic feature related to the exponential modes and their axial decay behaviour, it becomes interesting to assess their attenuation length. The real part of the eigenvalue determines the attenuation length. The higher the eigenvalue, the shorter the attenuation length is. Hence, an attenuation length can be defined as:

$$L_a = \frac{\epsilon}{|\mathrm{Re}(\lambda)|} \tag{41}$$

in which ϵ defines a lower level of interest where the decay has lead to a diminished displacement, which could be taken as 5% of the peak value. This results in ϵ being around three. Jönsson [39] introduces a value of $\epsilon = \pi$ giving a lower level of: $e^{-\pi} \approx 4\%$. Giavotto et al. [40] use a value of $\epsilon = 3$, which results in: $e^{-3} = 5\%$ as the lower level. The use of $\epsilon = \pi$ is relevant due to the equivalence to half the harmonic wavelength or a buckling length.

Depending on the attenuation length, the displacement modes found in Equation (21) can be characterised as global distortional modes or local distortional plate modes. The latter has an attenuation length typically less than the main cross-section dimension, whereas the former often has an attenuation length being several times the cross-section dimension.

5. Examples

In this section, four examples are used to illustrate and assess the results of the presented thin-walled beam element formulation. Both the geometry and the type of load vary in the four examples:

1. A cantilever having a hollow rectangular box section loaded in shear. This example illustrates the deformation behaviour, the normal stresses and shear stresses, as well as the shear stress transition at cross-section corners.

2. An open channel section with a non-symmetric transverse load, which induces torsional deformations, torsional warping stresses and bending stresses.

3. A short simply supported box section loaded in bending and exhibiting shear lag with non-linear normal stresses in the flanges.

4. The final example is a longitudinal assembly of three similar channel elements with a distortional load. The attenuation length related to exponential modes, mode intensities, and transverse bending stresses are assessed.

For each example, both stresses and nodal displacements will be compared to results obtained with the commercial finite element program `Abaqus` [41]. The finite element analysis is performed on a model with isotropic material and four node shell elements (S4-shell element in `Abaqus` syntax) using full integration. Furthermore, the linear elastic finite element calculations are based on a structured rectangular mesh with a side length of 5 mm.

5.1. Ex. 1 – Tip loaded cantilever box section

The first example considers a cantilevered beam with a closed rectangular cross-section as shown in Figure 5, in which the parameters of the example also are listed. The load at the tip is applied as evenly distributed line loads along the two webs of the end cross-section in `Abaqus` and as nodal loads in the theory presented here. Solving the beam element formulation from Equation (37) and then determining the deformation using Equation (38) renders a deformation as illustrated to the left in Figure 6 mainly having flexural bending deformation. In Table 2 nodal displacements are listed, which are extracted from the present theory and from the analysis using the commercial finite element program. Furthermore, a comparison between the nodal displacements and their relative deviation is given in Table 2. The values are extracted from the nodes at the free end ($Z = \ell$) in the upper and lower right corners of the cross-section. In the vertical direction, a relative derivation of 0.10 % is seen. If the horizontal displacements in u_x are compared, given in the table, a relatively high deviation is seen but at the same time the displacements are small, and therefore this deviation corresponds to $0.1 \cdot 10^{-3}$ mm which is equal to three millions of the

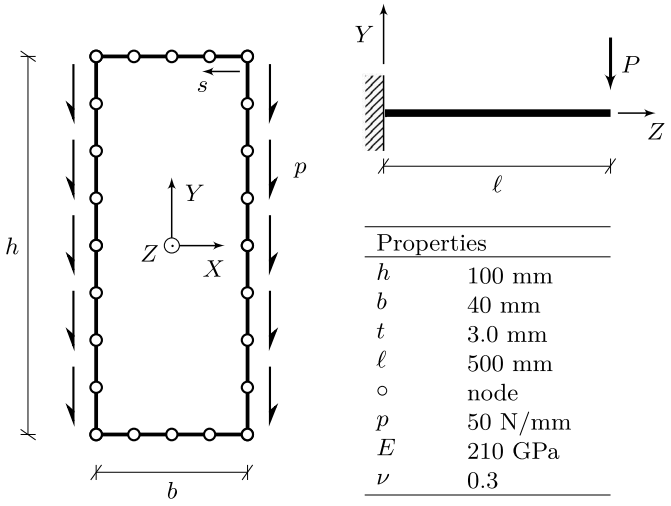

Properties	
h	100 mm
b	40 mm
t	3.0 mm
ℓ	500 mm
$\circ$	node
p	50 N/mm
E	210 GPa
ν	0.3

Figure 5: Ex. 1 – discretisation and geometrical properties of the cantilever beam with a closed box section including local set-up and general load/support configurations

width only. The u_x-deformations represent a contraction of the top flange and a widening of the lower flange. This is a result of the Poisson effect since the top flange is exposed to axial tension and the bottom flange is in axial compression.

The stresses will be analysed next and for this purpose, the cross-section at mid-span ($Z = \ell/2$) is assessed in order to alleviate the local effects that may occur near loaded or supported nodes. To the right in Figure 6, a three-dimensional illustration of the normal stresses is shown and in Figure 7, the values found at mid-span are seen. The axial stresses are obtained along the centre line of the cross-sectional wall elements. A good agreement is seen between the two models with a maximum relative deviation of -0.54 % found at the corners.

To be assessed next are the shear stresses. Due to the kinematics and the constitutive relations in Equation (7), we have τ_{sz}-stresses as well as τ_{nz}-stresses. On the other hand, the shell model in `Abaqus` considers τ_{sz}-stresses only. Comparing the τ_{sz}-stresses yields overall, good similarities and the relative deviation of the largest τ_{sz}-stresses is

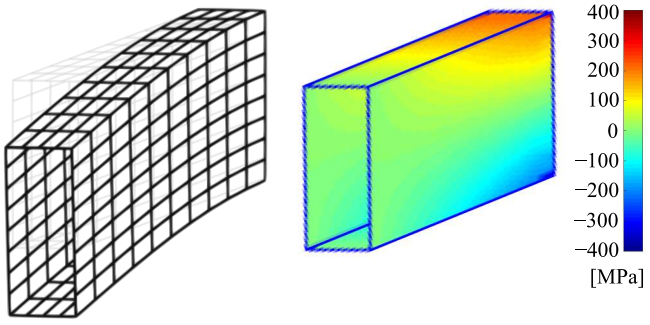

Figure 6: Ex. 1 – Deformation and σ_{zz}-stresses. Deformations are scale by a factor 20

Table 2: Ex. 1 – Nodal deformations at the upper and lower right corners comparing the two models. Measurements in [mm]

$(\frac{b}{2}, \pm\frac{h}{2}, \ell)$ $(n = 0)$	Present theory	`Abaqus`	Relative deviation
u_x	± 0.0013	± 0.0012	$-8.33\,\%$
u_y	-1.9060	-1.9080	$0.10\,\%$
u_z	± 0.2711	± 0.2712	$-0.04\,\%$

around 0.15 % depending on the mesh density. Figure 8 illustrates the shear stresses at $Z = \ell/2$ and for $n = 0\,\text{mm}$, i.e. the middle surface of the wall. The different mesh densities illustrated in Figure 8 have been considered to investigate the local shear effects near the corners. Thus, in the upper flange, two, four, six and eight elements are used as shown from the left to the right in the figure. Especially the τ_{nz}-plots indicate that the stresses are locally peaking near the corners. Additionally, if comparing the τ_{sz}-stresses obtained to those from `Abaqus`, deviations are significant at corners. However, with an increased mesh density this effect becomes more isolated near the corners. This local effect has inspired us to perform a detailed investigation of the stress transmission around corners. Therefore, a solid finite element model is created in `Abaqus` as well. In this model, an eight-node linear brick element (C3D8 in `Abaqus` syntax) has been used to discretise the beam in a structured mesh. A section cut-out of the upper right corner at mid-span is illustrated in Figure 9 and the stress variations along the middle of the walls are likewise shown here. From Figure 9, it can be seen how the stress variations follows the same pattern as the one obtained considering the present theory (Figure 8). However, Figure 9 also indicates that the decay of the τ_{nz}-stresses is less than two times the wall thickness. Therefore, the results from this solid finite element model indicate exactly what was seen in the stress distributions in Figure 8. This result supports that small elements near the corners should be considered when adapting the present theory in combination with this type of wall element. An example of this is illustrated in Figure 10 showing the results of an analysis with an element mesh having small wall elements at the corners only.

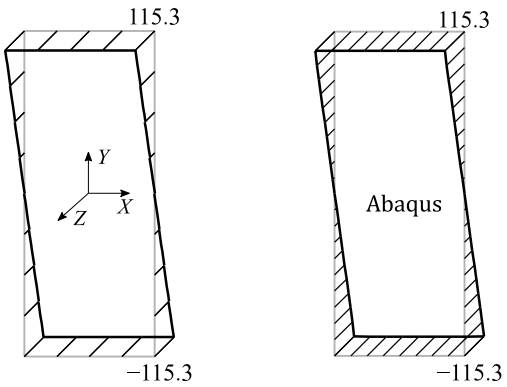

Figure 7: Ex. 1 – Axial stresses, σ_{zz}, in [MPa] at $Z = \ell/2$ and $n = 0$ mm. To the left stresses found from the theory presented here, to the right stresses extracted from `Abaqus`

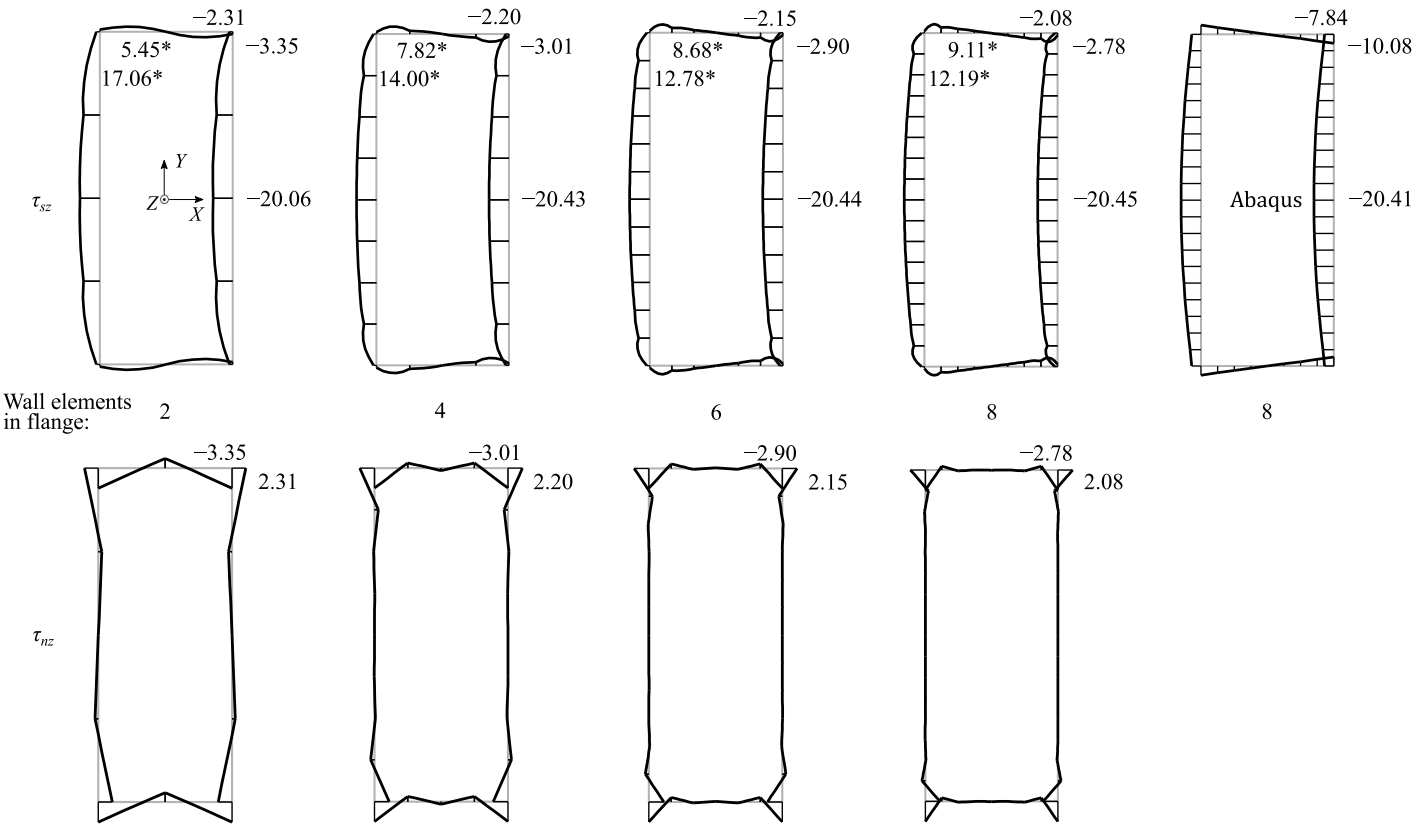

Figure 8: Ex. 1 – Shear stresses at $n = 0$ mm and $Z = \ell/2$ with an increasing mesh density. Also including stresses subtracted from the finite element analysis in `Abaqus`. Stresses given in [MPa]. The τ_{sz}-stresses marked with an asterisk indicates the highest stress value obtained in the wall element closest to the corner either in the web or flange (the stress is computed at teen points along each wall element)

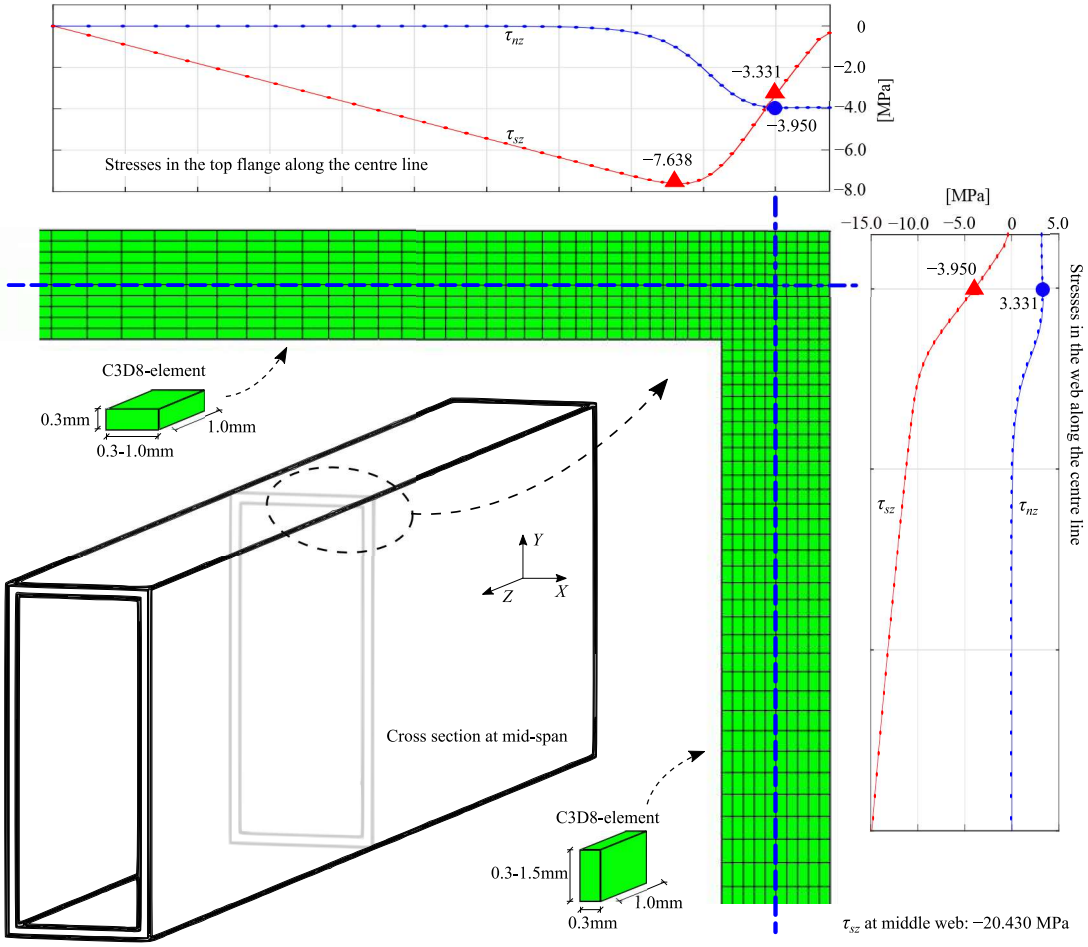

Figure 9: Ex. 1 – Results from the `Abaqus` model using solid elements

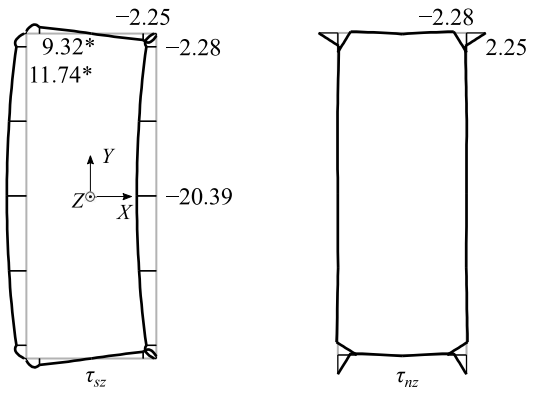

Figure 10: Ex. 1 – Shear stresses using a special mesh with small elements near corners. Stresses in [MPa] at $Z = \ell/2$ and $n = 0$ mm

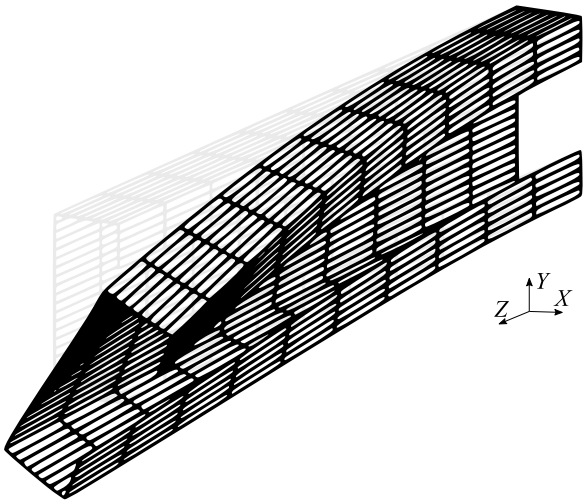

Figure 12: Ex. 2 – Three-dimensional deformation of the cantilever drawn with a scaling factor equal 20

5.2. Ex. 2 – Shear loaded cantilevered channel section

This example examines a mono-symmetric cantilever channel section exposed to a load which induces flexural and torsional displacements. The load configurations, as well as the geometrical properties, are shown in Figure 11. In the present implementation, the end cross-section load is applied as point loads distributed to each node in the web and in the finite element program `Abaqus` as a line load acting on the web. The clamped boundary condition is modelled by restraining all degrees of freedom within the end cross-section. Due to the load configuration, the beam element deforms partly in bending and partly in torsion as illustrated in Figure 12.

This example is chosen such that it includes the added effects of classic flexure, torsion and torsional warping. The channel section is loaded along the web and thus, the beam is expected to flexure about the strong principle axis and twists about the shear centre. Furthermore, since the beam is cantilevered with a completely clamped boundary condition at one end, the beam will exhibit torsional warping. Therefore, it is chosen to compare the resulting displacements at the free end and the stresses close to the clamped end of the beam with those found using finite shell elements.

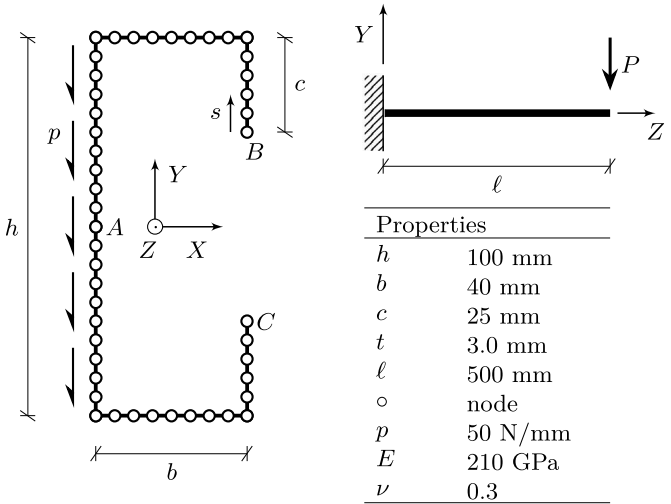

Properties	
h	100 mm
b	40 mm
c	25 mm
t	3.0 mm
ℓ	500 mm
$\circ$	node
p	50 N/mm
E	210 GPa
ν	0.3

Figure 11: Ex. 2 – Geometric properties, discretisation, and load properties of the shear loaded channel section

Let us first compare the displacement of the beam end at the central node point A in the web to an `Abaqus` shell model. The points A, B and C are shown in Figure 11. First of all, the displacements in u_x and u_z of point A vanish in both models. The present theory results in a vertical displacement of $u_y = -1.8392$ mm and `Abaqus` results in $u_y = -1.8473$mm giving a relative deviation of the present theory compared to `Abaqus` of 0.44%. The influence of torsion and the related warping can be illustrated by simply comparing the nodal displacements of the outer most free edge point of the lip, i.e. at point B. In Table 3, the three displacements of the upper lip are given. It can be seen that the maximum relative deviation of the displacements at this nodal point B is 0.87 % and it is related to the axial warping displacements of warping and flexure. Similar displacements are of course found at point C in the lower lip, however, u_x and u_z change signs.

Next, the normal stress and shear stresses of the model are compared to those found using an `Abaqus` shell model.

Table 3: Ex. 2 – The nodal displacements in [mm] of the free end of the upper lip at point B, i.e. at $Z = 500$ mm.

	Present theory	`Abaqus`	Relative deviation
u_x	1.1055	1.1107	0.47 %
u_y	−2.9155	−2.9324	0.58 %
u_z	−0.1488	−0.1501	0.87 %

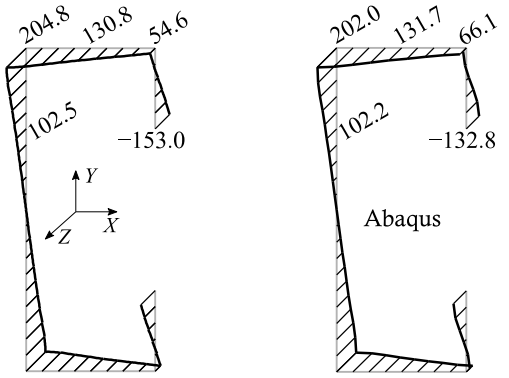

Figure 13: Ex. 2 – A comparison of normal stresses, σ_{zz} in [MPa], measured 10mm from the fixed end, i.e. at $Z = 10$mm, and $n = 0$ mm

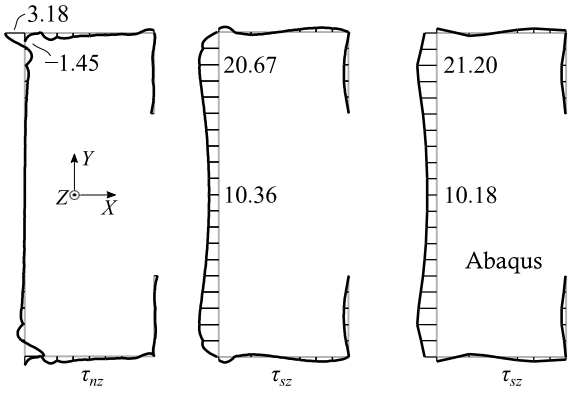

Figure 14: Ex. 2 – The shear stresses are shown in [MPa] at a cross-section 10 mm from the support, i.e. $Z = 10$ mm, moreover, $n = 0$ mm

Since the modelling of displacements and therefore also shear stresses are quite different at section corners and therefore difficult to compare, especially at the fixed end, we have chosen to compare stresses that occur quite close to the fixed end, having $Z = 10$ mm. The mid surface normal stresses measured 10mm from the fixed end are shown in Figure 13 and the stress values are given at the cross-section corners, at the lip end, at the web quarter point, and at the centre of the flange. This clearly shows that there are torsional warping stresses and bending stresses of the beam. Comparing the stresses obtained using Equation (40) and those from `Abaqus` it is seen that there is some difference, which is maximised at the upper right corner with a relative deviation of −17.4 %.

The shear stresses that occur 10 mm from the fixed end are shown in Figure 14. In general, the τ_{sz}-stresses have a similar distribution in both models.

Overall, the results obtained using the two different models agree. This despite the fact that the theory presented includes 564 degrees of freedom only, whereas the shell finite element model in `Abaqus` includes 28482 degrees of freedom. Indeed, this is due to the use of exact axial beam interpolation functions since the discretisation of the cross-section in the two models coincide.

5.3. Ex. 3 – Box section exposed to shear lag

This example assesses the effect of shear lag, which, for example, can be seen in relatively short thin-walled members with relative wide flanges. Consequently, this example examines a simply supported closed box beam with wide flanges.

The effect of shear lag is typically seen in box bridge sections with wide flanges and short spans. The shear lag effect is often of importance near supports (for example for uniformly loaded multi span members) and also near other large local transverse loads. This is because the shear with the associated shear deformation (warping) has to "transfer" the effects of the shear force (local transverse load) out into the flanges in order to build up the normal stresses needed for equilibrium. This effect is not included in classic theories of torsional beam theories, but it is included in the present model.

In this example, the beam is exposed to bending about the weak axis by a central transverse load. The load is applied on the central cross-section as line loads acting along the webs as shown in Figure 15. The figure also illustrates the cross-section and gives the necessary parametric values.

The boundary conditions are introduced as a restriction of the in-plane translations at the two end cross-sections, and as an axial restraint to a single node within the cross-section at $Z = 0$ mm. The rotational degrees of freedom are not restrained, and the load is distributed and applied as concentrated nodal loads in both models.

The vertical displacement of the lower left corner node at mid-span of the present model is compared to the results of an `Abaqus` shell model. Using the presented model a

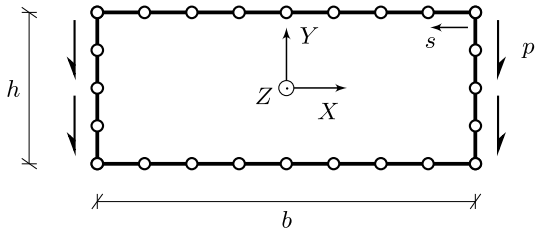

Properties			
h	40 mm	∘	node
b	100 mm	p	50 N/mm
t	0.5 mm	E	210 GPa
ℓ	200 mm	ν	0.3

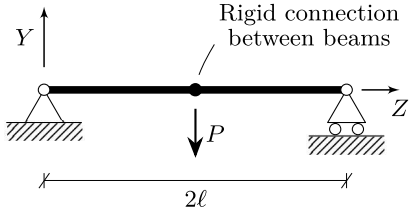

Figure 15: Ex. 3 – General configurations used in this example

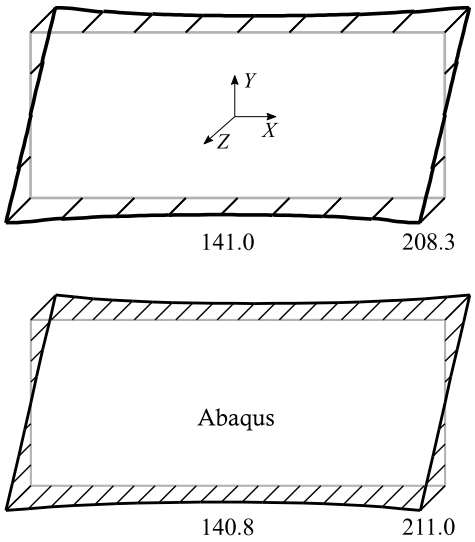

Figure 16: Ex. 3 – Normal stresses in [MPa] measured 10 mm from the middle of the beam, i.e. at $Z = 190$ mm

vertical displacement of $u_y = 0.7325$mm is found and using `Abaqus` a vertical displacement of $u_y = 0.7408$mm is found with a relative deviation of 1.12 %.

The normal stress variation in a cross-section situated 10 mm from the centre of the beam is used to assess whether the present theory will cover shear lag. Hence, the stress variations in Figure 16 shows that the present theory covers shear lag. A relative reduction in the normal stresses between the flange middle and the corner is 32.3 %. If the results are compared to those obtained from the commercial finite element software `Abaqus` the maximum relative deviation is found to be 1.28% at the corners.

5.4. Ex. 4 – Open lipped channel section

This final example considers a simply supported beam with an open channel section. The beam is assembled by three similar beam elements each of length ℓ. The beam is loaded at: $Z = 2\ell$ with a point load at the end of each lip. The cross-section parameters, cross-section discretisation, and load set-up are shown in Figure 17. The support conditions are achieved by prohibiting any transverse deformations at each end. Furthermore, at the one end, a single node is restricted to have no axial deformation. The rotational degrees of freedom at the two ends are kept as free variables.

The overall deformation is illustrated in Figure 18. It corresponds to a global bending behaviour combined with a local deformation close to the loaded nodes. A cut-out side-view near the loaded nodes is illustrated in Figure 19. This figure shows clearly how a global bending and local deformations influence the deformed shape. Besides, the figure highlights how local deformations decay over a certain distance.

Let us in the following look into the behaviour of the central beam element. First of all, the constants computed by Equation (33) are found. They determine how the cross-sectional displacement modes are linearly combined based on the intensities given by the components of $\mathbf{c}$. The constants are illustrated in Figure 20 where the absolute real values are given above the horizontal axis, and the absolute imaginary parts are given below the horizontal axis,

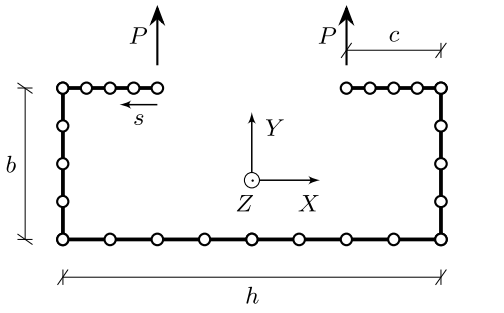

Properties			
h	100 mm	○	node
b	40 mm	P	1 kN
c	25 mm	E	210 GPa
t	3.0 mm	ν	0.3
ℓ	500 mm		

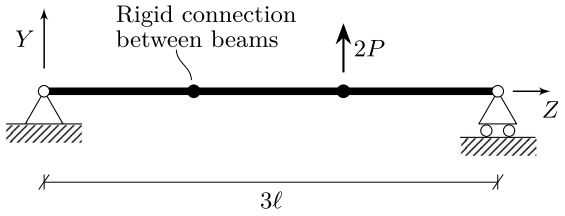

Figure 17: Ex. 4 – Open profile with simple supports, properties and overall static system

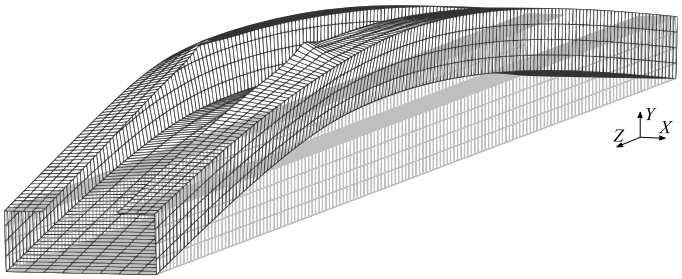

Figure 18: Ex. 4 – Three-dimensional visualisation of the deformation corresponding to the simply supported beam with two single loads attached to its lips. The deformation is scaled by a factor of 20

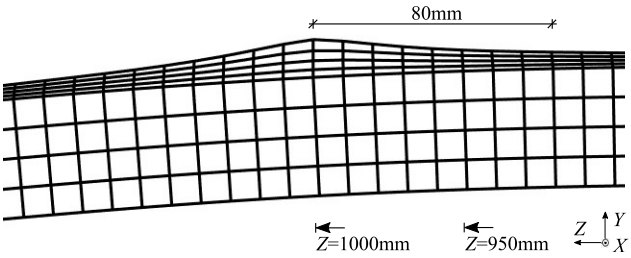

Figure 19: Ex. 4 – Decay length seen in the Y, Z-plane

respectively. The first twelve constants correspond to the fundamental modes and should always be considered. In Table 4, the most pronounced constants are listed with respect to the exponential modes.

To assess those modes contributing to the deflected shape, focus will be on the cross-section where the loads are applied ($Z = 1000$ mm). In addition, only the transverse displacement part of the modes will be considered. The total transverse deformation of the cross-section is given in Figure 21a, which is found computing: $\mathbf{u}(z) = \mathbf{V}\mathbf{\Psi}(z)\mathbf{T}_c\mathbf{c}$. Figure 21b and 21c illustrates the contributions from the polynomial and exponential modes, respectively. Hence, the polynomial modes contribute with a rigid vertical deformation whereas the exponential modes gives the distortional deformations.

From the graph in Figure 20, it was indicated that not all modes were activated and Table 4 listed the eight most pronounced exponential modes. If these eight modes are added together the shape shown in Figure 21d is achieved and it is very close to the one including all 288 exponential modes in Figure 21c. Now, a further assessment of these eight exponential modes are illustrated in Figure 22a to 22e. In these figures the light grey deformed cross-section represents the combined shape from Figure 21d. The deformation in Figure 22f is a combination of all remaining exponential modes showing a very small contribution. This confirms that the primary exponential deformation is a result of the eight selected modes. Figure 22b, 22c and 22d are contributions from three pairs of complex modes, which becomes real when they are added together in pairs.

Table 4: Ex. 4 – The eight highest constants with respect to the exponential modes regarding beam segment two (written in a decreasing order)

mode i	c_i	L_a [mm]
23	0.655	84.28
15	$0.214 + 0.267i$	540.90
16	$0.214 - 0.267i$	540.90
45	$-0.173 + 0.109i$	38.13
46	$-0.173 - 0.109i$	38.13
31	$0.141 - 0.057i$	79.75
32	$0.141 + 0.057i$	79.75
53	0.123	31.52

For each of the exponential modes, an axial attenuation length may be found considering Equation (41) letting $\epsilon = \pi$. These attenuation lengths are listed in Table 4. Hence, mode 23 has an attenuation length: $L_a = 84.28$mm that corresponds very well with the observed deformation pattern seen in Figure 19. The modes 15 and 16 are those having the largest decay length, which harmonise well with the cross-sectional deformation seen in Figure 22b.

Next, let us perform a comparison between the obtained stresses using Equation (40) and those obtained from the shell model in `Abaqus`. To avoid effects from singularities, a cross-section located 50 mm from the loaded nodes is analysed, which is at $Z = 950$mm. The axial stresses along the cross-sectional wall centre lines are shown in Figure 23. A maximum relative deviation of 0.30% is found at the upper right corner whereas the relative deviation at the web middle is only -0.08 %. Due to the load configurations, transverse bending stresses will occur. Figure 24 illustrates the distribution of these obtained at the outer surface. Since the transverse stresses are interpolated linearly within each element, the found stress distribution is discontinuous between elements. The stresses obtained from `Abaqus` are extrapolated averaged nodal stresses, which therefore are continuous. Nonetheless, the overall shapes are similar, and the stresses deduced from the two models coincide with a relative deviation between -0.37 % and -4.66 %.

6. Discussion

The formulation of an advanced thin-walled beam element has been presented. The beam element facilitates not only classic displacement patterns with rigid cross-section movements but also in-plane displacements related to the Poisson effect as well as distortional deformations with associated warping modes.

One of the main advantages obtained with this thin-walled beam theory is the use of exact beam interpolation functions in the axial direction. This allows the beam element to be used for any lengths. Consequently, a beam element is not limited to a finite length, which is the case in GBT since polynomial shape functions govern the axial variation.

Thus, the presented beam theory only has nodes and degrees of freedom at its end cross-sections and therefore,

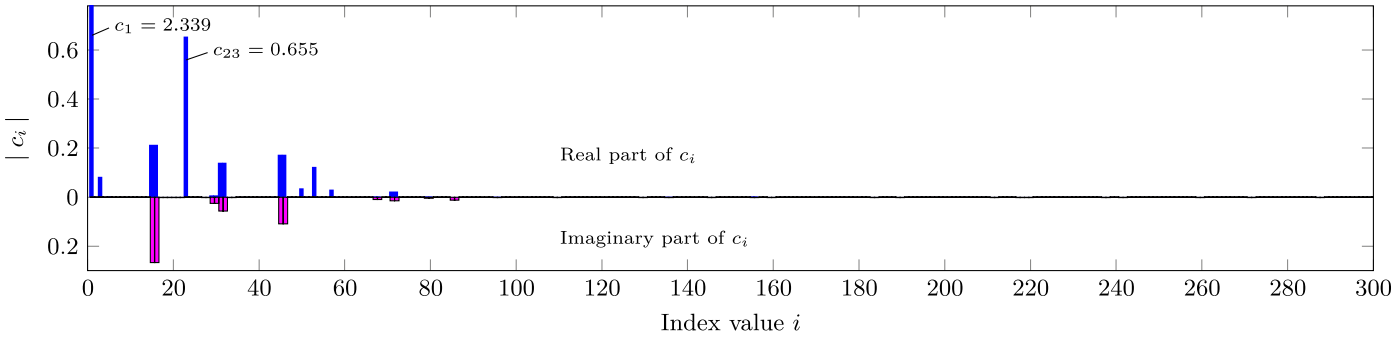

Figure 20: Ex. 4 – The absolute values of the real and imaginary part of the constants in **c**, respectively

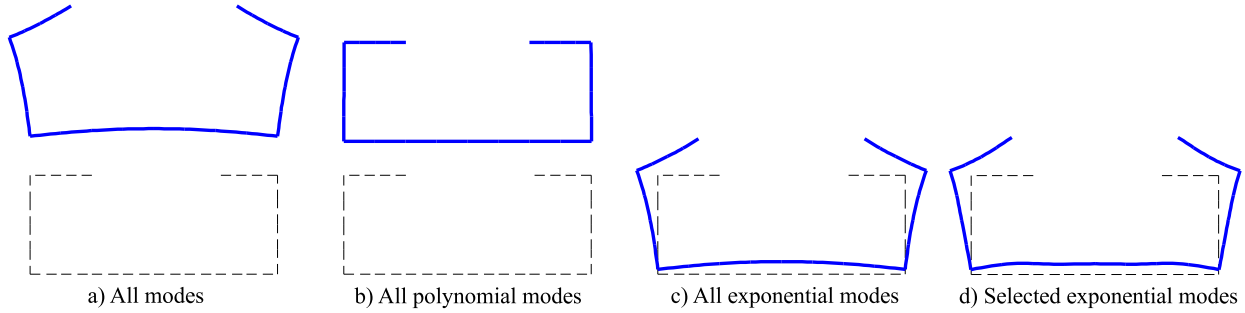

Figure 21: Ex. 4 – The transverse cross-sectional deformation at the point where the loads are acting (this is at $Z = 1000$ mm). The deformations are scaled 20 times

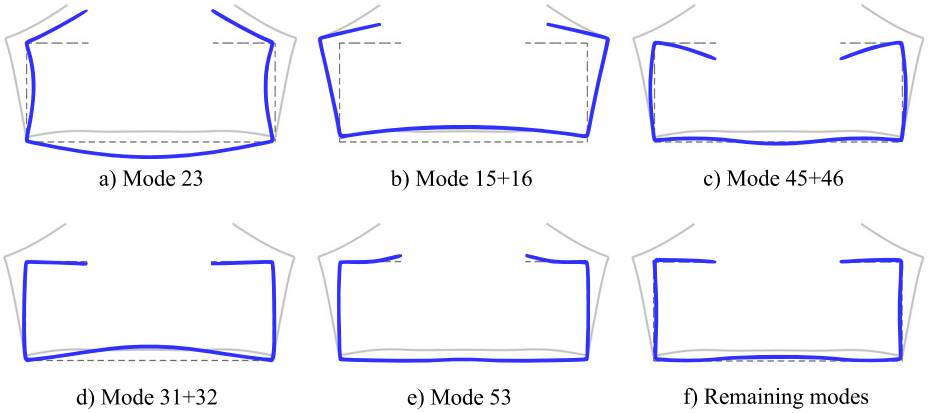

Figure 22: Ex. 4 – Transverse exponential displacement modes at $Z = 1000$ mm. The light grey cross-section is the one from Figure 21d. The displacement modes are scaled by a factor of 20

only include a limited number of degrees of freedom compared to, for example, a similar analysis using finite shell elements in the framework of the finite element method. Again, this is a result of the exact beam interpolation functions. Hence, the derivation of these axial interpolation functions is a result of the procedure deducing the beam element stiffness matrix, which is based on the novel semi-analytic cross-section analysis presented by the authors in [31]. Straight wall elements is used to discretise the thin-walled cross-section centre line, and with a strain energy formulation, a system of cross-sectional equilibrium equations is deduced. This formulation is purely based on linear elastic constitutive relations and isotropic material properties. The system of equilibrium equations is solved as a polynomial eigenvalue problem, and cross-sectional displacement fields are computed as eigenvectors with the associated eigenvalues being related to axial amplitude functions. The derivation of beam displacement modes is decomposed into two parts. One is related to fundamental beam modes and the other to distortional beam modes. The former part of the modes is belonging to the zero eigenvalues, which is found through a systematic decomposition and combination of the related eigenvectors. This is a procedure which is used by Morandini et al. [42] and Genoese et al. [25, 26]. The latter part of the modes is based on the non-zero eigensolutions.

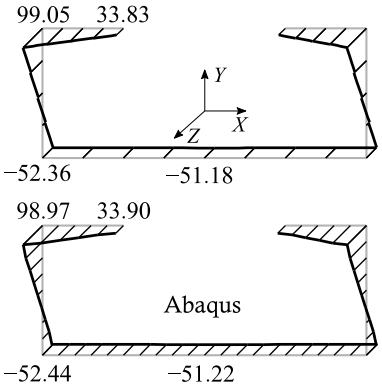

Figure 23: Ex. 4 – Axial stresses, σ_{zz}, in [MPa] at $Z = 950$mm and $n = 0$ mm

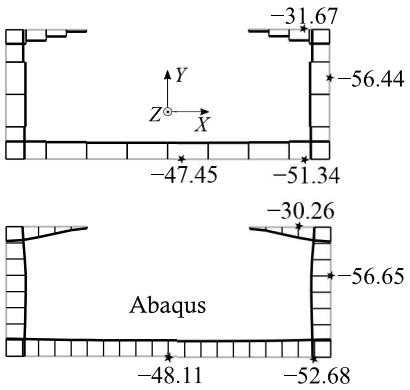

Figure 24: Ex. 4 – Transverse bending stresses, σ_{ss}, in [MPa] at $Z = 950$ mm and $n = t/2$. The star indicates to which element or node a given stress corresponds

Through examples, usability of the beam element is illustrated and reasonable agreement with results obtained with a commercial finite element program is achieved. However, near corners, in the cross-section, local shear effects occur due to the transmission of shear stresses around corners. This leads to a shear stress distribution that deviates from those shear stresses obtained in more classic shell models obeying the Kirchhoff plate hypothesis. Nonetheless, considering detailed solid finite element models, a similar transmission of shear stresses is seen confirming the results obtained in this theory. As a consequence, this theory results in a detailed assessment of shear stress transmission between non-aligned wall elements. However, a fine discretisation with wall elements is to be preferred close to these regions to get improved results. This is due to the attenuation of the shear stresses being no more than twice the wall thickness.

It has been shown in one of the examples how deformation of a cross-section can be decomposed into displacement modes. This mode decomposition is directly found from the solutions as the displacement mode intensity factors, which indicates the influence of each mode. Thus, in-depth knowledge of the beam deformation can be obtained right away and is an integrated part of the solution. This is one of the main advantages of this theory in comparison with for example cFSM where constraint equations are to be added to the kinematic equations to obtain a similar mode decomposition.

During a mode decomposition, the attenuation of the exponential distortion modes can be found since this is directly related to the eigenvalues, which were deduced computing the cross-sectional beam displacement modes. This is exemplified and verified in one of the examples. Furthermore, this mode decomposition may be utilised in future formulations of efficient beam elements with a reduced number of modal degrees of freedom based on a subset of modes. Besides, the identification of displacement modes becomes essential extending the theory to include buckling and post-buckling analysis of the beam members as well. Indeed, higher-order exponential displacement modes play a crucial role here, which is also highlighted in [27].

7. Acknowledgement

The first author wishes to thank the Danish consultancy company NIRAS A/S and the Innovation Fund Denmark, grant 5189-00005B, for funding this project.

References

[1] K. E. Kurrer, History of the Theory of Structures: From Arch Analysis To Computational Mechanics, John Wiley & Sons, 2009 (2009). doi:10.1002/9783433600160.

[2] V. Z. Vlasov, Thin-Walled Elastic Beams, 2nd Edition, Jerusalem, 1961, israel Program for scientific translations (1961).

[3] C. F. Kollbrunner, N. Hajdin, Dünnwandige Stäbe · Band 1, Stäbe mit undeformierbaren Querschnitten, Springer-Verlag, 1972 (1972).

[4] D. Krajcinovic, A consistent discete elements technique for thin-walled assemblages, International Journal of Solids and Structures 5 (1969) 639–662 (1969). doi:10.1016/0020-7683(69)90085-7.

[5] R. S. Barsoum, R. H. Gallagher, Finite element analysis of torsional and torsional-flexural stability problems, International Journal for Numerical Methods in Engineering 2 (1970) 335–352 (1970). doi:10.1002/nme.1620020304.

[6] R. Schardt, Eine erweiterung der technishen biegelehre für die berechnung biegestreifer prismatischer falfwerke, Der Stahlbau 35 (1966) 161–171 (1966).

[7] R. Schardt, Verallgemeinerte Technische Biegetheorie - Band 1, Lineare Theorie, 2nd Edition, Metrum-Verlag,Darmstadt, 1989 (1989).

[8] C. F. Kollbrunner, N. Hajdin, Dünnwandige Stäbe · Band 2, Stäbe mit deformierbaren Querschnitten - Nicht-elastiches Verhalten dünnwandiger Stäbe, Springer-Verlag, 1975 (1975).

[9] J. M. Davies, P. Leach, First-order generalised beam theory, Journal of Constructional Steel Research 31 (1994) 187–220 (1994). doi:10.1016/0143-974X(94)90010-8.

[10] J. M. Davies, P. Leach, D. Heinz, Second-order generalised beam theory, Journal of Constructional Steel Research 31 (1994) 221–241 (1994). doi:10.1016/0143-974X(94)90011-6.

[11] P. Simão, L. S. da Silva, A unified energy formulation for the stability analysis of open and closed thin-walled members in the framework of the generalized beam theory, Thin-Walled Structures 42 (2004) 1495–1517 (2004). doi:10.1016/j.tws.2004.03.021.

[12] N. Silvestre, D. Camotim, First-order generalised beam theory for arbitrary orthotropic materials, Thin-Walled Structures 40 (2002) 755–789 (2002). doi:10.1016/S0263-8231(02)00025-3.

[13] N. Silvestre, D. Camotim, Second-order generalised beam theory for arbitrary orthotropic materials, Thin-Walled Structures 40 (2002) 791–820 (2002). doi:10.1016/S0263-8231(02)00026-5.

[14] N. Silvestre, D. Camotim, Nonlinear generalized beam theory for cold-formed steel members, International Journal of Structural Stability and Dynamics 3 (4) (2003) 461–490 (2003). doi:10.1142/S0219455403001002.

[15] N. Silvestre, D. Camotim, N. F. Silva, Generalized beam theory revisited: from kinematical assumptions to the deformation mode determination, International Journal of Structural Stability and Dynamics 11 (2011) 969–997 (2011). doi:10.1142/S0219455411004427.

[16] D. Camotim, C. Basaglia, Buckling Analysis of Thin-Walled Structures Using Generalized Beam Theory (GBT): A State-of-the-art Report, Steel Construction 6 (2013) 117–131 (2013). doi:10.1002/stco.201310021.

[17] C. Basaglia, D. Camotim, N. Silvestre, Global Buckling Analysis of Plane and Space Thin-Walled Frames in the Context of GBT, Thin-Walled Structures 46 (2008) 79–101 (2008). doi:10.1016/j.tws.2007.07.007.

[18] G. Taig, G. Ranzi, Generalised beam theory (gbt) for stiffened sections, International Journal of Steel Structures 14 (2014) 381–397 (2014). doi:10.1007/s13296-014-2017-x.

[19] G. Taig, G. Ranzi, A. Luongo, Gbt pre-buckling and buckling analyses of thin-walled members under axial and transverse loads, Continuum Mechanics and Thermodynamics 28 (2016) 41–66 (2016). doi:10.1007/s00161-014-0399-9.

[20] Y. K. Cheung, Finite Strip Method in Structural Analysis, Pergamon Press, Oxford, New York, Toronto, Sydney, Paris, Frankfurt, 1976 (1976).

[21] S. Ádány, B. W. Schafer, Buckling mode decomposition of single-branched open cross-section members via finite strip method: Derivation, Thin-Walled Structures 44 (2006) 563–584 (2006). doi:10.1016/j.tws.2006.03.013.

[22] S. Ádány, B. W. Schafer, Buckling mode decomposition of single-branched open cross-section members via finite strip method: Application and examples, Thin-Walled Structures 44 (2006) 585–600 (2006). doi:10.1016/j.tws.2006.03.014.

[23] S. Ádány, B. W. Schafer, A full modal decomposition of thin-walled, single-branched open cross-section members via the constrained finite strip method, Journal of Constructional Steel Research 64 (1) (2008) 12–29 (2008). doi:10.1016/j.jcsr.2007.04.004.

[24] S. Ádány, N. Silvestre, B. W. Schafer, D. Camotim, GBT and cFSM: Two modal approaches to the buckling analysis of unbranched thin-walled members, Advanced Steel Construction 5 (2) (2009) 195–223 (2009).

[25] A. Genoese, A. Genoese, A. Bilotta, G. Garcea, A generalized model for heterogeneous and anisotropic beams including section distortions, Thin-Walled Structures 74 (2014) 85–103 (2014). doi:10.1016/j.tws.2013.09.019.

[26] A. Genoese, A. Genoese, A. Bilotta, G. Garcea, Buckling analysis through a generalized beam model including section distortion, Thin-Walled Structures 85 (2014) 125–141 (2014). doi:10.1016/j.tws.2014.08.012.

[27] G. Garcea, R. Gonçalves, A. Billota, D. Manta, R. Bebiano, N. Leonetti, D. Magisano, D. Camotim, Deformation modes of thin-walled members: a comparison between the method of generalized eigenvectors and generalized beam theory, Thin-Walled Structures 100 (2016) 192–212 (2016). doi:10.1016/j.tws.2015.11.013.

[28] J. Jönsson, M. J. Andreassen, Distortional eigenmodes and homogeneous solutions for semi-discretized thin-walled beams, Thin-Walled Structures 49 (2011) 691–707 (2011). doi:10.1016/j.tws.2010.12.009.

[29] R. F. Vieira, F. B. E. Virtuoso, E. B. R. Pereira, A higher order thin-walled model including warping and shear modes, International Journal of Mechanical Sciences (2013) 67–82 (2013). doi:10.1016/j.ijmecsci.2012.10.009.

[30] R. F. Vieira, F. B. Virtuoso, E. B. R. Pereira, A higher order model for thin-walled structures with deformable cross-sections, International Journal of Solids and Structures (2014) 575–598 (2014). doi:10.1016/j.ijsolstr.2013.10.023.

[31] A. B. Hansen, J. Jönsson, Displacement modes of a thin-walled beam model with deformable cross section, Thin-Walled Structures 141 (2019) 576–592 (2019). doi:10.1016/j.tws.2019.01.052.

[32] R. F. Vieira, A higher order thin-walled beam model, Ph.D. thesis, Universidade Técnica de Lisboa - Instituto Superior Técnico (2010).

[33] A. B. Hansen, J. Jönsson, A gbt-framework towards modal modelling of steel structures, John Wiley & Sons, Ltd – ce/papers (2017) 1822–1830 (2017). doi:10.1002/cepa.226.

[34] S. P. Timoshenko, LXVI. On the Correction for Shear of the Differential Equation for Transverse Vibrations of Prismatic Bars, Philosophical magazine series 6 41 (245) (1921) 744–746 (1921). doi:10.1080/14786442108636264.

[35] G. R. Cowper, The shear coefficient in timoshenko's beam theory, Journal of Applied Mechanics (1966) 335–340 (1966). doi:10.1115/1.3625046.

[36] R. D. Cook, D. S. Malkus, M. E. Plesha, Concepts and applications of finite element analysis, 3rd Edition, John Wiley & Son, NewYork Chichester Brisbane Toronto Singapore, 1989 (1989).

[37] F. Tisseur, K. Meerbergen, The quadratic eigenvalue problem, Society for Industrial and Applied Mathematics 43 (2) (2001) 235–286 (2001). doi:10.1.1.32.9042.

[38] M. J. Andreassen, J. Jönsson, Distortional solutions for loaded semi-discretized thin-walled beams, Thin-Walled Structures 50 (2012) 116–127 (2012). doi:10.1016/j.tws.2011.08.013.

[39] J. Jönsson, Distortional theory of thin-walled beams, Thin-Walled Structures 33 (1999) 269–303 (1999). doi:10.1016/S0263-8231(98)00050-0.

[40] V. Giavotto, M. Borri, P. Mantegazza, G. Ghiringhelli, Anisotropic beam theory and applications, Computers & Structures 16 (1983) 403–413 (1983). doi:10.1016/0045-7949(83)90179-7.

[41] Abaqus, Abaqus/CAE 2016; Abaqus® and SIMULIA® used for finite element analysis, 2016, abaqus Inc., SIMULIA © Dassault Systèmes, 2015, Version 2016 (2016).

[42] M. Morandini, M. Chierichetti, P. Mantegazza, Characteristic behavior of prismatic anisotropic beam via generalized eigenvectors, International Journal of Solids and Structures 47 (2010) 1327–1337 (2010). doi:10.1016/j.ijsolstr.2010.01.017.

Paper IV

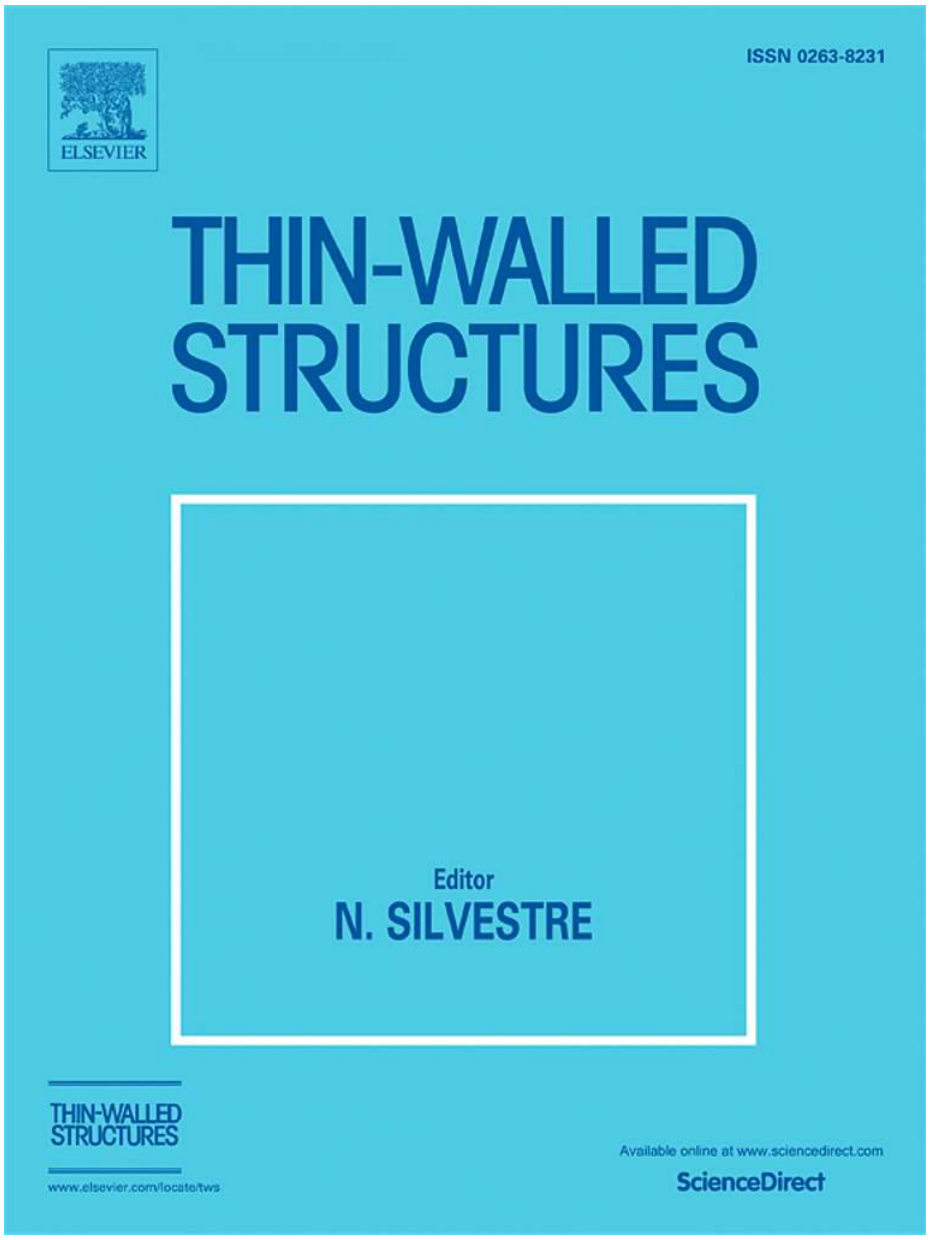

Mode-based assessment of joints and structural elements in thin-walled steel frames

Anders B. Hansen[a,b], Jeppe Jönsson[a,*], Ricardo F. Vieira[c]

[a] *Technical University of Denmark, Department of Civil Engineering, Brovej Building 118, DK-2800 Kgs. Lyngby, Denmark*
[b] *NIRAS A/S, Sortemosevej 19, DK-3450 Allerød, Denmark*
[c] *Universidade Técnica de Lisboa, Instituto Superior Técnico, Department of Civil Engineering, Architecture and Georesources, Av. Rovisco Pais, 1049-001 Lisboa, Portugal*

Abstract

A generic methodology to perform a first-order linear elastic analysis of thin-walled steel frames based on an advanced beam model and a specific joint finite element model capable of transmitting deformation modes between beam elements. The advanced beam model has been previously developed by the authors and relies on a set of displacement modes of the cross-section so as to accurately reproduce the structural behaviour of a thin-walled element. The joint model consists in a mesh of finite elements properly discretised to represent the joint geometry and to allow the connection between advanced beam elements. The main novelty within the present paper is the expression of interfaces between beam elements and joint elements by a number of generalised cross-sectional beam displacement modes. Hence, standard degrees of freedom at connected faces are transformed into a reduced number of cross-sectional beam displacement mode-related degrees of freedom – in general a base change in the degree of freedom formulation. Consequently, this methodology enables the effects of local cross-sectional distortion to be accounted for as well as transmitted through joints. This transmission is possible due to the inclusion of joint elements, which couples advanced beam elements that include higher order deformation effects. Therefore, with this methodology, it is possible to perform structural analyses of large frameworks with advanced beam elements and joints that allow for distortional effects to be included with only a reasonable number of degrees of freedom due to the novel mode-based approach. Two illustrative examples have been included to highlight the usability of the approach. In conclusion, the mode-based methodology analysing steel frames has indicated promising results, and the generic formulation allows it to be used in the context of any mode-based beam element formulation.

Keywords: Connections, steel frames, mode-based formulation, thin-walled structures

1. Introduction

The analysis of steel frame structures through beam elements is common practice. The connections between elements (joints) are modelled based on simplifying hypotheses concerning the rigidity. Commonly, hinges or direct transfer of beam displacements without any relative displacements are considered. This, however, might be erroneous when analysing beams with thin-walled cross-sections since local distortional effects are prone to occur. Effects such as cross-sectional distortion are not included in traditional beam element theories. Furthermore, the assumed joint behaviour may also lead to poor non-economical and over-sized designs.

With this paper and based on a background overview given by the authors in a companion paper [1] the authors propose an approach in which local cross-section effects are taken into account by using an advanced thin-walled beam theory, which was recently developed by the authors as well [2, 3]. In addition to this beam element formulation, the complexity that might occur when assembling two non-aligned beam elements is taken care of by introducing a three-dimensional joint element. This joint element is modelled as an assembly of finite elements and therefore it can be adapted to complex geometries. Moreover, this also ensures that the joint element include necessary mechanical properties.

The main advantage of this methodology is the use of beam displacement modes because this allows a the use of a reduced number of degrees of freedom. The mode-based formulation is seen as a powerful tool for analyses of thin-walled beam members. Among others, the *Generalised Beam Theory* (GBT) could be mentioned as an approach to utilise the efficiency related to mode-based formulations. An example could be Abambres et al. [4]. It follows that within the framework of GBT an approach to analysing entire frame structures has been developed by Basaglia et al. [5, 6]. Nonetheless, this methodology has some difficulty in formulating a fully mode-based formulation because the implementation of joint elements is not compatible with the mode-based GBT formulation. Thus, beam ends are transformed from the mode formulation into the seven generalised beam displacements, which was introduced in line with the Vlasov thin-walled beam

*Corresponding author
Email address: jej@byg.dtu.dk (Jeppe Jönsson)

theory [7]. Consequently, the advantages from the mode-based GBT formulation are lost concerning the joint elements. Moreover, to include local effects, such as distortion, constraint equations need to be identified based on a previous finite element assessment and then added to the seven generalised degrees of freedom, [8].

The methodology presented here includes arbitrary joint configurations in a global frame analysis. For simplicity, the formulation considers only direct connections, not including components such as bolts, but reflects welded connections. The frame is subdivided into beam and joint elements in a global Cartesian reference system.

The analysis of frames presented in this paper is performed as a first-order linear elastic analysis assuming isotropic material behaviour and small displacements without second-order effects. Furthermore, the methodology gives the ability to decompose an arbitrary deformation into well-known displacement modes. In extension, the substructuring technique may be utilised as well as duplicating identical elements within the frame.

2. Mode-based methodology

The generic methodology, which is presented, is based on a formulation where beam displacement modes govern the connections between beam elements. Let us outline the methodology. A beam element is formulated based on a set of beam displacement modes where each mode consists of a cross-sectional displacement field consist of an in-plane part and an out-of-plane part. An amplitude function is used to describe the variation of the cross-sectional displacement field along the beam element. Hence, instead of conventional finite element degrees of freedom at the beam end, the cross-sectional beam displacement fields are used as novel set of modal degrees of freedom. Consequently, the connected faces at a joint element must likewise be transformed into this modal degree of freedom space governed by the beam elements.

2.1. General beam element formulation

In general, the formulation uses advanced beam elements which relies on the definition of uncoupled cross-sectional displacmenet fields , such as GBT [9, 10] or the approach presented by the authors in [2, 3]. The advanced beam uses a set of orthogonal cross-sectional displacement modes, to derive a standard linear elastic stiffness equation that governs the problem.

$$\mathbf{K}^{\mathsf{B}}\,\mathbf{u}^{\mathsf{B}} = \mathbf{f}^{\mathsf{B}} \tag{1}$$

where the superscript B is introduced to specify terms related to beam elements. In the following, the index may be followed by a number that refers to a specific beam element number. The components in Equation (1) are the beam stiffness matrix $\mathbf{K}^{\mathsf{B}}$, the displacement and load vectors, $\mathbf{u}^{\mathsf{B}}$ and $\mathbf{f}^{\mathsf{B}}$ respectively. Regarding the displacement vector, it shall be organised such that the degrees of freedom at each beam end are grouped separately in such a way that the displacement vector explicitly will be written as:

$$\mathbf{u}^{\mathsf{B}} = \begin{bmatrix} \mathbf{u}_0^{\mathsf{B}} \\ \mathbf{u}_\ell^{\mathsf{B}} \end{bmatrix} \tag{2}$$

in which $\mathbf{u}_0^{\mathsf{B}}$ and $\mathbf{u}_\ell^{\mathsf{B}}$ relates to the displacements at each end cross-section, respectively. Similar separation follows for the load vector $\mathbf{f}^{\mathsf{B}}$. To clarify this notation a simple two-dimensional example is illustrated in Figure 1a. Here, only in-plane degrees of freedom are considered.

2.2. General formulation of a joint element

Besides the general formulations of a beam element in previous subsection, the methodology introduces a novel joint element. This element is a three-dimensional super-element that is a result of a discretisation of the joint geometry by finite elements, e.g. shell elements. Based on the standard finite element method, a linear elastic equation system for a joint element is derived by numerical integrations:

$$\mathbf{K}^{\mathsf{J}}\,\mathbf{u}^{\mathsf{J}} = \mathbf{f}^{\mathsf{J}} \tag{3}$$

where the superscript J refers to joint elements. Similar to the beam element notation, the index may be followed by a number referring to a global joint element number. The components in Equation (3) are the joint stiffness matrix $\mathbf{K}^{\mathsf{J}}$, the displacement vector $\mathbf{u}^{\mathsf{J}}$, and the load vector $\mathbf{f}^{\mathsf{J}}$, respectively. Based on the degrees of freedom in Equation (3), the system is organised such that the degrees of freedom in each beam-to-joint interface are clustered. Therefore, the displacement vector can be written as:

$$\mathbf{u}^{\mathsf{J}} = \begin{bmatrix} \mathbf{u}_1^{\mathsf{J}} \\ \vdots \\ \mathbf{u}_i^{\mathsf{J}} \\ \vdots \\ \mathbf{u}_{n_{\mathrm{I}}}^{\mathsf{J}} \\ \hdashline \mathbf{u}_{\mathsf{o}}^{\mathsf{J}} \end{bmatrix} \tag{4}$$

where $\mathbf{u}^{\mathsf{J}}$ without an index contains all degrees of freedom related to a single joint element whereas each vector $\mathbf{u}_i^{\mathsf{J}}$ relates to an interface, for $i = 1, .., n_{\mathrm{I}}$ and n_{I} is the number of interfaces, i.e. number of adjacent beam elements. The vector $\mathbf{u}_{\mathsf{o}}^{\mathsf{J}}$ holds the remaining degrees of freedom, which are internal degrees of freedom, degrees of freedom with a boundary conditions or a load. The categorisation in Equation (4) is also illustrated in the simplified two-dimensional example in Figure 1a for a joint element.

2.3. Transformation and base change

One of the main requirements with this approach is that the interfaces between beam elements and joint elements share the same number as well as location of nodes (and consequently also degrees of freedom).

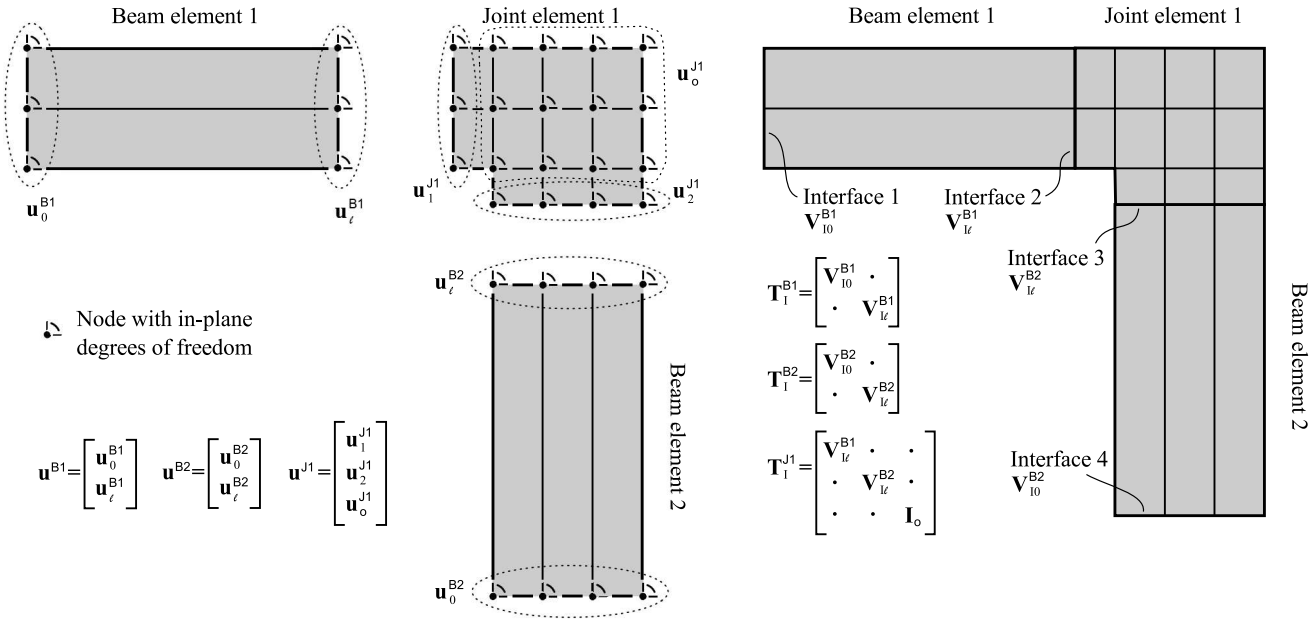

(a) Individual elements and their clustering of the degrees of freedom

(b) Assembly of individual elements and interfaces are identified

Figure 1: Illustration of the subdivision and categorisation of degrees of freedom with respect to individual elements. The assembly of beam elements and joint elements illustrates the interfaces that are located at element boundaries

The idea is that the degrees of freedom at the interfaces shall be expressed in terms of uncoupled displacement modes. To do so, a base change is introduced from standard degrees of freedom into cross-sectional beam displacement mode-related degrees of freedom. Thus, each set of degrees of freedom in the element at a specific interface is transformed according to:

$$\mathbf{u} = \mathbf{V}_\mathrm{I}\, \mathbf{u}_\mathrm{I} \tag{5}$$

where the displacement vector $\mathbf{u}$ can either be $\mathbf{u}_0^\mathsf{B}$ or $\mathbf{u}_\ell^\mathsf{B}$ from Equation (2), or one of the vectors $\mathbf{u}_i^\mathsf{J}$ from Equation (4) containing standard degrees of freedom, and the subscript I is introduced to identify interface terms. Accordingly, the columns in the transformation matrix $\mathbf{V}_\mathrm{I}$ contains orthogonal cross-sectional displacement modes. These modes will be referred to as interface modes. One of the key stones in this methodology is that the number of interface modes in $\mathbf{V}_\mathrm{I}$ can be reduced such that the number of modal degrees of freedom will be less than the number of conventional degrees of freedom. Note that the modes chosen are governed by the beam element connected to the interface. Furthermore, $\mathbf{u}_\mathrm{I}$ is the column vector containing the intensities of the interface modes – This being the new set of modal degrees of freedom.

At each interface the transformation in Equation (5) shall be executed, meaning that a beam element, which has two interfaces, has two identical transformations related to the two interfaces – one at each beam end – and thus the entire beam element transformation and transformation matrix can be written as:

$$\mathbf{u}^\mathsf{B} = \mathbf{T}_\mathrm{I}^\mathsf{B}\, \mathbf{u}_\mathrm{I}^\mathsf{B} \quad \text{with } \mathbf{T}_\mathrm{I}^\mathsf{B} = \begin{bmatrix} \mathbf{V}_{\mathrm{I}0}^\mathsf{B} & \cdot \\ \cdot & \mathbf{V}_{\mathrm{I}\ell}^\mathsf{B} \end{bmatrix} \tag{6}$$

in which $\mathbf{V}_{\mathrm{I}0}^\mathsf{B}$ and $\mathbf{V}_{\mathrm{I}\ell}^\mathsf{B}$ are sets of cross-sectional displacement modes chosen to represent the possible displacement field of the particular interface at each of the beam ends, respectively. An example of the beam element transformation matrix and its two matrices containing the interface modes are shown in Figure 1b. Moreover, Figure 2 presents the idea of interface modes, i.e. cross-sectional beam displacement fields, with respect to Beam element 1 from Figure 1. The interface modes are contained in $\mathbf{V}_{\mathrm{I}\ell}^{\mathsf{B}1}$, which occur at Interface 2 according to Figure 1b

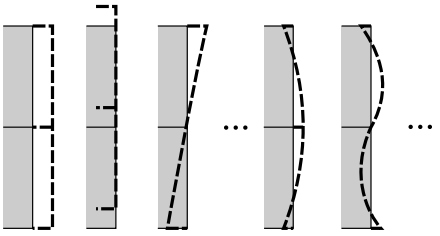

Figure 2: Visualisation of interface modes at the right end of Beam element 1 in Figure 1a

With respect to a joint element the number of interfaces, and thereby the size of the transformation matrix needed, depends on the number of adjacent beam elements. In accordance with Equation (4) and (5) the transformation and the transformation matrix with respect to a joint ele-

ment will be:

$$\mathbf{u}^{\mathsf{J}} = \mathbf{T}_{\mathrm{I}}^{\mathsf{J}}\, \mathbf{u}_{\mathrm{I}}^{\mathsf{J}} \quad \text{with } \mathbf{T}_{\mathrm{I}}^{\mathsf{J}} = \left[\begin{array}{ccc:c} \mathbf{V}_{\mathrm{I}1} & & & \\ & \ddots & & \\ & & \mathbf{V}_{\mathrm{I}n_{\mathrm{I}}} & \\ \hdashline & & & \mathbf{I}_{\mathsf{o}} \end{array}\right] \tag{7}$$

Here, $\mathbf{I}_{\mathsf{o}}$ is an identity matrix of size equal to the number of degrees of freedom of the joint element that are not located at an interface, that is the size of $\mathbf{u}_{\mathsf{o}}^{\mathsf{J}}$, in the case of not having all the internal degrees of freedom eliminated. Each set of cross-sectional displacement modes contained in the matrices $\mathbf{V}_{\mathrm{I}i}$ for $i = 1, .., n_{\mathrm{I}}$ may differ in size depending on the number of nodes at the specific interface as well as the number of interface modes to be included. However, two elements sharing the same interface must use the same interface modes for the transformations. Thus, the matrix $\mathbf{V}_{\mathrm{I}0}^{\mathsf{B}}$ or $\mathbf{V}_{\mathrm{I}\ell}^{\mathsf{B}}$ from Equation (6) must equal the same interface mode matrix in $\mathbf{T}_{\mathrm{I}}^{\mathsf{J}}$ for the same interface. For clarity, see also Figure 1b, where it has been illustrated how the different transformation matrices are composed. Note that nodes may not be shared between interfaces.

Applying the transformation laws with the transformation matrices in Equation (6) and (7), respectively, on both the beam element equation system in Equation (1) and the joint element equation system in Equation (3) these systems of equations can be expressed in terms of cross-sectional beam displacement modes.

To this end, the methodology is presented, illustrating how a beam element and a joint element can be transformed into a mode-based formulation. Finally, an entire equilibrium equation system for an entire frame structure can be assembled according to standard assembly procedures, e.g. described by Cook et al. [11]. Hence, this assembly results in:

$$\mathbf{K}^{\mathsf{sys}}\, \mathbf{u}^{\mathsf{sys}} = \mathbf{f}^{\mathsf{sys}} \tag{8}$$

In which the system degrees of freedom $\mathbf{u}^{\mathsf{sys}}$ are the modal interface degrees of freedom describing the displacement mode intensities at the interface. Throughout the next two sections, the specific joint element and beam element formulation and modelling used in the present work, will be deduced.

3. Joint modelling

This section introduces a procedure to formulate a joint element that is compatible with the methodology previously outlined.

For simplicity, it has been chosen to use plane triangular shell elements with three nodes and six degrees of freedom at each node (see also Figure 3), which is the simplest element allowing the modelling of complex geometries. This shell element is a combination of the following plane constant strain triangular element and plane flexural element.

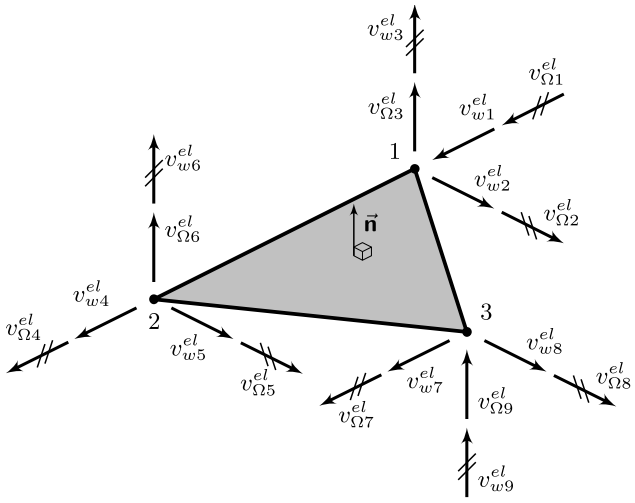

Figure 3: Triangular finite shell element and its degrees of freedom. Degrees of freedom related to in-plane deformations are denoted with a w-subscript and degrees of freedom related to out-of-plane deformations are denoted with an Ω-subscription. Element normal indicated by $\vec{\mathbf{n}}$

- A *Constant Strain Triangle*-element (CST-element) with an extra drilling degree of freedom parallel to the plate normal. The stiffness of this rotational degree of freedom is applied as an artificial stiffness being defined as a fraction of the largest value in the element stiffness matrix diagonal. Furthermore, this element includes degrees of freedom related to membrane actions only and are denoted with a w-subscript (the in-plane displacements). See also Cook et al. [11] for more detailed elaboration.

- A *Specht*-element presented by Specht [12]. This element covers the flexural displacements and can deform out of the element plane. Its degrees of freedom are denoted with an Ω-subscript.

The derivation of stiffness matrices of these two subelements are not included here, nor is the combination of these, which yields an element stiffness matrix of size 18×18. Depending on the joint discretisation, an entire joint element stiffness matrix $\mathbf{K}^{\mathsf{J}}$ with corresponding boundary and load vectors, $\mathbf{u}^{\mathsf{J}}$ and $\mathbf{f}^{\mathsf{J}}$, respectively, is derived and leads to the linear equation system in Equation (3). The joint element standard finite nodal degrees of freedom given in $\mathbf{u}^{\mathsf{J}}$ will be divided into three categories:

$\mathbf{u}_{\mathsf{j}}$ Degrees of freedom that overlap with beam degrees of freedom at the interface between connected faces. Hence, according to Equation (4) we have: $\mathbf{u}_{\mathsf{j}}^{\mathsf{T}} = \left[\, \mathbf{u}_1^{\mathsf{J}\,\mathsf{T}}, \cdots, \mathbf{u}_{n_{\mathrm{I}}}^{\mathsf{J}\,\mathsf{T}} \,\right]$.

$\mathbf{u}_{\mathsf{f}}$ Joint element degrees of freedom selected for boundary or load properties since these effects must be included in the joint element as a consequence of the methodology. These, we keep as standard finite ele-

ment degrees of freedom throughout the entire formulation.

$\mathbf{u}_\mathsf{i}$ Internal degrees of freedom. These represent all the remaining degrees of freedom. Due to speed optimisation these may be eliminated by condensation.

The remaining degrees of freedom $\mathbf{u}_\mathsf{o}^\mathsf{J}$ from Equation (4) is separated into the two parts $\mathbf{u}_\mathsf{f}$ and $\mathbf{u}_\mathsf{i}$. Having rearranged the system from Equation (3), based on the three categories of degrees of freedom listed above, we may write the equilibrium equations more explicitly:

$$\left[\begin{array}{c|c|c} \mathbf{K}_\mathsf{j} & \mathbf{K}_\mathsf{jf} & \mathbf{K}_\mathsf{ji} \\ \mathbf{K}_\mathsf{fj} & \mathbf{K}_\mathsf{f} & \mathbf{K}_\mathsf{fi} \\ \hline \mathbf{K}_\mathsf{ij} & \mathbf{K}_\mathsf{if} & \mathbf{K}_\mathsf{i} \end{array}\right] \left[\begin{array}{c} \mathbf{u}_\mathsf{j} \\ \mathbf{u}_\mathsf{f} \\ \hline \mathbf{u}_\mathsf{i} \end{array}\right] = \left[\begin{array}{c} \mathbf{f}_\mathsf{j} \\ \mathbf{f}_\mathsf{f} \\ \hline \mathbf{f}_\mathsf{i} \end{array}\right] \tag{9}$$

The internal degrees of freedom located in the vector $\mathbf{u}_\mathsf{i}$ can be eliminated such that:

$$\mathbf{u}_\mathsf{i} = \left[\mathbf{K}_\mathsf{i}\right]^{-1} \left(\mathbf{f}_\mathsf{i} - \left[\mathbf{K}_\mathsf{ij} \;\; \mathbf{K}_\mathsf{if}\right] \left[\begin{array}{c} \mathbf{u}_\mathsf{j} \\ \mathbf{u}_\mathsf{f} \end{array}\right] \right) \tag{10}$$

and thus, the equation system is rewritten as:

$$\tilde{\mathbf{K}}^\mathsf{J}\, \tilde{\mathbf{u}}^\mathsf{J} = \tilde{\mathbf{f}}^\mathsf{J} \tag{11}$$

where the stiffness matrix is computed according to Equation (12) and the boundary and load vectors follow in Equation (13).

$$\tilde{\mathbf{K}}^\mathsf{J} = \left[\begin{array}{cc} \mathbf{K}_\mathsf{j} & \mathbf{K}_\mathsf{jf} \\ \mathbf{K}_\mathsf{fj} & \mathbf{K}_\mathsf{f} \end{array}\right] - \left[\begin{array}{c} \mathbf{K}_\mathsf{ji} \\ \mathbf{K}_\mathsf{fi} \end{array}\right] \left[\mathbf{K}_\mathsf{i}\right]^{-1} \left[\mathbf{K}_\mathsf{ij} \;\; \mathbf{K}_\mathsf{if}\right] \tag{12}$$

$$\tilde{\mathbf{u}}^\mathsf{J} = \left[\begin{array}{c} \mathbf{u}_\mathsf{j} \\ \mathbf{u}_\mathsf{f} \end{array}\right] \;\text{ and }\; \tilde{\mathbf{f}}^\mathsf{J} = \left[\begin{array}{c} \mathbf{f}_\mathsf{j} \\ \mathbf{f}_\mathsf{f} \end{array}\right] - \left[\begin{array}{c} \mathbf{K}_\mathsf{ji} \\ \mathbf{K}_\mathsf{fi} \end{array}\right] \left[\mathbf{K}_\mathsf{i}\right]^{-1} \mathbf{f}_\mathsf{i} \tag{13}$$

After the elimination of internal degrees of freedom, the remaining ones are listed such that we have the degrees of freedom at beam interfaces followed by those degrees of freedom at the boundaries and the loaded ones. Hence, the non-condensed degrees of freedom are explicitly written as:

$$\tilde{\mathbf{u}}^\mathsf{J} = \left[\begin{array}{c} \mathbf{u}_{\mathsf{j}_1} \\ \vdots \\ \mathbf{u}_{\mathsf{j}_i} \\ \vdots \\ \mathbf{u}_{\mathsf{j}_{n_\mathrm{I}}} \\ \hline \mathbf{u}_\mathsf{f} \end{array}\right] \tag{14}$$

where a vector $\mathbf{u}_{\mathsf{j}_i}$ having an index is a subset of $\mathbf{u}_\mathsf{j}$. Each subset contains all the conventional degrees of freedom at the beam-to-joint interface i. The total number of interfaces at a specific joint element is denoted n_I. For illustration purpose, Figure 4 represents the two-dimensional joint element from Figure 1a in terms of the notation introduced through Equation (14).

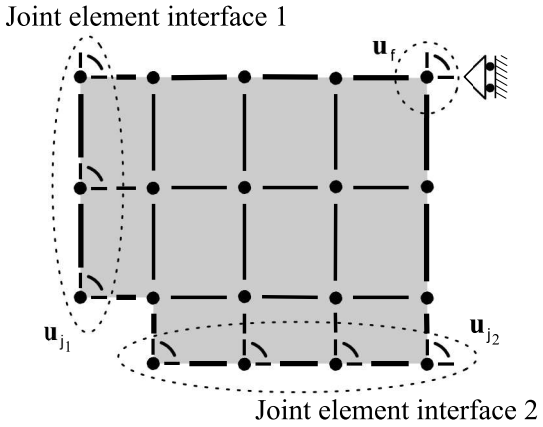

Figure 4: Joint element with degrees of freedom according to Equation (14) being $\mathbf{u}_{\mathsf{j}_1}$ and $\mathbf{u}_{\mathsf{j}_2}$ at the interfaces and $\mathbf{u}_\mathsf{f}$ at the upper right corner where a support is introduced. The internal degrees of freedom $\mathbf{u}_\mathsf{i}$ are condensed

4. Beam modelling

Any displacement mode-based beam theory may be adopted here. The main requirement, which must be fulfilled is that the beam element shall be able to be expressed in terms of displacement modes and deduce a set of orthogonal cross-sectional displacement fields that occur at the beam ends. This could, for example, be beam elements formulated by the GBT where beam displacement modes are deduced based on orthogonal cross-sectional displacement fields. Nonetheless, it has been chosen to adopt the advanced beam theory presented by the authors in [2, 3], which is briefly summarised in Appendix A as well. Hence, the beam element formulation in Equation (1) is valid according to Equation (A.20).

The cross-section displacement modes to be used in the mode transformation are deduced as a part of the beam element formulation. To explain, the beam cross-section is discretised by straight wall elements and by use of strain energy the beam equilibrium equations are derived. This equation system is then used to determine cross-sectional displacement fields with associated axial variations as solution modes to the beam equilibrium equations. Examples of the cross-sectional displacement fields are illustrated in Figure 5 and 6, where Figure 5 includes those cross-sectional displacement fields that corresponds to the polynomial beam modes and Figure 6 contains those displacement fields that corresponds to the exponential beam modes. The modes are deduced with respect to the cross-section assessed in Example 1 in Section 5.1.

The mode determination procedure is an exact solution method for the second-order differential equation system, which is solved as a quadratic eigenvalue problem. Consequently, twice as many solution modes are deduced and therefore, the modes do not span an orthogonal vector-space. Hence, a selection procedure is required to formulate the transformation matrix $\mathbf{V}_\mathrm{I}$ used in Equation (6).

The cross-sectional beam displacement modes are given

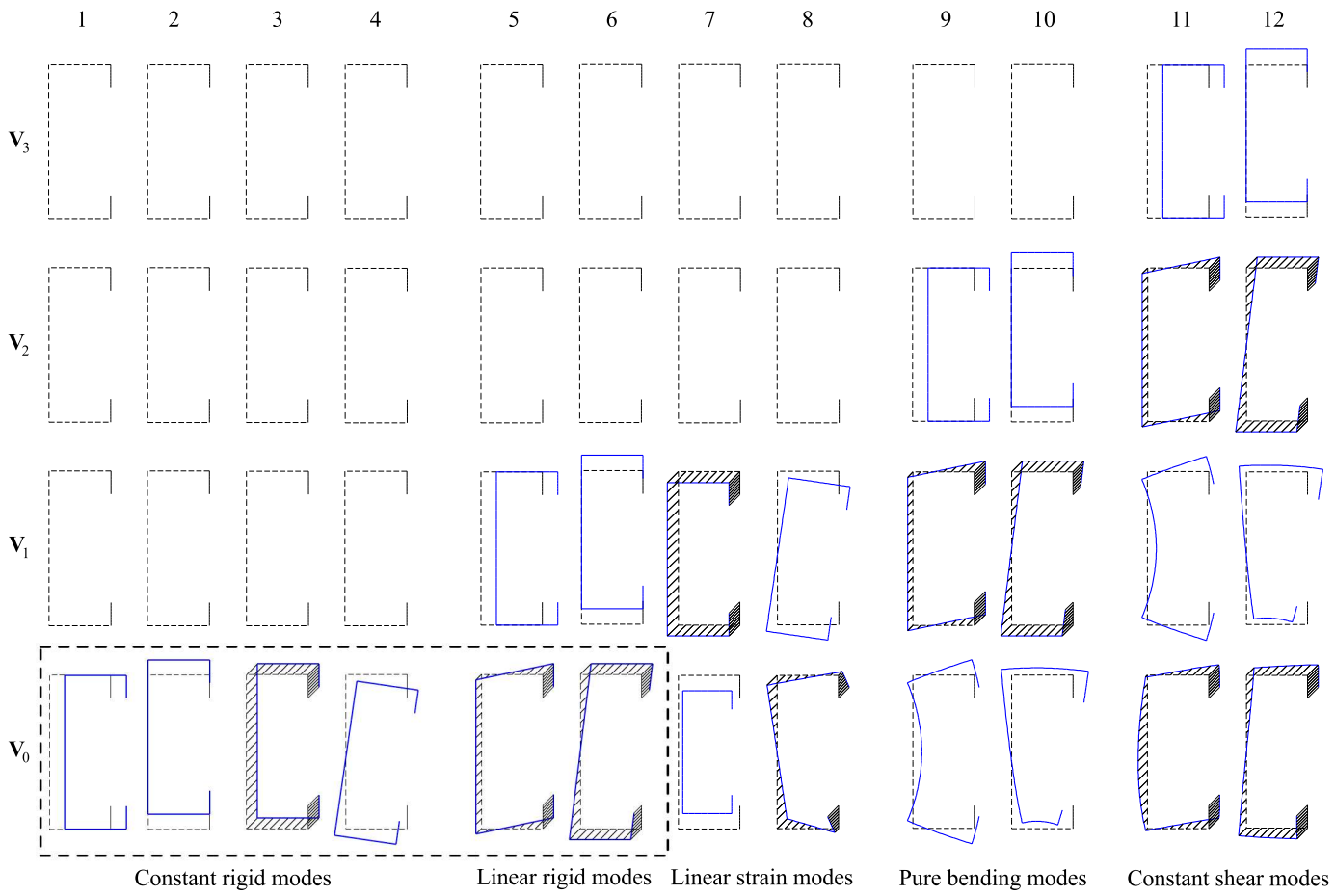

Figure 5: Cross-sectional displacement modes used to represent the fundamental beam displacement modes, which have the polynomial amplitude function. Each row represents the content in the four matrices $\mathbf{V}_3$ to $\mathbf{V}_0$, respectively. The dotted-line-box highlights the six rigid motions adopted as part of the interface modes

as columns in the matrix $\mathbf{V}$ (see also Equation (A.18)). The modes both represent solutions with a polynomial axial variation (Figure 5) as well as solutions with exponential axial variations (Figure 6). The modes are categorised as fundamental and distortional modes, respectively. Thus, the matrix $\mathbf{V}$ may, therefore, be subdivided into two subsets, which we write as:

$$\mathbf{V} = \left[\mathbf{V}_p \ , \ \mathbf{V}_e \right] \tag{15}$$

The polynomial modes are contained in $\mathbf{V}_p$ and consists of four submatrices, hence $\mathbf{V}_p = [\mathbf{V}_3 \ \mathbf{V}_2 \ \mathbf{V}_1 \ \mathbf{V}_0]$, where each subscript refers to the polynomial order that the specific mode refers to. For clarity see also Equation (A.12) and Figure 5 in which each row represents the content of the four matrices $\mathbf{V}_3$ to $\mathbf{V}_0$, respectively. According to [3] the modes in $\mathbf{V}_1$, $\mathbf{V}_2$ and $\mathbf{V}_3$ are repetitions of the modes in $\mathbf{V}_0$, and therefore these are not relevant for the procedure finding a set of orthogonal cross-sectional beam displacement modes. Through an in-depth assessment of the modes in $\mathbf{V}_0$ only the six rigid cross-sectional displacement modes should be used, which are highlighted in Figure 5 with the dotted box as well. The remaining six modes in $\mathbf{V}_0$ corresponds to distortional behaviours, e.g. due to Poisson effects and shear stresses, which can be found as combinations of the cross-sectional displacement modes in the distortional set of modes contained in $\mathbf{V}_e$.

Because the solution modes in $\mathbf{V}$ are found as solutions to a quadratic eigenvalue problem, the distortional modes are determined as either real pairs or complex quadruples. Within each pair of modes or quadrupled set of modes, the mode-vectors are similar only with different signs. Moreover, each set shares the same eigenvalue, which only deviates in the sign as well. To avoid repeated modes in the transformation matrix, Equation (5), and thereby a singular transformation matrix, a procedure is implemented choosing the correct modes from the full set of modes in $\mathbf{V}_e$. Accordingly, in case of a real pair of cross-sectional displacement modes we have, $[\mathbf{v} \ -\mathbf{v}] \in \mathbf{V}_e$. Here, the first vector is chosen for the transformation, and the other one is rejected (see for example mode 13 and 14 in Figure 6, where mode 13 is chosen but mode 14 has been rejected). In the case of having a set of complex quadruples, the selection is a bit more sophisticated. A complex set of modes can be written as:

$$\left[\mathbf{v} \ \ -\mathbf{v} \ \ \ \overline{\mathbf{v}} \ \ -\overline{\mathbf{v}} \right] \in \mathbf{V}_e \tag{16}$$

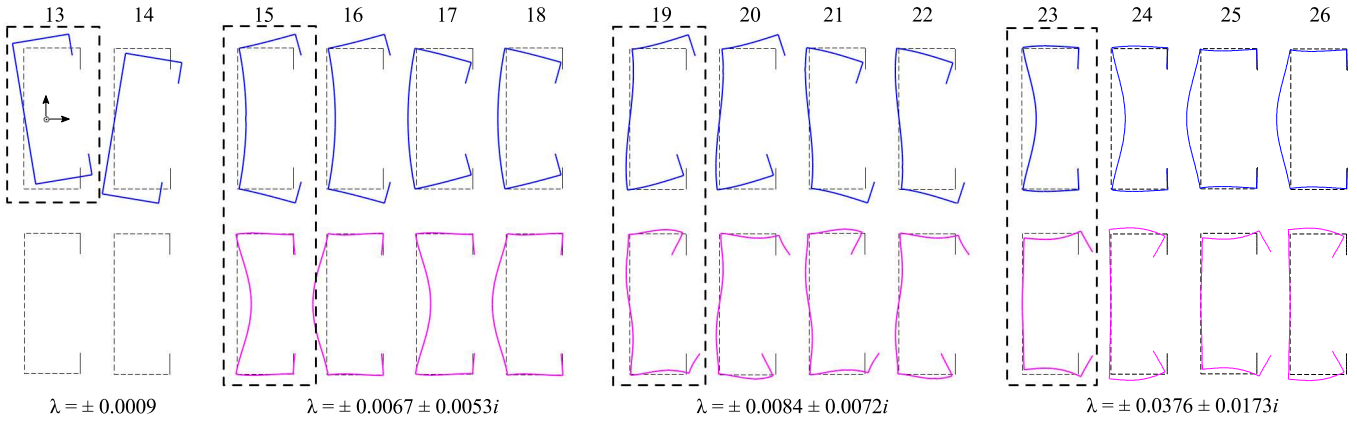

(a) The in-plane part of cross-sectional displacement modes. The upper row represents the real part and the lower row represents the imaginary part

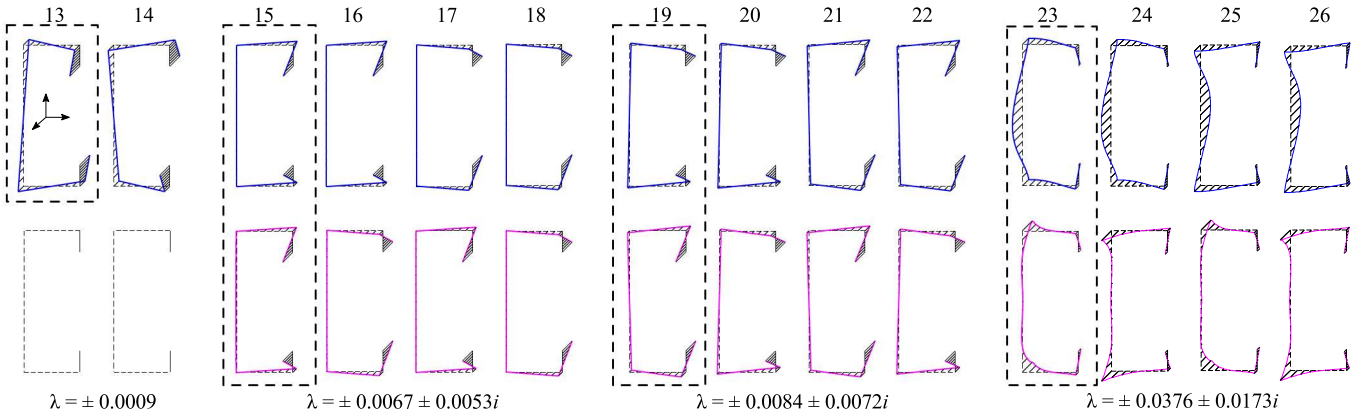

(b) The out-of-plane part of the cross-sectional displacement modes (warping). The upper row represents the real part and the lower row represents the imaginary part

Figure 6: The first number of cross-sectional displacement modes from $\mathbf{V}_e$ that have an exponential axial variation. The modes are represented by one pair of real modes and three quadruples of complex modes (each mode eigenvalue is represented as well). The dotted boxes indicates those modes chosen for interface modes

where a single mode is: $\mathbf{v} = \mathbf{a} + \mathbf{b}i$ and $\mathbf{a}$ and $\mathbf{b}$ represents the real and imaginary part of the vector, respectively. To represent the complex quadruples in Equation (16), the vectors $\mathbf{a}$ and $\mathbf{b}$ are chosen as the unique modes for the transformation and therefore added separately to the matrix $\mathbf{V}_\mathrm{I}$ (see also Figure 6, where the modes 15, 19, and 23 are the modes used as interface modes, which have been illustrated in Figure 9 as well).

To test whether the chosen modes span an orthogonal vector-space it is convenient to compute the null-space of the mode-transformation-matrix $\mathbf{V}_\mathrm{I}$, that is:

$$\mathcal{N}(\mathbf{V}_\mathrm{I}) \in \emptyset \tag{17}$$

where $\mathcal{N}(\ )$ is the null-space operator. Fulfilling this, the mode orthogonality is confirmed.

4.1. Normalisation of interface modes

To be able to compare mode intensities in a later post-analysing assessment of elements based on modes, the modes in $\mathbf{V}_\mathrm{I}$ are normalised by letting the translational degree of freedom with the largest absolute magnitude in each mode be equal to unity.

5. Illustration of the methodology

Throughout this section, the approach, which has been presented in the present paper, is applied to two examples illustrating the versatility and usability. The examples are:

1. A right angled frame corner assembling two similar lipped open channel sections with different configurations of stiffeners in the joint.

2. A beam-to-column connection between rectangular hollow sections inducing plate bending and thus, influenced by local plate bending modes.

The present approach has been modelled by use of the numerical software MATLAB [13] and the general material properties used are Young's modulus: $E = 210$ GPa and a Poisson ratio equal to: $\nu = 0.3$. In general, the joint elements that will be used in the following examples are modelled using triangular shell finite elements, like the one in Figure 3. The artificial stiffness related to the rotational degrees of freedom (v^{el}_{w3}, v^{el}_{w6}, v^{el}_{w9}) is chosen as 10^{-9} times

the maximum absolute value in the diagonal of the element stiffness matrix.

5.1. Ex. 1 – Frame corner

This example analyses the mechanical behaviours of a connection in a portal frame. The connection is an orthogonal assembly of two equal length thin-walled lipped channel sections, as illustrated in Figure 7. The dimensions are given in the figure as well. The frame corner is modelled by two beam elements and three joint elements (one primary joint element at the corner and two secondary joint elements at the two free beam ends). The boundary conditions are applied to three individual nodes. One being pinned, one being pinned and movable in the Z-direction, and one being pinned and movable in the Y- and Z-directions. However, all three supports prevent translational movements out of the frame plane (in the global X-direction), which for example could be prevented by purlins in a real structure. The load P is applied as a nodal load with a magnitude of 100 N.

To present an in-depth assessment of the frame corner and the transmission of displacements through the corner joint element, different stiffening configurations have been tested to identify the influences from stiffeners on the frame behaviour. Hence, four different joint configurations have been used throughout this example being:

- a joint without any stiffening plates [non]
- a joint with a diagonal stiffening plate [dia]
- a joint with two stiffening plates (box stiffened) [box]

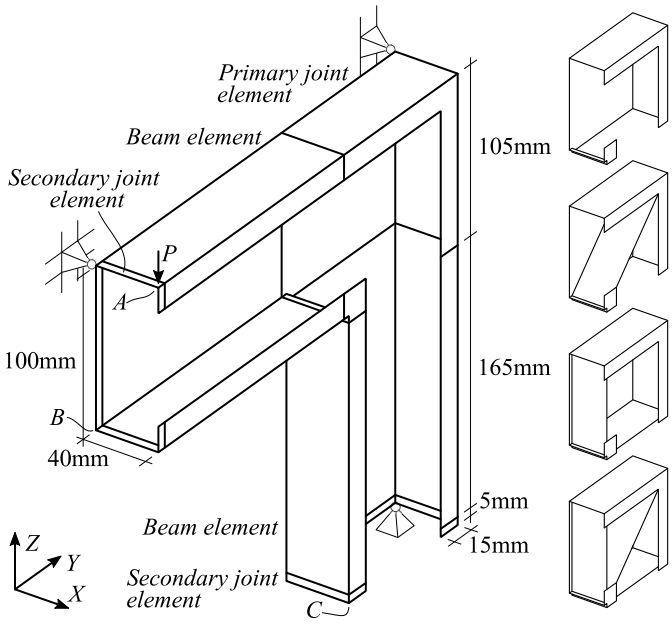

Figure 7: Ex. 1 – The set-up. All plates are 2 mm thick, and the point load is $P = 100$ N. To the right, the four different joint configurations are shown

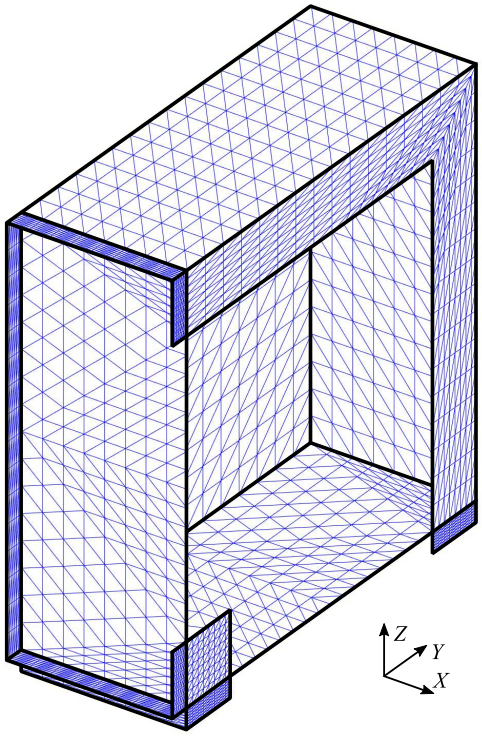

Figure 8: Ex. 1 – Mesh density of the primary joint element with the box stiffening configuration

- a joint fully stiffened with three stiffening plates (diagonal and box stiffeners) [full]

The names in squared parenthesis will be used when referring to the different stiffening configurations. Furthermore, these joint configurations are shown to the right in Figure 7 as well. Except the degrees of freedom chosen to represent boundary conditions, loads, and those at the connected faces, the remaining will be condensed according to the procedure in Section 3.

The discretisation of the joint elements are governed by the nodes chosen in the connected beam element. To illustrate the mesh density Figure 8 shows a discretised primary joint element with box stiffeners.

The beam element stiffness matrices are deduced using the approach outlined in Appendix A with a discretisation having eight wall elements in each lip, eight wall elements in the flanges, and sixteen wall elements along the web. This results in a total of 294 interface modes, i.e. degrees of freedom at each interface. The unique first 13 cross-sectional displacement modes used as part of the transformation matrix $\mathbf{V}_\mathrm{I}$ are illustrated in Figure 9. The order of the modes is based on the eigenvalues that relates to the beam displacement modes (see also Figure 6). The first six interface modes reflects the rigid displacements of the interface, then follows the global distortional modes and after these modes the local displacement modes follow. Because the two beam elements are identical, they share the same stiffness matrix as well as the same cross-sectional displacement modes to be used, transforming the

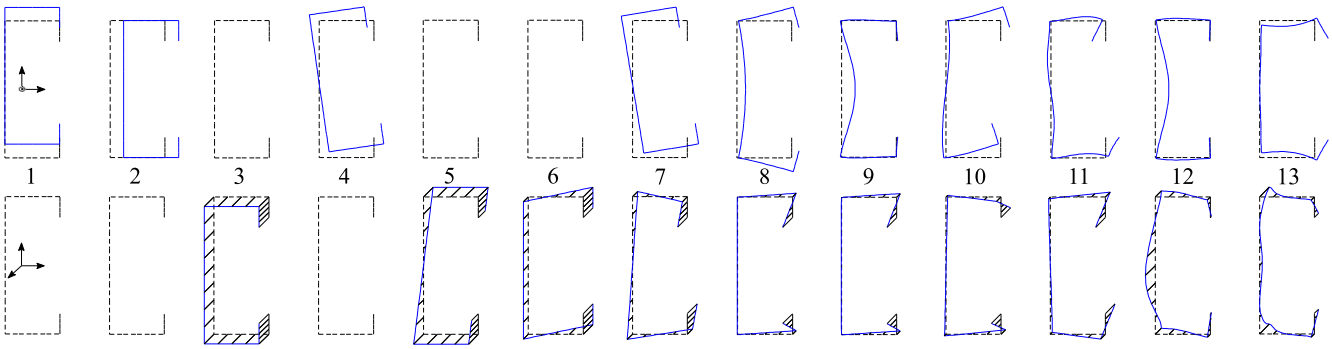

Figure 9: Ex. 1 – The first 13 modal-degrees of freedom out of 294 modes representing the interface modes. The upper row represents the in-plane part and the lower row represents the displacements orthogonal to the cross-sectional plane (warping)

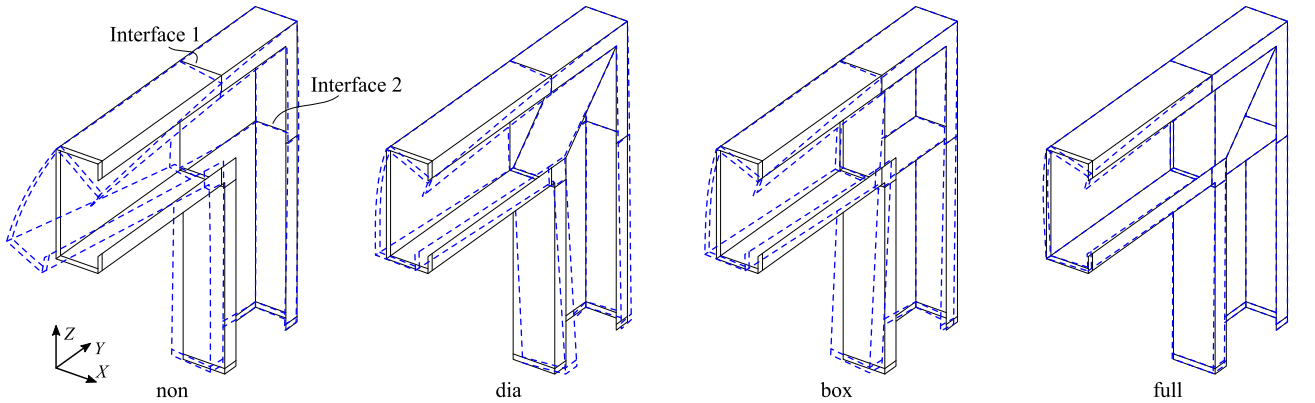

(a) Global deformations (the illustrated displacements are scaled 30 times)

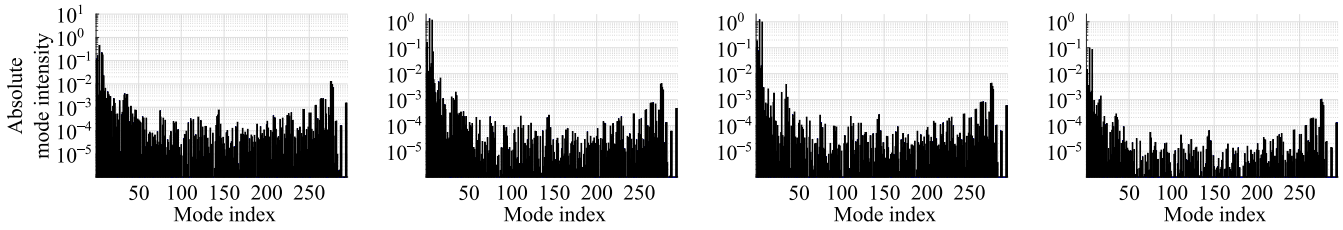

(b) Absolute mode intensities at Interface 1

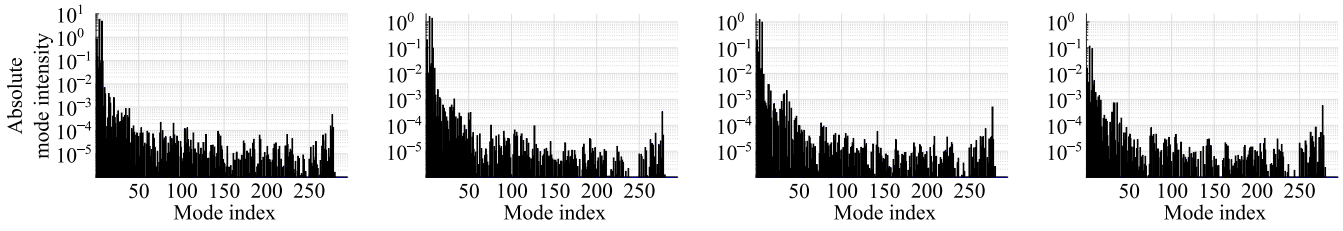

(c) Absolute mode intensities at Interface 2

Figure 10: Ex. 1 – Global deformation and mode intensities at the two interfaces related to the primary joint element with different stiffness configurations

formulation into the mode-based formulation.

5.1.1. Verification

Before a detailed assessment of the frame corner is conducted, a comparison of the present approach is conducted comparing with a full finite element analysis. To this purpose the commercial finite element software `Abaqus` [14] has been used. Hence, the frame corner with the box-stiffened joint configuration has been chosen to verify against `Abaqus`. The finite element model discretises the entire frame corner with triangular shell finite elements (S3 in `Abaqus` nomenclature) with full integration and in a structured mesh. The meshing is conducted with a maximum element side length of maximum 5 mm, and in some regions, even a finer mesh has been used. The displacements at the three locations A, B, and C have been measured and listed in Table 1 (see also Figure 7). The largest displacement at each point is highlighted with boldface and the relative deviations for these displacements are at point A: $\Delta u_Z = 1.40\,\%$, at point B: $\Delta u_X = -1.18\,\%$, and at point C: $\Delta u_X = -1.88\,\%$, respectively.

5.1.2. Mode-based assessment

Figure 10a shows each of the four frame corners with their associated global displacements. The first to be observed is the reduction in displacements at the ends when the stiffening configurations at the corner is increased. Additionally, it is seen how the transmission of rotation is more and more prevented increasing the number of stiffening plates, with almost no deformations being transmitted with the fully stiffened joint configuration.

Now, continuing the assessment, the mode identification is considered next. In Figure 10b and 10c the intensities of each mode at the interface between a beam element and the primary joint element are shown as bar-diagrams. These intensities are directly extracted from $\mathbf{u}_\mathrm{I}$. Each graph relates to one of the two joint corner interfaces. In each diagram, a bar represents a mode, and the intensity is given at the vertical axis. To be noticed is that the vertical axis is logarithmic. Common for all graphs in Figure 10 is that those modes with the highest intensity, i.e. the most pronounced displacement modes at an interface, are the first ones. This is the case for all four kinds of joint configurations. In Table 2, the ten modes with the highest absolute intensity values are listed for each stiffening configuration. This table indicates that the primary modes being activated are the modes related to rigid movements (mode 1–6) and the first torsional and distortional modes (mode 7–9)(see also Figure 9). However, what is observed as well is that a few modes with a high intensity belong to the upper mode index (modes 275–278). A tendency that is seen in all four joint configurations according to Figure 10. Therefore, an assessment of these modes has been conducted and resulted in the conclusion that these modes contribute only with a small displacement being

Table 1: Ex. 1 – Displacements measured for the frame corner with the box stiffening configuration, $[\,\cdot\,10^{-2}\mathrm{mm}]$

		A	B	C
Present	u_X	−0.02	**−39.42**	**−40.91**
theory	u_Y	−0.70	0.33	−11.22
	u_Z	**−56.44**	−0.77	−6.13
`Abaqus`	u_X	−0.02	**−39.89**	**−41.69**
	u_Y	−0.66	0.27	−11.45
	u_Z	**−55.66**	−0.66	−6.25

Table 2: Ex. 1 – Interface mode intensities

	Interface 1		Interface 2	
	Index	Intensity	Index	Intensity
non	4	−0.4513	4	5.8202
	7	0.2142	7	4.8942
	8	−0.1710	1	0.7937
	2	−0.1634	2	−0.1452
	1	0.1184	6	0.0983
	9	−0.0221	8	−0.0923
	275	−0.0124	5	−0.0766
	276	0.0124	3	−0.0488
	277	−0.0093	10	0.0068
	278	0.0069	15	−0.0039
dia	4	1.3149	4	1.5613
	7	−1.1488	7	1.3515
	1	−0.1621	1	0.1982
	8	−0.0698	8	−0.0966
	6	−0.0238	6	0.0235
	5	0.0177	5	−0.0181
	3	0.0121	10	−0.0160
	2	−0.0077	3	−0.0105
	17	−0.0067	2	0.0073
	9	−0.0058	14	−0.0024
box	4	−1.2067	4	1.2249
	7	0.9689	7	0.9761
	1	0.1821	1	0.1844
	2	−0.0754	2	−0.0674
	6	0.0199	6	0.0157
	5	−0.0158	5	−0.0136
	3	−0.0101	9	0.0094
	276	0.0043	3	−0.0073
	275	−0.0042	8	−0.0047
	35	−0.0037	14	0.0038
full	4	−0.0975	4	0.1153
	7	0.0852	7	0.0918
	1	0.0146	1	0.0164
	2	−0.0034	9	0.0053
	6	0.0021	2	0.0046
	5	−0.0018	8	−0.0035
	17	−0.0013	6	−0.0022
	3	−0.0010	3	0.0019
	276	−0.0010	11	0.0018
	275	0.0010	15	−0.0014

very localised at the end of each lip.

Consequently, it seems intuitive to start out reducing the number of modes (i.e. the number of degrees of freedom) by eliminating modes with a high mode index in the transformation matrix, i.e. Equation (6) and (7). This is done by eliminating modes with a high index in the transformation matrix. To explain the procedure, at first, we keep the first 250 columns, i.e. modes, in $\mathbf{V}_\mathrm{I}$ at all interfaces. Then, we reduce to 225 columns in $\mathbf{V}_\mathrm{I}$, and so forth until the six rigid modes are left. After each reduction of modes (degrees of freedom at each interface) the displacements at the locations A, B and C are measured. The relative deviations, compared to the case, including all 294 modes, is illustrated in Figure 11. It is seen that nearly no variation is observed when reducing to 250 modes, which confirms our hypothesis that the transformation modes with the highest index relate to modes with very localised effects, an do not influence the global deformations. When reducing further, it is observed that the frames with no, a diagonal, or a box stiffening configuration do not receive relative deviations above 5 % until only the first 50 modes are included. The same behaviour is seen for the frame configuration with both the diagonal and box stiffening plates at point A. Nonetheless, at point B and C, the relative deviation increases when reducing from 250 modes to 225 modes. However, it should be noticed that due to the very stiff joint configuration, the displacements at the points B and C are limited and therefore the relative deviations may be considered as misleading. To illustrate, when including the first 100 modes only, the displacements at point B and C are -0.0168mm and -0.0311mm, respectively, whereas at point A the displacement is -0.3791mm being approximately ten times larger.

5.1.3. The joint eigenmodes

Throughout this subsection, a detailed analysis of the primary joint element with box stiffeners is conducted. This analysis has been performed in order to assess if it is possible to deduce meaningful displacement modes related to the joint element itself letting the joint element displacement field be governed by the beam displacement modes occurring at the interfaces. In this analysis the condensed stiffness matrix $\tilde{\mathbf{K}}^\mathsf{J}$ from Equation (11) is used without boundary degrees of freedoms, i.e. $\mathbf{u}_\mathsf{f} \in \emptyset$ and $\mathbf{f}_\mathsf{f} \in \emptyset$. However, before the stiffness matrix is assessed through an eigenvalue problem, the stiffness matrix is reduced by only including a few number of modal degrees of freedom at the interfaces. This reduction is chosen because it is hypothesised that the primary displacement modes will be governed by the first number of interface modes. Hence, by using Equation (5) and (7) with $\mathbf{V}_\mathrm{I}$ containing the six rigid cross-section displacement modes the joint element stiffness matrix $\tilde{\mathbf{K}}^\mathsf{J}$ is transformed into a 12×12 mode-space-governed stiffness matrix $\mathbf{K}^\mathsf{J}_\mathsf{m}$ that is spanned by the first six interface modes at each interface (see also Figure 9). Then, orthogonal displacement modes for the joint element are computed as eigenmodes by solving the eigenvalue problem:

$$\left(\mathbf{K}^\mathsf{J}_\mathsf{m} - \mathbf{\Lambda}\,\mathbf{I}\right)\mathbf{V}_\mathsf{m} = \mathbf{0} \tag{18}$$

It follows that the eigenvectors in $\mathbf{V}_\mathsf{m}$ corresponds to displacement modes of the joint element governed by the displacement modes at the interfaces enforced by the mode transformation. Moreover, the matrix $\mathbf{\Lambda}$ is a diagonal matrix containing the eigenvalues.

The modes deduced from Equation (18) given in $\mathbf{V}_\mathsf{m}$ are back-transformed according to Equation (5), (7) and (10) and drawn in Figure 12. The corresponding eigenvalues deduced in the diagonal of $\mathbf{\Lambda}$ are listed in Table 3. It is observed that the first six modes have null eigenvalues, which corresponds to rigid motions that are shown in Figure 12a, in which the motions are governed by the cross-sectional beam displacement modes at Interface 1. The remaining six joint element modes are modes having eigenvalues different from zero (Table 3) and results in displacement shapes deforming the joint element, see also Figure 12b. These displacement shapes are either symmetric or anti-symmetric with respect to the joint diagonal.

To conclude the joint element displacement modes deduced in Equation (18) reflect the six rigid displacements as well as displacement modes that could be used in a bilinear elasto-plastic formulation, which however, is beyond the scope of this paper. Nonetheless, a modal-based formulation of a joint element seems reasonable and such a mode formulation could be useful in order to extend this mode-based methodology to include non-linear behaviours as well, in future studies.

This final assessment of the joint element concludes this example regarding the frame corner.

Table 3: Ex. 1 – Eigenvalues that relates to the eigenmodes shown in Figure 12 for the joint element with the box stiffener configuration

Mode	Eigenvalue	Mode	Eigenvalue $[\cdot 10^6]$
1	0.0	7	0.4542
2	0.0	8	0.7100
3	0.0	9	0.7664
4	0.0	10	2.2631
5	0.0	11	3.7980
6	0.0	12	4.6623

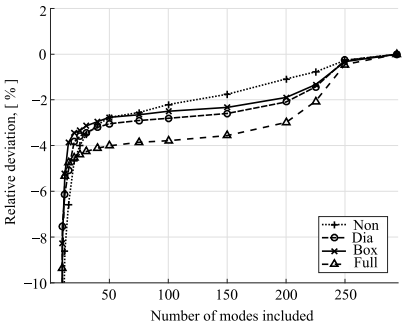

(a) The u_Z-displacements at point A

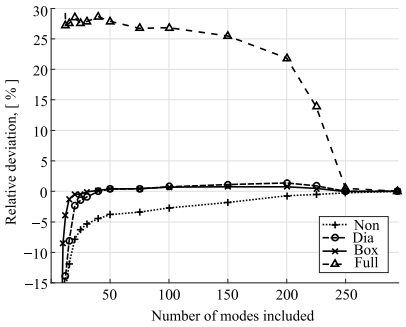

(b) The u_X-displacements at point B

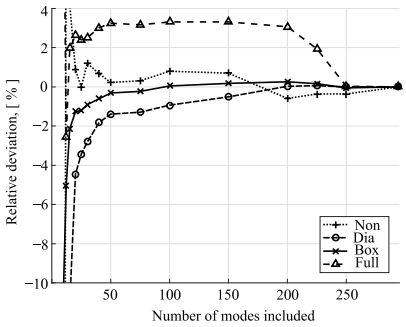

(c) The u_X-displacements at point C

Figure 11: Ex. 1 – The influence on the displacements at point A, B and C illustrated as relative deviations when reducing the number of modes within the elements

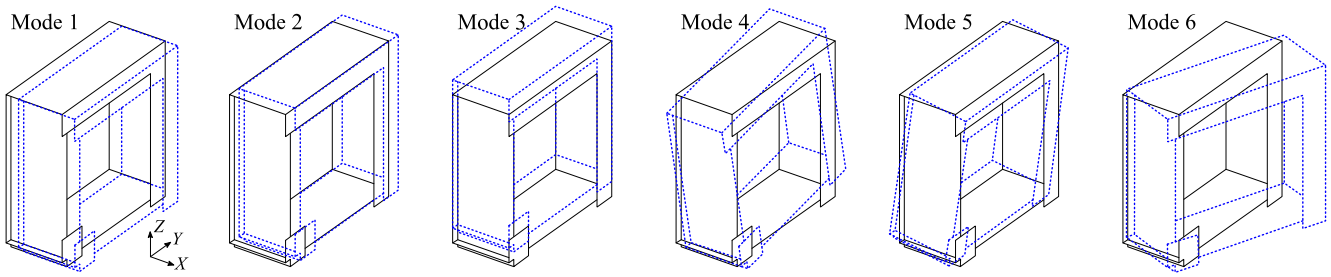

(a) Six rigid modes

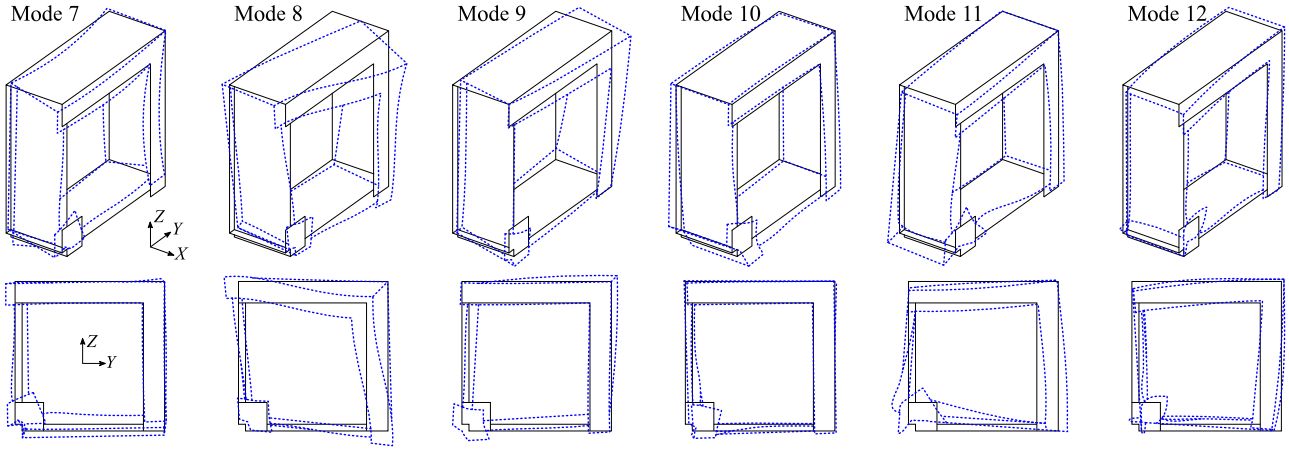

(b) Six non-rigid modes (three-dimensional view and side view)

Figure 12: Ex. 1 – Eigenmodes related to box stiffened joint element (the magnitude of the displacements are scale ten times)

5.2. Ex. 2 – Beam-to-column connection

This second example assesses a connection between a cantilever beam and a clamped column, as illustrated in Figure 13. The model consists of three beam elements (two used for the column part and a single beam element for the beam part). Furthermore, four joint elements are used (three secondary joint elements one for each beam element end and a primary joint element located where the three beam elements meet). The geometry and dimensions, as well as load and boundary conditions, are shown in Figure 13. The load of magnitude 160 N is applied at the secondary joint element located at the free end of the beam where it is evenly distributed along the two web-panels. Furthermore, all degrees of freedom at each of the two secondary joint elements at the ends of the column are restrained to fulfil the clamped support condition. The remaining degrees of freedom within all four joint elements not being at a connected face nor assigned for load or boundary conditions are condensed. It follows that the discretisation of the joint elements is mainly governed by the mesh chosen for the beam elements and is illustrated in Figure 14. The cross-section of the two beam elements forming the column consists of 16 wall elements at the narrow sides and 12 wall elements at the other side. This discretisation results in 56 nodes in total within a cross-section and thus, a total of 336 interface modes at each

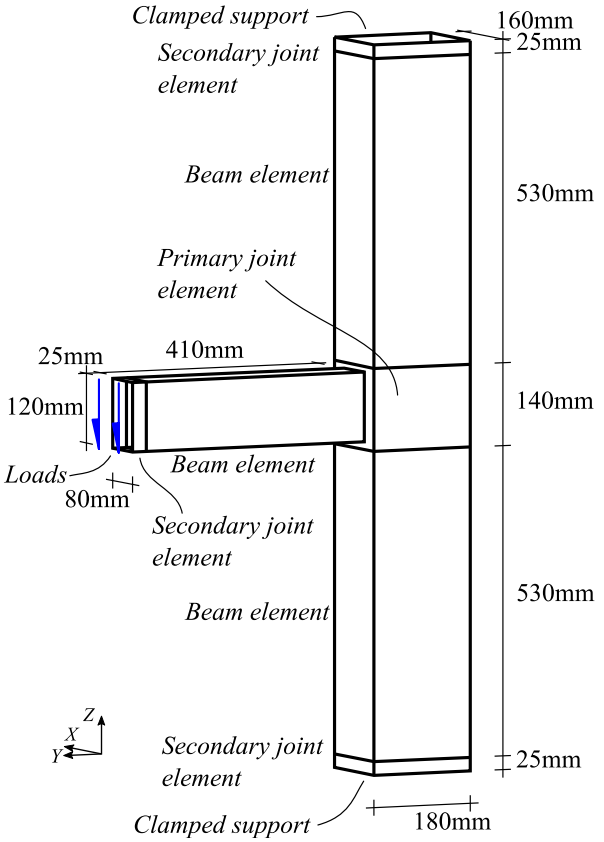

Figure 13: Ex. 2 – The beam-to-column set up. The thickness of all plates are 2 mm

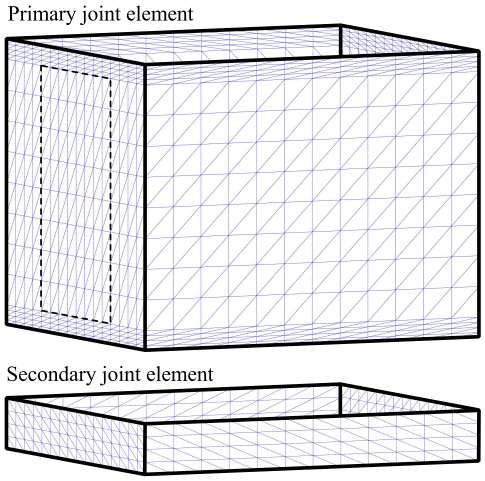

Figure 14: Ex. 2 – Visualisation of the mesh density for the different kind of joint elements

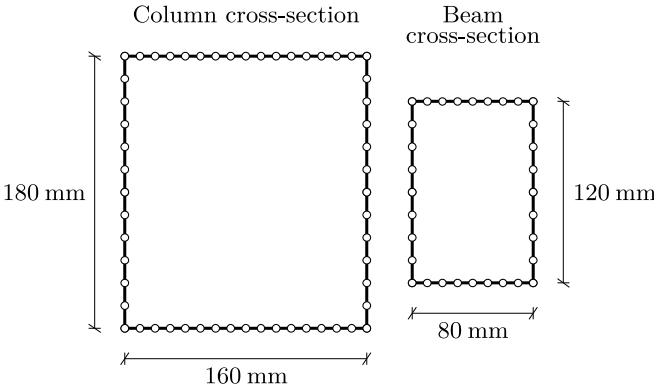

Figure 15: Ex. 2 – Discretisation of the two types of beam elements used

beam element interface. Regarding the cantilever beam, eight wall elements have been used at each of the four edges, which results in 32 nodes in total and hence, 192 interface modes as a maximum related to this connected face. The discretisation of the beam element cross-sections are shown in Figure 15 for clarity.

5.2.1. Verification

Verification of the model has been performed by comparisons with a finite element model from `Abaqus`. The finite element model in `Abaqus` uses triangular shell elements (S3 elements in `Abaqus` nomenclature) in a structured mesh and with full integration. The mesh is chosen such that the column has 16 elements along each edge in the cross-section whereas the beam has eight elements at the narrow sides and 16 elements at the others. In general, the finite element side length is approximately 10 mm.

The u_Y and u_Z displacements at the free end of the beam at the point located at the middle of the upper flange and at the plate centre line have been measured and are listed in Table 4. Comparing the main displacements in u_Z

Table 4: Ex. 2 – Displacements measured at the free end of the beam at the middle of the flange and at the centre line of the plate, $[\cdot 10^{-2}\text{mm}]$

	Present theory	`Abaqus`
u_Y	27.02	27.99
u_Z	−195.5	−202.6

obtained by the present theory with the results from the `Abaqus` model results in a relative deviation of −3.50 %.

5.2.2. Mode-based assessment

Figure 16 and 17 illustrates the global deformation of the beam-to-column connection. The intensities at each interface of the primary joint element are illustrated in Figure 16 as well. Due to the different discretisations of the beam and column elements, the number of interface modes varies. Hence, at Interface 1 and 3 there are 336 modes whereas at Interface 2 there are 192 modes. The tendency at Interface 1 and 3 is that the primary modes are the first ones and then the intensities decay for increasing mode indices. However, at Interface 2, a single mode stands out from the others, which is mode five and has an intensity being atleast ten times higher compared to the other modes, which are at a more constant level not decreasing in the same ways as seen at Interface 1 and 3. The first number of interface modes regarding Interface 2 are illustrate in Figure 18.

Now, as in the previous example, the number of modes used for the analysis is decreased. The displacements u_Y and u_Z at the beam flange are measured, and the relative

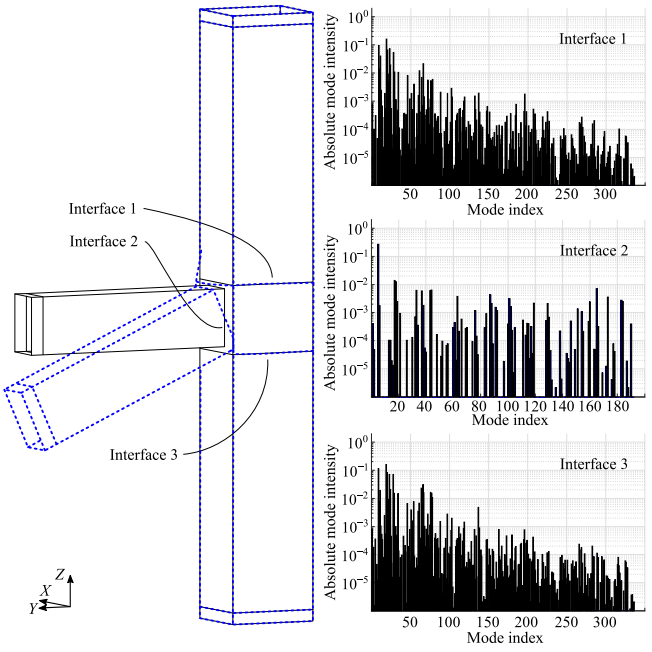

Figure 16: Ex. 2 – Global deformation and intensities at interfaces related to the primary joint element. The magnitude of the displacements are scaled 100 times

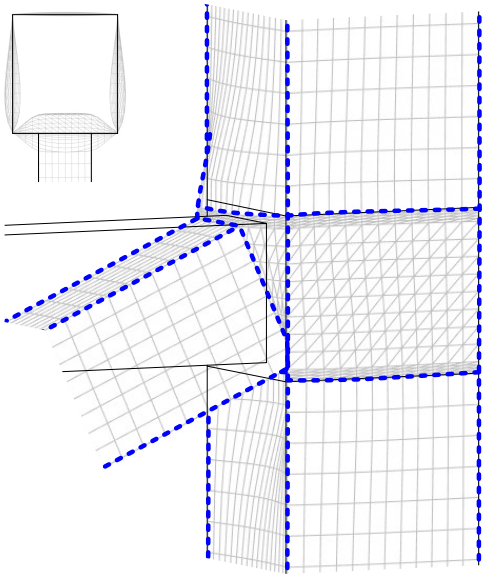

Figure 17: Ex. 2 – A close-up of the deformation at the connection and a top view illustrating the bending of the column panels. The magnitude of the displacements are scale 100 times

deviation compared to the full mode formulation is illustrated in Figure 19. It is seen that a rapid increase in the relative deviation is measured as we reduce the number of modes. The main reason for this shall be found in the fashion the frame deforms. Because the beam width does not equal the column width, the bending that occurs at the connection will be obtained by plate bending in the column plate panels. The interface modes supporting this behaviour are modes with a high index number and thus, not including these modes, the induced error will be significant. Furthermore, the stiffness of this type of connection is limited, and therefore, the following section introduces a re-design of the connection, results in an stiffer joint.

5.2.3. Re-design

This subsection focus on an optimisation of the connection in order to increase the bearing capacity by avoiding plate bending in the column. Hence, the beam width is increased, such that it equals the column width. Then, the displacements at the middle of the upper flange at the free end are reduced to: $u_Y = 0.399 \cdot 10^{-2}$ mm and $u_Z = 2.83 \cdot 10^{-2}$ mm, which is a significant decrease compared to the displacements in Table 4 with almost a factor 100. Of cause, the moment of inertia is increased in the beam due to the increase flange width; however, the main strengthen is mainly obtained because the bending is transferred to the web and flange panels directly without inducing as much local plate bending within the column plate panels.

With the re-designed set up of the beam-to-column configuration, the mode assessment is conducted. Figure 20 shows the global deformation as well as the intensities of the modes at the interfaces similar to Figure 16. In ac-

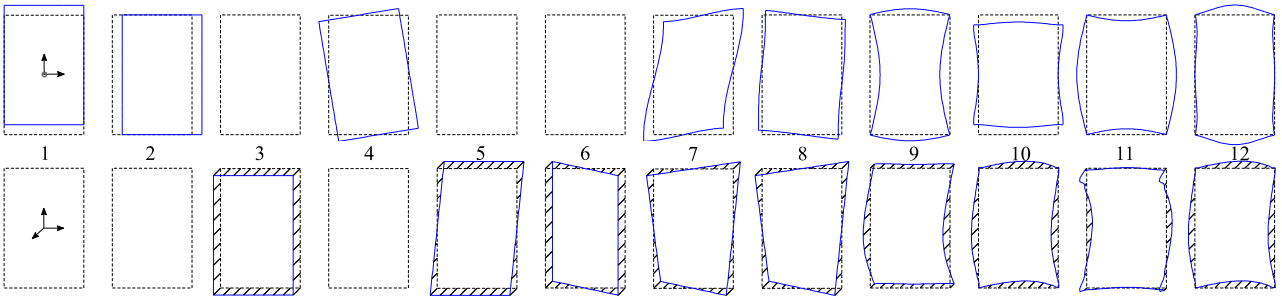

Figure 18: Ex. 2 – The first twelve interface modes used at Interface 2 in Figure 16. The upper row represents the in-plane part of the displacement modes and the lower row represents the out-of-plane displacements of the modes (warping)

cordance with the increased stiffness and the reduction in displacements, the intensities are generally decreased compared to those in Figure 16. Moreover, since this design avoids main plate bending in the column panels, it is seen how the number of modes with high intensities is reduced, especially at Interface 1 and 3. Also, at Interface 2, we see a decrease in the number of modes with a clear influence. Nonetheless, what is more interesting is that executing the procedure, reducing the number of interface modes in the analysis, the relative deviation in displacements is not as significant as in the case of the poor design. The relative deviations obtained in the displacements when reducing the number of interface modes are illustrated in Figure 19. The graph illustrates how the local modes with a high mode index do not influence the displacement to the same extent as in the case with the narrow beam. When only the first 100 modes are kept, the relative deviation is still below 6 % whereas for the poor design this number if 26 %.

6. Discussion

A generic methodology to perform a first-order linear elastic frame analysis of steel frame structures based on displacement modes have been presented here.

The analysis is based on a systematic method and detailed description of each element within the frame, i.e. beam elements and joint elements. The joint elements are modelled by use of finite shell elements and are versatile in the sense of covering any complex geometry associated with the connection between beam elements. The beam elements, on the other hand, are described by an advanced mode-based beam theory that includes cross-sectional displacement modes. These cross-sectional beam displacement modes are used as a novel set of degrees of freedom instead of standard degrees of freedom, and thus, interfaces between beam elements and joint elements are transformed

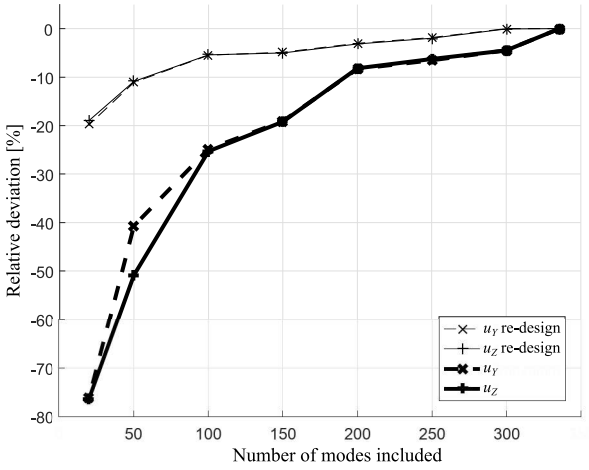

Figure 19: Ex. 2 – Relative deviations when reducing the number of modes within the model. Displacements measured at the middle of the upper flange at the free end of the cantilever beam

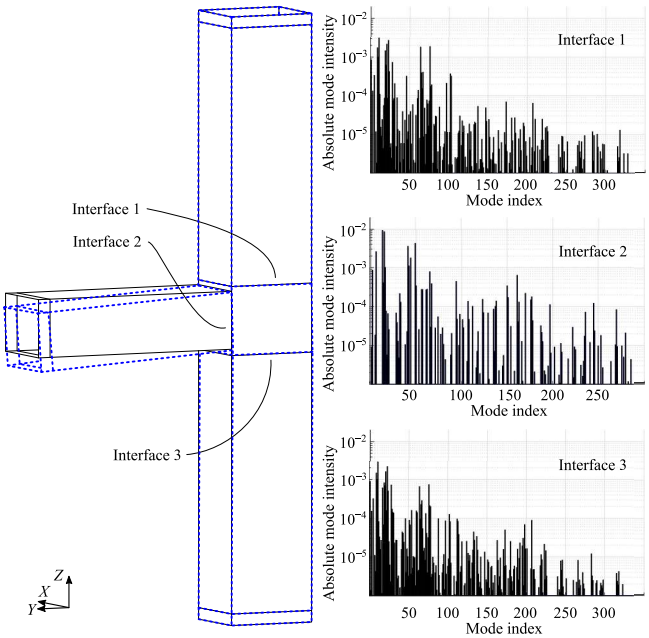

Figure 20: Ex. 2 – Global deformation of the re-designed model (magnitude of the deformations are scale 1000 times). The intensities of the interface modes related to the primary joint element are illustrated as well

into a cross-sectional beam displacement mode-based degree of freedom space. Thereby, the entire frame structure is described by a set of interface displacement modes instead of the standard nodal degrees of freedom. Through an assessment of these modes, it is observed that with proper joint design it is reasonable to reduce the number of mode related-degrees of freedom but still retain a sufficient level of accuracy as well as including advanced displacements such as cross-sectional distortion. Because the reduction in the number of degrees of freedom is directly related to the computational time, the presented methodology is especially interesting when larger frame structures have to be analysed since the computational capacity may be a limiting factor.

Two examples have been included, and consistent results have been obtained compared to a full shell finite element model computed in a commercial finite element software. The joint elements within the two examples are modelled exclusively by shell elements. However, future studies will focus on the inclusion of other kinds of elements to be able to handle components within a connection, such as bolts.

A unique feature with this approach is the identification of activated displacement modes. The deformation of a beam element can be decomposed into pre-established beam displacement modes, and hence, extended informative knowledge regarding a global frame deformation may be obtained. Furthermore, based on this knowledge, a redesign may be considered. Not only the beam elements may be decomposed into structural meaning full displacement modes, but the joint elements may also be assessed to deduce displacement modes as well. Moreover, the joint displacement modes may be used in future studies of the influence of non-linear geometric or material behaviours by pursuing an interactional modal formulation.

Due to the general formulation, this methodology can be used with most advanced beam theories that are based on a displacement mode-based formulation.

7. Acknowledgement

The first author thankfully acknowledges the financial support given by the Danish consultancy company NIRAS A/S and the Innovation Fund Denmark (grant 5189-00005B). Moreover, on behalf of the first author, a great thank is given to Associate Professor Ricardo F. Vieira for supervision during his two-month research stay at the Technical University of Lisbon in 2018.

References

[1] A. B. Hansen, J. Jönsson, Modelling of steel frames using advanced beam and joint elements with a beam mode governed interface, submitted to: Thin-Walled Structures.

[2] A. B. Hansen, J. Jönsson, Displacement modes of a thin-walled beam model with deformable cross sections, submitted to: Thin-Walled Structures.

[3] A. B. Hansen, J. Jönsson, A thin-walled beam element formulated on exact displacement modes, submitted to: Thin-Walled Structures.

[4] M. Abambres, D. Camotim, N. Silvestre, K. J. R. Rasmussen, GBT-based structural analysis of elastic-plastic thin-walled members, Computers & Structures 136 (2014) 1–23 (2014). doi:10.1016/j.compstruc.2014.01.001.

[5] C. Basaglia, D. Camotim, N. Silvestre, GBT-based global buckling analysis of plane and space thin-walled steel frames, in: Proceedings of the International Collquium on Stability and Ductility of Steel Structures, SDSS 2006 (2006) 381–388 (2006).

[6] C. Basaglia, D. Camotim, N. Silvestre, Global Buckling Analysis of Plane and Space Thin-Walled Frames in the Context of GBT, Thin-Walled Structures 46 (2008) 79–101 (2008). doi:10.1016/j.tws.2007.07.007.

[7] V. Z. Vlasov, Thin-Walled Elastic Beams, 2nd Edition, Jerusalem, 1961, israel Program for scientific translations (1961).

[8] C. Basaglia, D. Camotim, N. Silvestre, GBT-based local, distortional and global buckling analysis of thin-walled steel frames, Thin-Walled Structures 47 (2009) 1246–1264 (2009). doi:10.1016/j.tws.2009.04.003.

[9] R. Schardt, Verallgemeinerte Technische Biegetheorie - Band 1, Lineare Theorie, 2nd Edition, Metrum-Verlag,Darmstadt, 1989 (1989).

[10] N. Silvestre, D. Camotim, First-order generalised beam theory for arbitrary orthotropic materials, Thin-Walled Structures 40 (2002) 755–789 (2002). doi:10.1016/S0263-8231(02)00025-3.

[11] R. D. Cook, D. S. Malkus, M. E. Plesha, Concepts and applications of finite element analysis, 3rd Edition, John Wiley & Son, NewYork Chichester Brisbane Toronto Singapore, 1989 (1989).

[12] B. Specht, Modified shape functions for the three-node plate bending element passing the patch test, International Journal for Numerical Methods in Engineering 26 (1988) 705–715 (1988). doi:10.1002/nme.1620260313.

[13] MATLAB, MATLAB® and Simulink® used for technical computing, 2016, MATLAB - © 1984-2016 The MathWorks, Inc., Version 2016a (2016).

[14] Abaqus, Abaqus/CAE 2016; Abaqus® and SIMULIA® used for finite element analysis, 2016, abaqus Inc., SIMULIA © Dassault Systèmes, 2015, Version 2016 (2016).

[15] A. B. Hansen, J. Jönsson, A gbt-framework towards modal modelling of steel structures, John Wiley & Sons, Ltd – ce/papers (2017) 1822–1830 (2017). doi:10.1002/cepa.226.

[16] F. Tisseur, K. Meerbergen, The quadratic eigenvalue problem, Society for Industrial and Applied Mathematics 43 (2) (2001) 235–286 (2001). doi:10.1.1.32.9042.

[17] G. Strang, Introduction to Linear Algebra, Wellesley-Cambridge Press, 2009 (2009).

[18] R. F. Vieira, A higher order thin-walled beam model, Ph.D. thesis, Universidade Técnica de Lisboa - Instituto Superior Técnico (2010).

[19] M. Morandini, M. Chierichetti, P. Mantegazza, Characteristic behavior of prismatic anisotropic beam via generalized eigenvectors, International Journal of Solids and Structures 47 (2010) 1327–1337 (2010). doi:10.1016/j.ijsolstr.2010.01.017.

Appendix A. Advanced beam theory

In accordance with the advanced beam theory presented in [2, 3], some of the key-points will be highlighted in this appendix.

The beam geometry is defined by the cross-section located in the xy-plane and then being extruded continuously in the direction of the z-axis. Within the thin-walled cross-section, a local Cartesian coordinate system (n, s, z) is introduced. Here, n is the wall normal, s is the wall tangential, and z is parallel to the beam axis. An example of a beam element is illustrated in Fig. A.21.

The deformation of a beam element is found as a sum of beam displacement modes. Each mode consists of two cross-sectional displacement fields that are associated with an axial amplitude function. These amplitude functions are linear independent, which guarantee a continuity of the displacement fields along the beam axis. The two cross-sectional displacement fields are one related to in-plane motions and the other one relates to motions perpendicular to the cross-sectional plane.

A cross-section is constituted by straight wall elements, which gives the freedom to form any cross-sectional geometry, being a member with an open or a closed cross-section. An example of a cross-sectional wall element is shown in Fig. A.22. The division into minor elements is done for better approximation features and the wall element supports both flexural and membrane behaviours. The kinematic presumptions consider a Kirchhoff formulation in the n, s-plane, a Mindlin formulation in the n, z-plane, and a Timoshenko formulation in the s, z-plane. To fulfil these kinematics, we formulate three equations to describe the displacement of a wall element as functions of the z-axis. Hence, the displacement of a single wall element is defined from the plate element centre surface on its three local coordinate directions, $\boldsymbol{u} = [u_n \; u_s \; u_z]^\mathsf{T}$.

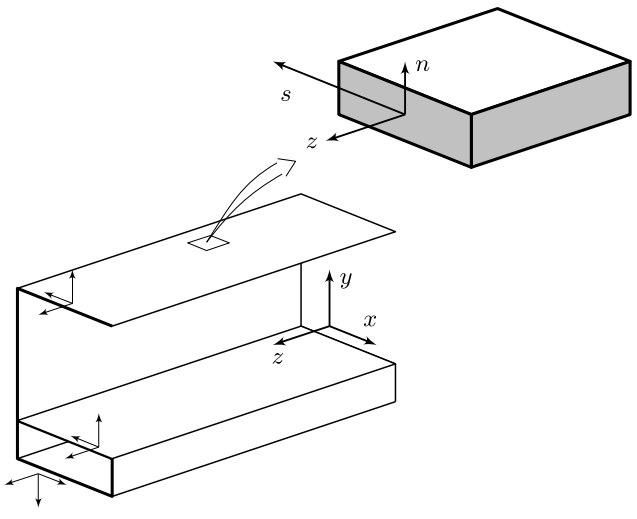

Figure A.21: Cartesian beam coordinate system (x, y, z) and local cross-sectional coordinate systems (n, s, z) regarding a thin-walled beam member

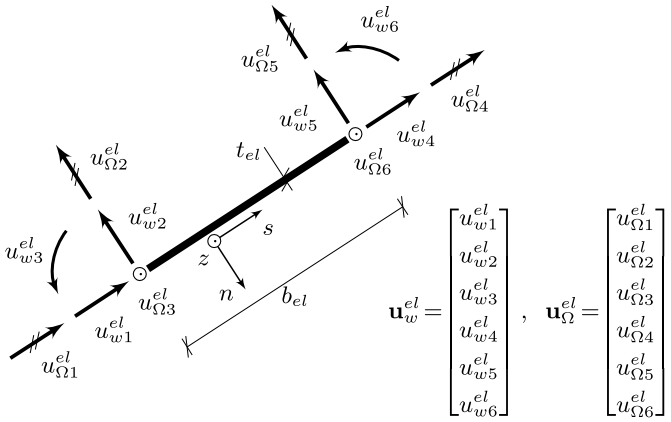

Figure A.22: Wall element, which is used to discretize the cross-section also illustrating the displacement components from $\mathbf{u}^{el}_w$ and $\mathbf{u}^{el}_\Omega$, respectively

These are independently approximated through interpolation functions along the coordinate s. The interpolation functions are governed by the nodal displacement components at the wall element ends as the degree of freedom vectors $\mathbf{u}^{el}_w(z)$ and $\mathbf{u}^{el}_\Omega(z)$, which relates to in-plane (index w) and out-of-plane (index Ω) translations and rotations as illustrated in Fig. A.22. To be mentioned, the degrees of freedom in the vectors $\mathbf{u}^{el}_w(z)$ and $\mathbf{u}^{el}_\Omega(z)$ are sums of m displacement modes and can be computed as:

$$\begin{aligned} \mathbf{u}^{el}_w(z) &= \sum_{i=1}^{m} \mathbf{v}^{el\,i}_w \; \psi^i(z)\, c_i \\ \mathbf{u}^{el}_\Omega(z) &= \sum_{i=1}^{m} \mathbf{v}^{el\,i}_\Omega \; \eta^i(z)\, c_i \end{aligned} \tag{A.1}$$

in which $\mathbf{v}^{el}_w$ and $\mathbf{v}^{el}_\Omega$ are wall element mode displacement vectors, $\psi(z)$ and $\eta(z)$ are the axial amplitude functions, and c is a mode intensity factor used to scale the intensity of each mode.

Accordingly, the displacements of a single wall element are approximated as follows:

$$\begin{aligned} u_n(s, z) &= \mathbf{N}_n(s)\, \mathbf{u}^{el}_w(z) \\ u_s(n, s, z) &= \Big[\; \mathbf{N}_s(s) - n\, \mathbf{N}_{n,s}(s) \;\Big]\, \mathbf{u}^{el}_w(z) \\ u_z(n, s, z) &= \Big[\; \mathbf{N}_\Omega(s) + n\, \mathbf{N}_\alpha(s) \;\Big]\, \mathbf{u}^{el}_\Omega(z) \end{aligned} \tag{A.2}$$

The interpolation vectors $\mathbf{N}_n$ and $\mathbf{N}_\alpha$ contain linear Lagrange interpolation functions, and the vectors $\mathbf{N}_s$ and $\mathbf{N}_\Omega$ includes cubic Hermite interpolation functions, see also [15]. Furthermore, an n or s-index that follows a comma indicates a derivative, e.g.: $(\,\cdot\,)_{,s} = d(\,\cdot\,)/ds$, whereas axial derivatives will be signed using the Lagrange notation, i.e. a prime: $(\,\cdot\,)' = d(\,\cdot\,)/dz$.

Displacements are obtained under the small displacement hypothesis, and thus, the strains are obtained calculating:

$$\boldsymbol{\varepsilon} = \boldsymbol{\mathcal{S}}\, \boldsymbol{u} \quad \text{with } \boldsymbol{\varepsilon} = [\varepsilon_{nn},\; \varepsilon_{ss},\; \varepsilon_{zz},\; \gamma_{sz},\; \gamma_{nz},\; \gamma_{ns}]^\mathsf{T} \tag{A.3}$$

having the strains written in Voigt notation and the strain operator given by:

$$\boldsymbol{\mathcal{S}} = \begin{bmatrix} \frac{\partial}{\partial n} & \cdot & \cdot & \cdot & \frac{\partial}{\partial z} & \frac{\partial}{\partial s} \\ \cdot & \frac{\partial}{\partial s} & \cdot & \frac{\partial}{\partial z} & \cdot & \frac{\partial}{\partial n} \\ \cdot & \cdot & \frac{\partial}{\partial z} & \frac{\partial}{\partial s} & \frac{\partial}{\partial n} & \cdot \end{bmatrix}^{\mathsf{T}} \tag{A.4}$$

In this expression, a dot $[\,\cdot\,]$ represents a suitable zero matrix, which is a notation used throughout this appendix.

From Eq. (A.3) and the displacements in Eq. (A.2) it follows that $\varepsilon_{nn} \equiv 0$ and $\gamma_{ns} \equiv 0$. Now, the stresses are formulated on the assumption of linear elastic isotropic material properties and thereby the Generalised Hooke's law is used. As a consequence, the shear stress $\tau_{ns} \equiv 0$ and the normal stress $\sigma_{nn} \equiv 0$ are defined zero. The remaining non-null stress field is found from the constitutive relation:

$$\boldsymbol{\sigma} = \boldsymbol{D}\,\boldsymbol{\varepsilon} \tag{A.5}$$

in which the stress components are written in the vector format: $\boldsymbol{\sigma} = [\,\sigma_{ss}\,,\ \sigma_{zz}\,,\ \tau_{sz}\,,\ \tau_{nz}\,]^{\mathsf{T}}$, the strain vector only include non-null terms, and the elastic stiffness matrix $\boldsymbol{D}$ is defined for a plane stress state taking into account the Poisson effect as follows:

$$\boldsymbol{D} = \begin{bmatrix} E_s & \nu E_s & \cdot & \cdot \\ \nu E_s & E_s & \cdot & \cdot \\ \cdot & \cdot & G & \cdot \\ \cdot & \cdot & \cdot & G \end{bmatrix} \tag{A.6}$$

Here, E_s is the plate type elastic modulus: $E_s = E/(1-\nu^2)$, where E is the modulus of elasticity; ν is the Poisson coefficient; and G is the shear modulus: $G = E/(2(1+\nu))$.

Equilibrium for the beam element is found using the linear elastic strain energy, which is derived by integrating the strain energy density over the full continuum V. Hence, in its purest form, the strain energy is expressed as:

$$U = \frac{1}{2}\int_V \boldsymbol{\sigma}^{\mathsf{T}}\,\boldsymbol{\varepsilon}\;dV \tag{A.7}$$

The volume integral is separated into an integration over the beam length ℓ along z, and integration over each wall element thickness t_{el} and wall element width b_{el} being supplemented by assembling of wall elements. Hence, substituting Eq. (A.2) into the strain and stress formulations, in Eq. (A.3) and (A.5), local wall element stiffness matrices can be computed as indicated in Tab. A.5. To that end, assembling the wall elements based on standard transformations and their degrees of freedom, the strain energy from Eq. (A.7) is rewritten into the following expression based on stiffness matrices and displacement vectors.

$$U = \frac{1}{2}\int_0^{\ell} \begin{bmatrix} \mathbf{u}_w \\ \mathbf{u}_\Omega \\ \mathbf{u}'_w \\ \mathbf{u}'_\Omega \end{bmatrix}^{\mathsf{T}} \begin{bmatrix} \mathbf{K}^{s}_{ww} & \cdot & \cdot & \mathbf{K}^{s\sigma}_{w\Omega} \\ \cdot & \mathbf{K}^{\gamma}_{\Omega\Omega} & \mathbf{K}^{\gamma}_{\Omega w} & \cdot \\ \cdot & \mathbf{K}^{\gamma}_{w\Omega} & \mathbf{K}^{\gamma}_{ww} & \cdot \\ \mathbf{K}^{\sigma s}_{\Omega w} & \cdot & \cdot & \mathbf{K}^{\sigma}_{\Omega\Omega} \end{bmatrix} \begin{bmatrix} \mathbf{u}_w \\ \mathbf{u}_\Omega \\ \mathbf{u}'_w \\ \mathbf{u}'_\Omega \end{bmatrix} dz \tag{A.8}$$

The superscripts s, σ and γ on the stiffness matrices identifies terms related to transverse, axial and shear strains, respectively.

A system of second-order beam differential equilibrium equations is deduced from the strain energy in Eq. (A.8). This is done by seeking a minimum of energy and requiring the strain energy to be stationary using the principle of variation when introducing virtual displacement fields, which is kinematic admissible, then perform partial integration on selected terms. A homogeneous system of differential equilibrium equations in terms of displacements is then deduced as follows:

$$\mathbf{K}_2\mathbf{u}''(z) \;+\; \mathbf{K}_1\mathbf{u}'(z) \;+\; \mathbf{K}_0\mathbf{u}(z) \;=\; \mathbf{0} \tag{A.9}$$

where the matrices $\mathbf{K}_0$, $\mathbf{K}_1$ and $\mathbf{K}_2$ are defined as blocks of cross-sectional stiffness matrices and the common displacement vector $\mathbf{u}(z)$ is introduced containing both the translational and warping displacement vectors. To clarify:

$$\mathbf{K}_0 = \begin{bmatrix} \mathbf{K}^{s}_{ww} & \cdot \\ \cdot & -\mathbf{K}^{\gamma}_{\Omega\Omega} \end{bmatrix},\quad \mathbf{K}_2 = \begin{bmatrix} -\mathbf{K}^{\gamma}_{ww} & \cdot \\ \cdot & \mathbf{K}^{\sigma}_{\Omega\Omega} \end{bmatrix},\quad \mathbf{K}_1 = \begin{bmatrix} \cdot & \mathbf{K}^{s\sigma}_{w\Omega} - \mathbf{K}^{\gamma}_{w\Omega} \\ \mathbf{K}^{\sigma s}_{\Omega w} - \mathbf{K}^{\gamma}_{\Omega w} & \cdot \end{bmatrix},\quad \mathbf{u}(z) = \begin{bmatrix} \mathbf{u}_w(z) \\ \mathbf{u}_\Omega(z) \end{bmatrix} \tag{A.10}$$

Each block matrix is $n \times n$, where n is six times the number of nodes within a beam cross-section.

A full homogeneous solution space to Eq. (A.9) is a summation of two parts, that is: $\mathbf{u} = \mathbf{u}_p + \mathbf{u}_e$. The first part of the solution space relates to solutions with a polynomial variation along z. The second part of the solution space is reserved for those solutions having an exponential variation. In paper [3], it was found that the solutions having a polynomial variation relates to the fundamental beam modes and is a set of twelve solutions. Consequently, $\mathbf{u}_p$ contains $n_z = 12$ solution modes. The other part, the exponential solutions $\mathbf{u}_e$, corresponds to displacement modes of higher order and has an exponential attenuation of the mode along the beam axis. The number of modes related to this part of the solution space depends on the cross-sectional discretisation and is: $n_e = 2n - n_z$. These solutions might include pairs of complex conjugate solutions.

In the following section, solutions to the differential equation system from Eq. (A.9) is computed as cross-sectional displacement fields with associated axial amplitude functions.

Cross-sectional displacement field

Thus, the deformation of the cross-section is governed by a set of displacement fields, which is assumed by interpolation functions of generic straight wall elements. Such straight wall element is also illustrated in Fig. A.22. To this end, a set of cross-sectional stiffness matrices are deduced, and a strain energy formulation is written. Solutions to Eq. (A.9) are computed by a generalised eigenvalue problem, [16]. To solve the system it is assumed

Table A.5: Local stiffness matrices

Stiffness matrices related to normal stresses	Stiffness matrices related to shearing stresses
$\mathbf{k}^{s}_{ww} = \int_0^{b_{el}} \left(t_{el} E_s \mathbf{N}^{\mathsf{T}}_{s,s} \mathbf{N}_{s,s} + \frac{t^3_{el}}{12} E_s \mathbf{N}^{\mathsf{T}}_{n,ss} \mathbf{N}_{n,ss} \right) ds$	$\mathbf{k}^{\gamma}_{ww} = \int_0^{b_{el}} \left(t_{el} G \mathbf{N}^{\mathsf{T}}_{n} \mathbf{N}_{n} + t_{el} G \mathbf{N}^{\mathsf{T}}_{s} \mathbf{N}_{s} + \frac{t^3_{el}}{12} G \mathbf{N}^{\mathsf{T}}_{n,s} \mathbf{N}_{n,s} \right) ds$
$\mathbf{k}^{\sigma}_{\Omega\Omega} = \int_0^{b_{el}} \left(t_{el} E_s \mathbf{N}^{\mathsf{T}}_{\Omega} \mathbf{N}_{\Omega} + \frac{t^3_{el}}{12} E_s \mathbf{N}^{\mathsf{T}}_{\alpha} \mathbf{N}_{\alpha} \right) ds$	$\mathbf{k}^{\gamma}_{\Omega\Omega} = \int_0^{b_{el}} \left(t_{el} G \mathbf{N}^{\mathsf{T}}_{\alpha} \mathbf{N}_{\alpha} + t_{el} G \mathbf{N}^{\mathsf{T}}_{\Omega,s} \mathbf{N}_{\Omega,s} + \frac{t^3_{el}}{12} G \mathbf{N}^{\mathsf{T}}_{\alpha,s} \mathbf{N}_{\alpha,s} \right) ds$
$\mathbf{k}^{s\sigma}_{w\Omega} = \int_0^{b_{el}} \left(t_{el} \nu E_s \mathbf{N}^{\mathsf{T}}_{s,s} \mathbf{N}_{\Omega} - \frac{t^3_{el}}{12} \nu E_s \mathbf{N}^{\mathsf{T}}_{n,ss} \mathbf{N}_{\alpha} \right) ds$	$\mathbf{k}^{\gamma}_{w\Omega} = \int_0^{b_{el}} \left(t_{el} G \mathbf{N}^{\mathsf{T}}_{n} \mathbf{N}_{\alpha} + t_{el} G \mathbf{N}^{\mathsf{T}}_{s} \mathbf{N}_{\Omega,s} - \frac{t^3_{el}}{12} G \mathbf{N}^{\mathsf{T}}_{n,s} \mathbf{N}_{\alpha,s} \right) ds$
$\mathbf{k}^{\sigma s}_{\Omega w} = \int_0^{b_{el}} \left(t_{el} \nu E_s \mathbf{N}^{\mathsf{T}}_{\Omega} \mathbf{N}_{s,s} - \frac{t^3_{el}}{12} \nu E_s \mathbf{N}^{\mathsf{T}}_{\alpha} \mathbf{N}_{n,ss} \right) ds$	$\mathbf{k}^{\gamma}_{\Omega w} = \int_0^{b_{el}} \left(t_{el} G \mathbf{N}^{\mathsf{T}}_{\alpha} \mathbf{N}_{n} + t_{el} G \mathbf{N}^{\mathsf{T}}_{\Omega,s} \mathbf{N}_{s} - \frac{t^3_{el}}{12} G \mathbf{N}^{\mathsf{T}}_{\alpha,s} \mathbf{N}_{n,s} \right) ds$

that $\eta(z) = \psi(z)$ in Eq. (A.1). Thus, cross-sectional displacement fields are determined as eigenvectors, and the associated eigenvalues relate to the axial amplitude functions.

Fundamental modes

Those eigenvectors having eigenvalues equal to zero represents the fundamental modes, which have polynomial amplitude functions that are limited to third-order. Since these modes share the same eigenvalue, it follows that since the algebraic and geometric multiplicity of the eigenvalues do not coincide some generalised eigenvectors are related to these solutions as well, Strang [17]. This was solved by Vieira [18] and Morandini et al. [19] using a Jordan Chain method extracting these additional solution modes. Hansen & Jönsson [2] outlined a more engineering-based procedure and adopted here as well. The result is an extension of the twelve eigenvectors with associated null-eigenvalues into four sets of twelve cross-sectional displacement fields. This we write as:

$$\mathbf{V}_p = \begin{bmatrix} \mathbf{V}_3 & \mathbf{V}_2 & \mathbf{V}_1 & \mathbf{V}_0 \end{bmatrix} \tag{A.11}$$

A single displacement field is then a combination of four columns – one from each of the matrices $\mathbf{V}_0$ to $\mathbf{V}_3$. The displacement for a single mode j is expressed as:

$$\mathbf{u}_{p_j}(z) = \left(\frac{z^3}{3!} \mathbf{v}_{3j} \; + \; \frac{z^2}{2!} \mathbf{v}_{2j} \; + \; z \mathbf{v}_{1j} \; + \; \mathbf{v}_{0j} \right) c_{p_j} \tag{A.12}$$

where the j-subscript refers to a column index in $\mathbf{V}_i$ for $i = 0, .., 3$ and $j = 1, .., 12$. The c_p is a constant regulating the intensity of the mode.

The solution to Eq. (A.9) related to the polynomial displacement is conveniently written as:

$$\mathbf{u}_p(z) = \mathbf{V}_p \; \mathbf{\Psi}_p(z) \; \mathbf{T}_p \; \mathbf{c}_p \tag{A.13}$$

where $\mathbf{V}_p$ is given in Eq. (A.11) and the remaining components are outline below.

$$\mathbf{\Psi}_p(z) = \begin{bmatrix} \frac{z^3}{6}\mathbf{I}_p & \cdot & \cdot & \cdot \\ \cdot & \frac{z^2}{2}\mathbf{I}_p & \cdot & \cdot \\ \cdot & \cdot & z\mathbf{I}_p & \cdot \\ \cdot & \cdot & \cdot & \mathbf{I}_p \end{bmatrix}, \; \mathbf{T}_p = \begin{bmatrix} \mathbf{I}_p \\ \mathbf{I}_p \\ \mathbf{I}_p \\ \mathbf{I}_p \end{bmatrix}, \; \mathbf{c}_p = \begin{bmatrix} c_{p_1} \\ c_{p_2} \\ \vdots \\ c_{p_{n_z}} \end{bmatrix} \tag{A.14}$$

in which $\mathbf{I}_p$ is an identity matrix of size $n_z \times n_z$, and $\mathbf{c}_p$ contains the twelve mode intensity constants.

Exponential modes

The eigenvectors having a non-null eigenvalue are sorted with decreasing eigenvalues and stored as column vectors in the matrix $\mathbf{V}_e$. The associated eigenvalues are substituted into exponential functions in the diagonal of the amplitude matrix $\mathbf{\Psi}_e(z)$. To explain this amplitude matrix we have:

$$\mathbf{\Psi}_e(z) = \begin{bmatrix} e^{\lambda_1 z} & & & \\ & e^{\lambda_2 z} & & \\ & & \ddots & \\ & & & e^{\lambda_{n_e} z} \end{bmatrix} \tag{A.15}$$

where λ is the eigenvalue and n_e is the number of exponential solution modes. Now, the solution space to Eq. (A.9) related to the exponential part can be written as:

$$\mathbf{u}_e(z) = \mathbf{V}_e \; \mathbf{\Psi}_e(z) \; \mathbf{I}_e \; \mathbf{c}_e \tag{A.16}$$

Here, $\mathbf{I}_e$ is a "dummy" unit matrix of size $n_e \times n_e$ and has been introduced to ease the later summation with fundamental modes. The mode intensity constants are stored in $\mathbf{c}_e$ as:

$$\mathbf{c}_e = \begin{bmatrix} c_{e_1} & c_{e_2} & \dots & c_{e_{n_e}} \end{bmatrix}^{\mathsf{T}} \tag{A.17}$$

Full displacement formulation

The full homogeneous solution space to the beam equilibrium equation system (A.9) corresponds to a summation of the displacement formulations in Eq. (A.13) and (A.16). These we add together and receive a full homogeneous solution space expressed in terms of displacement modes being:

$$\begin{aligned} \mathbf{u}(z) &= \mathbf{u}_p(z) + \mathbf{u}_e(z) \\ &= \begin{bmatrix} \mathbf{V}_p & \mathbf{V}_e \end{bmatrix} \begin{bmatrix} \mathbf{\Psi}_p(z) & \cdot \\ \cdot & \mathbf{\Psi}_e(z) \end{bmatrix} \begin{bmatrix} \mathbf{T}_p & \cdot \\ \cdot & \mathbf{I}_e \end{bmatrix} \begin{bmatrix} \mathbf{c}_p \\ \mathbf{c}_e \end{bmatrix} \\ &= \mathbf{V} \; \mathbf{\Psi}(z) \; \mathbf{T}_c \; \mathbf{c} \end{aligned} \tag{A.18}$$

in which the components are defined in Eq. (A.11), (A.14), (A.15), and (A.17).

In conclusion, we can describe the beam deformation as a combination of cross-sectional displacement fields with exact axial amplitude functions. The intensity constants in $\mathbf{c}$ regulate each mode intensity.

Beam equation system

A linear beam element formulation can be obtained using the potential energy. The strain energy contribution was defined in Eq. (A.8) and for simplicity only nodal loads at beam end cross-sections are taken into account regarding the potential contribution from loads. Hence, to formulate the beam element stiffness matrix from the strain energy, the integration in Eq. (A.8) is solved by using the beam displacement modes from Eq. (A.18) as interpolation functions. Thus, the potential energy follows as:

$$V = U + \Pi \quad \Leftrightarrow \quad V = \tfrac{1}{2}\ \mathbf{u}_b^{\mathsf{T}}\ \mathbf{K}^{\mathsf{B}}\ \mathbf{u}_b - \mathbf{u}_b^{\mathsf{T}}\ \mathbf{f} \tag{A.19}$$

Using the variational principles on the potential energy introducing the virtual displacement field $\delta\mathbf{u}_b^{\mathsf{T}}$, onto Eq. (A.19) and apply the condition of stationarity by requiring kinematic admissible boundary conditions, we obtain the beam element formulation:

$$\mathbf{K}^{\mathsf{B}}\ \mathbf{u}_b = \mathbf{f} \tag{A.20}$$

where $\mathbf{K}^{\mathsf{B}}$ is the beam element stiffness matrix deduced from Eq. (A.8), $\mathbf{u}_b$ is a boundary vector containing the end cross-sectional degrees of freedom and $\mathbf{f}$ is a load vector likewise related to the degrees of freedom at the beam end cross-sections. The choice of interface modes is derived in Section 4.

Structural systems of thin-walled members such as steel frames in power plants and sport facilities have reached increasing attention throughout the last decades. This increased attention is mainly due to an efficient material utilisation. However, the methods for structural analysis existing today are primarily based on single member analysis, which does not include the actual interaction between the members. Despite that, the modelling of the beams, columns, and especially their connections is essential for the assessment of the overall structural performance and for the ability to provide more economical design.

This thesis presents a novel methodology to analyse thin-walled frame structures. In general, the method consists of two different types of elements - advanced thin-walled beam elements and detailed joint elements. The computational efficiency of the process is achieved by the use of beam displacement modes, which reduces the number of equations needed. Furthermore, an in-depth assessment of each component is possible due to a displacement-based decomposition procedure. This procedure subdivides the deformation of each element into structurally meaningful displacement modes, whereby the user gains informative knowledge of the structural response.

The obtained results show that the methodology has potential and is well-suited for further development and practical use by enabling a full mechanical analysis of thin-walled frames. Furthermore, this general formulation is suitable for implementation in other approaches that uses displacement modes when analysing structural systems.

DTU Civil Engineering

Brovej 118
2800 Kongens Lyngby
Tel. 45251700

www.byg.dtu.dk

87-7877-508-6